Contribution to Advanced Modelli of Turbulent Natural and Mixed Convection

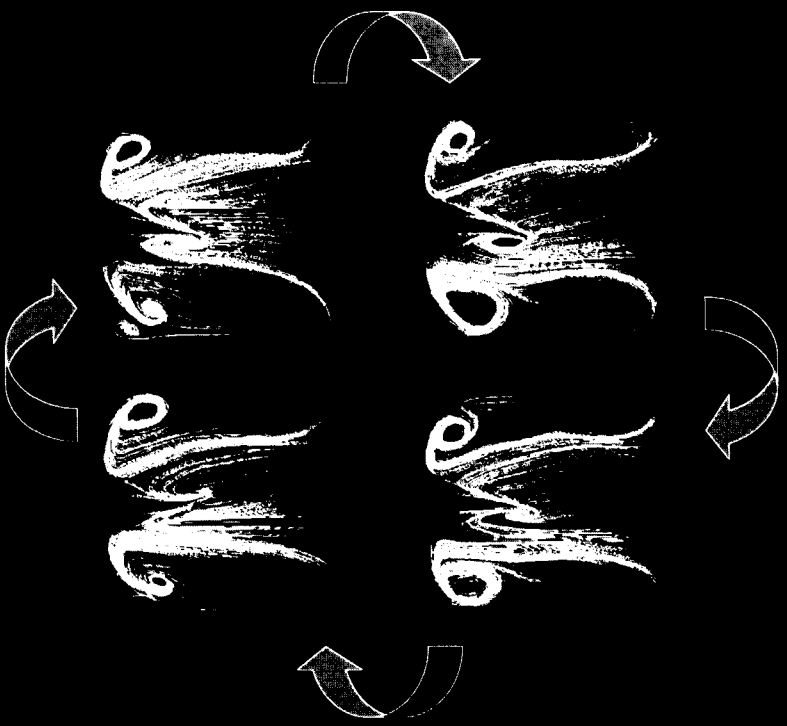

Gunarjo Suryanto Budi

Propositions

belonging to the doctoral dissertation

Contribution to advanced modelling of turbulent natural and mixed convection

by Gunarjo Suryanto Budi

1. It is worthwhile spending time and effort on thorough testing of turbulence models in simple generic fluid flows, not only because generic phenomena are present in most complex flows, but also because such tests can disclose subtle model deficiencies, which will make them unreliable for predicting real-life complex flows.

2. A good turbulence model does not always need to be sophisticated and very advanced: the optimum model is harmony and balance between accuracy, robustness, computational cost, applicability, and complexity.

3. The $k - \varepsilon - \overline{v^2} - f - \overline{\theta^2}$ model developed in this thesis is at present the optimum model for complex turbulent flows driven or affected by thermal buoyancy: it has provided relatively accurate results in a range of applications with affordable mesh density.

4. Turbulence models are like fashion in dressing: fashionable models appear and disappear in cycles: new releases remain in fashion for some time, then they disappear and suddenly they are back again with new minor modification and new success claims. Only the $k-\varepsilon$ model remains eternal.

5. Most CFD model developers are fond of Reynolds Stress Models, because they provide the soundest physical rationale within the framework of RANS modelling. However, because of formidable demands on computer power and personal computational skill, people in industry facing dynamic market demands, consider these models as a nightmare!

6. Natural is a heavenly word for many groups of people: for women it means plants, health and beauty; for environmentalists it means clean water, fresh air and green forests; for artists it means mountains, blue ocean, green valley, and clear sky. For engineers, unfortunately, natural is mostly related to convection.

7. To spend four years working on turbulence models developing and testing seems like one season. To spend one season in a cold, wet, windy weather in winter time it seems like 4 years. That is the relativity.

8. Sometimes it is not easy to distinguish between an abstract painting and turbulence feature, because both of them exhibit unclear looks. For an artist, a painting can be expressed in thousands beautiful words: harmony, heavenly, moonlight, rainbow, aurora. On the other hand, for an experimentalist or CFD modeller, the feature of turbulence can be explained with only several odd words: random, chaotic, irregular and disorder.

9. The thing that comes first into our mind after we wake up in the morning is usually the most important one in our life on that day. If during five years one has thought about turbulence at least 555 times after getting up from bed, one is certainly qualified and legitimized to work professionally in the field of turbulence modelling and computations.

These propositions are considered defendable and as such have been approved by the supervisor prof dr. K. Hanjalić

Stellingen

behorende bij het proefschrift

Contribution to advanced modelling of turbulent natural and mixed convection

van Gunarjo Suryanto Budi

1. Het is de moeite waard tijd en energie te investeren in het grondig testen van turbulentie modellen in eenvoudige generieke stromingen, niet alleen omdat generieke verschijnselen optreden bij complexe stromingen, maar ook om subtiele onvolkomenheden in de modellen te ontdekken, die anders tot onbetrouwbare voorspellingen leiden in complexe stromingen.

2. Een goed turbulentie model hoeft niet altijd ingewikkeld en zeer geavanceerd te zijn: het optimum model weerspiegelt balans en harmonie tussen nauwkeurigheid, robuustheid, hoeveelheid rekenwerk, toepasbaarheid en complexiteit.

3. Het $k - \varepsilon - \overline{v^2} - f - \overline{\theta^2}$ model, dat ontwikkeld werd in dit proefschrift, is momenteel het optimum model voor complexe turbulente stromingen die gedreven of beïnvloed worden door dichtheidsverschillen: relatief nauwkeurige resultaten werden ermee behaald met haalbare roosterdichtheden, in een reeks toepassingen.

4. Turbulentie modellen zijn als mode voor kleding: modieuze modellen verschijnen en verdwijnen in cycli: nieuwe publicaties blijven een tijd in de mode, verdwijnen dan, en duiken plotseling weer op met nieuwe kleine aanpassingen en nieuwe succes verhalen. Alleen het $k - \varepsilon$ model is immer aanwezig.

5. De meeste CFD-modelbouwers zijn erg gecharmeerd van Reynolds Stress Modellen, omdat ze de krachtigste fysische basis hebben in de RANS modellering. Echter, door hun grote vraag naar rekenkracht van computers en rekenervaring van de gebruiker, beschouwen mensen, die op de industriële markt met een continu veranderende vraag te maken hebben, ze als een nachtmerrie!

6. 'Natuurlijk' is een hemels woord voor vele groepen mensen: voor vrouwen betekent het planten, gezondheid en schoonheid; voor milieudeskundigen betekent het schoon water, frisse lucht en groene wouden; voor kunstenaars betekent het bergen, een blauwe oceaan, een groene vallei en een heldere hemel. Voor wetenschappers is 'natuurlijk' helaas meestal verbonden met convectie.

7. Vier jaar doorbrengen, werkend aan het ontwikkelen en testen van turbulentie modellen, lijkt slechts een seizoen te duren. Eén seizoen doorbrengen in koud, nat en winderig winterweer lijkt vier jaar te duren. Dat is de relativiteit.

8. Soms is het onderscheid tussen een abstract schilderij en turbulente structuur moeilijk te maken, omdat beide een onduidelijk uiterlijk hebben. Een kunstenaar kan een schilderij uitdrukken in een duizendtal prachtige woorden: harmonie, hemels, maanlicht, regenboog, dageraad. Daarentegen, een experimentalist of CFD-modelbouwer kan de structuur van turbulentie alleen uitdrukken in een aantal vreemde woorden: willekeurig, chaotisch, onregelmatig en wanorde.

9. Hetgeen het eerst in ons opkomt na het ontwaken in de ochtend is meestal hetgeen dat het belangrijkst voor ons is op die dag. Als je vijf jaar lang op zijn minst 555 keren aan turbulentie gedacht hebt na het ontwaken, dan ben je zeker bekwaam genoeg en is het je geoorloofd om professioneel te werken op het gebied van turbulentie modellering en berekeningen.

Deze stellingen worden verdedigbaar geacht en zijn als zodanig goedgekeurd door de promotor prof. dr. K. Hanjalić

Contribution to Advanced Modelling of Turbulent Natural and Mixed Convection

Proefschrift

ter verkrijging van de graad van doctor
aan de Technische Universiteit Delft,
op gezag van de Rector Magnificus prof. dr. ir. J.T. Fokkema,
voorzitter van het College voor Promoties,
in het openbaar te verdedigen
op vrijdag 10 Oktober 2003 om 10.30 uur

door

Gunarjo Suryanto Budi

Master of Science, Physics, The University of New England, Australia
geboren te Sukoharjo, Indonesië

Dit proefschrift is goedgekeurd door de promotor:
Prof. dr Dipl.-Ing. K. Hanjalić

Samenstelling promotiecommissie:

Rector Magnificus,	voorzitter
Prof. dr Dipl.-Ing. K. Hanjalić	TU Delft, promotor
Prof. dr D. Roekaerts	TU Delft
Prof. dr ir. Th. van der Meer	Twente Universiteit
Prof. dr ir. A.A. van Steenhoven	TU Eindhoven
Prof. dr ir. H. van der Ree	TU Delft
Dr Dipl-Ing. Saša Kenjereš	TU Delft
Ir. A.D. Lemaire	TNO BOUW

This work was financially supported by The Indonesian Government and CICAT.

Printed by [OPTIMA] Grafische Communicatie, Rotterdam

ISBN: 90-6734-018-9

Dedicated to my wife Tripancani
and to my sons Esa and Gema

Contents

CHAPTER 1

Turbulent convective flows

1.1 Introduction

Computational Fluid Dynamics (CFD) modellers and experimentalists should be grateful to CNN for promoting their field of interest: *turbulence*. Although the TV channel talks about it in the sense of *turbulent time*, the term turbulence is acknowledged as an important aspect of life. From the CNN point of view turbulence means "*hurry, chaotic, difficult to predict*". It is so often that in everyday life an intuitive understanding of turbulence is adopted in different sense. Not surprising if what "other part of the world" understands about turbulence is somewhat similar to what is understood by scientists and engineers. The above mentioned *"turbulent time"* is one of many examples.

According to Oxford dictionary, "*hurry*" is a kind of eagerness to get a thing done quickly, or great urgency of movement. From physical view point *hurry* might be related to irregular or something that can be associated with hurricane. *Chaotic* is the most common feature of turbulence which is associated with disorderly. The third of the characteristic properties, *difficult to predict*: it is the most distinguished behavior of turbulence. It is well known among the CFD community that turbulence is a phenomenon with several characteristics, that are very difficult to predict. Many scientists and engineers have dedicated their life to develop a theory for turbulence. Although large progress has been made, more research is still needed. Not to be pessimistic, the necessity of having a universal turbulence model is like a pursue of a universality in heavenly diversity. It is therefore not surprising that Rotta [94] expressed his opinion about a turbulence model: *"A really universal turbulence model is a dream and will be a dream possibly forever"*. A similar remark, which is attributed to either Sommerfeld, Einstein, and Feynman, says: "*Turbulence is the last great unsolved problem of classical physics*". To some extent in view of an optimist, this can in part be disputed by the fact that great improvements have been achieved in the last few years by both experimental and computational research, thanks to the developments in supercomputers and new experimental techniques.

Convection is a mode of heat transport associated with the flow of fluids. The word convection has its roots in the Latin verbs *"convecto-are"* and *"convehovehere"*, which mean to bring together or to carry from one place to another, Bejan [2]. It is often referred to as free or natural convection when it is caused by density difference in gravitational field. The natural term emphasises that the convection occurs due to neither an imposing flow nor an external intervention.

Temperature difference in a cavity causes a difference in the density of fluid particles, i.e fluid with higher temperature would be less dense while cold fluid would be more dense. Due to the gravitational force, dense particles move downward and light particles move upward. This process happens over and over again, and that is how the natural convection in a cavity occurs.

If the ratio between the convective (inertial) force and the viscous force is low, the flow is considered to be laminar. On the other hand when the ratio is sufficiently high the process becomes turbulent. An example of natural convection in our daily life, especially in a four season country, is a heating system of a house. Moreover, natural convection also occurs in the atmosphere, for instance motion of hot air from subtropical region to the neighboring areas, motion of air (wind) from sea to land and vice versa. Apart from the temperature difference, the density difference can also be caused by concentration difference between chemical species. Example is motion in sea due to salinity difference of the sea water.

When flow is driven by an imposed external force -usually a pressure difference and the presence of buoyancy is negligible, it is regarded as forced convection. When the imposed force and buoyancy are comparable, the flow is referred to as mixed convection. Example is a convection in rooms due to heating or during summer time, where for comfort reason, windows are opened allowing external air to enter or a cold air is injected into a room through vents. Other example is an air conditioning system that supplies cold air jet in providing thermal comfort.

1.2 Computational Fluid Dynamics

1.2.1 Why CFD

It is difficult to imagine what wold be our present knowledge of turbulence without computational fluid dynamics, by which turbulence is studied with the aid of computer hardware and software. Though the Navier-Stokes equations that govern the fluid flow have been known since the nineteenth century, turbulence theory advanced very slowly until the significant computer resources became available. The slow development was not only due to the limiting accuracy of experimental apparatus, but also due to the fact that many turbulent flows are too expensive or even impossible to access by the existing experimental techniques. When experimental problems exist, CFD is an alternative to investigating turbulence. While it is true that CFD will never replace the role of experimental study, it reduces some part of expensive work and possibly gives an insight and guidelines to experimentalists to a better and more effective design of their work. Recent development in advanced techniques, such as supercomputers for CFD and laser-based as optical measuring technique in experiment, has improved the way turbulence is studied. This parallel development is likely to accelerate better understanding

of turbulence.

The seemingly rapid development of computational study as compared to experiment can be attributed to several reasons. First, the availability of computers has attracted many researcher to employ this resource in turbulence modelling. Second, in the computational approach there is a huge flexibility in modifying geometry and boundary conditions. Moreover, measuring equipment with high precision is not only expensive, but also often cannot be used in certain flows. Another reason is the difficulty to modify the experimental set up, for example to change Rayleigh number, since such a modification requires great effort.

Experimental data are practically always used for validation of computational studies. The reason lies not only because they are result of direct measurement, but also due to "psychological" real life reflection of the experiment. However, experiments hardly ever provide all information we would like to have, and it is therefore reasonable to give more research attention to CFD.

1.2.2 Why RANS

There are three different approaches by which computational fluid dynamics is conducted: Direct numerical simulation (DNS), Large eddy simulation (LES), and Reynolds averaged Navier-Stokes equation (RANS). Each approach introduces some advantages and disadvantages over the other and therefore it is difficult to judge which one is the most appropriate approach in computing turbulent flows. Instead, one approach is more suitable in one case while the other is more appropriate in other conditions.

Properties of a turbulent fluid flow, such as velocity, pressure, and temperature and their variation in space and time, can be captured by numerically solving the Navier-Stokes equations. The calculation of the instantaneous turbulent variables can only be done by direct numerical simulation (DNS). Since such a calculation uses no approximation, the results are assumed to represent the real feature of turbulence which can be used for validation research of both the modelling and experimental work. In fact, DNS can calculate the complete turbulent budget that often can not be accessed by experiment, and therefore new ideas and theory can be evaluated.

However, despite advances in computer technology and in simulation methods, it is still not feasible to perform DNS for turbulent flows occurring in most engineering applications. This is due to the fact that all turbulence scales, which range from large scale of the size of the flow geometry to the smallest scale, must be resolved in the numerical grid with the high order of computational accuracy. As the smallest scale that must be resolved is in the size of $O(\eta)$, where $\eta = (\nu^3/\varepsilon)^{1/4}$ is the Kolmogorov scale, such a simulation needs a very fine mesh. As an illustration of how fine the mesh should be to resolve the smallest scales by different differencing schemes, we quote here some requirements for mesh spacing.

A second order central differencing scheme requires mesh spacing 0.26η, fourth order of central differencing scheme needs 0.95η, while Fourier spectral scheme requires mesh spacing about 1.5η. One can say that the lower the order of the differencing scheme, the smaller the mesh spacing. In other words, lower order schemes need greater resolution. In addition, the number of grid points of the computation domain depends on Reynolds number. The number of required grid points N_g is proportional to $Re^{9/4}$, and the number of numerical operations N_{op} is proportional to $Re^{11/4}$. According to observation on the computer development, the speed of computer becomes twice faster in every one and half year, known as Moore's law. If this trend continues to hold true, it will be possible to perform DNS of flows for ten times higher Re number within the next 15 years. It is therefore wise not to expect a giant leap in DNS in the near future. Therefore, DNS will remain available for only relatively low Reynolds numbers and simple geometries. Yet, DNS data can serve as a basis for model and experiment validation.

In order to overcome the drawback of DNS, other approach that offers attractive solution is Large Eddy Simulation. LES resolves only large scales as the major target of calculation, while the small scale or subgrid-scale motion is modelled. The main argument behind LES is that most transport of momentum or energy are carried out by large eddies, while the small eddies do not contribute to the transport process significantly. Hence, LES requires relatively coarser mesh spacing and thus needs less computer resources. It is a fact that important heat transfer process in turbulent natural convection mostly occurs at near-wall region. Unfortunately, the size of the large scale eddies in the near wall regions of a turbulent flow is as small as the size of small scale ones. And inevitably, simulation of turbulent natural convection must put high attention on the treatment in this regions, including how to create proper mesh. As a result, LES also employs large number of grid points which is still expensive for most industrial applications.

Turbulence models based on Reynolds Averaged Navier-Stokes Equation have been widely used by most industrial community and university researchers. The reasons are primarily for the practicality and computer resources availability. Foe most engineering problems, calculations using RANS model are considered to be sufficient, while the availability of computers at the recent days is adequate for the RANS based models. It is well known that turbulence quantities calculated using models based on RANS approach are only approximation of the real turbulence. This is due to the fact that RANS relies on the statistical averaging rather than treating instantaneous properties of turbulence fluid flows. With the statistical approach, one can approximate the turbulence in simpler way and solve flow problem with much less effort. Since most engineers need only the mean field properties, the RANS approach has been well accepted by industry.

1.2.3 Turbulence model

Turbulence modelling has received a lot of research attention by industrial communities and universities in the past years. Some CFD users, for the sake of practicality, have been satisfied with the available models, while others, especially ones who really put lot attention on the quality of model performance, have looked for better models. In spite of successful application of existing models, in many situations some shortcomings and deficiencies still exist. Despite considerable progress in modelling the turbulence, more research attention should be directed towards developing more fundamental formulation so that the general behavior of turbulence can be better reproduced. A robust and sufficiently accurate prediction is the main challenge for turbulence models.

Turbulence modelling has its roots in the Reynolds averaging which introduces new unknown quantities. These are called Reynolds stresses and turbulent heat flux and this quantities make the Navier-Stokes equations no longer a closed system. In order to calculate the Reynolds stress and turbulent heat flux, a model should be developed. The turbulent viscosity hypothesis that relates the Reynolds stress to the velocity gradients is the first known turbulence model. This proposal was relatively successful for very simple flows, but its applicability is very limited. Improvement is proposed by introducing two equation models, such as $k - \varepsilon$ model, in which the model transport equations are solved for two turbulent quantities, namely turbulent kinetic energy k and its dissipation rate ε. Here, the turbulent viscosity is independent to any a priori prescription in form of bulk flow parameters. As a result, the range of applicability is much wider. In addition, the $k - \varepsilon$ model is relatively simple, and has been tested in many engineering applications. However, the model has revealed a number of shortcomings and deficiencies. Those are poor performances whenever the stress transport is important, insensitivity to the orientation of turbulence structure and anisotropy of normal stress, inability to account for extra-strain and so on. In order to overcome the limitation of the model, higher level of modelling approach is proposed. The task is conducted by introducing further differential equations that describes the relation between the Reynolds stress and the turbulent heat flux and the mean quantities. This approach is known as the second moment closure model, which is considered as the highest model level in RANS approach.

A turbulence model is considered to be a good model if it possess features: generality, physical meaning, simple, and suitable for incorporation into numerical code. Generality refers to the applicability of the model to any turbulent flows in addition to basic flows, in which the model was calibrated. The model must also work for a wide range of turbulence levels, from very weak to strong turbulent flows. In addition, the model should be based on physical conception of turbulence structure expressed by the mathematical formulation. The model must be as simple as possible but without leaving out any important factors, and should be suitable for incorporation into a numerical code. Ideally, any turbu-

lent model should be robust to available solution method and mesh. However this requirement is hard to fulfill by the existing turbulence models. The reason is that turbulence takes place almost everywhere ranging from simple to very complex geometries, and with various levels from very low to very high turbulence intensities. Indeed, it is not expected that one simple model can perfectly compute any turbulent flow. Alternatively, a moderately sophisticated turbulent model that can be applied in any kind of flows with considerable performance is demanded. Of course, that kind of model will not fit perfectly in every case. However reasonable results must be predicted. Therefore a trade off between model's complexity, robustness, application and accurateness is unavoidable, the priority is given to aspects that are most important in the case considered.

1.3 Objective of the study

The aim of this study is to expand and improve a turbulence model for flows driven or affected by thermal buoyancy, which would be applicable to a range of problems encountered in engineering and nature. At the early step, a new second moment closure turbulence model is developed based on the work of Hanjalić and Jakirlić [43] for Reynolds stress model and the work of Dol *et al.* [26] for scalar flux model. In this study, attention is given to the buoyancy effects. The buoyancy is introduced in the Reynolds stress equation and in pressure strain correlation. Moreover, a reduction in the complexity level of previous model is also the aim of the study. The first objective is to simplify the turbulent heat flux model of Dol *et al.* [26]. The main purpose of this modification is to reduce the complicated model of the pressure scrambling into moderate model by cutting out insignificant terms, and optimising the important terms in order to maintain the performance of the model. The model is then applied to one of the generic flow cases, namely natural convection in a vertical channel heated from the side. For completion, algebraic calculation based on the second moment closure model is also studied and comparison is made with the full differential model.

Despite its success, it is recognised that the second moment closure model is indeed more complicated than the standard $k-\varepsilon$ model. Since most industries have been using the $k-\varepsilon$ model, and are still reluctant to employ the second moment closure model, it is for practical reasons that this study to focus on enhancement of the $k-\varepsilon$ model with an elliptic relaxation equation. The model is first introduced by Durbin [28] known as $k-\varepsilon-\overline{v^2}-f$ model. In this approach, the Reynolds stress is calculated using the modified Eddy Viscosity Model in terms of $\overline{v^2}$, k and ε, while heat flux is calculated by Algebraic Flux Model. The effect of buoyancy on the Reynolds stress is accounted by buoyancy terms in the extended EVM.

The proposed model ($k-\varepsilon-\overline{v^2}-f-\overline{\theta^2}$) is tested in several types of flows ranging from simple infinite vertical and horizontal channel to real life free and mixed

convection. The application of the model covers a range of Rayleigh numbers, from $Ra = 5 \times 10^6$ for vertical channel to $Ra = 5 \times 10^{10}$ for three-dimensional enclosure. For validation purposes, experimental data are used to test the model performance. In addition, comparison is also made with direct numerical simulation data which are available in the literature and are relevant to this study. In order to demonstrate its wide range of application, the model was applied to turbulent mixed convection, which is relevant to many practical engineering problems. Two different mixed convection cases have been studied:

(i) Mixed convection in an two-dimensional enclosure with supply and exhaust in stable thermal stratification; the case is matched to the experimental study of Blay *et al.* [4] and numerical study of Murakami *et al.* [79], and

(ii) Indoor-climate mixed convection under summer cooling condition.

1.4 Outline of the thesis

This book consists of seven chapters: Introduction, Literature review, Survey of relevant models for turbulent buoyant flow, Advancement and improvement of models, Application of the model for turbulent natural convection and Application of the model in mixed convection under summer cooling condition.

After some introductory material in Chapter 1, Chapter 2 presents a review of the phenomena of turbulent natural and mixed convection, and of turbulent closures with reference to previous related studies. The focus is given on the review of development in turbulence modelling, followed by discussion of advantage and disadvantage of different approaches.

Mathematical description of turbulent flows is discussed in Chapter 3. The first part summarises the governing equations and Reynolds averaging technique used. A brief discussion of transport equations for turbulent kinetic energy and dissipation rate is also given, followed by a review on several versions of eddy viscosity and diffusivity models. A close look at turbulence modelling is given by discussing the transport equation for the Reynolds stress. Attention is also paid to transport equation for turbulent heat flux, temperature variance, and dissipation of temperature variance. In addition, algebraic models are also shortly reviewed. Here the budget of Reynolds stress and turbulent heat flux are discussed.

Chapter 4 presents the proposed second moment closure and algebraic $k - \varepsilon - \overline{v^2} - f - \overline{\theta^2}$ models. In the mechanical part of the second moment closure model, attention is paid to the enhancement of the pressure-strain correlation and in the dissipation rate equations. In the thermal part of the second moment closure model, the focus is given on the pressure scrambling term, which is one of the main targets of the modification. To close the chapter, a comprehensive discussion of the proposed $k - \varepsilon - \overline{v^2} - f - \overline{\theta^2}$ model is given.

Chapter 5 reviews the computational method used. A short discussion is given on control volume methods, collocated grid arrangements, differencing schemes, and discretisation procedures. In the last part of this chapter, application of the numerical method in unsteady state laminar natural convection is presented in order to test the accuracy of the method.

Applications of the second moment closure to turbulent natural convection in vertical channel is given in Chapter 6. In order to validate the turbulence model, comparison is made with DNS data and previous second moment closure model. The focus is then given on the application of the $k - \varepsilon - \overline{v^2} - f - \overline{\theta^2}$ model in turbulent natural convection heated from side and heated from below. In the case of heating from the side, several flow cases are presented: vertical channel, 2-D enclosures of different aspect ratios, followed by comparisons with several experimental data. Moreover, application of the proposed model in turbulent natural convection in a cubical enclosure is presented and comparison is made with experimental study of Opstelten [85]. The last part of this chapter reviews the application of the model in turbulent natural convection heated from below.

Chapter 7 provides a discussion of turbulence mixed convection. Here two different cases are presented: 2-D mixed convection in stably stratified fields, and 3-D mixed convection under summer cooling condition. The latter case is the real application of numerical simulation in practical engineering design, where ventilation system in summer time or air conditioning system are the major means for providing the thermal comfort for human.

CHAPTER 2

Literature Review

2.1 Overview

In the last few decades, there have been a large number of studies of natural and mixed convection. Numerical studies on the subject have attracted much research attention following rapid increase in the computer power. This is also motivated by the fact that natural and mixed convection have important technological applications. Some of the applications are thermal insulation of buildings using double glass air gaps, heating and cooling system in rooms, nuclear reactor systems, electronics compartment system, solar energy collectors, indoor-climate optimisation, smoke dispersion and others.

This chapter presents a literature review on recent computational and experimental studies of natural and mixed convection in enclosures. The focus is given on several studies of turbulence closure that are closely related to the current work. This includes studies of modelling of transport terms, pressure correlation processes, and the near wall treatment in $k-\varepsilon$, algebraic and differential second moment closure models.

2.2 Convective flows in enclosures

There have been a number of reports on experimental and numerical studies of laminar natural convection in two and three dimensional enclosures, which were aimed at serving as benchmark cases. Examples are numerical studies of de Vahl Davis [22], Lankhorst and Hoogendoorn [51], and Leong *et al.* [72]. An important trend has been the steady increase in level of the Rayleigh number considered. Some studies have taken into account the effect of partitions in the cavities, see Nansteel and Greef [80]. In addition, attention has been given to heat transfer modification due to change of inclination between the imposed heat flux and the gravitational orientation, Hamady *et al.* [40] for two-dimensional enclosure and Kenjereš [60] for three-dimensional enclosure.

Leong *et al.* [72] performed an experimental study on a physically realizable benchmark problem in internal natural convection. He argued that, despite the interest as a benchmark problem, the adiabatic boundary conditions are considered physically not realisable. In that study, the natural convection in a cube was set up with two opposing isothermal walls and the remaining walls having a linear temperature variation from the cold wall to the hot wall. The argument

was supported by the study of Le Quere [69] who conducted a study of the square thermally driven cavity at high Rayleigh number. Leong *et al.* [72] and Le Quere [69] concluded that benchmark problems should be physically realisable.

A significant research attention has been given to convection resulting from thermal buoyancy, while convection due to purely concentration buoyancy have received less attention. Similarly, a lot attention is given to situation where combined buoyancy effect due to temperature and concentration gradients exist. Van der Eyden *et al.* [100] reported results of numerical and experimental study of turbulent double-diffusive natural convection of a mixture of two gases in a trapezoidal enclosure with imposed thermal stratification. The turbulent fluxes of momentum, heat and mass were modelled by standard and low-Re-number $k - \varepsilon$ eddy diffusivity model with inclusion of thermal and mass buoyancy. It was shown that the computed mean velocity, temperature, and concentration agreed quite well with the measurement. Numerical study of the dynamics of the temperature and concentration fields in simulated salt-gradient solar ponds was reported by Hanjalić and Musemić [47]. The method of simulation employs a two-equation model of turbulence with variable turbulent Prandtl-Schmidt numbers, modified to account for thermal and mass buoyancy. Good agreement between the computed results with several sets of experimental data is obtained. Study of computational modelling of double diffusive flows in stratified media is conducted by Armitage [1]. Here, two-layer modelling strategy was applied to a one-dimensional double diffusive flow. The calculation for the near wall region is conducted by using a buoyancy extended low-Reynolds number model that has been interfaced to the high-Reynolds number second moment closure model for flow in the core of the enclosure.

During the past three decades experimental studies of natural convection in enclosures heated from sides have been reported by a number of authors. Cheesewright *et al.* [9] presented data on heat transfer, velocity, and velocity fluctuation for turbulent vertical boundary layers of a large air-filled cavity ($5:1$ aspect ratio) at sufficiently high Rayleigh number ($Ra = 5 \times 10^8$). Olson *et al.* [84] performed experiments on three-dimensional natural convection in empty and partitioned enclosures. Their experiments indicated that at Rayleigh number up to 3×10^{10} the boundary layers are still laminar. Opstelten *et al.* [86] presented experimental data of velocity and velocity fluctuations for turbulent boundary layers. They have shown with flow visualisation, that the resulting experimental boundary conditions obtained with optimal insulation at horizontal walls show different flow structures when compared to numerically predicted adiabatic case.

Convective transport under the combined influence of buoyancy force and external imposed flow, known as mixed convection, occur in many practical applications, and hence this type of flow has also received a lot of research attention. Neiswanger *et al.* [82] conducted experimental study of high Rayleigh number mixed convection in a rectangular enclosure. The experiment was performed in a small-scale test section with uniformly heated vertical side walls and adiabatic

remaining walls using water as the test fluid. Kasagi and Nishimura [59] performed a study of direct numerical simulation of combined forced and natural turbulent convection in a vertical plane channel. The Reynolds number based on the channel half-width and friction velocity was 150, while the Grashof number based on the channel width and the wall temperature difference was varied up to 1.6×10^6. It was shown that the buoyancy force has a substantial effect on the near wall force balance, which governs the distribution of shear stress. Numerical study of laminar mixed convection in a horizontal square channel with heated side walls, at Reynolds number $Re = 500$, and the Grashof number varied around $Gr = 10^5$, was conducted by Sillekens *et al.* [97]. The computed velocity was validated with result of particle-tracking experiments, while that of temperature was compared to liquid crystal measurements. It is shown that the numerical results agree quite well with the experimental data.

2.3 Turbulence closure studies

There have been many numerical studies relating to turbulence models, and more recently a very advanced second moment closure models have been developed. It is well recognised that the turbulence closure problem is very challenging, and therefore a lot of efforts have been devoted to development and evaluations of turbulence models. Generally, such models give a global overview of behaviour of turbulence flows in a wide range of situation and practical application. Impressive progress has been made, but until now it is very difficult to find a model that is both accurate, sufficiently general and robust.

One of the earliest works dealing with turbulence closure was that by Rotta [94], who suggested that transport equation of Reynolds stress could be derived in an exact form but contains terms that must be modelled to close the system. Specifically, the work was about modelling the pressure strain correlation. Monin [78] reported a model for pressure temperature gradient correlation that appears in heat flux transport equation. Extension of those models was made by Gibson and Launder [37] by introducing effects due to buoyancy in both pressure correlation processes. Rodi[91] proposed an interesting and useful algebraic simplification to Reynolds stress model. The primary purpose of this simplification was to reduce the computational complexity of solving the differential transport equation for the Reynolds stress tensor. In the algebraic model the pressure strain correlation is still retained, with an assumption that the total (convective plus diffusive) transport of the Reynolds stress is proportional to the convection and diffusion of the turbulent kinetic energy. Similar approach was made to reduce the transport equation for heat flux into algebraic flux model, Gibson and Launder [37]. Although the model exhibited some limitations, especially when convective and diffusive transports are very important, it appeared to be relatively acceptable for several flows types.

Unlike the standard $k-\varepsilon$ model which is relatively simple to solve, Reynolds stress models contain large number of partial differential equations and coefficients, by which several effects such as buoyancy and anisotropy are taken into account without ad hoc treatment. With that, Reynolds stress models can overcome some of deficiencies that appear in simpler models. In recent years, many Reynolds stress and heat flux models modifications have been proposed and a number of computational studies have been carried out. Lumley [76] recommended the direction in which in order to obtain accurate prediction, modellers should focus on extending linear pressure strain models by including higher order terms. Following the works of Shih and Lumley [96] and Fu [36], Craft [18] extended models to derive pressure-strain and pressure-temperature gradient correlations which contain cubic order terms. With this model, the need for empirical wall reflection terms which are normally added in order to account for the incorrect behaviour of pressure correlations terms near a wall is avoided. It was shown that by including buoyancy and higher order terms in the pressure correlations, satisfactory prediction of turbulent fields in several flows including separating and impinging flows are obtained.

Peeters and Henkes [89] performed a numerical study on turbulent natural convection boundary layer along a heated vertical plate, using both full differential stress and algebraic models. Several model functions are modified in order to obtain better prediction in the near wall region. The pressure strain is modelled using the return to isotropy assumption of Rotta [94], while the diffusion term is calculated through generalised gradient diffusion model of Daly and Harlow [21]. In order to accurately capture the near-wall turbulence fields, wall correction term of Gibson and Launder [38] was used. This study showed that some RSM constants are very influential for overall predictions, while others are important only in thermal field. This analysis of the RSM coefficients is very important since it gave the overall view about the behaviour of terms in the second moment closure model of natural convection boundary layer along a vertical plate. They reported that Reynolds stress model is superior to the algebraic model, as local equilibrium assumption is not always valid. Craft *et al.* [19] used a cubic eddy viscosity model of turbulence in order to improve performance of linear and quadratic stress strain correlation model. Despite its complexity, the model has shown consistently better than the lower order model over a range of flows, from simple shear at high strain rates and pipe flow, to flows involving strong streamline curvature and stagnation. Because of very specific features of the near-wall turbulence in buoyancy driven flows, several authors focused on modifying the model for near wall behaviour. An example is the model of Hanjalić and Jakirlić [44]. In principle, this model is a modification of high-Re number model, to account for the vanishing near wall Reynolds number, wall blocking effects, strong inhomogeneity and large stress anisotropy. The obvious extension of the high-Re number model to low-Re model is the idea of using the model function in terms of stress invariants and turbulence Reynolds number to capture near wall be-

haviour. The wall effect is accounted for through coefficients, expressed in terms of anisotropy invariants for the stress and dissipation rate. The model is applied to many flows and produced a significant improvement in predicting turbulence fields, particularly in the near wall region. In the later version Jakirlić and Hanjalić citeJakirlic02, the model is modified by using homogeneous dissipation rate , which is free from any wall configuration parameters. This new approach has been applied to flows in a pipe, plane channel, constant pressure boundary layer, behind a backward facing step and in an axially rotating pipe, all showing good near wall behaviour.

Dol [27] conducted numerical study on turbulent natural convection in differentially heated tall cavity for a range of Rayleigh numbers. He adopted the model of Hanjalić and Jakirlić [44] for pressure strain correlation and dissipation rate, while the model of the thermal part for the pressure scrambling based on the model of Craft [17]. For validation purpose, Dol [27] used Direct numerical simulation of Nieuwstadt and Versteegh [83]. With the availability of term by term DNS budget, the task is quite successful. It is worth to mention that the important aspect of his model is in proper prediction of coefficients based on term by term modelling of the pressure scrambling term.

While the second moment closure has demonstrated its superiority over simpler models, it has often suffered from numerical difficulties that hinders its wider application to industrial flow computations. The difficulties are mainly caused by loose coupling of the mean velocity and turbulent stress field. For more detail, a comprehensive review about higher turbulence closure and numerical implication can be found in Hanjalić [42]. In order to expand the use of turbulence model to research communities and industry, a moderate complexity of turbulence model is desired. An example is the work of Kenjereš [62] who used low-Re number $k-\varepsilon$ and AFM model in turbulent natural convection. In the three-equation model, turbulent kinetic energy k, its dissipation rate ε, and temperature variance $\overline{\theta^2}$ are solved, while in the four-equation model one additional transport equation is solved for the dissipation rate of the temperature variance ε_θ. In the former case, ε_θ is calculated using algebraic relation for the ratio of thermal to mechanical time scales, which is assumed to be constant. The model is applied to flows with different geometries ranging from generic flows in enclosure, in annuli, in real three dimensional configurations, and in flows under the influence of magnetic field.

Finally, Durbin [28] proposed an elliptical relaxation method in the framework of the eddy viscosity hypothesis. This approach is aimed to account for near wall behaviour. Wall treatment in a low-Reynolds number model is usually provided by introducing damping functions. Such dumping functions are derived on ad hoc basis and are often unsatisfactory. Because such a treatment is often conducted with the use of parameters dependence on wall distance, their generality is limited. It is obvious that any model possessing wall distance dependency is less preferable, because it is difficult to be used in complex flows and hence

it is not suitable for industrial applications. In this approach, computation is conducted by solving k and ε with one additional transport equation for the new velocity scale $\overline{v^2}$, and an elliptic equation for the relaxation function and therefore known as $k - \varepsilon - \overline{v^2} - f$ model. The equation for $\overline{v^2}$ can be derived from the transport equation for the wall normal Reynolds stress component and it can be used to account for anisotropy of the flow in the near wall region. The elliptic relaxation approach allows an integration of equations up to the wall and hence the eddy viscosity is correctly damped without using damping function.

CHAPTER 3

A Survey of Relevant Models of Turbulent Buoyant Flows

3.1 Introduction

This chapter presents a review of fundamental principles and mathematics that have served as a basis for studying of the turbulent convective flows driven or affected by thermal buoyancy. The beginning of the chapter reviews the general partial differential equations of conservation of mass, momentum and energy that govern the fluid flows and their averaging. This is followed by the discussion of the basic turbulence models of different levels, starting from the eddy-viscosity type to Reynolds stress models, followed by the outline of the equations for turbulent kinetic energy, and its dissipation rate. In addition, a brief review of the problem of closing the equations, known as turbulence closure, is presented. Next, we discuss the problem of modelling the transport equation for heat flux and for the temperature variance. This chapter also presents the truncation approach to the transport equations for Reynolds stress and turbulent heat flux which leads to algebraic stress/flux model. In the context of algebraic models, the weak equilibrium hypothesis is discussed. The details of the proposed model are presented in Chapter 4.

3.2 Governing Equation and Review of Models

Turbulent fluid flow and heat transfer are fully defined by the equations for conservation for mass, momentum, and energy for the instantaneous motion. The conservation of mass equation, which is commonly referred to as the continuity equation, is:

$$\frac{\partial \hat{\rho}}{\partial t} + \frac{\partial \hat{\rho}\hat{U}_i}{\partial x_i} = 0 \tag{3.1}$$

where ρ is the density, U_i is velocity vector and " ˆ " denotes instantaneous values. Momentum equation reads:

$$\frac{\partial \hat{\rho}\hat{U}_i}{\partial t} + \hat{U}_j \frac{\partial \hat{\rho}\hat{U}_i}{\partial x_j} = \hat{F}_i - \frac{\partial \hat{P}}{\partial x_i} + \frac{\partial}{\partial x_j}\left[\mu\left(\frac{\partial \hat{U}_i}{\partial x_j} + \frac{\partial \hat{U}_j}{\partial x_i}\right)\right] \tag{3.2}$$

where μ is fluid viscosity and $\hat{F}_i$ is the body force acting on the fluid. The general momentum balance of equation (3.2) describes the motion of fluid driven by body force $\hat{F}_i$, pressure gradient and the strain tensor gradient. The equation for energy conservation is derived from the first law of thermodynamics, and in the absence of internal heat source it can be written as:

$$\frac{\partial \hat{\rho}\hat{T}}{\partial t} + \hat{U}_j \frac{\partial \hat{\rho}\hat{T}}{\partial x_j} = \frac{\partial}{\partial x_j}\left(\frac{\mu}{Pr}\frac{\partial \hat{T}}{\partial x_j}\right) \tag{3.3}$$

In equation (3.3) the left hand side represents time-dependent and convective terms, and on the right hand side is the rate of heat diffusion term.

3.2.1 The Reynolds-averaged Navier Stokes Equation

Introducing the Reynolds averaging and Boussinesq hypothesis for the buoyancy force, equation (3.1)-(3.3) can be written as:

$$\frac{\partial \rho}{\partial t} + \frac{\partial \rho U_j}{\partial x_j} = 0 \tag{3.4}$$

$$\frac{\partial \rho U_i}{\partial t} + U_j \frac{\partial \rho U_i}{\partial x_j} = -\frac{\partial P}{\partial x_i} + \frac{\partial}{\partial x_j}\left[\mu\left(\frac{\partial U_i}{\partial x_j} + \frac{\partial U_j}{\partial x_i}\right) - \rho\overline{u_i u_j}\right] - \rho g_i \beta (T - T_{ref}) \tag{3.5}$$

$$\frac{\partial \rho T}{\partial t} + U_j \frac{\partial \rho T}{\partial x_j} = \frac{\partial}{\partial x_j}\left(\frac{\mu}{Pr}\frac{\partial T}{\partial x_j} - \rho\overline{\theta u_j}\right) \tag{3.6}$$

The averaged equations, known also as the Reynolds Averaged Navier Stokes (RANS) have the same form as the instantaneous equations (3.2)-(3.3), with the exception of the new unknown quantities, the second-moments $\overline{u_i u_j}$, and $\overline{\theta u_i}$, the former being the Reynolds stress tensor and the latter the turbulent heat flux vector.

3.2.2 Eddy viscosity models

In order to close the averaged equation, the unknown variables $\overline{u_i u_j}$ and $\overline{\theta u_i}$ have to be provided. The auxiliary algebraic or differential equation set that provides these quantities are commonly known as a turbulence model. The level of turbulence modelling ranges from very simple to very sophisticated ones. The simplest approach is based on eddy viscosity/diffusivity concept, where the Reynolds stress and heat flux are expressed in terms of averaged ("mean") velocity and temperature gradient, respectively, i.e.:

$$\overline{u_i u_j} = \frac{2}{3}k\delta_{ij} - \nu_t\left(\frac{\partial U_i}{\partial x_j} + \frac{\partial U_j}{\partial x_i}\right) \tag{3.7}$$

$$\overline{\theta u_i} = \frac{\nu_t}{\sigma_t}\frac{\partial T}{\partial x_i} \tag{3.8}$$

where σ_t denotes the turbulent Prandtl number. The eddy viscosity is a turbulence parameter and should be defined in term of turbulence quantities. On dimensional ground, the eddy viscosity can be defined as:

$$\nu_t \propto VL \tag{3.9}$$

where V and L are the turbulence velocity and length scale, respectively. By specifying suitable values of the velocity and the length scale, the system is closed. There have been numerous ways to model the eddy viscosity. The closure level of the eddy viscosity model is related to the manner in which the velocity and length scales are defined. It is common to relate the eddy viscosity with measurable quantities that can be interpreted physically. The square root of the turbulent kinetic energy has been used as the velocity scale, i.e.

$$\nu_t = C_\mu L k^{1/2} \tag{3.10}$$

This leads to the requirement for solving the transport equation for the turbulent kinetic energy k. The definition of the length scale is less obvious. The most common approach is to use the length scale of the energy containing eddies unaffected by fluid viscosity (high Reynolds number assumption), which can be defined on pure similarity arguments and dimensional analysis in term of turbulent kinetic energy and its dissipation rate $L \propto k^{3/2}/\varepsilon$. In this case the eddy viscosity is defined as:

$$\nu_t = C_\mu \frac{k^2}{\varepsilon} \tag{3.11}$$

where the coefficient C_μ equals to 0.09. This value of C_μ arises from the assumption of turbulence energy equilibrium. For low-Reynolds number and near wall flows when the integration is conducted up to the wall, the high-Reynolds number approach needs to be modified. The conventional modification involves one or more damping functions. For the eddy viscosity models usually a function f_μ expressed in terms of turbulent Reynolds number is added to equation (3.11), Jones and Launder [57]. Despite its relatively simple formulation, the model works quite well for most near-equilibrium flows. Unfortunately, in most real flows of practical relevance, eddy viscosity is usually anisotropic.

3.2.3 Turbulent kinetic energy and dissipation-rate equations

The exact transport equation for the turbulent kinetic energy k=0.5 $\overline{u_i u_i}$ reads:

$$\underbrace{\frac{Dk}{Dt}}_{L_k} = \underbrace{\frac{\partial k}{\partial t}}_{L_k} + \underbrace{U_k \frac{\partial k}{\partial x_k}}_{C_k} = \underbrace{\frac{\partial}{\partial x_k}\left(\underbrace{\boxed{-\overline{u_k k}}}_{\mathcal{D}_k^t} - \underbrace{\boxed{\frac{1}{\rho}\overline{u_k p}}}_{\mathcal{D}_k^p} + \underbrace{\nu \frac{\partial k}{\partial x_k}}_{\mathcal{D}_k^\nu} \right)}_{\mathcal{D}_k} - \underbrace{\overline{u_i u_k}\frac{\partial U_i}{\partial x_k}}_{P} - \underbrace{\beta g_i \overline{\theta u_i}}_{G} - \underbrace{\boxed{\nu \overline{\left(\frac{\partial u_i}{\partial x_k}\right)^2}}}_{\varepsilon} \tag{3.12}$$

where terms in boxes: turbulent diffusion, pressure diffusion, and dissipation rate need to be modelled, while the remaining terms can be treated in their exact form.

The pressure diffusion is usually modelled together with the turbulent velocity diffusion using a simple gradient diffusion hypothesis:

$$\mathcal{D}_k^t = \frac{\partial}{\partial x_k}\left(\frac{\nu_t}{\sigma_k} \frac{\partial k}{\partial x_k} \right) \tag{3.13}$$

This leads to the final form of the model transport equation for the turbulent kinetic energy:

$$\frac{\partial k}{\partial t} + U_k \frac{\partial k}{\partial x_k} = (P + G) - \varepsilon + \frac{\partial}{\partial x_k}\left[\left(\nu + \frac{\nu_t}{\sigma_k} \right) \frac{\partial k}{\partial x_k} \right] \tag{3.14}$$

The exact transport equation for the dissipation rate of the turbulent kinetic energy can be written as:

$$\underbrace{\frac{D\varepsilon}{Dt}}_{L_\varepsilon} = \underbrace{\frac{\partial \varepsilon}{\partial t}}_{L_\varepsilon} + \underbrace{U_k \frac{\partial \varepsilon}{\partial x_k}}_{C_\varepsilon} = \underbrace{\frac{\partial}{\partial x_k}\left(\underbrace{\boxed{-2\frac{\nu}{\rho}\overline{\frac{\partial p}{\partial x_l}\frac{\partial u_k}{\partial x_l}}}}_{\mathcal{D}_\varepsilon^p} - \underbrace{\boxed{\nu u_k \overline{\left(\frac{\partial u_i}{\partial x_l}\right)^2}}}_{\mathcal{D}_\varepsilon^t} + \underbrace{\nu \frac{\partial \varepsilon}{\partial x_k}}_{\mathcal{D}_\varepsilon^\nu} \right)}_{\mathcal{D}_\varepsilon} - \underbrace{\boxed{2\nu \frac{\partial U_i}{\partial x_k}\left(\overline{\frac{\partial u_i}{\partial x_l}\frac{\partial u_k}{\partial x_l}} + \overline{\frac{\partial u_l}{\partial u_i}\frac{\partial u_l}{\partial x_k}} \right)}}_{P_{\varepsilon_1} + P_{\varepsilon_2}} - \underbrace{\boxed{2\nu u_k \overline{\frac{\partial u_i}{\partial x_l}\frac{\partial^2 U_i}{\partial x_k \partial x_l}}}}_{P_{\varepsilon_3}} \tag{3.15}$$

$$\boxed{\underbrace{-2\nu\overline{\frac{\partial u_i}{\partial x_l}\frac{\partial u_k}{\partial x_l}\frac{\partial u_i}{\partial x_k}}}_{P_{\varepsilon_4}}} \boxed{\underbrace{-2\nu\left(\overline{\frac{\partial^2 u_i}{\partial x_k \partial x_l}}\right)^2}_{Y_\varepsilon}} \boxed{\underbrace{-2\beta\nu g_i\overline{\frac{\partial u_i}{\partial x_l}\frac{\partial \theta}{\partial x_l}}}_{G_\varepsilon}} \tag{3.16}$$

where terms in the boxes: turbulent diffusion, pressure diffusion, productions and destruction need to be modelled, while the only term that can be treated in the exact form is the viscous diffusion. For modelling the turbulent diffusion of ε due to velocity fluctuation, the simple gradient diffusion hypothesis of Daly and Harlow [21] is often employed:

$$\mathcal{D}_\varepsilon^t = \frac{\partial}{\partial x_k}\left(\frac{\nu_t}{\sigma_\varepsilon}\frac{\partial \varepsilon}{\partial x_k}\right) \tag{3.17}$$

where σ_ε is the turbulent Prandtl number for ε for which most authors take $\sigma_\varepsilon = 1.3$.

For high Reynolds number flows, the "mixed" production $P_{\varepsilon 1}$ and $P_{\varepsilon 2}$ are negligibly small. The main production of ε is attributed to P_{ε_4}, while the major destruction is Y_ε. It is worth to mention that the difference between P_{ε_4} and Y_ε is roughly balanced with the diffusion transport terms. These two dominant terms are usually modelled together:

$$P_{\varepsilon_4} + Y = \frac{\varepsilon}{k}\left(C_{\varepsilon_1} P_k - f_\varepsilon C_{\varepsilon_2}\varepsilon\right) \tag{3.18}$$

For high Reynolds number model the standard value of f_ε is 1. However for low Reynolds number model Jones and Launder [57] introduced f_ε as a function of turbulent Reynolds number Re_t:

$$f_\varepsilon = 1 - 0.3exp(-Re_t^2) \tag{3.19}$$

The buoyancy term G_ε is modelled in a similar form as its analogous in the transport equation for the turbulent kinetic energy:

$$G_\varepsilon = -C_{\varepsilon 3}\beta g_i \overline{\theta u_i}\frac{\varepsilon}{k} \tag{3.20}$$

The model transport equation for the dissipation rate becomes:

$$\frac{\partial \varepsilon}{\partial t} + U_k\frac{\partial \varepsilon}{\partial x_k} = \left[C_{\varepsilon_1}(P+G) - C_{\varepsilon 2}\varepsilon\right]\frac{\varepsilon}{k} + \frac{\partial}{\partial x_k}\left[\left(\nu + \frac{\nu_t}{\sigma_\varepsilon}\right)\frac{\partial \varepsilon}{\partial x_k}\right] \tag{3.21}$$

where $C_{\varepsilon 1}$ equals to $C_{\varepsilon 3}$.

3.3 Second Moment Closure

The two equation models, and among them the most popular $k-\varepsilon$ model, are the most widely used for research and engineering application. A considerable amount of work has been invested in testing of the $k-\varepsilon$ model and a number of modifications and improvements have been proposed, though with a limited success. In many complex flows the restrictions imposed by equilibrium assumptions inherent in of the $k-\varepsilon$ model reduce its performance. These are the assumption of the isotropic (scalar) turbulent viscosity, and the assumption of the proportionality of the stresses to the rate of mean strain.

The Reynolds stress and turbulent heat flux that appear in momentum equation are the turbulence second moments for which exact differential transport equations can be derived. These equations contain a number of terms that cannot be treated exactly, but need to be modelled in order to close the equations. The closure at this level is known as the second moment closure. Because the second moments are now obtained by solving the model transport equations in differential form, this closure level should provide more accurately prediction of turbulence quantities than when using standard EVM and EDM such as $k-\varepsilon$ model. Several levels of second moment closures have been proposed, (see e.g. Hanjalić [42]) The main difference appears in modelling the term involving the correlation between the fluctuating pressure and velocity or temperature, for which the simplest second moment closure use linear models with constant coefficient in both Reynolds stress and heat flux equations.

3.3.1 Reynolds Stress Equation

For incompressible buoyant flow under the Boussinesq approximation, the partial differential equation for the Reynolds stress tensor reads:

$$\frac{D\overline{u_iu_j}}{Dt} = \underbrace{\frac{\partial \overline{u_iu_j}}{\partial t}}_{L_{ij}} + \underbrace{U_k\frac{\partial \overline{u_iu_j}}{\partial x_k}}_{C_{ij}} =$$

$$\underbrace{\frac{\partial}{\partial x_k}\Bigg(\underbrace{\nu\frac{\partial \overline{u_iu_j}}{\partial x_k}}_{\mathcal{D}^{\nu}_{ij}} - \boxed{\underbrace{\overline{u_iu_ju_k}}_{\mathcal{D}^{t}_{ij}}} - \boxed{\underbrace{\overline{\frac{p}{\rho}\left(u_i\delta_{jk}+u_j\delta_{ik}\right)}}_{\mathcal{D}^{p}_{ij}}}\Bigg)}_{\mathcal{D}_{ij}} \underbrace{-\left(\overline{u_iu_k}\frac{\partial U_j}{\partial x_k} + \overline{u_ju_k}\frac{\partial U_i}{\partial x_k}\right)}_{P_{ij}}$$

$$\underbrace{-\beta(g_j\overline{\theta u_i} + g_i\overline{\theta u_j})}_{G_{ij}} \boxed{\underbrace{\overline{\frac{p}{\rho}\left(\frac{\partial u_i}{\partial x_j}+\frac{\partial u_j}{\partial x_i}\right)}}_{\Phi_{ij}}} - \boxed{\underbrace{2\nu\overline{\frac{\partial u_i}{\partial x_k}\frac{\partial u_j}{\partial x_k}}}_{\varepsilon_{ij}}} \quad (3.22)$$

where L_{ij} is local time rate of change, and C_{ij} is the convection, D^{ν}_{ij} is the viscous diffusion, D^{t}_{ij} is the turbulent diffusion by velocity fluctuations, D^{p}_{ij} is the turbulent diffusion by pressure fluctuations, P_{ij} is the mean strain production, G_{ij} is the buoyant production, Φ_{ij} is the pressure strain correlation, and ε_{ij} is the stress dissipation rate. The terms in boxes need to be modelled.

Reynolds stress budget

In order to properly develop a turbulence model of Reynolds stress, it is useful to study how the budget of the stress is distributed in some generic flows. Ideally, a second moment closure model should reproduce each term in the Reynolds stress and scale providing equation, i.e the model should affect the budget of the stress. Studying the budget discloses the importance of various terms and difficulties in term-by-term modelling. As an illustration, we consider here the stress budget for natural convection between two infinite vertical plates heated from the side, using the DNS data of Versteegh and Nieuwstadt [102]. The budget of the Reynolds stress $\overline{uu}, \overline{vv}$, and $\overline{ww}$ and shear stress $\overline{uv}$ are shown in Figs. (3.1)ab -(3.2)ab. Note that the adopted coordinate system is: x-horizontal, y-vertical and z-spanwise direction. The corresponding velocity arguments are denoted as $u = u_x$, $v = u_y$, and $w = u_z$. It is clear that the shear and buoyancy productions appear in the Reynolds stress budget of the vertical stress $\overline{vv}$. The former is a consequence of the velocity gradient, while the latter is caused by the vertical heat flux. It is worth mentioning that the production term for the Reynolds stress $\overline{vv}$ budget has a negative value in the near-wall region. However this negative value is compensated by either the transport by velocity fluctuation or the buoyant production, ensuring that $\overline{vv}$ has always positive value. Note that the pressure strain correlation Φ_{ij} is very influential not only in the near wall region, but also in the far away from the wall. This term will be discussed in more details in Chapter 4.

For the horizontal Reynolds stress $\overline{uu}$ budget, the transport by pressure fluctuation and pressure strain correlation in the near wall region are quite large and almost in equilibrium. On the other hand, pressure transport is relatively small in the center region. Note that dissipation is important in the center region. It is notable that transport by viscosity is very small, indicating small viscous effect. For Reynolds stress $\overline{ww}$ budget, the pressure strain correlation and the dissipation are almost in equilibrium, especially in the center region, while the other components are very small. The budget of shear stress and the vertical stress are similar. An interesting feature of the shear stress budget is the balance between the shear production and the pressure scrambling, and between buoyant production and dissipation rate. Since the shear production is more dominant, the negative value of the shear stress in that region is still observed.

a.

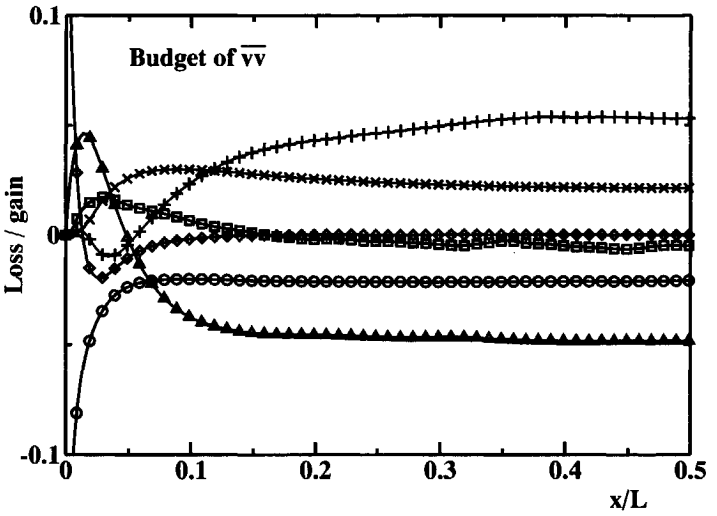

b.

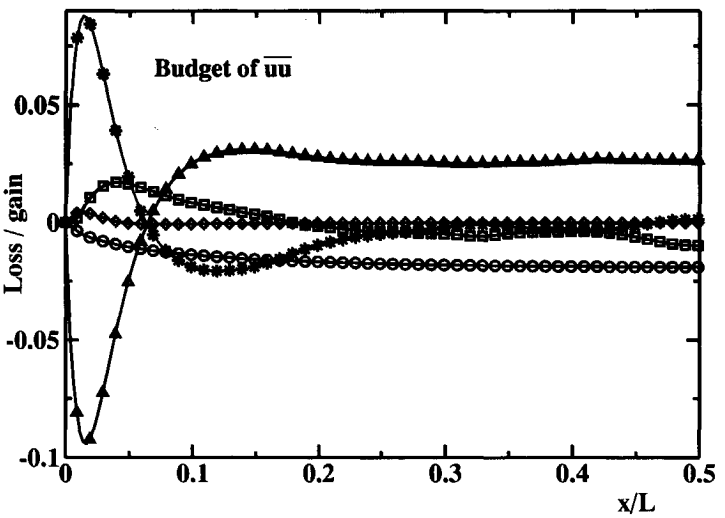

Figure 3.1: The budget of stress $\overline{vv}$ (a), $\overline{uu}$ (b), in a side-heated infinite cavity at $Ra = 5 \times 10^6$ of Versteegh [102]: $D^{\nu}_{ij}(-\diamond-)$, D^{t}_{ij} $(-\square-)$, $D^{p}_{ij}(-*-)$, $P_{ij}(-+-)$, $G_{ij}(-\times-)$, $\Phi_{ij}(-\triangle-)$ and $\varepsilon_{ij}(-\circ-)$.

a.

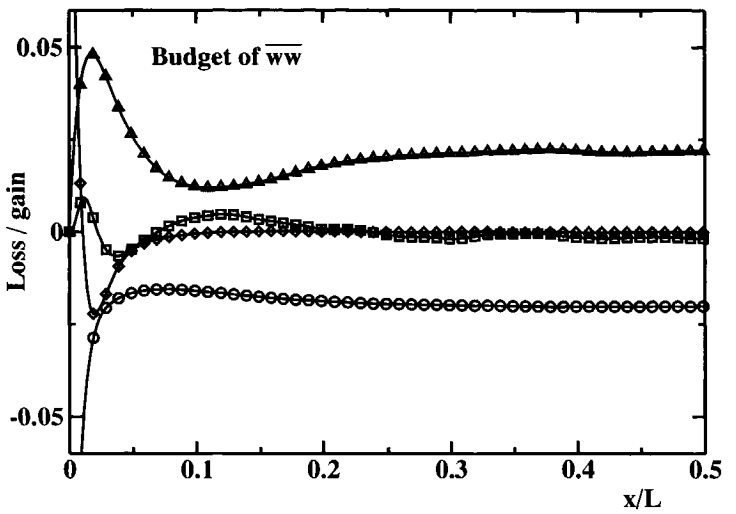

b.

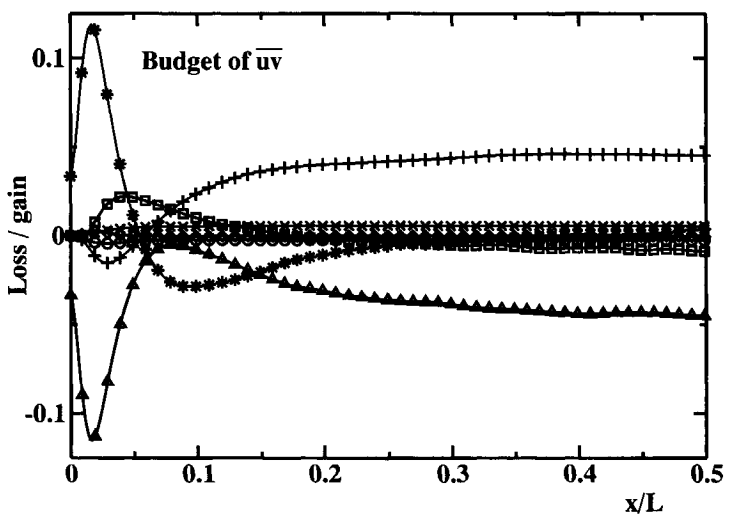

Figure 3.2: The budget of stress $\overline{ww}$ (a), and $\overline{uv}$ (b), in a side-heated infinite cavity at $Ra = 5.0 \times 10^6$ of Versteegh [102] : $D^{\nu}_{ij}(-\diamond-)$, D^{t}_{ij} $(-\square-)$, $D^{p}_{ij}(-*-)$, $P_{ij}(-+-)$, $G_{ij}(-\times-)$, $\Phi_{ij}(-\triangle-)$, and $\varepsilon_{ij}(-\circ-)$.

3.3.2 Turbulent heat flux equation

The derivation of the transport equation for turbulent heat flux can be conducted in analogous way to the Reynolds stress equation:

$$\frac{D\overline{\theta u_i}}{Dt} = \underbrace{\frac{\partial}{\partial x_k}\left[\underbrace{\boxed{\nu\overline{\frac{\partial u_i}{\partial x_k}\theta} + \alpha u_i \overline{\frac{\partial \theta}{\partial x_k}}}}_{\mathcal{D}^{\nu}_{\theta i}} - \underbrace{\boxed{\overline{u_i u_k \theta}}}_{\mathcal{D}^{t}_{\theta i}}\right]}_{\mathcal{D}_{\theta i}} \underbrace{-\overline{u_i u_k}\frac{\partial T}{\partial x_k}}_{P^{th}_{\theta i}}$$
$$\underbrace{-\overline{\theta u_k}\frac{\partial U_i}{\partial x_k}}_{P^{m}_{\theta i}} \underbrace{\boxed{-g_i\beta\overline{\theta^2}}}_{G_{\theta i}} \underbrace{\boxed{-\overline{\frac{\partial p}{\partial x_i}\frac{\theta}{\rho}}}}_{\Phi_{\theta i}} - \underbrace{\boxed{(\nu+\alpha)\overline{\frac{\partial u_i}{\partial x_k}\frac{\partial \theta}{\partial x_k}}}}_{\varepsilon_{\theta i}} \tag{3.23}$$

The term on the left hand-side is the material rate of change (time rate of change plus convection). On the right hand-side are the molecular diffusion $\mathcal{D}^{\nu}_{\theta i}$, the turbulent velocity diffusion $\mathcal{D}^{t}_{\theta i}$, the thermal production $P^{th}_{\theta i}$, the mechanical production $P^{m}_{\theta i}$, the buoyancy production $G_{\theta i}$, the pressure scrambling $\Phi_{\theta i}$, and the molecular dissipation rate $\varepsilon_{\theta i}$. It is clear that the mechanical and thermal productions are exact and therefore need not be modelled. On the other hand, the turbulent diffusion, buoyant production, pressure scrambling and the dissipation which are shown in boxes, should be modelled. It is interesting that unlike in the stress transport equation, even the molecular diffusion needs to be modelled if Prandtl number $Pr = \nu/\alpha$ is different from 1. In general, the terms of the transport equation of turbulent heat flux are modelled in the similar manner as those in the transport equation for the Reynolds stress. Both transport equations contain exact production terms, while the rest need to be modelled. It is noted that the mean quantity in the Reynolds stress equation is only the gradient of the mean velocity, while in the turbulent heat flux equation it is the gradient of the mean velocity and the mean temperature. These brings to a conclusion that turbulent heat flux depends not only on the thermal field, but also on the velocity field. Similar to the Reynolds stress equation, the pressure scrambling in the budget of turbulent heat flux plays an important role (see e.g. Dol [27]).

Turbulent heat flux budget

The budget of the two components of turbulent heat flux for the side-heated infinite vertical channel, $\overline{\theta u}$ and $\overline{\theta v}$, are shown in Figs. (3.3)a-b. The most distinguished feature of both budgets is their similarity in the sense that molecular and turbulent diffusion are significant in the near wall region, while in the core region they are negligibly small. The difference between the two budgets is the

a.

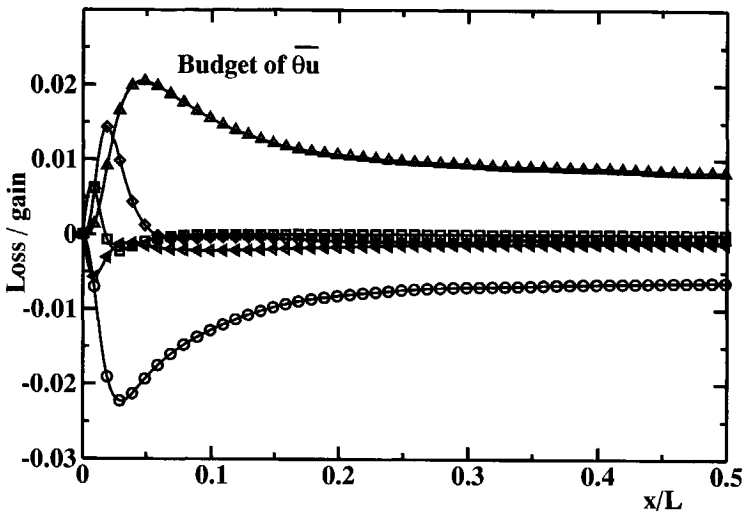

b.

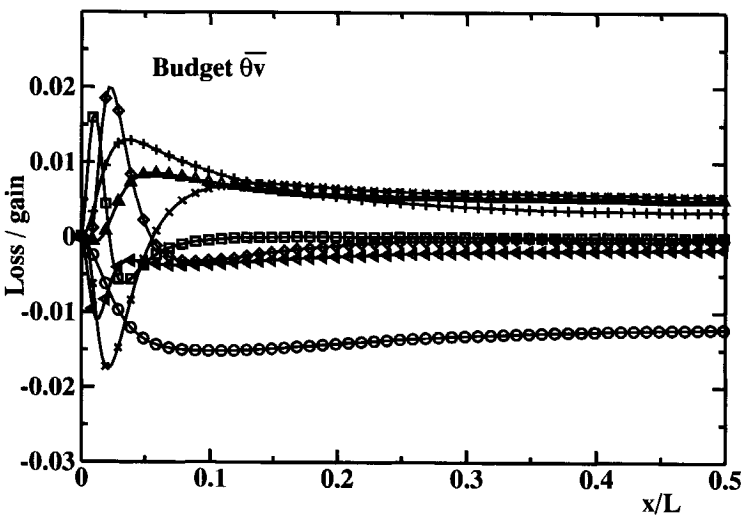

Figure 3.3: The budget of the turbulent heat flux $\overline{\theta u}$ (a) and $\overline{\theta v}$ (b) in a side-heated infinite cavity at $Ra = 5.0 \times 10^6$ of Versteegh [102]: $D^{\nu}_{\theta i}(-\diamond-)$, $D^{t}_{\theta i}$ $(-\square-)$, $P^{th}_{\theta i}(-\ \triangle\ -)$,$P^{m}_{\theta i}(-\times-)$, $G_{\theta i}(-+-)$, $\Phi_{\theta i}(-\circ-)$ and $\varepsilon_{\theta i}(-\triangleleft-)$.

absence of the buoyancy and mechanical production in the horizontal component. In addition, the production of $\overline{\theta u}$ is roughly balanced by the pressure scrambling term. Similarly, the pressure scrambling term in $\overline{\theta v}$ is also balanced by the sum of the thermal, mean-strain, and buoyancy production, especially in the region far away from the wall. In the the near wall region all budget contributions are influential. An interesting feature is observed in the shear production of $\overline{\theta v}$ where it has negative value in the near wall region. The positive values of $\overline{\theta v}$ is ensured by the turbulent and molecular diffusion, which compensates the negative terms in this region.

3.3.3 Temperature variance

In order to calculate the buoyancy generation $G_{\theta i}$ in equation (3.23), the temperature variance $\overline{\theta^2}$ must be evaluated. Temperature variance is an important parameter that affects the whole thermal field. The transport equation for $\overline{\theta^2}$ can be derived in a similar manner as for turbulent kinetic energy equation:

$$\frac{D\overline{\theta^2}}{Dt} = \underbrace{\frac{\partial}{\partial x_k}\left[\underbrace{\alpha\frac{\partial\overline{\theta^2}}{\partial x_k}}_{\mathcal{D}_\theta^\nu} \boxed{\underbrace{-\overline{\theta^2 u_k}}_{\mathcal{D}_\theta^t}}\right]}_{\mathcal{D}_\theta} \underbrace{-2\overline{\theta u_k}\frac{\partial T}{\partial x_k}}_{P_\theta} \boxed{\underbrace{-2\alpha\overline{\left(\frac{\partial\theta}{\partial x_k}\right)^2}}_{\varepsilon_\theta}} \tag{3.24}$$

Equation (3.24) contains three terms: the diffusion, the production, and the dissipation terms. The molecular diffusion and the production can be treated exactly, whereas the turbulent diffusion and the dissipation rate need to be modelled. In equation (3.24) one can notice the similarity of the corresponding terms in the transport equation for the turbulent kinetic energy. In addition, several experimental studies have shown that close similarity does exist between the budget of k and $\overline{\theta^2}$, Sommer [98].

3.3.4 Algebraic stress and flux models

The full differential Reynolds stress/flux model presumes that equation for each stress and flux are solved plus at least two equations for variables providing turbulence scale. For a general 3-dimensional flow this involves in total 11 transport differential equation in addition to the mean continuity momentum and energy. This requires additional computer resources as compared with similar isothermal flows. For buoyancy driven flows where temperature and velocity gradients in the near-wall region are being of the main concern, a large number of grid points is required if the near-wall flow fields needs to be well captured. In order to reduce this complexity, it is useful to approximate the differential form of the transport

equations of the Reynolds stress and heat flux. A common way to achieve this is to truncate the differential Reynolds stress and turbulent heat flux equations into algebraic formulation. As a result, only a few differential scalar transport equations need to be solved and this is the best compromise between physical representation and numerical robustness.

This simplification eliminates the convective and diffusive transport terms in the Reynolds stress and turbulent heat flux equations (3.22) and (3.23). This approach leads to an algebraic formulation of the Reynolds stress and heat flux models and is known as Algebraic Stress Model (ASM) and Algebraic Flux Model (AFM). Although the transport terms are truncated, the important redistribution Φ_{ij} and productions P_{ij}, G_{ij} are still kept as in the full differential stress model. Similarly, the important redistribution $\Phi_{\theta i}$, productions $P_{\theta i}^{m}$, $P_{\theta i}^{th}$, and $G_{\theta i}$ are still kept as in the full differential flux model. In this approach, only major scalar quantities need to be solved, these are turbulent kinetic energy, dissipation rate and temperature variance, and therefore ASM/AFM is considered as an extended $k-\varepsilon$ model.

When the transport term of Reynolds stress is neglected, $D\overline{u_iu_j}/Dt - \mathcal{D}_{ij} = 0$, $\overline{u_iu_j}$ can be expressed as a function of the nondifferential terms in the right hand side of equation (3.22). The Reynolds stress reads (Rodi [92]):

$$\overline{u_iu_j} = \frac{2}{3}k\delta_{ij} + \frac{k}{\varepsilon}\left[\frac{1-C_2}{C_1}\left(P_{ij} - \frac{2}{3}P\delta_{ij}\right) + \frac{1-C_3}{C_1}\left(G_{ij} - \frac{2}{3}G\delta_{ij}\right)\right] \tag{3.25}$$

where $C_1 = 1.8$, $C_2 = C_3 = 0.6$. Equation (3.25) is called the reduced algebraic stress model. In order to still account for the stress and flux transport and thus to improve the model performance, Rodi [92] proposed to assume the proportionality between the transport terms of Reynolds stress and turbulent kinetic energy k:

$$\frac{D\overline{u_iu_j}}{Dt} - \mathcal{D}_{ij} = \frac{\overline{u_iu_j}}{k}(P + G - \varepsilon) \tag{3.26}$$

Introducing equation (3.26) into the modelled Reynolds stress equation (3.22), we obtain expression of full algebraic stress model similar to the equation (3.25):

$$\overline{u_iu_j} = \frac{2}{3}k\delta_{ij} + \frac{k}{\varepsilon}\left[\frac{1-C_2}{C_1'}\left(P_{ij} - \frac{2}{3}P\delta_{ij}\right) + \frac{1-C_3}{C_1'}\left(G_{ij} - \frac{2}{3}G\delta_{ij}\right)\right] \tag{3.27}$$

where $C_1' = C_1 + (P+G)/\varepsilon - 1$. Similarly, when the transport term of the heat flux is neglected $D\overline{\theta u_i}/Dt - \mathcal{D}_{\theta i} = 0$, $\overline{\theta u_i}$ can be expressed as a function of the non-differential terms in the right hand side of equation (3.23). The algebraic expression for the turbulent heat flux vector reads:

$$\overline{\theta u_i} = -C_\theta\frac{k}{\varepsilon}\left(\overline{u_iu_k}\frac{\partial T}{\partial x_k} + \xi\overline{\theta u_k}\frac{\partial U_i}{\partial x_k} + \eta g_i\beta\overline{\theta^2}\right) \tag{3.28}$$

Based on the assumption of "weak equilibrium", Gibson and Launder [37] extended Rodi's idea to express the transport terms of $\overline{\theta u_i}$ as a function of the transport terms of k and $\overline{\theta^2}$, to derive an algebraic flux model:

$$\begin{aligned}\frac{D\overline{\theta u_i}}{Dt} - D_{\theta i} &= \frac{\overline{\theta u_i}}{\left(\overline{\theta^2} k\right)^{1/2}} \left[\frac{D}{Dt}(\overline{\theta^2} k)^{1/2} - \mathcal{D}_{(\overline{\theta^2} k)^{1/2}}\right] \\ &= \frac{1}{2}\overline{\theta u_i}\left[\frac{1}{\overline{\theta^2}}\left(\frac{D\overline{\theta^2}}{Dt} - \mathcal{D}_\theta\right) + \frac{1}{k}\left(\frac{Dk}{Dt} - \mathcal{D}_k\right)\right] \end{aligned} \tag{3.29}$$

Providing the transport of k and $\overline{\theta^2}$ by their sources, and substituting equation (3.29) into the modelled heat flux equation (3.23), we obtain:

$$\overline{\theta u_i} = \frac{\overline{u_i u_k}\dfrac{\partial T}{\partial x_k} + \xi\overline{\theta u_k}\dfrac{\partial U_i}{\partial x_k} + \eta g_i \beta \overline{\theta^2}}{-C_\theta^{-1}\dfrac{\varepsilon}{k} + \dfrac{1}{2\overline{\theta^2}}\left(2\overline{\theta u_k}\dfrac{\partial T}{\partial x_k} + \varepsilon_\theta\right) + \dfrac{1}{2k}\left(\overline{u_i u_k}\dfrac{\partial U_i}{\partial x_k} + g_i\beta\overline{\theta u_i} + \varepsilon\right)} \tag{3.30}$$

where $C_\theta = 0.2$, $\xi = 1 - C_{\theta 2}$, and $\eta = 1 - C_{\theta 3}$.

CHAPTER 4

Advancement and Improvement of Models

4.1 Introduction

This chapter outlines the adopted models of various terms in the model equations and describes the major contribution of this thesis. These novelties consist of:

(i) buoyancy extension of a low Re number second moment closures and its truncation to algebraic form,

(ii) introduction of the "homogeneous" dissipation rate equation,

(iii) buoyancy extension of the elliptic relaxation model, resulting in the $k-\varepsilon-\overline{v^2}-f-\overline{\theta^2}$ model, and

(iv) proposal and comparative assessment of several variants of the ASM/AFM models.

4.2 Buoyancy Extended Low-Re number Reynolds stress model

Most industrial CFD codes use high Reynolds number models which do not have any provision for accounting for near-wall viscous and blocking effects. In order to bridge the near-wall viscous layer, wall functions are used to bridge the viscous layer by providing flow parameter in the first grid point next to wall, which must lie outside the molecular layer. Because it allows a relatively coarse grid, the use of wall functions is very attractive for complex industrial flows at high Reynolds and Rayleigh numbers where integration of equations up to the wall would require a formidable computer resources. However, the common wall functions are based on energy-equilibrium, constant shear stress and validity of the semi-logarithmic velocity law in the near-wall layer and are inaccurate in more complex flows in regions where the turbulence dynamics departs from the equilibrium conditions. Although several attempts have been made to provide more general wall function for wider applications in non-equilibrium flows and for forced convective heat transfer, for examples by Chieng and Launder [12], Yuan [107], the results were only marginally successful. For example, no reliable wall functions exist for flows driven by thermal buoyancy.

In order to overcome the problem, it is necessary to provide a model that permits integration of the governing equations up to the wall and thus to use exact wall boundary conditions. Such a model must mimic the flow behaviour and its physics in the near-wall region which is affected both by molecular effects (viscosity, thermal conductivity) and non-molecular wall blocking effects. This is achieved by introducing molecular and wall-blocking modifications to the basic models developed for high Reynolds and Rayleigh numbers. The modifications must satisfy various physical constraints such as two-component turbulence limit at the edge of the viscous sublayer, and to capture the vanishing turbulent Reynolds number when approaching a solid wall. As a consequence, a low-Reynolds number model requires a very fine mesh in the near-wall region to resolve very high gradients of most mean and turbulence properties, that leads to a large number of grid points.

This chapter outlines a low-Re-number model for flows affected or driven by thermal buoyancy. The near-wall modifications are especially important for buoyant flows over heated and cooled walls because most interaction take place at near-wall region and therefore it is important to capture accurately all turbulent quantities in that region. We consider here in details the models of various terms in the new low Re-number second moment closure for buoyancy-driven flows.

4.2.1 Pressure strain correlation in the Reynolds stress equation

A considerable attention has been given in the literature to modelling the pressure-velocity correlations because this term plays an important role in the turbulence stress dynamics. The pressure strain correlation represents a stress redistribution process that redistributes turbulent energy among stress components acting towards stress isotropisation, without affecting directly the value of turbulent kinetic energy. In order to get a physical insight into the process and make it easier to model this term, the pressure-strain correlation is decomposed into: slow, rapid, buoyant and wall contributions:

$$\Phi_{ij} = \Phi_{ij,1} + \Phi_{ij,2} + \Phi_{ij,3} + \Phi^w_{ij,1} + \Phi^w_{ij,2} + \Phi^w_{ij,3} \tag{4.1}$$

This decomposition follows from the analysis of Chou [13] and Rotta [94] based on Poisson equation for pressure fluctuation to obtain an integral expression in which four different contributions can be distinguished: turbulence-turbulence interaction (the "slow" term) $\Phi_{ij,1}$, turbulence-mean flow interaction (the "rapid" term) $\Phi_{ij,2}$, buoyancy effect $\Phi_{ij,3}$, and wall effect Φ^w_{ij}. The turbulence-turbulence term is known as the slow term, because it is associated with the slow relaxation of the turbulence toward isotropy. The turbulence-mean flow interaction is known as the rapid term, which is associated with the rapid response of the turbulence to imposed mean velocity gradient or to buoyancy and other body forces.

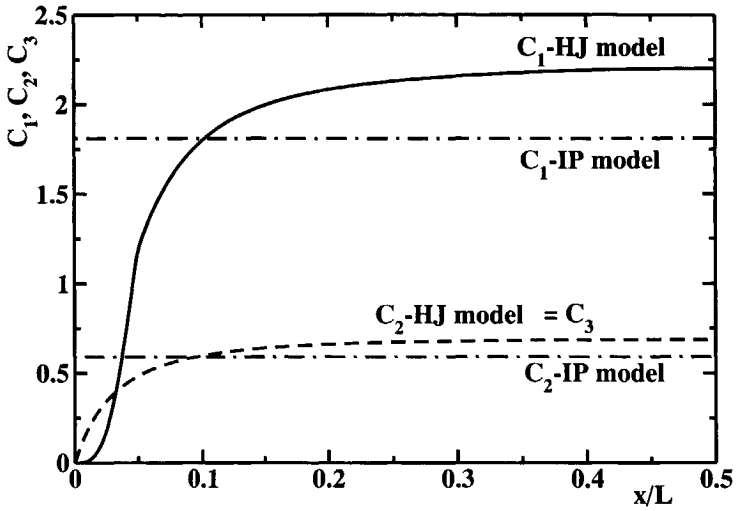

Figure 4.1: The coefficients C_1, C_2 and C_3 for a side-heated infinite vertical channel using DNS data of Versteegh [101] at $Ra = 5.0 \times 10^6$

For modelling the slow term, Rotta [94] proposed a simple linear model:

$$\Phi_{ij,1} = -C_1 \frac{\varepsilon}{k}(\overline{u_i u_j} - \frac{2}{3}k\delta_{ij}) \tag{4.2}$$

where the value of C_1 varies between 1.5 to 3.0. Lumley [76] pointed out that C_1 is not a universal constant, but it depends on the turbulent Reynolds number and the rate of anisotropy and proposed a quadratic model in term of stress anisotropy. The differences in the value of C_1 proposed by various authors arises mainly from the difference in features of flows considered for model tuning. Recent DNS data for a plane channel flow showed that C_1 is not constant across the flow irrespective whether the linear or quadratic model is considered, as shown in Fig.(4.1), and that the closest value for the outer wall layer is about 1.8, though the DNS of the buoyancy driven flow in a vertical channel suggest in the outer region the value of 2.2.

For the rapid term originating from the mean rate of strain, Naot *et al.* [81] proposed a model analogous to the slow term, but in terms of the redistribution of the stress production:

$$\Phi_{ij,2} = -C_2(P_{ij} - \frac{2}{3}P_k\delta_{ij}) \tag{4.3}$$

where most authors take the coefficient $C_2 = 0.6$

It is well known that for any flow affected by buoyancy, i.e. where the variation in fluid density caused by temperature or concentration stratification, the body

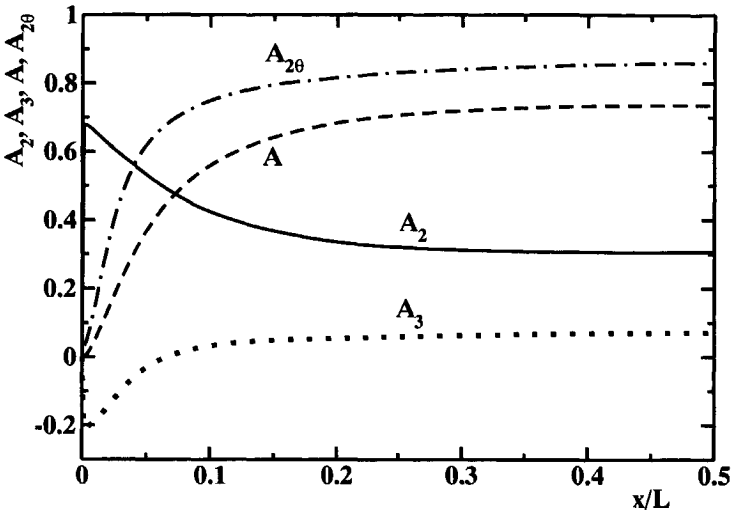

Figure 4.2: The stress and scalar flux invariants in a side-heated infinite channel using DNS data of Versteegh [101] at $Ra = 5.0 \times 10^6$.

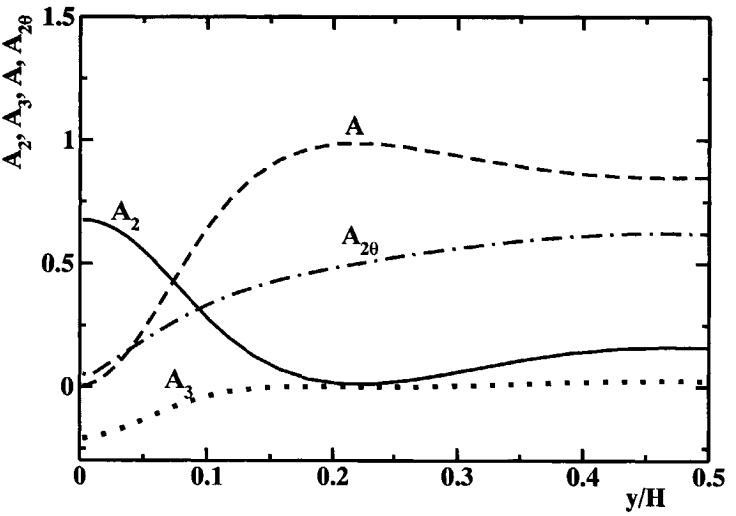

Figure 4.3: The stress and scalar flux invariants in infinite horizontal channel heated from below using DNS data of Wöerner [104] at $Ra = 6.3 \times 10^5$

force plays an important role not only in the stress production or destruction, but also in the stress redistribution dynamics, and therefore it should be introduced in the mechanical field equation. The buoyant contribution to the pressure strain correlation can be modelled in a similar manner as the rapid term reflecting the redistribution and isotropisation of the buoyant production:

$$\Phi_{ij,3} = -C_3(G_{ij} - \frac{2}{3}G_k\delta_{ij}) \tag{4.4}$$

Due to the lack of experimental or DNS information on the buoyant pressure-redistribution term, most authors take $C_3 = C_2$. Gibson and Launder [37] proposed, in contrast $C_3 = 0.5$, whereas Launder [67] adopted $C_3 = 0.33$.

The non-viscous wall blocking effect tends to retard the redistributive action of the fluctuating pressure. The most popular model of this ("wall echo") effect is that of Gibson and Launder [37]:

$$\Phi^w_{ij,1} = C^w_1 f_w \frac{\epsilon}{k}\Big(\overline{u_k u_m}n_k n_m\delta_{ij} - \frac{3}{2}\overline{u_i u_k}n_k n_j - \frac{3}{2}\overline{u_k u_j}n_k n_i\Big) \tag{4.5}$$

$$\Phi^w_{ij,2} = C^w_2 f_w\Big(\Phi_{km,2}n_k n_m\delta_{ij} - \frac{3}{2}\Phi_{ik,2}n_k n_j - \frac{3}{2}\Phi_{kj,2}n_k n_i\Big) \tag{4.6}$$

$$\Phi^w_{ij,3} = C^w_3 f_w\Big(\Phi_{km,3}n_k n_m\delta_{ij} - \frac{3}{2}\Phi_{ik,3}n_k n_j - \frac{3}{2}\Phi_{kj,2}n_k n_i\Big) \tag{4.7}$$

In equations (4.5)-(4.7) the coefficients have constant values, i.e. $C^w_1 = 0.6$, $C^w_2 = 0.3$ and $C^w_3 = 0$.

Low Re number and near wall modification

For integration up to the wall the pressure strain needs to be modified to account for viscous effects, but also for possible variation of the coefficients from constant values. Following Hanjalić and Jakirlić [43] (see also Jakirlić [54]) these modifications can be accomplished by expressing all coefficients in the models of the pressure-strain terms as functions of local turbulence Reynolds number $Re_t = k^2/(\nu\varepsilon)$ and stress- and dissipation-rate anisotropy invariants. This model was tested successfully in several turbulent flows, such as boundary layers at strong favourable and adverse pressure gradients, oscillatory flows, and other unsteady flows, channel flow, back-step, rotating and swirling flows and many more. These functions have been designed to satisfy various near-wall constraints, such a two-component limit and vanishing Reynolds number at a solid wall.

The coefficients used in the pressure-strain correlation model is given by the following expression:

$$C_1 = C + \sqrt{A}E^2 \qquad C_2 = C_3 = 0.8A^{1/2} \tag{4.8}$$

$$C^w_1 = max(1 - 0.7C; 0.3) \qquad C^w_2 = min(A; 0.3) \tag{4.9}$$

The functions used in the pressure-strain correlation coefficients are:

$$C = 2.5AF^{\frac{1}{4}}f \qquad F = min\{0.6; A_2\} \tag{4.10}$$

$$f = min\left\{\left(\frac{Re_t}{150}\right)^{\frac{3}{2}}; 1\right\}, \qquad f_w = min\left[\frac{k^{\frac{3}{2}}}{2.5\varepsilon x_n}; 1.4\right], \qquad Re_t = k^2/(\nu\varepsilon) \tag{4.11}$$

where Reynolds stress anisotropy invariants can be written as:

$$A_2 = a_{ij}a_{ji}, \qquad A_3 = a_{ij}a_{jk}a_{ki}, \qquad A = 1 - 9/8(A_2 - A_3) \tag{4.12}$$

and dissipation rate anisotropy invariants can be expressed similarly as:

$$E_2 = e_{ij}e_{ji}, \qquad E_3 = e_{ij}e_{jk}e_{ki}, \qquad E = 1 - 9/8(E_2 - E_3) \tag{4.13}$$

$$a_{ij} = \overline{u_iu_j}/k - 2/3\delta_{ij}, \qquad e_{ij} = \varepsilon_{ij}/\varepsilon - 2/3\delta_{ij} \tag{4.14}$$

Figure (4.1)a shows the variation of the coefficients used in the slow, rapid, buoyant terms of pressure scrambling. In the away-from-the-wall region, C_1 and C_2 are approaching values recommended by previously mentioned authors. The obvious difference is found in the near-wall region, where these coefficients approach zero values at the wall to satisfy the wall limits of the stress budget. The coefficient C_1 is modified as function of the Reynolds stress and dissipation rate anisotropy invariants A and E, respectively. In addition, the coefficient C_2 is modified as a function of the stress second invariant A_2, while the coefficient $C_3 = C_2$. The variation of the stress anisotropy invariants A_2, A_3, A and of the flux anisotropy invariant $A_{2\theta}$ in two generic buoyancy driven flows, infinite vertical and horizontal channels, is given in Figs.4.2 and 4.3.

4.2.2 Diffusion

The diffusion term $\mathcal{D}_{ij}$ consists of three terms: turbulent diffusion by pressure and velocity fluctuations and the viscous diffusion. Since the molecular diffusion is an exact expression, only the turbulent diffusion that originate from triple correlation $\overline{u_iu_ju_k}$ and the pressure diffusion must be modelled. Ideally, these triple correlation should be provided from their exact differential transport equations, that should be closed (modelled) in similar way as the transport equation for the Reynolds stress. However, this route would end up with correlation of third and fourth order that need to be modelled further. In order to overcome the modelling task, Hanjalić and Launder [45] proposed a simplified model, where the transport terms and the mean flow contributions of the $\overline{u_iu_ju_k}$ are omitted leaving simple algebraic formulation. Daly and Harlow [21] introduced a simpler but not frame invariant formulation of the turbulent diffusion which is known as gradient diffusion hypothesis.

$$D_{ij}^t = \frac{\partial}{\partial x_k}\left(C_s\frac{k}{\varepsilon}\overline{u_ku_l}\frac{\partial\overline{u_iu_j}}{\partial x_l}\right) \tag{4.15}$$

The pressure diffusion is often modelled in a similar way of the turbulent diffusion model. Dol [27], used this model to calculate the turbulent flow in vertical channel. However, since the pressure diffusion is relatively small, Peeters and Henkes [89] neglected the term.

4.2.3 Stress Dissipation Rate

For high Re number flows and away from a solid wall the dissipation rate ε_{ij} is modelled with isotropic assumption. These is due to the fact that viscous dissipation of isotropic turbulence occurs at the smallest eddies. The isotropic model of the dissipation reads:

$$\varepsilon_{ij} = \frac{2}{3}\varepsilon\delta_{ij} \tag{4.16}$$

This isotropic model is not valid in the near-wall region and for flows at low Re numbers. To account for the viscous effect and anisotropy of the near-wall small eddies, Hanjalić and Launder [46] proposed a formulation of the stress dissipation rate ε_{ij}:

$$\varepsilon_{ij} = (1 - f_s)\frac{2}{3}\varepsilon\delta_{ij} + f_s\frac{\varepsilon}{k}\overline{u_i u_j} \tag{4.17}$$

$$f_s = \frac{1}{(1 + 0.1Re_t)} \tag{4.18}$$

Since the expression (4.17) does not satisfy the wall limiting values of ε_{ij}, several modifications have been proposed, the most recent being that of Hanjalić and Jakirlić [44]:

$$\varepsilon_{ij} = (1 - f_s)\frac{2}{3}\varepsilon\delta_{ij} + f_s\varepsilon^*_{ij} \tag{4.19}$$

$$\varepsilon^*_{ij} = \frac{\frac{k}{\varepsilon}\left[\overline{u_i u_j} + (\overline{u_i u_k}n_j n_k + \overline{u_j u_k}n_i n_k + \overline{u_k u_l}n_k n_l n_i n_j)f_d\right]}{1 + \frac{3}{2}\frac{\overline{u_p u_q}}{k}n_p n_q f_d} \tag{4.20}$$

$$f_s = 1 - \sqrt{A}\ E^2 \tag{4.21}$$

$$f_d = \frac{1}{(1 + 0.1Re_t)} \tag{4.22}$$

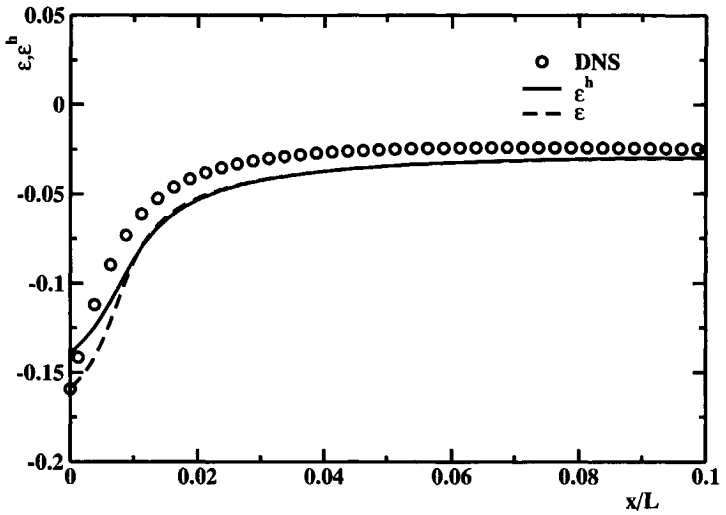

Figure 4.4: The profiles of the homogeneous dissipation rate at side-heated cavity at $Ra = 5.0 \times 10^6$ of Versteegh [101]

4.2.4 Homogeneous dissipation

Recently, Jakirlić and Hanjalić [55] proposed a new model for the dissipation rate ε and the anisotropy of the dissipation rate tensor ε_{ij}. The model of the dissipation rate is derived in term of homogeneous part ε^h. The derivation is based on the two-point velocity covariance analysis of Jovanović *et al.* [58] and reinterpretation of the viscous term. The anisotropy of the dissipation rate ε_{ij} is expressed in term of ε^h to provide the wall limit condition. With this new model, the algebraic expression for the components of ε_{ij} is independent of any wall-configuration parameters.

$$\varepsilon_{ij}^h = (1 - f_s)\frac{2}{3}\delta_{ij}\varepsilon^h + f_s\frac{\overline{u_i u_j}}{k}\varepsilon^h \tag{4.23}$$

Here ε^h is provided from its transport equation, which differs marginally from the conventional equation:

$$\frac{D\varepsilon^h}{Dt} = -C_{\varepsilon 1}\overline{u_i u_j}\frac{\partial U_i}{\partial x_j}\frac{\varepsilon^h}{k} - 2\nu\left(\frac{\partial \overline{u_i u_k}}{\partial x_l}\frac{\partial^2 U_i}{\partial x_k \partial x_l} + C_{\varepsilon 3}\frac{k}{\varepsilon^h}\frac{\partial \overline{u_k u_l}}{\partial x_j}\frac{\partial U_i}{\partial x_k}\frac{\partial^2 U_i}{\partial x_j \partial x_l}\right)$$
$$-C_{\varepsilon 2}f_\varepsilon\frac{\tilde{\varepsilon}^h\,\varepsilon^h}{k} + \frac{\partial}{\partial x_k}\left[\left(\frac{1}{2}\nu\delta_{kl} + C_\varepsilon\frac{\varepsilon^h}{k}\overline{u_k u_l}\right)\frac{\partial \varepsilon_h}{\partial x_l}\right] \tag{4.24}$$

where $f_s = 1 - \sqrt{A}E^2$, $C_{\varepsilon 1} = 1.44$, $f_\varepsilon = 1 - (C_{\varepsilon 2} - 1.4)/C_{\varepsilon 2}exp[-(Re_t/6)^2]$. The new equation for homogeneous dissipation rate can be solved with the model of

transport equation for the Reynolds stress $\overline{u_i u_j}$. The only difference from the conventional dissipation rate is that ε^h serves as the sink term in the Re-stress equation, and factor of 0.5 appears in the viscous diffusion terms of both the $\overline{u_i u_j}$ and ε^h equations. In addition, the low-Re-number production term in the ε^h equation is somewhat different. It was reported by Jakirlić and Hanjalić [55] that the use of ε^h gave considerable improvement as compared to the conventional dissipation rate equation. Examples of this application are flows in a pipe, plane channel, constant-pressure boundary layer, backward-facing step, and in an axially rotating pipe.

4.3 Modelling the transport equation for turbulent heat flux

4.3.1 Thermal Pressure scrambling

In this study the pressure diffusion is modelled together with the pressure - temperature-gradient correlation, known as pressure scrambling. Many authors neglect the pressure diffusion, e.g Peeters and Henkes [89], whereas others treated this term separately. Lumley [76] proposed a separate model for the pressure diffusion, however the model behaved badly, especially in the near wall region. As demonstrated by Dol *et al.* [25] the joint treatment of the pressure diffusion and the pressure - temperature-gradient correlation is much easier to model and the result shows better agreement with DNS. As mentioned in Chapter 3 that pressure scrambling dominates the budget of turbulent heat flux, consequently the performance of the complete model is affected heavily by this contribution. The pressure scrambling is conventionally decomposed into four parts: slow, rapid, buoyant, and wall parts.

Slow term

The simplest way to model the slow term $\Phi_{\theta i,1}$ is by expressing it in a "return to isotropy" form. In the absence of all turbulence generating mechanism, the slow term returns the turbulence heat flux field to the isotropic state. The model proposed by Monin [78] reads:

$$\Phi_{\theta i,1} = -C_{\theta 1}\frac{\varepsilon}{k}\overline{\theta u_i} \tag{4.25}$$

Different authors used different values of $C_{\theta 1}$. For example, Monin [78] took $C_{\theta 1}$ equals 3, while Peeters and Henkes [89] took $C_{\theta 1}$ is equal 3.75. Equation (4.25) is the most widely used form of the slow part of the pressure scrambling term and it is known as the linear or basic model. In order to improve the basic

model, a modification have been proposed to the coefficient $C_{\theta 1}$ to be a function of Reynolds stress invariants. A more complex model function of $C_{\theta 1}$, including stress invariants, Reynolds stress, heat flux, and time scale ratio R, has been proposed by Shih and Lumley [95]. However, the attempt was not very successful.

It was reported by Dol [27] that the model cannot be improved through the modification of $C_{\theta 1}$. This leads to extension of the basic model of the slow term to a higher-order expression. The inclusion of non-linear term has been adopted by Launder [66]. The model reads:

$$\Phi_{\theta i,1} = -C_{\theta 1}\frac{\epsilon}{k}\left(\overline{\theta u_i} + C'_{\theta 1}a_{ij}\overline{\theta u_j}\right) \tag{4.26}$$

Similar attempt has been proposed by Dol [27] to model the pressure scrambling of heat flux. He expanded the slow term into quadratic and cubic expressions, which are linear in $\overline{\theta u_i}$ and quadratic to a_{ij}:

$$\Phi_{\theta i,1} = -\frac{\epsilon}{k}(C_{\theta 1}\overline{\theta u_i} + C'_{\theta 1}a_{ij}\overline{\theta u_j} + C''_{\theta 1}a_{ij}a_{jk}\overline{\theta u_k}) \tag{4.27}$$

The model given by equation (4.27) reduces to the slow term of the basic model when coefficient $C'_{\theta 1} = C''_{\theta 1} = 0$ and $C_{1\theta}$ constant. This higher order model was adopted in order to match the DNS data for the infinite side-heated vertical channel. The coefficients $C_{\theta 1}$, $C'_{\theta 1}$ and $C''_{\theta 1}$ are exponential functions defined by four parameters. As the slow term dominates the pressure scrambling, these coefficients have important impact on the modelling of the total pressure scrambling contributions. It was shown by Dol *et al.*[26] that the performance of this model of the pressure scrambling model is very good and matches to the DNS data for the vertical channel very well. However, this model introduces more empirical coefficients. The difference between the quadratic and the cubic model is the number of terms in the slow part of the pressure scrambling, where $C''_{\theta 1} = 0$ for the quadratic model. It was also reported that the quadratic model is very sensitive and can produce oscillation during the computations. The problem could be overcome by using adequate value of the parameters r and s.

The coefficient involved in the pressure scrambling model are defined as:

$$C_{\theta 1}, C'_{\theta 1}, C''_{\theta 1} \subset F_{pqrs}(A_{2\theta}) = \frac{p[1 - exp(-qA_{2\theta})]}{1 + rexp(-sA_{2\theta})} \tag{4.28}$$

where $A_{2\theta}$ is the scalar flux invariant. It is important to mention that $A_{2\theta}$ has replaced the stress invariant A, which is used in the previous model. The scalar flux invariant is defined as :

$$A_{2\theta} = \frac{\overline{\theta u_k}\ \overline{\theta u_k}}{\overline{\theta^2}k} \tag{4.29}$$

As shown in Fig.(4.2) the profiles of $A_{2\theta}$ in both the vertical channel and in the horizontal channel of Fig.(4.3) are similar. In the vertical channel both

	Dol et al model			Present model		
	$C_{\theta 1}$	$C'_{\theta 1}$	C''_{θ}	$C_{\theta 1}$	$C'_{\theta 1}$	C''_{θ}
p	4.9	$-2C_{\theta 1}$	12.9	6	$-1.5C_{\theta 1}$	-
q	3.6	∞	1.2	4	-	-
r	10	0	-0.94	1	-	-
s	37	-	10	20	-	-

Table 4.1: The values of the shape factors constituting $F_{pqrs}(A_{2\theta})$ for the new model

invariants A and $A_{2\theta}$ have similar shape, but they differ in magnitude. On the other hand, in the horizontal channel they are obviously different in both the shape and magnitude.

The final goal of this study is to develop new models that can be applied for a range of different turbulent flows driven by thermal buoyancy. In order to have a robust model and avoid numerical instability, a simple form with less number of coefficients is desired. We propose here a new model of the slow term of the pressure scrambling process that reads:

$$\Phi_{\theta i,1} = -C_{\theta 1}\frac{\epsilon}{k}(\overline{\theta u_i} - 1.5a_{ij}\overline{\theta u_j}) \tag{4.30}$$

where $C_{\theta 1}$ is given by equation (4.28). Equation (4.30) reduces to basic model when $C_{\theta 1}$ is constant and the second term is omitted. This new model is more preferable, since it consists of less terms. It is mentioned before that the pressure scrambling is dominated by the slow term. Indeed, the proper modelling of the slow term is required, not only for physical reasons, but also for making it possible to define and use unique model coefficients $C_{\theta 1}$ and $C'_{\theta 1}$, where $C_{\theta 1}$ is expressed as a function of $A_{2\theta}$, with parameters p, q, r, s specified in Table 4.1. The new model of the equation (4.30) is relatively simple, but it works well for more general cases. The new model with introduction of $A_{2\theta}$ produced $\Phi_{\theta i}$ in close agreement with DNS data.

Rapid and Buoyant term

In analogy with the rapid part of the pressure scrambling term in the Reynolds stress equation, which is associated with the rapid response of the turbulence to imposed mean velocity gradient, the rapid term of turbulent heat flux is modelled in association with the mechanical production. Peteers and Henkes [89] use rapid term model as:

$$\Phi_{\theta i,2} = -C_{\theta 2}P^m_{\theta i} \tag{4.31}$$

with $C_{\theta 2} = 0.5$ as most authors take. Equation (4.31) is the most common model for the rapid term of the turbulent heat flux.

The buoyant term is often modelled in analogy with equation (4.31):

$$\Phi_{\theta i,3} = -C_{\theta 3} G_{\theta i} \tag{4.32}$$

For most application, $C_{\theta 2} = C_{\theta 3} = 0.5$ is the appropriate choice. Launder [68] argued that for the correct value in the limit of vanishing anisotropy, $C_{\theta 3}$ should be about 0.33. A more advanced model for the rapid and buoyant terms was introduced by Craft[17] by expanding the turbulent-interaction part in terms of the stress anisotropy a_{ij} and $\overline{\theta u_i}$. Similarly, Dol *et al.* [26] lumped the rapid term of the pressure scrambling $\Phi_{\theta i,2}$ together with the buoyant term $\Phi_{\theta i,3}$, denoted as $\Phi_{\theta i,2/3}$. They represent the action of pressure fluctuation to produce isotropisation of turbulence production due to strain rate for and buoyancy. The rapid and buoyant term can be expressed as:

$$\Phi_{\theta i,2/3} = -C_{\theta 2} P^m_{\theta i} - C'_{\theta 2} P^{th}_{\theta i} - C_{\theta 3} G_{\theta i} \tag{4.33}$$

where coefficients $C_{\theta 2}$, and $C'_{\theta 2}$, are functions of local invariant turbulence properties $A_{2\theta}$, while $C_{\theta 3} = 0.45$. The model function of $C'_{\theta 2}$ is set to match $\Phi_{\theta 1,2/3}/P^{th}_{\theta 1}$, while function of $C_{\theta 2}$ has been approximated to $-(\Phi_{\theta 2,2/3} + C'_{\theta 2} P^{th}_{\theta 2} + C_{\theta 3} G_{\theta 2})/P^m_{\theta 2}$. The profiles of coefficients $C_{\theta 1}, C_{\theta 2}$ and $C_{\theta 3}$ are shown in Figs.4.5.

The coefficients used in the new model read:

$$C_{\theta 2} = 1.25 A^2_{2\theta} \tag{4.34}$$

$$C'_{\theta 2} = 6.A^2_{2\theta} - 19.A^3_{2\theta} + 15.0 A^4_{2\theta} \tag{4.35}$$

Modelling the wall term

Wall reflection is an important effect that must be considered in any turbulence model. The wall causes a blocking effect on the normal heat flux much more than on the parallel component. There have been several proposals to model the wall reflection, an example is by Gibson and Launder [38]. The model has been adopted by Peeters and Henkes [89], Craft [16], Dol *et al.*[25], to mention a few. Following the model of Dol *et al.* [26], the wall term is expressed as:

$$\Phi^w_{\theta i} = C^w_\theta |a_{ij}| \left(\Phi_{\theta i,1} + \Phi_{\theta i,2/3} \right) \tag{4.36}$$

$$C^w_\theta = max \left(0, 0.58 - 0.69 A^{1/2} \right) \tag{4.37}$$

Figures (4.6)a-b show the performance of the new pressure scrambling model for side-heated infinite channel. It is evident that the term by term modelling of the pressure scrambling, especially of the slow term, shows a good agreement

a.

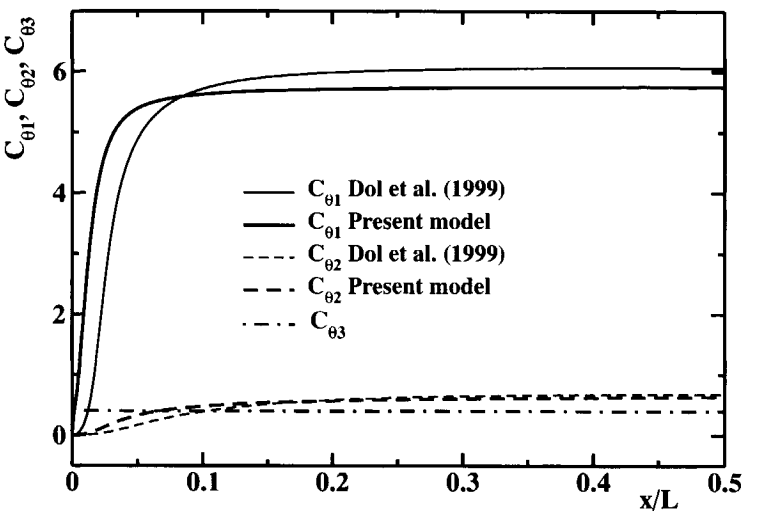

b.

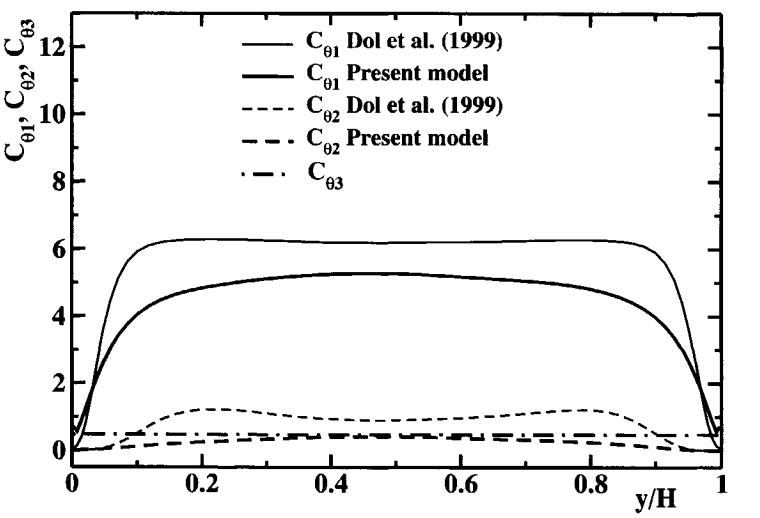

Figure 4.5: The profiles of $C_{\theta1}, C_{\theta2}$ and $C_{\theta3}$ of vertical channel of DNS data by Versteegh [101] at $Ra = 5.10^6$ (a) and horizontal channel (b) of DNS data by Wöerner [104] at $Ra = 6.3 \times 10^5$.

a.

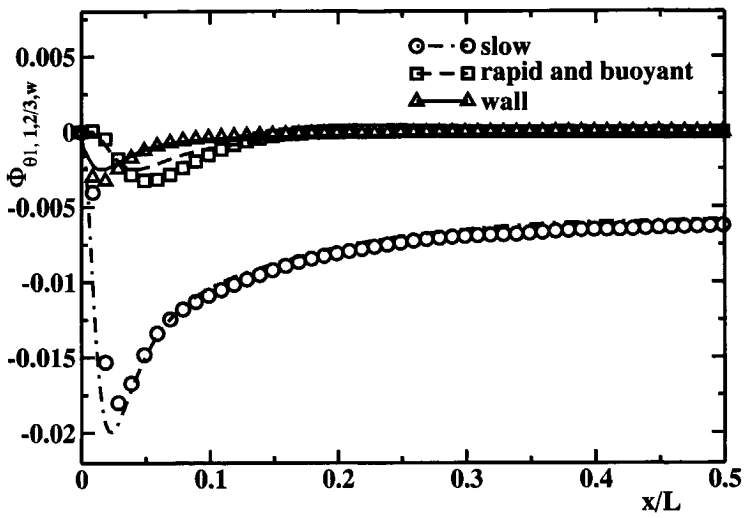

b.

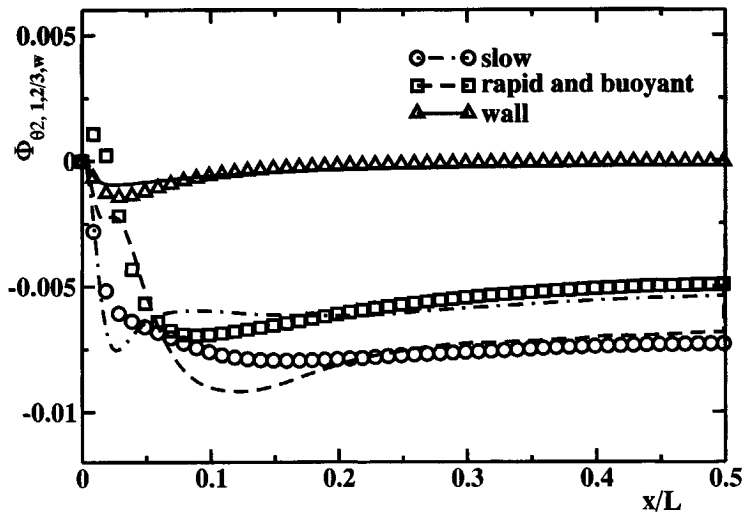

Figure 4.6: The performance of the slow, rapid and buoyant, and wall models of horizontal (a) and vertical (b) components compared to DNS of Versteegh [101] at $Ra = 5.10^6$

a.

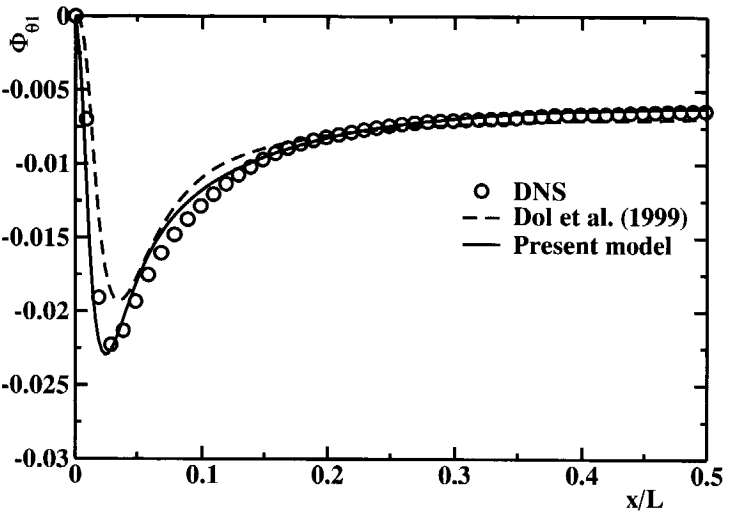

b.

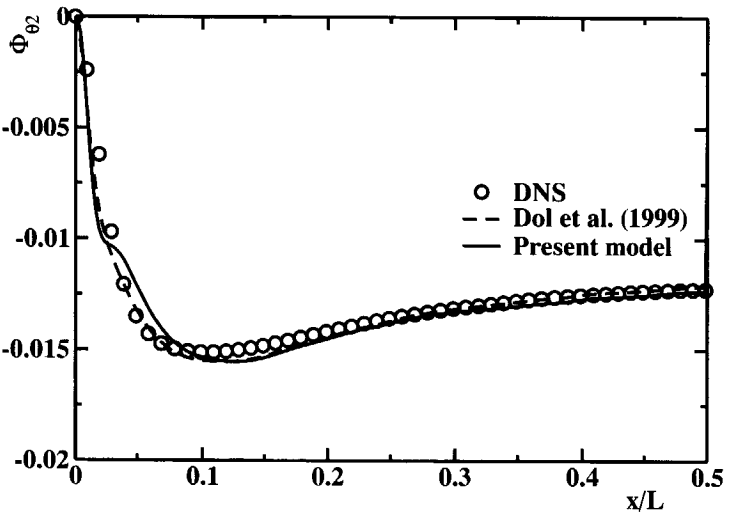

Figure 4.7: The performance of the new pressure scrambling models of horizontal (a) and vertical (b) components compared to DNS of Versteegh [101] at $Ra = 5.10^6$

with the DNS data, especially for the horizontal component. Since these term dominates the pressure scrambling, the remaining terms are less influential in affecting the whole performance. The contribution of the second term of equation (4.30) is very influential since it makes possible to reduce the growth of the pressure scrambling in region far away from the wall due to the effect of the $C_{\theta 1}$. The presence of the scalar flux invariant $A_{2\theta}$ instead of A is aimed to broaden the use of the model in other flow situations. The vertical component of the pressure scrambling also shows as good performance as the horizontal component.

4.3.2 Molecular Diffusion

In modelling the viscous diffusion, Peeters and Henkes [89] derived:

$$D^{\nu}_{\theta i} = \nu \frac{\partial^2 \overline{\theta u_i}}{\partial x_k^2} + (\alpha - \nu) \overline{u_i \frac{\partial^2 \theta}{\partial x_k^2}} + (\alpha - \nu) \overline{\frac{\partial u_i}{\partial x_k} \frac{\partial \theta}{\partial x_k}} \tag{4.38}$$

Clearly, the viscous diffusion of equation (4.38) consists of three terms, in which the first term is the most influential. In a similar manner, Dol [27] proposed the same formula for viscous diffusion. Additional modification of diffusion coefficient is required to obtain suitable value, and decomposition of α with ν is often the best choice giving the mean value $(\alpha + \nu)/2$.

4.3.3 Turbulent diffusion

The turbulent velocity diffusion represented by the triple correlation of fluctuating velocity and temperature is often modelled in similar way as the turbulent diffusion of the Reynolds stress by using invariant modelling. The turbulent diffusion is expressed :

$$\mathcal{D}^{t}_{\theta i} = \frac{\partial}{\partial x_k} \left[C_\theta \frac{k}{\varepsilon} \left(\overline{u_k u_l} \frac{\partial \overline{\theta u_i}}{\partial x_l} + \overline{u_i u_l} \frac{\partial \overline{\theta u_k}}{\partial x_l} + \overline{\theta u_l} \frac{\partial \overline{u_i u_k}}{\partial x_l} \right) \right] \tag{4.39}$$

Ideally, the triple correlation is modelled by considering its transport equation in a similar manner as in modelling the triple velocity correlation in the second moment closure. As a consequence, higher order correlations appear. In fact for most engineering flows, this diffusion contributes only a small part to the mean turbulent quantities, and therefore GGDH model is considered to be sufficient.

4.3.4 Dissipation rate of heat flux

The dissipation rate of the turbulent heat flux can usually be neglected for high Re number flow regions, but close to a solid wall it becomes significant. Several

models have been proposed in the literature. We adopt here the model of Dol *et al.* [26]:

$$-\varepsilon_{\theta i} = -f^* \varepsilon^*_{\theta i} - \varepsilon'_{\theta i} \tag{4.40}$$

where

$$-\varepsilon^*_{\theta i} = -\frac{1}{2}\left(1 + \frac{1}{Pr}\right)\frac{\varepsilon}{k}\overline{\theta u_i} \tag{4.41}$$

$$-\varepsilon'_{\theta i} = -\frac{1}{2}\mathcal{D}^{\nu}_{\theta i} + \frac{1}{4}\left(1 + \frac{1}{Pr}\right)\frac{\mathcal{D}^{\nu}_{k}}{k}\overline{\theta u_i} \tag{4.42}$$

where $f^* = exp(-3/4A^{3/2})$. The inclusion of the molecular diffusion of turbulent kinetic energy introduces the second derivative of k. However, this disadvantage has been compensated by not using any topology-dependent parameters, Dol [27].

4.4 Modelling the Equation for Thermal Variance

Dol *et al.* [26] used a model for the turbulent diffusion of the temperature variance $\overline{\theta^2}$ in the same way as for the turbulent diffusion in equation (4.39), by including the production of the triple correlation $\overline{u_i\theta^2}$. This inclusion, although of an ad hoc nature improved matching with the Direct Numerical Simulation of Versteegh [101]. In this approach the turbulent diffusion of $\overline{\theta^2}$ reads:

$$\mathcal{D}^t_{\theta} = \frac{\partial}{\partial x_k}\left[C_{\theta\theta}\tau_m\left(\overline{u_k u_l}\frac{\partial\overline{\theta^2}}{\partial x_l} + 2\overline{\theta u_l}\frac{\partial\overline{\theta u_k}}{\partial x_l} + 2\overline{\theta u_k u_l}\frac{\partial T}{\partial x_l}\right)\right] \tag{4.43}$$

The modelled term contains a triple correlation of fluctuating velocities and fluctuating temperature, and again these needs to be modelled:

$$\overline{\theta u_k u_l} = -C_{\theta\theta 2}\tau_m\left(\overline{u_k u_l}\frac{\partial\overline{\theta u_i}}{\partial x_l} + \overline{u_i u_l}\frac{\partial\overline{\theta u_k}}{\partial l}\right) \tag{4.44}$$

By omitting the last two terms, equation (4.43) reduces to GGDH model, which was used by Kenjereš [62], Peeters and Henkes [89]. The coefficient $C_{\theta\theta} = 0.22$ is adopted by most authors, with slightly different proposal by Launder [66] who chose $C_{\theta\theta}$ to be 0.11. When the last term is omitted, the most appropriate value of $C_{\theta\theta}$ is 0.11. In order to improve the performance of the model, Dol [27] replaced the mechanical time scale in equation (4.43) by the thermal time scale. However this attempt was not successful. Boudjemadi [6] modified the mechanical time scale with a lower bound of $C_T(\nu/\varepsilon)^{1/2}$, but this does not give any better result. It is worth that the proposal of the GGDH model for the turbulent diffusion of $\overline{\theta^2}$ can be adopted for both the low- and high-Reynolds number flows.

In order to close the equation for the thermal variance, it is necessary to provide its dissipation rate. Ideally, the dissipation rate ε_θ is derived as an exact

differential equation similar to the dissipation rate ε equation in standard $k-\varepsilon$ model. The transport equation for the dissipation of temperature variance can be written:

$$\frac{D\varepsilon_\theta}{Dt} = \underbrace{\frac{\partial}{\partial x_k}\left(\underbrace{\boxed{-\overline{\varepsilon_\theta u_k}}}_{\mathcal{D}^t_{\varepsilon_\theta}} + \underbrace{\alpha\frac{\partial \varepsilon_\theta}{\partial x_k}}_{\mathcal{D}^\nu_{\varepsilon_\theta}}\right)}_{\mathcal{D}_{\varepsilon_\theta}} - \underbrace{\boxed{2\alpha\overline{\frac{\partial u_k}{\partial x_l}\frac{\partial \theta}{\partial x_l}\frac{\partial \theta}{\partial x_k}}}}_{P_{\varepsilon_{\theta 4}}}$$
$$- \underbrace{\boxed{2\alpha\overline{\frac{\partial u_k}{\partial x_l}\frac{\partial \theta}{\partial x_l}\frac{\partial T}{\partial x_k}} + \overline{\frac{\partial \theta}{\partial x_k}\frac{\partial \theta}{\partial x_l}\frac{\partial U_k}{\partial x_l}} + u_k\overline{\frac{\partial \theta}{\partial x_l}\frac{\partial^2 T}{\partial x_k \partial x_l}}}}_{P_{\varepsilon_{\theta 1}} + P_{\varepsilon_{\theta 2}} + P_{\varepsilon_{\theta 3}}} - \underbrace{\boxed{2\alpha\overline{\frac{\partial^2 \theta}{\partial x_k \partial x_k}}}}_{Y_{\varepsilon_\theta}} \tag{4.45}$$

Several closure of this equation have been proposed in the past, but none seems to be sufficiently tested to be used in predicting buoyancy driven flows. The equation has twice many terms as the equation for mechanical dissipation, introducing thus many new coefficients and a lot of uncertainty. For that reason we will avoid modelling and solving differential transport equation for ε_θ and use an algebraic approximation for the ratio of thermal to mechanical time scale, from which ε_θ can be deduced. As an illustration, we show here the model equation used by Peeters and Henkes [89]:

$$\frac{D\varepsilon_\theta}{Dt} = \frac{\partial}{\partial x_k}\left(\alpha\frac{\partial \varepsilon_\theta}{\partial x_k} - \overline{u_k \varepsilon'_\theta}\right) + \left(C_{P1}\frac{P_\theta}{\overline{\theta^2}} - C_{D1}\frac{\varepsilon_\theta}{\overline{\theta^2}}\right)\varepsilon_\theta$$
$$+ \left(C_{P2}\frac{P_k}{k} - C_{D2}\frac{\varepsilon}{k}\right)\varepsilon_\theta \tag{4.46}$$

It is noted that the thermal time scale $\tau_\theta = \overline{\theta^2}/2\varepsilon_\theta$ appears in the equation above in addition to the mechanical time scale τ_m. It is obvious from equation (4.46) that the last term in the right hand side resembles its thermal counterpart represented by the second term. In order to calculate ε_θ, without solving the transport equation for ε_θ one often employs the thermal to mechanical time scale ratio R which is then expressed in terms of stress and flux invariants, or even assuming it to be a constant. This topic is discussed in more details below.

4.4.1 Thermal to mechanical time-scale ratio R

There have been a number of attempts to develop a scalar second moment closure in which the dissipation rate of temperature variance ε_θ is calculated from the thermal to mechanical time scale ratio R. This approach is relatively simple as compared to modelling and solving the transport equation of ε_θ. The

dimensionless quantity of R is defined:

$$R = \frac{\tau_\theta}{\tau_m} \tag{4.47}$$

where $\tau_\theta = \overline{\theta^2}/2\varepsilon_\theta$ is the thermal time scale and $\tau_m = k/\varepsilon$ is the mechanical time scale. The turbulence quantities k, ε, and $\overline{\theta^2}$ are solved from their transport equations, while R is either expressed as a function of turbulent stress and flux invariants, or is set as a constant from experimental or DNS data. For forced convection Craft [16] expressed R as a function of the scalar flux invariant $A_{2\theta}$.

$$R = \frac{1}{1.5(1 + A_{2\theta})} \tag{4.48}$$

Equation (4.48) was applied in calculation of heat transfer in an inhomogeneous plane and axisymmetry jets. The use of the scalar flux invariant $A_{2\theta}$ helped to increase the value of R as required in the buoyant plumes.

In turbulent natural convective flow heated from the side, R is almost constant in the region not so close to a solid wall, with a relatively strong peak observed very close to the wall. DNS data indicate that R increases with a decrease in Rayleigh number, for example at $Ra = 5.4 \times 10^5$ $(x/L > 0.1)$ R is about 0.5, while that at $Ra = 5 \times 10^6$ R is around 0.4. In addition, the spike of R is smaller as the wall is approached with an increase in the Rayleigh number. Dol [27] proposed an analytical formula for the thermal to mechanical time scale ratio R, which reflects this behaviour:

$$R = min\left(2.2Ra_t^{-0.13}, 0.75\right) \tag{4.49}$$

where $Ra_t = g\beta(\overline{\theta^2})^{1/2}k^{9/2}Pr/(\nu^2\varepsilon^3)$ is the turbulent Rayleigh number. Indeed, no universal constant value of R is expected in all turbulent flows. It is therefore instructive to express R by relating it to scalar and stress invariants in order to define a more general formulation. While it is true that dissipation rate of temperature variance is not the weakest point in turbulent closure, resolving the transport equation for ε_θ shows a reasonable improvement of the turbulent thermal field, Kenjereš [62]. It is clear that R is not constant in the entire region, and therefore solving ε_θ makes it possible to mimic the behaviour of R, especially in near wall region where it shows a peak value.

We propose here the following model of R:

$$R = max\left[\left(\frac{A_2^{1/2}}{(1 + A_{2\theta})}\right), 0.6A\right] \tag{4.50}$$

The performance of the model equation (4.50) is shown if Fig.(4.8)a for a side-heated cavity and in Fig.(4.8)b for a cavity heated from below. In the same

a.

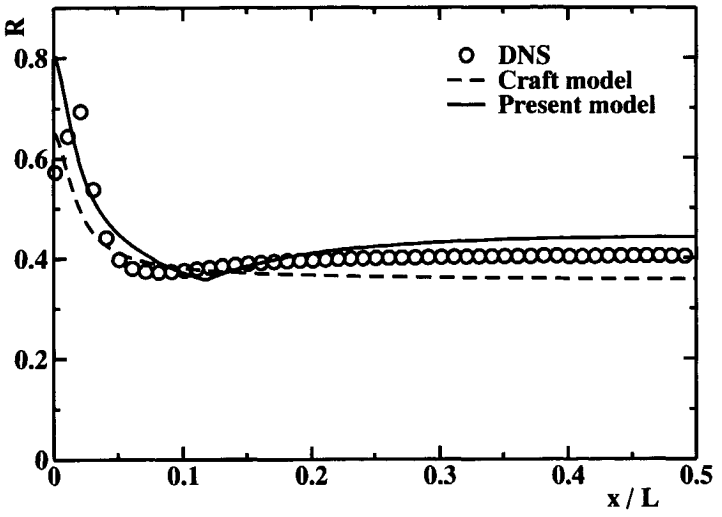

b.

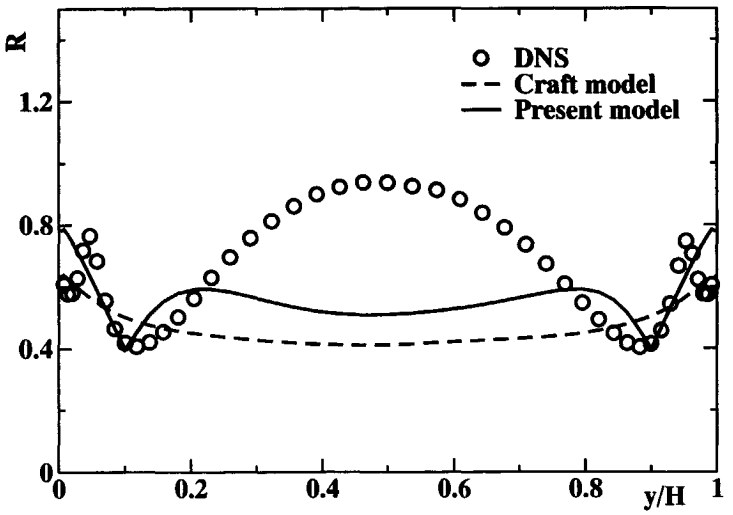

Figure 4.8: The thermal to mechanical time scale ratio R of a side-heated infinite vertical channel (a) at $Ra = 5.0 \times 10^6$ (Versteegh[101]) and a heated from below (b) infinite horizontal channel at $Ra = 6.3 \times 10^5$ (Wöerner [104])

figures, the model of Craft [16] is also presented. The wall value of R of the model of Craft [16] provides a satisfactory requirement to viscous effect, i.e. it yields approximately the value of Prandlt number, $R = 0.71$ (for air). On the other hand, the proposed model predicted a slightly higher Pr at the boundary. However, it can be seen that the new model predicts better the peaks in the near wall region for both cases. For region far away from the wall, the model corresponds to DNS only for side-heated cavity, while for heating from below it is underpredicted.

4.4.2 A priori test of the model

The DNS database of Versteegh [101] for natural convection in vertical channel at $Ra = 5.0 \times 10^6$ is used to perform a priori tests of the new model. Figures (4.9)a-b show results of a priori test for the side-heated tall cavity compared with DNS of Versteegh [101] and also with Dol [27], as well as with the basic model. The basic model refers to equation (4.25) for the slow term of pressure scrambling. The figures clearly show good agreement between the new model and DNS. This is as expected, because the pressure scrambling is well predicted by the model and the remaining parts are taken from the DNS. On the other hand, the basic model obviously fail to predict the DNS. The main cause for discrepancy lies in the linear model of the slow term as well as in the coefficient $C_{\theta 1}$. As explained in the previous section, it is impossible to reproduce DNS by simply changing the value of the coefficient $C_{\theta 1}$.

In the case of turbulent natural convection heated from below Rayleigh-Bénard convection the calculation is conducted at Rayleigh number $Ra = 6.3 \times 10^5$, to match the DNS data of Wörner [104]. The heat flux profile of a priori test using the new model, Dol model and the basic model are plotted against DNS in Fig.(4.10). It is evident that the basic model overpredicted the heat flux in the near wall region and this mainly due to the coefficient $C_{\theta 1}$ which is much lower than implied by the DNS. Similar disagreement is observed in Dol [27] model. This disagreement is attributed to the use of the stress invariant A in the coefficient $C_{\theta 1}$, $C'_{\theta 1}$, and $C_{\theta 2}$. The proposed model shows a considerable improvement as compared to the previous models. In the near wall region the new model yields some overpredictions, while in the far-wall region it gives a slightly lower value. The success of the new model is mainly attributed to the introduction of the second term in the slow part. The use of the new coefficient $C_{\theta 1}$ has also improved the performance of the models.

a.

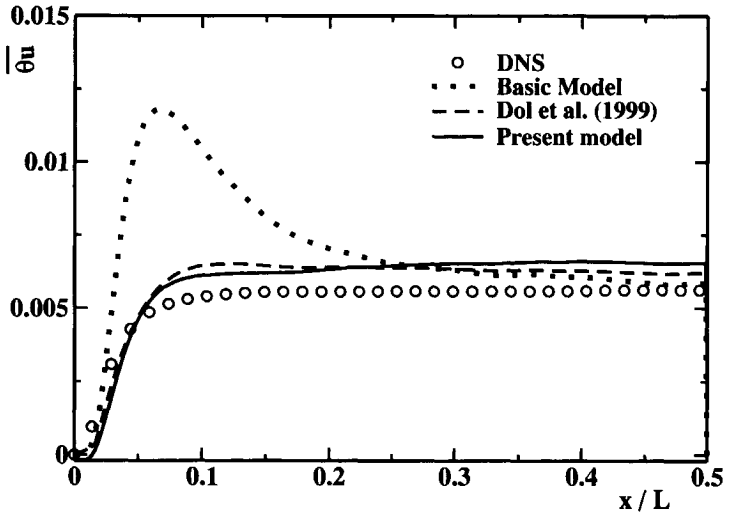

b.

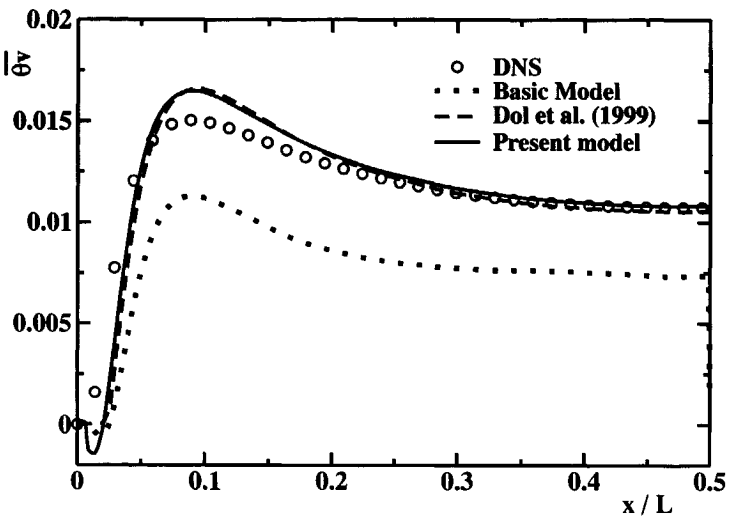

Figure 4.9: The profiles of $\overline{\theta u}$ (a) and $\overline{\theta v}$ (b) in a side-heated infinite cavity at $Ra = 5.0 \times 10^6$ of Versteegh [101]

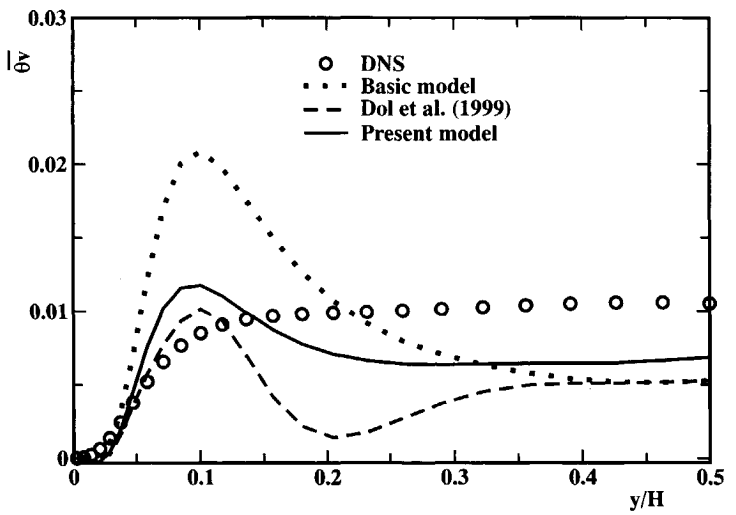

Figure 4.10: The profiles of $\overline{\theta v}$ in a heated from below horizontal cavity at $Ra = 6.3 \times 10^5$ of Wöerner [104]

.

4.5 Elliptic Relaxation

The modifications of fluid flow and turbulence in the vicinity of a solid wall comes from several effects that have different physical origin. Very close to the wall in the viscous sublayer (which is present irrespective of the bulk Reynolds number) the dominant effect comes from viscosity. However, the impermeability of a solid wall causes non-viscous blocking effect that damps the fluid velocity and its fluctuations, especially in the direction normal to the wall. That is why the wall-normal turbulent stress is mush smaller than the stream wise and span wise ones, not only very close to the wall, but also in the turbulent wall region which is much thicker than the viscous sublayer.

In most near-wall modifications of turbulence closures these two effects are modelled jointly, by introducing one or more damping functions in terms of non-dimensional wall distance, or in terms of turbulence Reynolds number $Re_t = k^2/(\nu\varepsilon)$. The best known damping function is $f_\mu = f(Re_t)$ in the expression for eddy viscosity, $\nu_t = C_\mu f_\mu k^2/\varepsilon$ in the so called "low-Re-number" $k-\varepsilon$ and similar eddy-viscosity models. It is obvious that such functions cannot capture the non-viscous wall-blocking effects, but nevertheless these models have proved reasonably successful in some simpler flows, thanks mostly to the fortunate variation of Re_t and other nondimensional parameters that increase with the distance from a wall, making it suitable to mimic the diminishing wall effects in terms of this parameter.

In second-moment closures where the reproduction of stress anisotropy close to the wall is essential for predicting wall-related phenomena-friction and heat transfer, the use of simple damping functions has not been successful. Instead, the wall-blockage effects has been modelled by introducing "wall reflection" modifications of the pressure-redistribution terms, such as given by expressions (4.5)-(4.7) and (4.36) in Reynolds stress equation and in pressure - temperature-gradient correlation of turbulent heat flux equation. Generally, such near-wall treatment has proved successful in predicting wall-attached flows, and with some modifications also in other flow types. However, the major shortcomings is the lack of physical foundation: the models have been derived intuitively using assumptions of quasi-homogeneity of velocity field, which is far from truth in the near-wall region, Bradshaw *et al.* [8]. The other deficiency is the need to use wall-normal unit vectors to distinguish between the wall-normal and other stress and flux components. This shortcoming is especially serious if flow with complex geometry are considered.

In order to account for the physics of the wall-blocking effect, which has an elliptic character, Durbin [28] proposed to relate the redistributive tensor with the elliptic effect. Because this effect primarily blocks the wall-normal velocity, Durbin proposed to solve a separate transport equation for a scalar quantity - another velocity scale (called "$\overline{v^2}$") directly derived from the transport equation of the wall-normal Reynolds stress, and which effectively reduces to this stress

component close to a solid wall (equation (4.53)). This equation is closed by an elliptic relaxation equation for the elliptic function f. Unlike conventional way of formulating the non-viscous wall effect by using the unit wall normal for turbulence properties, the wall effect thus is accounted for by the following:(i) through boundary conditions for $\overline{v^2}$ and f (ii) the model relaxes to quasi-homogeneous behaviour in far-wall region (iii) the effect then enters via solution of the governing equations.

The elliptic relaxation eddy viscosity model ($k-\varepsilon-\overline{v^2}-f-\overline{\theta^2}$) is formulated in the following way. First, instead of conventional expression, the eddy viscosity is defined as:

$$\nu_t = C_\mu^D \overline{v^2} T \tag{4.51}$$

where $C_\mu^D = 0.22$, instead of classical value $C_\mu = 0.09$ and the time scale T is defined as

$$T = max\left[\frac{k}{\varepsilon}, C_T\left(\frac{\nu}{\varepsilon}\right)^{1/2}\right] \tag{4.52}$$

where $C_T = 6$ is a model constant, which is an insensitive parameter and therefore variation of its value gives no appreciable affect on model. In the near wall-region where turbulent kinetic energy is very small the time scale T is bounded by the Kolmogorov time scale $6(\nu/\varepsilon)^{1/2}$ (the low bound of equation (4.52)). On the other hand, in the region far away from the wall, the contribution due to molecular effect is negligible and T takes the standard form k/ε. In addition, the function of the Kolmogorov time scale is to avoid a singularity in the source term of the dissipation rate equation.

Next, a transport equation for a scalar velocity scale $\overline{v^2}$ is formulated and modelled, based on the model-transport equation for the wall-normal Reynolds stress:

$$\frac{\partial \overline{v^2}}{\partial t} + U_j \frac{\partial \overline{v^2}}{\partial x_j} = P_{22} + G_{22} + \Phi_{22} + \frac{\partial}{\partial x_j}\Big((\nu + \frac{\nu_t}{\sigma_{\overline{v^2}}})\frac{\partial \overline{v^2}}{\partial x_j}\Big) - \varepsilon_{22} \tag{4.53}$$

Durbin proposed to split the dissipation ε_{22} into $\varepsilon_{22} - \varepsilon\overline{v^2}/k$ and $\varepsilon\overline{v^2}/k$, the former is lumped together with the pressure-strain term and modified by the elliptic relaxation effect, and the later is left as the destruction term.

$$\frac{\partial \overline{v^2}}{\partial t} + U_j \frac{\partial \overline{v^2}}{\partial x_j} = \Big(\Phi_{22} - \varepsilon_{22} + \varepsilon\frac{\overline{v^2}}{k}\Big) - \varepsilon\frac{\overline{v^2}}{k} + \frac{\partial}{\partial x_j}\Big((\nu + \frac{\nu_t}{\sigma_{\overline{v^2}}})\frac{\partial \overline{v^2}}{\partial x_j}\Big) \tag{4.54}$$

In order to account the wall effect, the first three terms on the right hand side are expressed as a function of the elliptic relaxation function kf, and equation (4.54) becomes

$$\frac{\partial \overline{v^2}}{\partial t} + U_j \frac{\partial \overline{v^2}}{\partial x_j} = kf - \varepsilon \frac{\overline{v^2}}{k} + \frac{\partial}{\partial x_j}\left((\nu + \frac{\nu_t}{\sigma_{\overline{v^2}}})\frac{\partial \overline{v^2}}{\partial x_j}\right) \tag{4.55}$$

This equation is closed with the conventional k and ε equations. In addition, an elliptic relaxation equation is solved for the elliptic function f:

$$f - L^2 \frac{\partial^2 f}{\partial x_j \partial x_j} = \frac{1}{k}\left(\Phi_{22}^h + \varepsilon \frac{\overline{v^2}}{k} - \frac{2}{3}\varepsilon\right) \tag{4.56}$$

Clearly, the homogeneous source term $(\varepsilon\overline{v^2}/k - 2/3\varepsilon)/k$ of equation (4.56) is added into the Φ_{22}^h to which the equation reduces in a homogeneous field. The source term Φ_{22}^h is then given by the slow $\Phi_{22,1}$, rapid $\Phi_{22,2}$ and buoyant $\Phi_{22,3}$ terms. Any model of the pressure strain term can be used for the homogeneous contribution. For example, by adopting the simple return to isotropy model of Rotta[94] and model of Naot *et al.* [81] for the rapid part with added buoyancy contribution, the equation for the elliptic relaxation function f reads:

$$f - L^2 \frac{\partial^2 f}{\partial x_j \partial x_j} = (C_1 - 1)\frac{\left(\frac{2}{3} - \frac{\overline{v^2}}{k}\right)}{T} + C_2 \frac{P + G}{k} \tag{4.57}$$

where L is the length scale that uses the Kolmogorov scale as a lower bound to prevent from going to zero at wall. Moreover, the length scale L makes the elliptic relaxation function f to relax to the value which correspond to homogeneous state away from the wall. By using the same approach as for the time scale, the length scale is expressed as:

$$L = C_L max\left[\frac{k^{3/2}}{\epsilon}, C_\eta\left(\frac{\nu^3}{\epsilon}\right)^{1/4}\right] \tag{4.58}$$

The low bound of equation (4.58) is significant only in the near wall region - though extending further from the wall than the low bound time scale (which has been recognized as an inconsistency of the Durbin model), while the first part dominates in the region far from a boundary. The boundary condition of f reads:

$$f_{wall} = -20\frac{\nu^2}{\varepsilon_{wall}}\frac{\overline{v^2}}{x_n^4} \tag{4.59}$$

where x_n is the direction normal to the wall, and ε_{wall} is the boundary condition for the energy dissipation rate at the wall. It can be seen that f_{wall} goes with $(1/x_n^4)$ and, as a consequence, it can cause numerical instabilities when a fine mesh is applied in the near wall region. Lien and Kalitzin [74] introduced a modification of the standard model. The way the standard model is modified is by splitting ε_{22} into $\varepsilon_{22} + n\varepsilon\overline{v^2}/k$ and $-n\varepsilon\overline{v^2}/k$. With this modification, the coefficient of $-\varepsilon\overline{v^2}/k$ in equation (4.54) becomes n, while equation (4.57) becomes:

a.

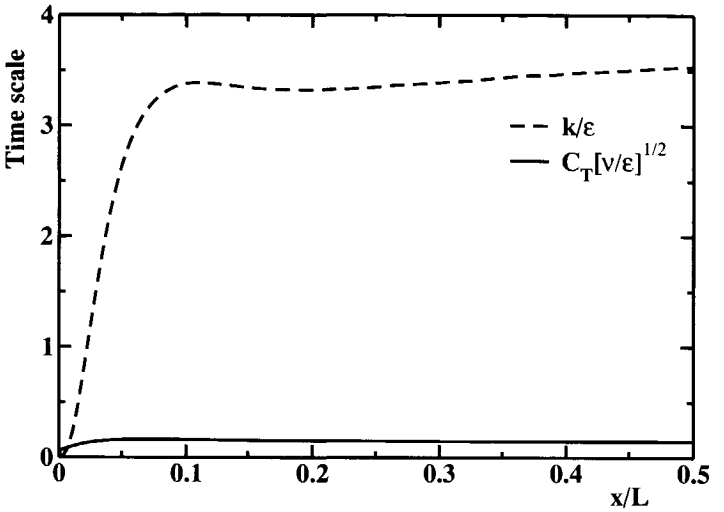

b.

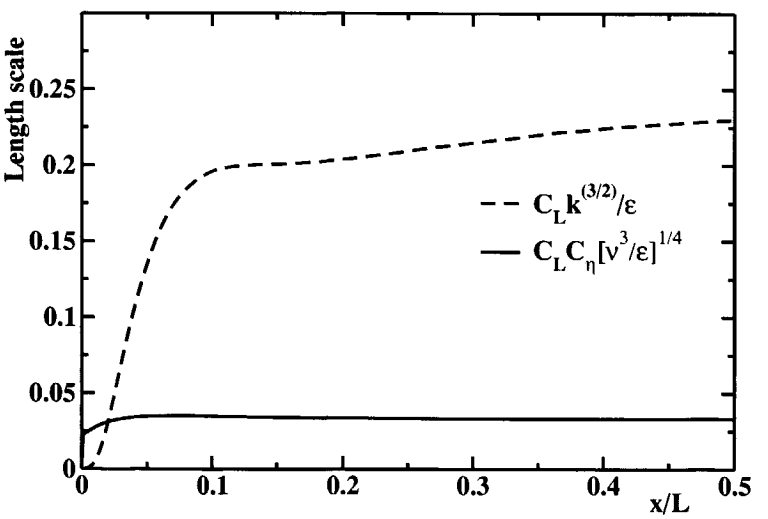

Figure 4.11: The time scale T (a) and length scale L (b) of the side-heated vertical channel at $Ra = 5.10^6$

$$f - L^2 \frac{\partial^2 f}{\partial x_j \partial x_j} = (n - C_1)\frac{\overline{v^2}}{k} + (1 - C_1)\frac{2}{3} + C_2 \frac{P + G}{k} \tag{4.60}$$

When $n = 6$ the boundary condition is $f = 0$.

The dissipation equation used is essentially the standard one, except for the time-scale switching and some modification of the coefficients. It can be written as

$$\frac{\partial \varepsilon}{\partial t} + U_j \frac{\partial \varepsilon}{\partial x_j} = \frac{C_{\varepsilon_1}(P + G) - C_{\varepsilon 2}\varepsilon}{T} + \frac{\partial}{\partial x_j}\left[\left(\nu + \frac{\nu_t}{\sigma_\varepsilon}\right)\frac{\partial \varepsilon}{\partial x_j}\right] \tag{4.61}$$

where the production term in equations (4.61) and (4.67) is given by:

$$P = \nu_t \left(\frac{\partial U_i}{\partial x_j} + \frac{\partial U_j}{\partial x_i}\right)\frac{\partial U_j}{\partial x_i} \tag{4.62}$$

The boundary condition for ε reads:

$$\varepsilon_{wall} = \nu \left(\frac{\partial^2 k}{\partial x_n^2}\right)_{wall} \tag{4.63}$$

To account for the nonequilibrium in the near wall region Durbin [29] suggested to modify the coefficient C_{ε_1} as a function of P/ε.

$$C_{\varepsilon_1} = 1.44\left[1 + 0.1\left(P\right)/\varepsilon\right] \tag{4.64}$$

or in an alternative form as:

$$C_{\varepsilon_1} = 1.3 + \frac{0.25}{[1 + (d/2L)^8]} \tag{4.65}$$

where d is the distance from the closest boundary and L is the length scale. The function of d/L was calibrated such that in attached boundary layers C_{ε_1} equals to 1.55, while in far-from-the-wall region is equal to 1.3. The coefficient C_{ε_1} is expressed in different manner by Manceau [77], namely as $k/\overline{v^2}$. The introduction of this functional form is aimed to enhance the generation of the ε close to the wall. The coefficient reads:

$$C_{\varepsilon_1} = 1.44\left(1 + 0.045(k/\overline{v^2})^{1/2}\right) \tag{4.66}$$

In this work, we extended the coefficient by including buoyancy production. The new coefficient can be written as:

$$C_{\varepsilon_1} = 1.44\left[1 + 0.1\left(P + G\right)/\varepsilon\right] \tag{4.67}$$

One important feature of the extended coefficient is its dependence to both shear and buoyant productions. A summary of the coefficients is given in Table 4.2

Coefficients							
C_1	C_2	$C_{\varepsilon 2}$	C_μ	C_T	C_L	C_η	C_θ^*
1.4	0.6	1.9	0.22	6	0.2	50	0.49

Table 4.2: The coefficients used in the proposed model

In order to calculate the heat flux, it is necessary to provide Reynolds stress components. Here, the buoyancy extended eddy viscosity model is used.

$$\overline{u_i u_j} = \frac{2}{3}k\delta_{ij} - \mu_t\left(\frac{\partial U_i}{\partial x_j} + \frac{\partial U_j}{\partial x_i}\right) + C_\theta \tau \beta\left(g_i\overline{\theta u_j} + g_j\overline{\theta u_i}\right) \tag{4.68}$$

The inclusion of the buoyancy in equation (4.68) is essential for flows driven or affected by buoyancy.

The turbulent heat flux is calculated using an algebraic flux model:

$$\overline{\theta u_i} = -C_\theta \tau\left[\overline{u_i u_j}\frac{\partial T}{\partial x_j} + \xi\overline{\theta u_j}\frac{\partial U_i}{\partial x_j} + \eta g_i \beta\overline{\theta^2}\right] \tag{4.69}$$

where where τ is the time scale, for which several options have been considered.

4.5.1 The choice of the time scale

The time scale τ that appears in equation (4.69) is an important parameter by which turbulent heat flux is calculated. From an *a priori* analysis of natural convection in an infinite vertical channel heated from the side, the AFM given by equation (4.69) with $\tau = k/\varepsilon$ yields an overprediction in the normal heat flux. This overprediction is mainly attributed to the normal Reynolds stress $\overline{uu}$, regardless whether it is expressed by eddy viscosity or by algebraic expression. It is recalled that the eddy viscosity expression yields in this case $\overline{uu} = 2/3k$. Although the eddy viscosity model is extended by accounting the buoyancy effect, it does not improve the performance since for the horizontal component the gravity effect is zero. This value, $2/3k$ is too large for $\overline{uu}$, especially in the near wall region. Similarly, when the normal stress is expressed in the algebraic form, the result is even larger, since the productions gives rise to $\overline{uu}$.

Several attempts have been made in order to capture the DNS performance of the normal heat flux. Firstly, the focus of modification is given to the coefficient C_θ. Although C_θ can be modified to predict well the normal heat flux, this approach is not appropriate since the required value of this coefficient is too small and this will negatively affect the other components of the heat flux.

The second possibility is to express $\overline{uu}$ in terms of $\overline{v^2}$. The reduction from $2/3k$ to $\overline{v^2}$ significantly improves the performance of the normal heat flux. However,

this approach is inappropriate not only because it leads to tensorial inconsistency of the equation but also because $\overline{uu}$ could be associated with $\overline{v^2}$ only when the flow is one-dimensional, while in the two and three-dimensional cavities they are quite different. For those reasons it was found necessary to perform further alternative approach. The solution was sought in the approach similar to that of Durbin [28] in modifying the new turbulent viscosity through the introduction of a new coefficient C_μ and replacement of k with $\overline{v^2}$. Here, a new function is introduced:

$$f_\tau = \frac{C_\mu^D k\overline{v^2}/\varepsilon}{C_\mu k^2/\varepsilon} \tag{4.70}$$

where $C_\mu^D = 0.22$ and $C_\mu = 0.09$ are coefficients proposed by Durbin [28] and the standard one, respectively. Basically, equation (4.70) is the ratio between the eddy viscosity ν_t of Durbin [28] and ν_t of the standard EVM. The coefficient in the equation can be replaced by $C_\mu^D/C_\mu = 2.44$. The introduction of the new damping function f_τ in equation (4.70) gives:

$$\overline{\theta u_i} = -f_\tau C_\theta \tau \left[\overline{u_i u_j}\frac{\partial T}{\partial x_j} + \xi\overline{\theta u_j}\frac{\partial U_i}{\partial x_j} + \eta g_i \beta\overline{\theta^2}\right] \tag{4.71}$$

where $f_\tau C_\theta \tau = \tau^* = 0.49\overline{v^2}/\varepsilon$ and this is regarded as the new time scale. The final heat flux expression reads:

$$\overline{\theta u_i} = -\tau^* \left[\overline{u_i u_j}\frac{\partial T}{\partial x_j} + \xi\overline{\theta u_j}\frac{\partial U_i}{\partial x_j} + \eta g_i \beta\overline{\theta^2}\right] \tag{4.72}$$

where $\tau^* = C_\theta^*\overline{v^2}/\varepsilon$ with $C_\theta^* = C_\theta C_\mu^D/C_\mu$.

At first, this new time scale is difficult to assign a physical meaning. However, the expression is correct mathematically, and essentially is consistent with the approach used by Durbin in arriving to his turbulent viscosity ν_t. In addition, from a priori test in calculating the normal heat flux in a vertical infinite cavity, it shows that this new time scale gives much better result than the classical time scale. Note that the same time scale τ^* in the third term of equation (4.68) yields better results.

A priory analysis of the new Algebraic Flux Model

Figure(4.12) show a priori analysis of heat flux using SGDH,GGDH, and AFM with different time scales. The difference between the models is illustrated in Table 4.3-4.4 where full terms in the AFM expression are given. Of course the SSGH and GGDH do not contain any other terms. This analysis is aimed at choosing the appropriate model that will predict with acceptable accuracy heat flux in both generic test cases: the turbulent natural convection in infinite vertical and horizontal cavities. It is obvious that GGDH model failed not only in the

vertical component which, in contrast to reality, is predicted zero, but also in the normal component which is severely overpredicted, especially in the region around $x/L = 0.075$ to 0.1. This failure on the normal component is mainly attributed to turbulent kinetic energy k, which is too large for this formulation. When Durbin's approach is applied into GGDH by simply changing $C_\mu^S k$ with $C_\mu \overline{v^2}$, a better performance is achieved. On the other hand, calculation using AFM gives a substantial improvement as compared to that of using GGDH. Although the normal heat flux is still overpredicted, the shape of the vertical component is considerably captured. Reasonable improvement is observed when the damping function is applied in AFM. The function is able to damp the overprediction of the normal heat flux. As can be seen from Fig.(4.12), perfect agreement is observed in the normal component with slightly discrepancy in the near wall region. Similarly, the model performs a fairly well in the natural convection heated from below of Fig.(4.13).

4.5.2 Conclusions

In this chapter second-moment closures for $\overline{u_i u_j}$ and $\overline{\theta u_i}$ have been developed. A priori testing is performed first, using DNS data for turbulent natural convection in the differentially heated vertically or horizontally oriented infinite channels. In addition, simplifications of parent transport equations for $\overline{u_i u_j}$ and $\overline{\theta u_i}$ resulted in their algebraic formulations. Both variants of model showed good agreement with the available DNS data. Despite these performances, the second-moment closures still posses mathematically complex forms with many empirical coefficients.

In order to simplify turbulence model, the elliptic relaxation method, previously developed for pressure-driven flows (Durbin [28]), has been extended with buoyancy effects. Several time scales which appear in the algebraic flux equation are extensively tested using a priori analysis. It has been found that $\overline{v^2}/\varepsilon$ is the best definition of time scale. Finally, the new 5-equation model ($k-\varepsilon-\overline{v^2}-f-\overline{\theta^2}$) is proposed as the best compromise between mathematical complexity and numerical behaviour.

a.

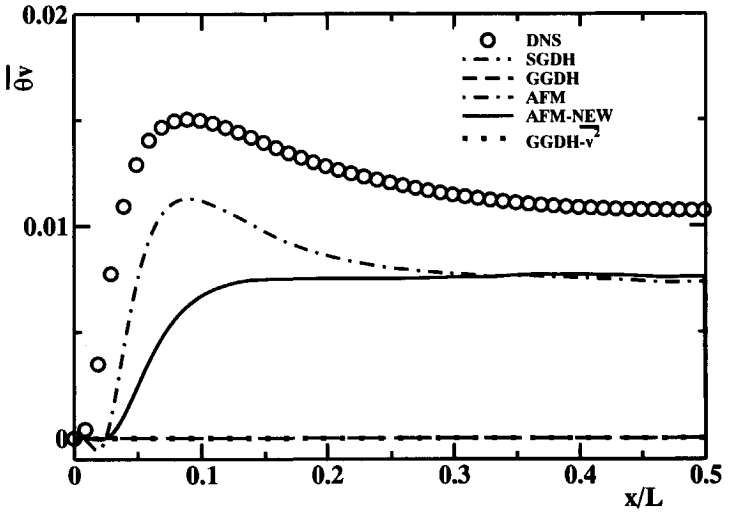

b.

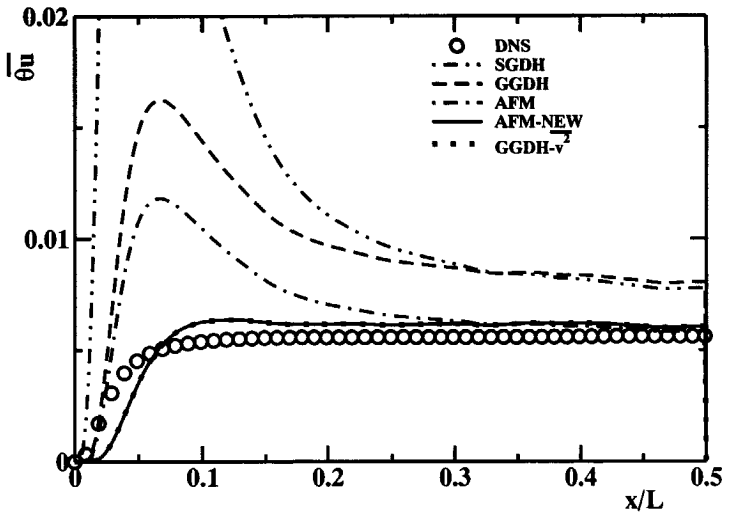

Figure 4.12: A priory test of vertical (a) and horizontal (b) heat flux against DNS of Versteegh [101] of different time scales in AFM at $Ra = 5.10^6$

Model	$\overline{\theta u_i}$	$\overline{\theta u}$ *(horizontal comp.)*	$\overline{\theta v}$ *(vertical comp.)*
$SGDH$	$-\frac{C_\mu}{Pr_t}\frac{k^2}{\varepsilon}\frac{\partial T}{\partial x_i}$	$-\frac{C_\mu}{Pr_t}\frac{k^2}{\varepsilon}\frac{\partial T}{\partial x}$	0
$GGDH$	$-\frac{C_\mu^D}{Pr_t}\frac{k\overline{v^2}}{\varepsilon}\frac{\partial T}{\partial x_i}$	$-\frac{C_\mu^D}{Pr_t}\frac{k\overline{v^2}}{\varepsilon}\frac{\partial T}{\partial x}$	0
AFM	$-C_\theta\frac{k}{\varepsilon}\left(\overline{u_iu_j}\frac{\partial T}{\partial x_j}+\xi\overline{\theta u_j}\frac{\partial U_i}{\partial x_j}+\eta\beta g_i\overline{\theta^2}\right)$	$-C_\theta\frac{k}{\varepsilon}\overline{uu}\frac{\partial T}{\partial x}$	$-C_\theta\frac{k}{\varepsilon}\left(\overline{uv}\frac{\partial T}{\partial x}+\xi\overline{\theta v}\frac{\partial V}{\partial x}+\eta\beta g\overline{\theta^2}\right)$
$AFM-NEW$	$-C_\theta^*\frac{\overline{v^2}}{\varepsilon}\left(\overline{u_iu_j}\frac{\partial T}{\partial x_j}+\xi\overline{\theta u_j}\frac{\partial U_i}{\partial x_j}+\eta\beta g_i\overline{\theta^2}\right)$	$-C_\theta^*\frac{\overline{v^2}}{\varepsilon}\overline{uu}\frac{\partial T}{\partial x}$	$-C_\theta^*\frac{\overline{v^2}}{\varepsilon}\left(\overline{uv}\frac{\partial T}{\partial x}+\xi\overline{\theta v}\frac{\partial V}{\partial x}+\eta\beta g\overline{\theta^2}\right)$
$GGDH-\overline{v^2}$	$-C_\theta^*\frac{\overline{v^2}}{\varepsilon}\overline{v^2}\frac{\partial T}{\partial x_i}$	$-C_\theta^*\frac{\overline{v^2}}{\varepsilon}\overline{v^2}\frac{\partial T}{\partial x}$	0

Table 4.3: The final expression for heat flux components resulting from different time scale proposals for the side-heated infinite channel flow.

Model	$\overline{\theta u_i}$	$\overline{\theta v}$ *(vertical component)*
$SGDH$	$-\frac{C_\mu}{Pr_t}\frac{k^2}{\varepsilon}\frac{\partial T}{\partial x_i}$	$-\frac{C_\mu}{Pr_t}\frac{k^2}{\varepsilon}\frac{\partial T}{\partial x_2}$
$GGDH$	$-\frac{C_\mu^D}{Pr_t}\frac{k\overline{v^2}}{\varepsilon}\frac{\partial T}{\partial x_i}$	$-\frac{C_\mu^D}{Pr_t}\frac{k\overline{v^2}}{\varepsilon}\frac{\partial T}{\partial x_2}$
AFM	$-C_\theta\frac{k}{\varepsilon}\left(\overline{u_iu_j}\frac{\partial T}{\partial x_j}+\xi\overline{\theta u_j}\frac{\partial U_i}{\partial x_j}+\eta\beta g_i\overline{\theta^2}\right)$	$-C_\theta\frac{k}{\varepsilon}\left(\overline{vv}\frac{\partial T}{\partial x_2}+\eta\beta g\overline{\theta^2}\right)$
$AFM-NEW$	$-C_\theta^*\frac{\overline{v^2}}{\varepsilon}\left(\overline{u_iu_j}\frac{\partial T}{\partial x_j}+\xi\overline{\theta u_j}\frac{\partial U_i}{\partial x_j}+\eta\beta g_i\overline{\theta^2}\right)$	$-C_\theta^*\frac{\overline{v^2}}{\varepsilon}\left(\overline{vv}\frac{\partial T}{\partial x_2}+\eta\beta g\overline{\theta^2}\right)$
$GGDH-\overline{v^2}$	$-C_\theta^*\frac{\overline{v^2}}{\varepsilon}\overline{v^2}\frac{\partial T}{\partial x_i}$	$-C_\theta^*\frac{\overline{v^2}}{\varepsilon}\overline{v^2}\frac{\partial T}{\partial x_2}$

Table 4.4: The final expression for heat flux components resulting from different time scale proposals for the heated from below infinite channel flow.

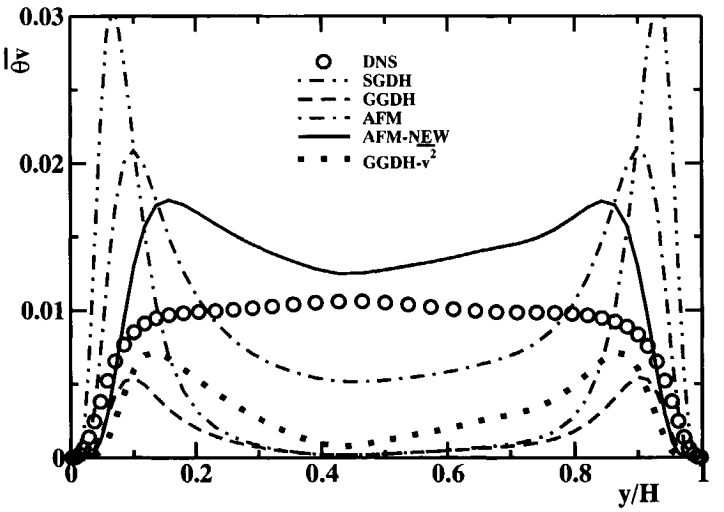

Figure 4.13: A priory test of heat flux against DNS Wöerner [104] of different time scales in AFM at $Ra = 6.3 \times 10^6$

CHAPTER 5

Numerical method

5.1 Introduction

Computational fluid dynamics is an approximate method for solving governing equations in order to obtain a numerical description of fluid flow and heat transfer of interest. There are several steps to perform such a computation. These includes pre-processing (grid generation), processing (calculation), and post-processing tasks (data analysis and visualisation). Since the main task of this study was development and validation of turbulent models, numerical method will be just briefly mentioned.

This chapter gives a general overview of the numerical method used in the current study. The discussion of control volume method and collocated grid arrangement together with differencing schemes is presented. A benchmark application of accepted numerical method in an unsteady laminar convection in cubical enclosures is presented in order to demonstrate the accuracy of the method.

5.2 Control volume method

In principle, the physical aspects of any fluid flow are described by three fundamental conservation equations: mass, momentum and energy. The general form of the conservation equations read:

$$\frac{\partial}{\partial \tau}(\rho\Phi) + div\,(\rho\vec{u}\Phi - \rho\Gamma_\Phi \nabla\Phi) = S_\Phi \tag{5.1}$$

where Γ_Φ is a diffusion coefficient, while Φ could represent an actual scalar, for example temperature; or it could be a vector such as velocity or heat flux; or a tensor for example Reynolds stress, and S_Φ denotes a source term. Since finite volume method is used in this computation, equation(5.1) needs to be integrated over control volume. By applying the Gauss-Ostrogradski theorem:

$$\int_V div\Phi dV = \int_A \Phi dA \tag{5.2}$$

the integral form of a general conservation law can be expressed in the following form:

$$\underbrace{\frac{\partial}{\partial t}\int_V \rho\Phi dV}_{unsteady} + \underbrace{\int_A \rho\vec{u}\Phi\vec{i}dA}_{convection} - \underbrace{\int_A \rho\Gamma_\Phi \nabla\Phi\vec{i}dA}_{diffusion} = \underbrace{\int_V S_\Phi dV}_{source} \tag{5.3}$$

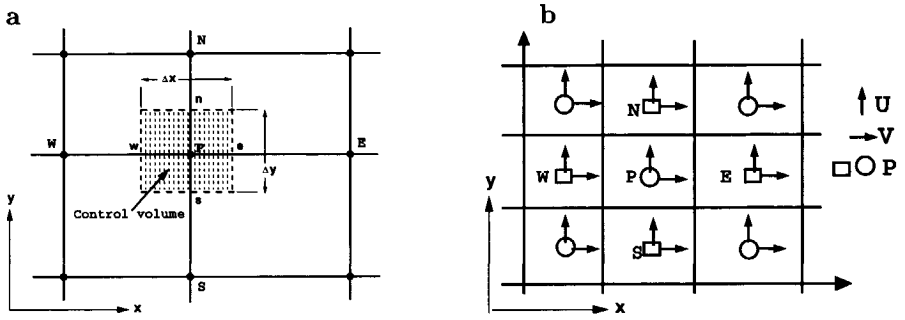

Figure 5.1: Two-dimensional control volume configuration (a) and collocated grid (b).

As an example, a two-dimensional control volume configuration is shown in Fig. (5.1) a. The rectangular dashed line shows one control volume at grid point P. Points W and E are the x-direction neighbors at west and east, respectively. While points S and N are the y-direction neighbors at south and north, respectively. The solution domain is subdivided into a finite number of control volumes by a numerical grid, within which the integration is carried out. Computational nodes at which the variable values are to be calculated are placed at the geometric center of each control volume. The advantage of control volume approach is that it keeps conservative properties of discretised variables. Moreover, implementation of boundary condition is relatively easy. Additional discussions of the control volume method in computation can be found in the literature, for example Ferziger and Perić [33].

Discretisation of the governing equations are often conducted using two popular approaches: collocated and staggered grids. Figure (5.1) b shows the collocated grid configuration, at which the quantities are located at the same center point of the grid. The obvious advantage of this arrangement is due to the fact that only a single control volume is used for all equations, and only a single set of grid metric is required. For complex grid systems, collocated arrangement is therefore preferable. Discussion on the advantages and disadvantages of using collocated and staggered grids in computation is given by Perić [90], Wesseling [103].

There have been several differencing schemes that are often used in turbulent numerical simulation, for example central differencing scheme (CDS), upwind differencing scheme (UDS), linear upwind differencing scheme (LUDS), quadratic upwind differencing scheme (QUDS), and total variation diminishing scheme (TVD). It is well recognised that any simulation should employ at least a scheme of second order in order to obtain good computation result. Examples of second order scheme are LUDS, QUDS or QUICK, and CDS. In this study, upwind scheme is used (for steady state flow) only at the beginning of calculation, be-

cause it exhibits computational stability. At convergence stage, all calculation is done using LUDS. For unsteady state flow, LUDS or QUICK is used from the beginning of calculation.

5.3 Discretisation procedure

The discretised form of equation(5.3) consists of four terms: unsteady rate of change, convection, diffusion, and source. The principle of their discretisation are given next.

Unsteady term

In this study, calculation of the unsteady term is conducted by employing the second order implicit three-level differencing scheme. The discretisation of the unsteady term can be derived using Taylor-series expansion and it reads:

$$\left.\frac{(\partial\Phi)}{\partial t}\right|_n = \frac{3(\Phi)_n - 4(\Phi)_{n-1} + (\Phi)_{n-2}}{2\Delta t} \tag{5.4}$$

where Φ is a variable, and $n, n-1$, and $n-2$ denote the current time, and two previous successive time instants, respectively.

Diffusion

The diffusion term for the flux term using average rule can be expressed as:

$$\int_{A_n} \rho\Gamma\nabla\Phi_n\vec{i}dA = \rho_n\Gamma_n\nabla\Phi_n\vec{i}A_n \tag{5.5}$$

where A_n is the surface over n cell face. The discretised diffusive flux can be expressed by using central differencing scheme as:

$$\left(\frac{\partial\Phi}{\partial x_i}\right)_P = \frac{\Sigma_j\ \Phi_j A_j}{\Delta\ V_P} \tag{5.6}$$

Convection

The rate at which variable Φ is convected into or out of the control volume through cell face is represented by the convective flux of Φ. Following Demirdžić and Muzaferija [23], the convective flux can be expressed as:

$$C_n = \int_{A_n} \rho\ \vec{u}\ \Phi\ \vec{i}\ dA \approx m_n\ \Phi_n \tag{5.7}$$

In the case for orthogonal mesh, the mass flux m_n through the cell face can be expressed:

$$m_n = \int_{A_n} \rho \, \vec{u} \, \vec{i} \, dA \approx \rho (U\Delta y - V\Delta x)_n \tag{5.8}$$

Source term

The source term is integrated by assuming linear variation of Φ over the control volume.

$$S_\Phi = \int_V \Phi \, dV \approx \Phi \Delta V \tag{5.9}$$

It is often necessary to linearise the source term, in order to enhance the convergence behaviour of the simulation. The practice of linearisation of source term is discussed more details in Patankar [88].

The discretisation of pressure and velocity coupling is done by using Semi Implicit Method for Pressure Linked Equations (SIMPLE) of Patankar [88]. The method is widely used and it is proved to be accurate and effective way for most computation. Velocity is calculated by using estimated pressure, and then improved from iteration to iteration to reach satisfaction of continuity equation. A detailed description of the SIMPLE algorithm can be found in Ferziger and Perić [33].

5.4 Boundary condition and convergence criterion

Boundary conditions can be classified in two groups: Dirichlet and Neumann boundary conditions. When the boundary condition of variable such as temperature is specified explicitly, the approach is called Dirichlet boundary condition. On the other hand, when they are specified in derivative form, the approach is called Neumann boundary condition. The boundary condition on walls assumes no relative velocity between the boundary and the fluid immediately to the walls, which is known as *no-slip* condition. For impermeable walls there is no mass flux across solid boundary. This leads to the constant condition of variable Φ. The wall boundary conditions are specified as follows:

$$U = V = W = k = \overline{\theta^2} = \overline{v^2} = 0 \tag{5.10}$$

Unlike other variables, the boundary conditions for the elliptic relaxation function f and dissipation rate ε are finite:

$$\varepsilon_{wall} = \nu \left(\frac{\partial^2 k}{\partial x_n^2} \right)_{wall} \tag{5.11}$$

$$f_{wall} = \frac{-20 \, \nu^2 \, \overline{v_1^2}}{\varepsilon_{wall} \, x_n^4} \tag{5.12}$$

In order to reach convergent solution in a proper way, it is recommended to use underrelaxation. In this study, all computations are performed with underrelaxation approach, but with different relaxation parameters for momentum pressure correction, and the turbulence transport equations. General rule is to use a small underrelaxation factor at the beginning of calculation and then to increase gradually until convergent solution is obtained. Convergence is achieved when the following criteria is satisfied:

$$\frac{\left|\Phi_n - \Phi_{n-1}\right|}{\left|\Phi_n\right|_{max}} \leq 10^{-6} \tag{5.13}$$

where n refers to the value of Φ at the n^{th} iteration level.

In principle, sufficiently fine grid is required in order to obtain an accurate solution, especially in regions where scalar and turbulent fields change very rapidly and this is usually observed in the near wall region. As a consequence, the grids are clustered against wall. On the other hand, relatively coarse grid could be employed in regions away from walls in order to save the computational expenses, especially when the change of quantities is mild. Paradoxical requirement is faced in dealing with near wall grid arrangement. On one side, as the flow is under buoyancy effect that creates very important fields in the near wall region, it requires very fine mesh. On the other side, because the boundary condition of f is proportional to $1/x_n^4$ very fine grid near the wall can cause numerical instability. Optimisation is made in order to satisfy these requirements by using fine mesh in the near wall region with adjustment of the first grid point.

5.5 Application of the numerical method in a benchmark problem

The laminar natural convection in a cubical cavity with various inclination angles has been studied extensively both numerically and experimentally. Examples are Leong *et al.* [73] for experimental work and Kenjereš *et al.* [60] for numerical work. It is of interest because it combines geometrical simplicity with a reasonable level of physical complexity (different orientation between imposed temperature gradients and gravitational vector).

The numerical method was tested first in the benchmark problem of laminar natural convection of side-heated cubical cavity which is characterised by two non-dimensional parameters: Rayleigh number and Prandtl number. This calculation is conducted with Boussinesq approximation. The vertical thermally active walls are kept at constant temperature difference (ΔT), while the remaining walls are treated as perfectly conducting (with linear temperature variation). The

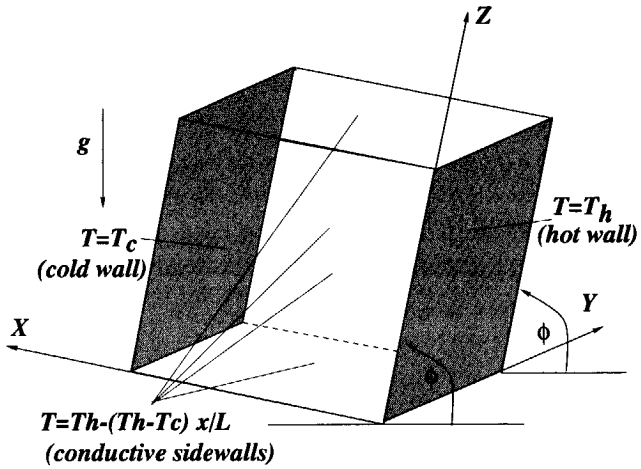

Figure 5.2: Specification of the boundary conditions and applied coordinate system for defined inclined cubical cavity.

temperature profile of the conducting walls is defined as :

$$T = T_h - (T_h - T_c)\frac{x}{L} \tag{5.14}$$

where x denotes the position and L is the length of the cavity. The calculation is conducted for various angles of inclination, namely $\phi = 0^o, 45^o$, and 90^o. The geometrical configuration of the cavity is shown in Fig. (5.2). It can be seen from the figure that when the inclination angle $\phi = 90^o$ the temperature gradient is perpendicular to the gravitational vector. On the other hand, when $\phi = 0^o$, the Rayleigh Bénard convection is obtained (gravitational vector and the initial temperature gradient are aligned). Calculations are performed using central differencing scheme and an implicit three-level scheme for the time integration. The grid size was $82 \times 82 \times 82$ clustered towards the walls in order to accurately capture the near wall region. The convergence solution is reached when all residuals of the quantities are less than 10^{-6}. The calculation is conducted in a range of Rayleigh numbers, $Ra = 10^6, 10^7$, and 10^8, for various inclination angles.

Figures (5.3)-(5.5) show the velocity and temperature distributions in the central $(x-z)$ plane of the cavity heated from the side at $Ra = 10^6$, for $\phi = 90^o$, 45^o, and 0^o, respectively. The figures show the effects of inclination angles on flow pattern, where the smaller the angle the more instabilities is created. The transient (T) behaviour was obtained for four specific situations: both simulations for ($\phi = 45^0$) inclination angle and highest Rayleigh numbers in other two configurations, i.e for the side-heated ($\phi = 90^0$,$Ra = 10^8$) and for heated from below ($\phi = 0^0$,$Ra = 10^6$). The final value of Nu number was obtained by time av-

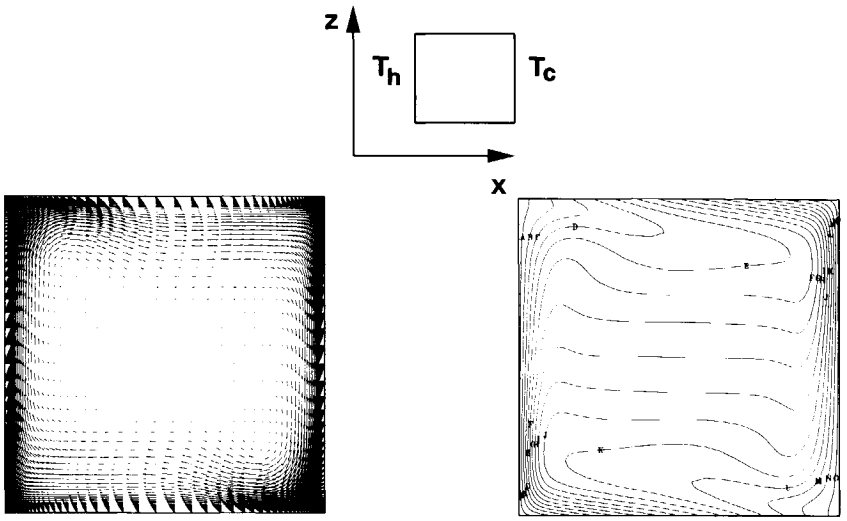

Figure 5.3: Velocity vectors and temperature contours in central vertical (x-z) plane at $Ra = 10^6$, $\phi = 90^o$.

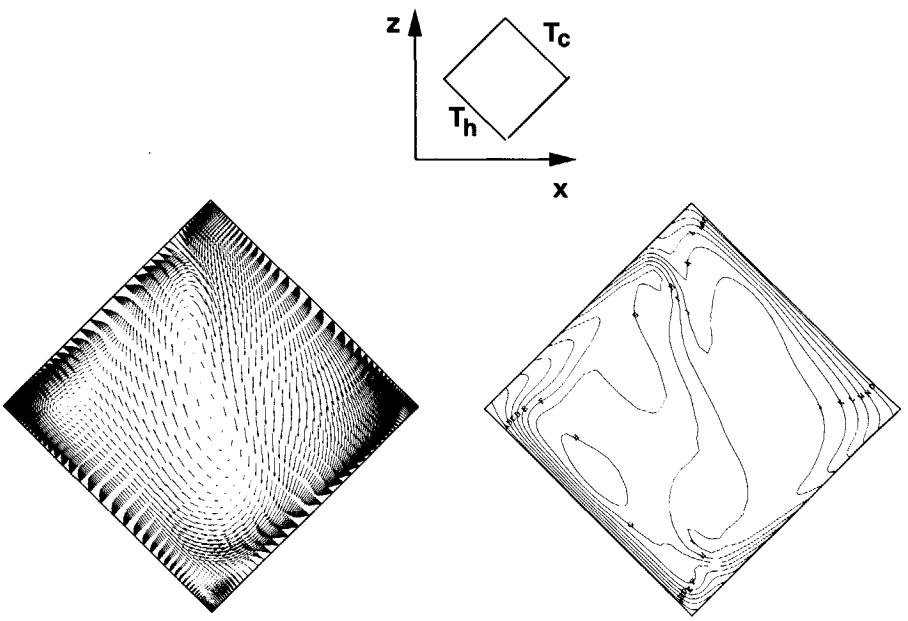

Figure 5.4: Velocity vectors and temperature contours in central vertical (x-z) plane at $Ra = 10^6$, $\phi = 45^o$.

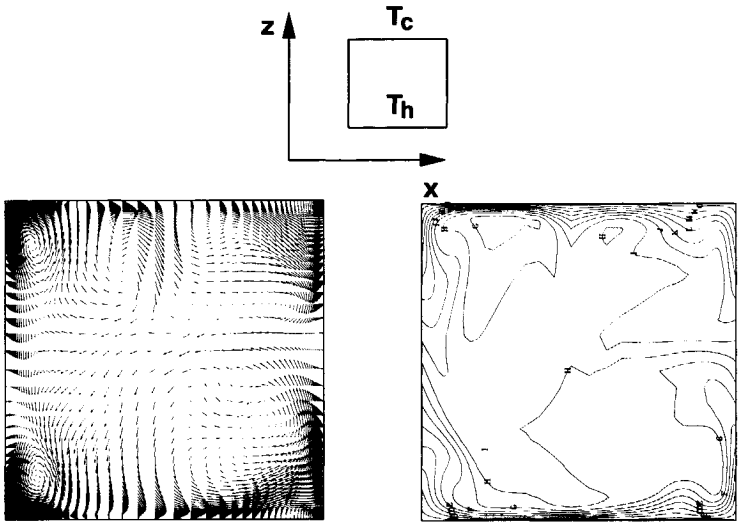

Figure 5.5: Velocity vectors and temperature contours in central vertical (x-z) plane at $Ra = 10^6$, $\phi = 0^o$.

Table 5.1: Comparison of integral Nusselt numbers between computations and experiment of Leong *et al.* [73]

$\phi = 90^0$				$\phi = 45^0$			$\phi = 0^0$		
Ra	Exp	CFD	ΔNu	Exp	CFD	ΔNu	Exp	CFD	ΔNu
10^5							3.91	3.98	1.6%(S)
10^6	6.3	6.4	1.8%(S)	8.83	8.81	-0.2%(T)	7.88	7.89	0.14%(T)
10^7	12.9	12.9	-0.3%(S)	17.50	17.35	-0.8%(T)			
10^8	26.7	25.0	-6.6%(T)						

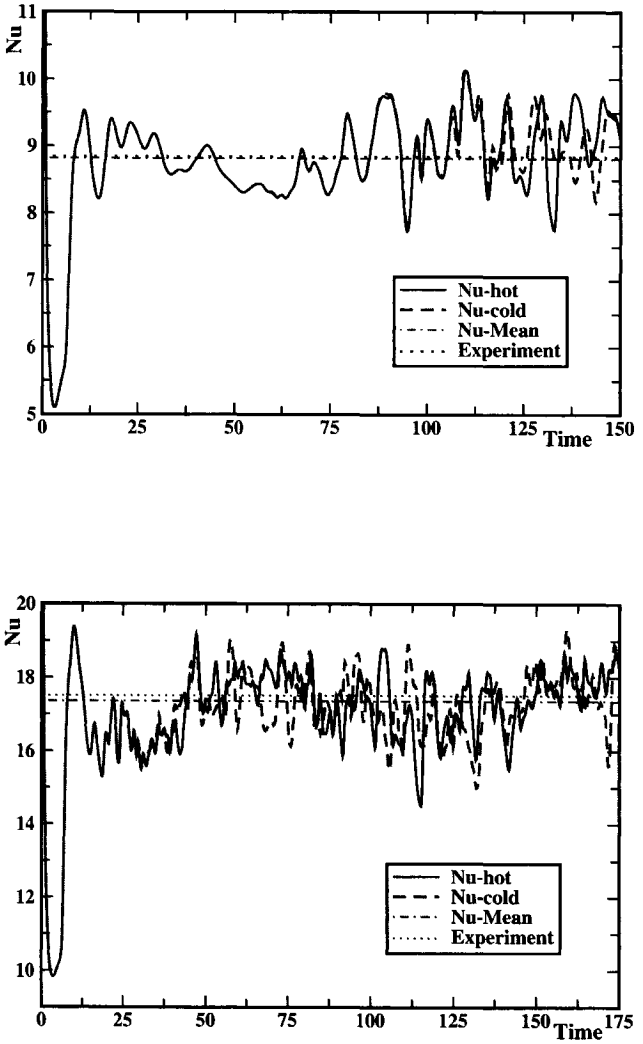

Figure 5.6: Time evolution of integral Nusselt number at hot (−) and cold (− −) walls; time averaged experimental value of Leong *et al.* [73] (···): Ra=10^6,ϕ=45^0 (above); Ra=10^7,ϕ=45^0 (below).

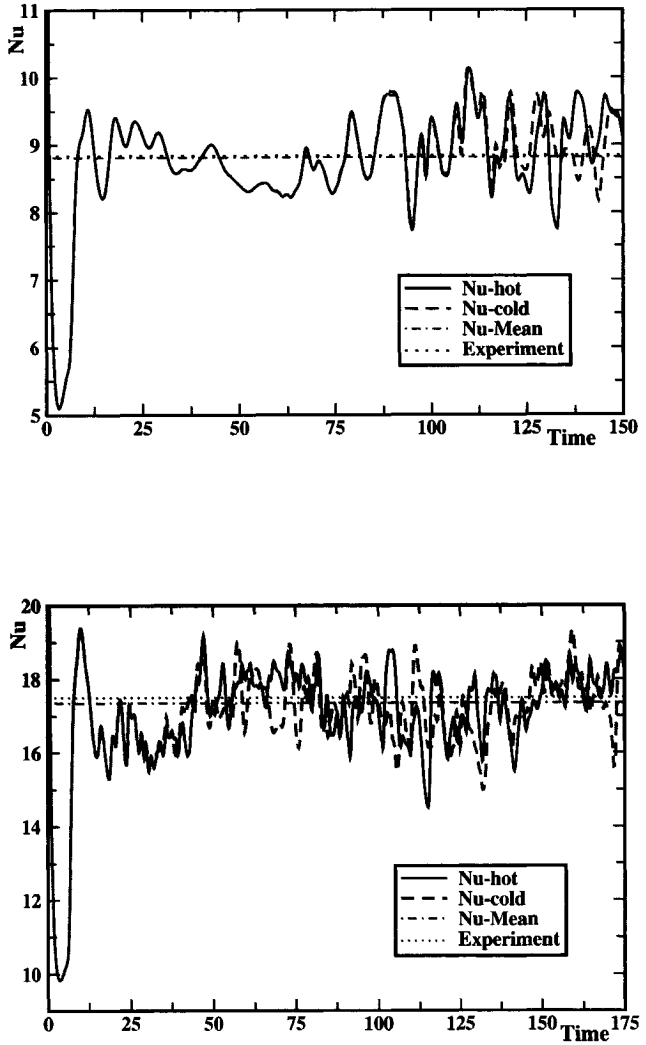

Figure 5.7: Time evolution of integral Nusselt number at hot (−) and cold (−−) walls; time averaged experimental value of Leong *et al.* [73] (···): Ra=10^6,ϕ=0^0 (above); Ra=10^8,ϕ=90^0 (below).

eraging over last 100 non-dimensional time units when the statistically steady state was established, Figs.(5.6)-(5.7). It is interesting to note the amplitude of oscillations for integral Nu number for different configurations. The maximum of oscillations was observed for heated from below ($\phi = 0^0$) situation at $Ra = 10^6$, with amplitude of 25% of time-averaged value. Despite its largest $Ra = 10^8$ value, the side-heated configuration produced time evolution with the minimal amplitude of oscillations (with 5% amplitude of time-averaged value). As seen from Table 5.1 as well as from Figs.(5.6)-(5.7), good agreement between experimental and simulated values of Nu number was obtained, except, at our surprise, for $\phi = 90^0$, $Ra = 10^8$ situation. Simulation underpredicted integral Nu by more than 5%. Since very good agreement was obtained for other configurations over range of Ra and different angles of inclination, we suspect that the imposed three-dimensionality as well as additional promotion of instabilities due to presence of perfectly-conductive walls probably promoted turbulence regime earlier than in situations with adiabatic side walls. Only with additional grid refinement or with a turbulence closure activation this hypothesis can be proved.

5.5.1 Conclusions

A numerical method has been presented to simulate turbulent natural and mixed convection. For evaluation purpose, the method is used to calculate three-dimensional laminar natural convection in an air-filled cubical enclosure heated from the side under different angles of inclination. The numerical method is tested, and it is found to produce results that are in agreement with experiments. In the simulation with angles of inclination $\phi = 45^o$ and 0^o, the results indicated a transient (unsteady) behaviour. Similar behaviour is observed at $\phi = 90^o$ for $Ra = 10^8$. In the case of simulations for $Ra = 10^6$ and 10^7, regardless of the inclination angles, the Nusselt numbers are well predicted. However, at $Ra = 10^8$, the numerical calculation yielded underpredicted values of Nusselt number. Since the method shows good performance, it can be used for simulation in turbulent flows.

CHAPTER 6

Turbulent Natural Convection Results

6.1 Introduction

Natural convection phenomena in an enclosure can exhibit very different features, depending on the geometry and mutual orientation between gravitational vector and initial temperature gradient. In this work we focus on natural convection in enclosures. Very different geometrical configurations can be encountered in engineering applications. However, in order to illustrate the performance of various models and to perform their validation two generic cases are usually considered: (i) enclosure heated from the side, (ii) enclosure heated from below. These two flow cases exhibit conditions, in which the imposed temperature gradient is aligned or perpendicular to the gravitational vector, respectively.

A side-heated turbulent natural convection in a vertical channel is shown in Fig.(6.1)a. Here, the flow is solely driven by density or temperature gradients in the gravity field. Due to temperature difference, higher temperature of the fluid means lower density ($T_h > T_c$, then $\rho_h < \rho_c$) and this creates the thermal buoyancy force which drives fluid to move. As a consequence, less dense fluid has a tendency to move upward and more dense fluid to move downward. Assuming that the transport properties are uniform, the flow field between the two isothermal walls would show anti-symmetric profiles. In general, the side-heated enclosures are characterised by the presence of two distinct regimes: boundary layers along the vertical walls and slowly rotating core region.

Figure (6.1)b shows a horizontal channel where the bottom wall is isothermally heated at temperature T_h and the top cold wall is maintained at a lower temperature T_c. Unlike the flow heated from the side where the temperature gradient is perpendicular to the gravitational vector, here the temperature gradient is parallel to the buoyancy force. This causes an unstable stratification not only in region close to the wall, but also in most part of the enclosure. As a result, this configuration promotes turbulence generation at much lower Rayleigh number compared to the side-heated enclosures. In addition, for the side-heated natural convection turbulence might occur only in a portion of flow domain (boundary layer) while in heated from below situation, turbulence occurs almost in the entire flow domain.

In this chapter, two different turbulent models are validated (run in full simulations mode): (i) the second moment closure and its algebraic simplification (ASM/AFM) (ii) $k-\varepsilon-\overline{v^2}-f-\overline{\theta^2}$ model. The second moment closure and ASM/AFM are used for simulation of:

- side-heated infinite vertical channel

The buoyancy-extended ($k-\varepsilon-\overline{v^2}-f-\overline{\theta^2}$) is applied for simulations of the natural convection in:

- side-heated infinite vertical channel
- side-heated natural convection in a 2-D enclosure of aspect ratio 5:1
- side-heated natural convection in a 3-D enclosure of aspect ratio 1:2:3
- side-heated turbulent natural convection in a 3-D cubical enclosure
- Natural convection heated from below of a 2-D enclosure with aspect ratio 1:1.5

The reason for selecting the above flow cases is based on the fact that in terms of geometry, flows in enclosure are very basic and have served to model testing. With a simple geometry, the model performance can be considered as the outcome of the turbulence model and the numerical method only, rather than due to the influence of geometrical complexity.

In this study, simulations are performed using Boussinesq approximation. The Boussinesq approximation is valid only when density of the fluid varies only with the temperature and only within a narrow range. Contrary to this, when the density variation is significant the Boussinesq approximation is no longer valid and therefore the variation of the density must be taken into account directly in all equations. The working fluid used in this study is air, because its properties are well known and majority of experimental and DNS studies are performed with air as the working fluid. For model validation and evaluation, comparisons are made with either experimental data or direct numerical simulation, or computational result of other models.

6.2 Simulations with second moment closure in side-heated infinite vertical channel

The present section considers the application of the second moment closure in differentially heated infinite vertical channel. The second moment closure model that was developed in Chapter 4 is the modification of model developed by Hanjalić and Jakirlić [43] for the mechanical part and by Dol *et al.* [26] for the thermal part. The development of this model is aimed to combine the necessity of proper level of physics represented by model of turbulence and its numerical stability. This is very important issue in computational fluid dynamics. Although second moment closure is the logical and natural level for modelling turbulent

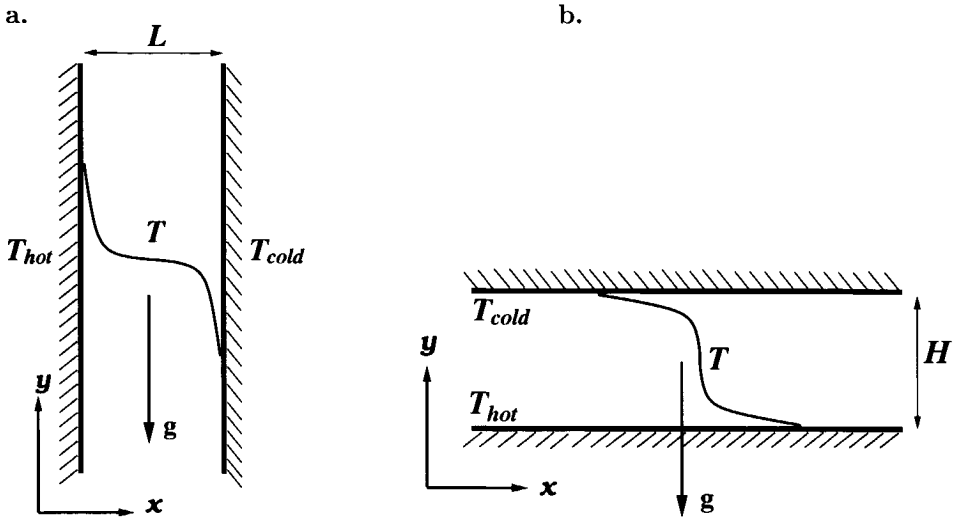

Figure 6.1: Geometrical configuration of natural convection in a side-heated vertical channel (a) and a horizontal channel (b)

fluid flow, heat and mass transfer within the framework of RANS, industrial users are still reluctant to use the model, Hanjalić [41]. It is therefore the goal of this investigation to develop a compromising model of turbulence. Requirement of proper turbulence modelling involving moderate level of complexity is vitally important to predict buoyancy driven flows, because natural convection has many engineering applications.

Natural convection in vertical channel corresponds to a very tall cavity with negligible influence from the horizontal walls. The flow described above has been extensively studied numerically by Versteegh [101] in direct numerical simulation, and experimentally by Dafa'ala and Betts [20]. The simulation is performed using control volume method with second order discretization scheme on $48 \times 90 \times 180$ and $96 \times 216 \times 432$ grid points, which are considered sufficiently fine with respect to the requirement of mean grid spacing as specified by Grötzbach [39]. The dimensionless parameters which describes the flow problem are Prandtl and Rayleigh numbers. The flow fluid used in this simulation is air with Pr=0.709. In addition, the simulation is performed in a range of Rayleigh numbers: Ra=5.4×10^5; 8.227×10^5; 2.0×10^6; and 5.0×10^6. Similar DNS data of the turbulent natural convection at Ra=5.4×10^5 is provided by Boudjemadi *et al.* [7].

In this section, the second moment closure is evaluated. In addition, calculations using algebraic Reynolds stress and heat flux model are also performed here. As explained in Chapter 3, the algebraic model is formulated by truncat-

ing the transport terms in the Reynolds stress and heat flux equations. This algebraic form is mathematically complex and special care should be taken in order to avoid singularity of solution. This is accomplished by keeping nonzero denominator in the equations of Reynolds stress and heat flux. In order to avoid complex mathematical formulation, fully implicit formulation of $\overline{u_i u_j}$ and $\overline{\theta u_i}$ is used.

The mean velocity profiles predicted by the second moment closure model is shown in Fig.(6.2)a. The velocity has been non-dimensionalised by the characteristic velocity $V_c = \sqrt{\beta g \Delta T L}$, and the temperature by the temperature difference ΔT. The figure indicates that the new model predicts the mean velocity reasonably well in the region far from the wall. Although the peak velocity is underpredicted, the position of the peak is well predicted. On the other hand, the algebraic model predicts the peak at location slightly closer to the wall. The mean temperature profile is plotted against DNS in Fig.(6.2)b. It is evident that the new model agrees well with DNS. Similar profile is shown by the algebraic model, with exception of small discrepancy in region between $(0.2 < x/L < 0.35)$.

The profiles of the Reynolds stress $\overline{vv}$, $\overline{uu}$, $\overline{ww}$, and the shear stress $\overline{uv}$, are plotted in Figs. (6.3)a-b and (6.4)a-b. It is worth noting the near wall behaviour of the Reynolds stress. The presence of a wall introduces reflection effect that influence the normal stress $\overline{uu}$. This indicates the importance of the wall reflection effect that damps the stress.

The normal stress $\overline{uu}$ is underpredicted by the new model in the central part of cavity but overpredicted in the near-wall region. This indicates a small wall reflection effect in the near-wall region but significant effect in the far-wall region reproduced by the wall term of pressure strain correlation. This discrepancy is due to the profile of the wall coefficient C_1^w used in the wall term. On the other hand, the vertical component $\overline{vv}$ is overpredicted in the central part, while in the near-wall region is underpredicted. The span-wise component $\overline{ww}$ and shear stress $\overline{uv}$ are well predicted by the new second moment closure model. The algebraic model gives a slightly lower prediction than the new second moment closure model. This is due to truncation of the transport term in the Reynolds stress equation.

The vertical heat flux $\overline{\theta v}$ profile predicted by the new model is plotted against DNS in Fig.(6.5)a. It is obvious that the second moment closure model does not agree well with DNS. In the near-wall region, DNS data increases very rapidly while the model increases gradually. In the core region the level of $\overline{\theta v}$ is higher than the DNS data. Figure (6.5)b shows the profile of the horizontal heat flux $\overline{\theta u}$. Contrary to the vertical heat flux $\overline{\theta v}$, the calculated horizontal heat flux $\overline{\theta u}$ agrees quite well with DNS. This good agreement is primarily attributed to the fact that the horizontal heat flux strongly depends on the gradient of temperature. Since the mean temperature is well predicted, the heat flux $\overline{\theta u}$ is also accurately calculated.

While it is true that the omission of the transport terms in both Reynolds

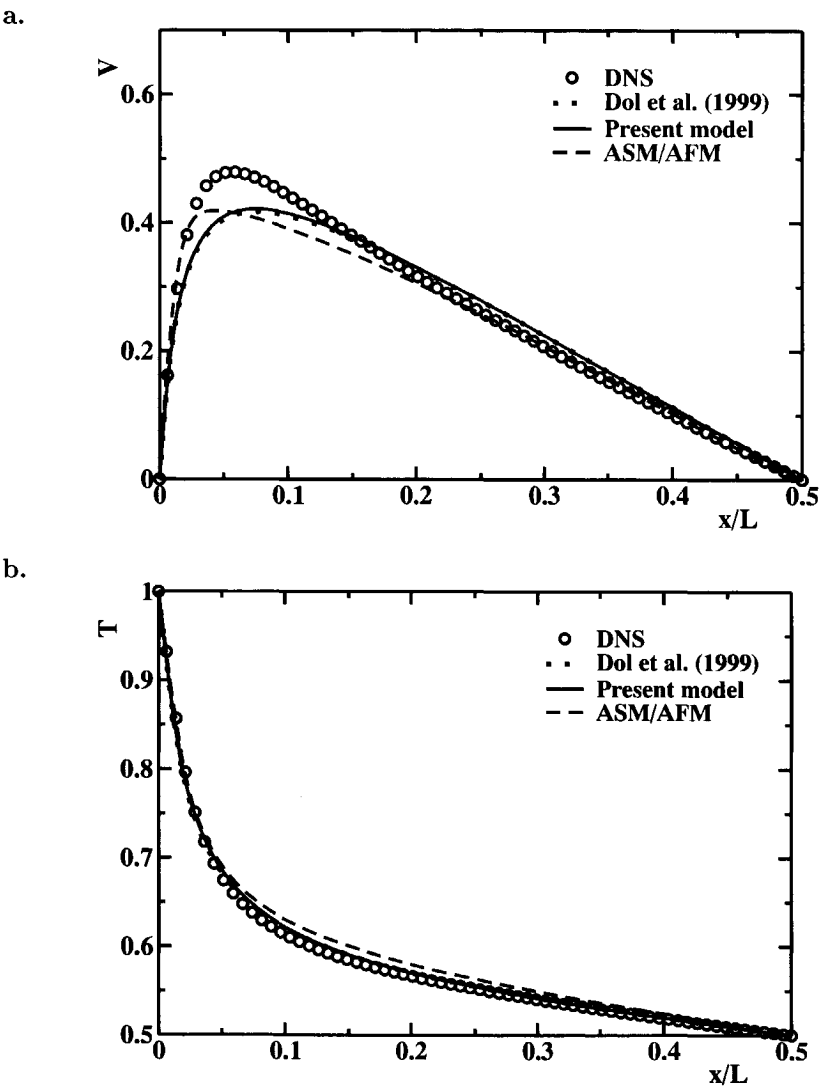

Figure 6.2: The vertical velocity distribution V (a) and temperature T (b) in an infinite vertical cavity heated from the side at $Ra = 5 \times 10^6$, $Pr = 0.71$ DNS data of Versteegh [101].

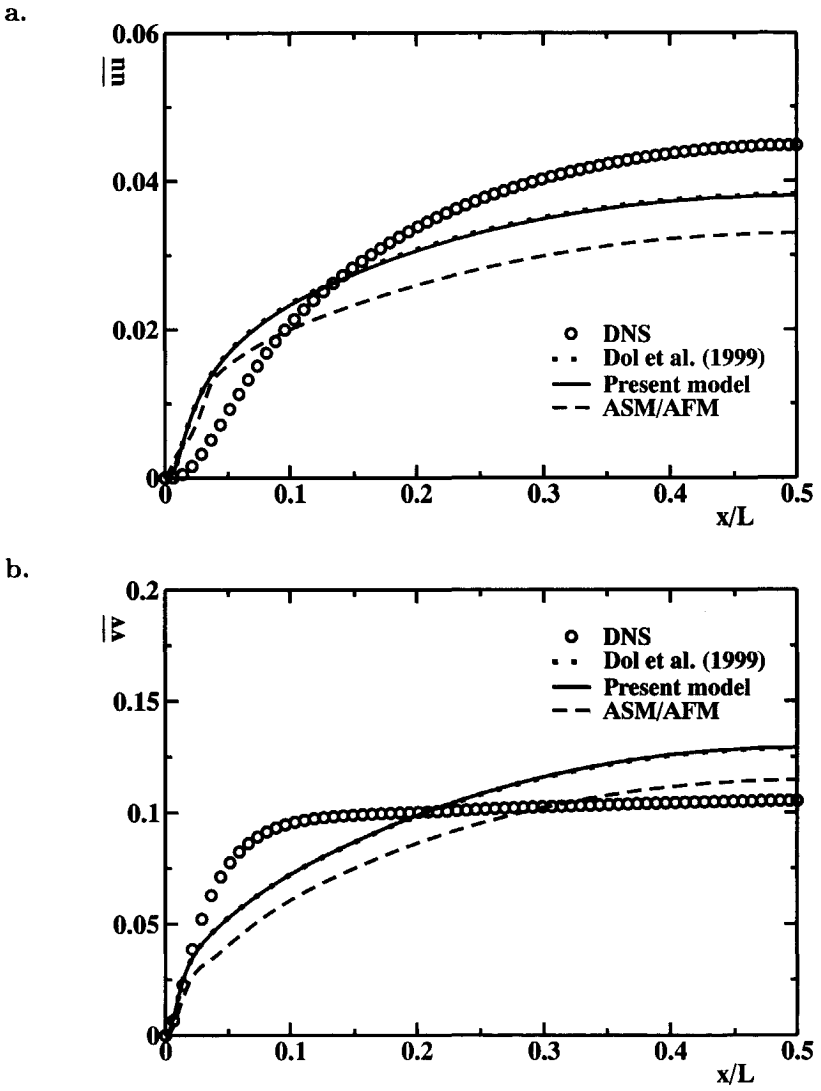

Figure 6.3: The horizontal Reynolds stress $\overline{uu}$ (a), and vertical stress $\overline{vv}$ (b) , in an infinite vertical cavity heated from the side at $Ra = 5 \times 10^6$, $Pr = 0.71$ DNS data of Versteegh[101].

a.

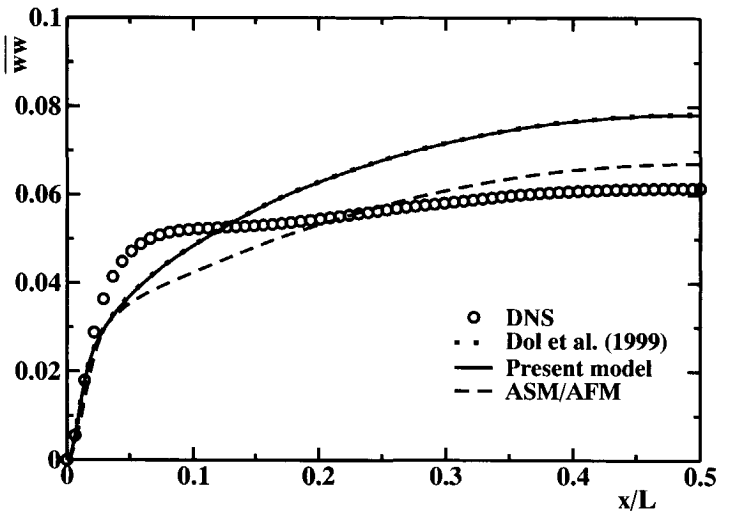

b.

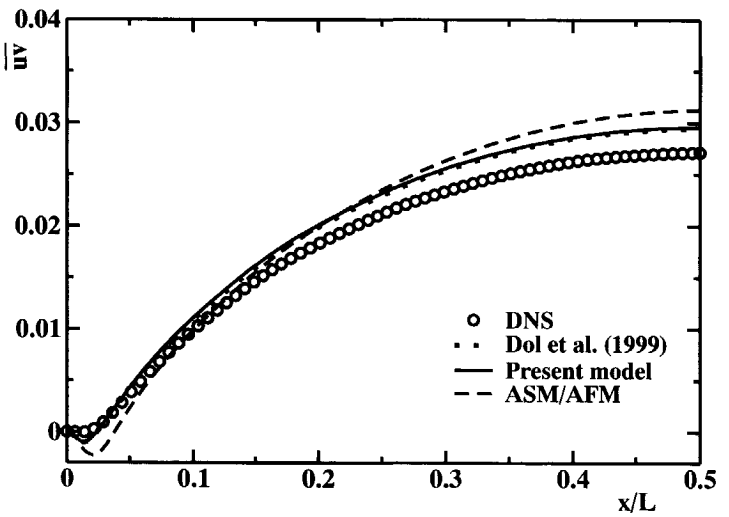

Figure 6.4: The Reynolds stress $\overline{ww}$ (a), and shear stress $\overline{uv}$ (b) in an infinite vertical cavity heated from the side at $Ra = 5 \times 10^6$ $Pr = 0.71$ DNS data of Versteegh [101].

a.

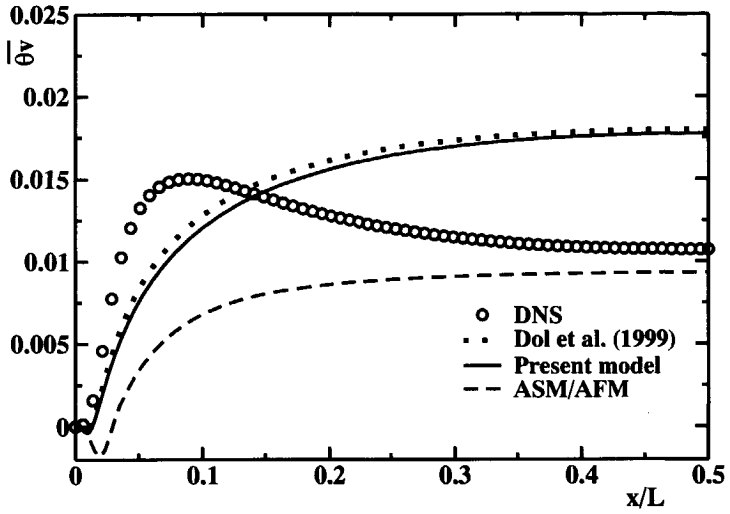

b.

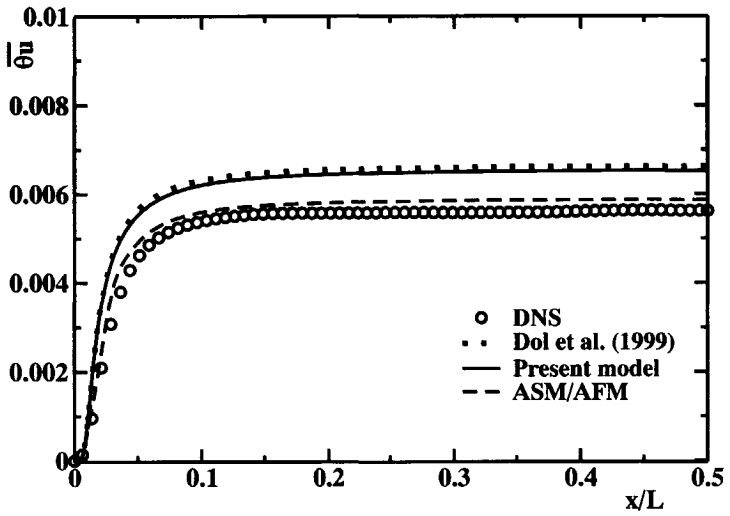

Figure 6.5: The vertical heat flux $\overline{\theta v}$ (a) and the horizontal heat flux $\overline{\theta u}$ (b) in an infinite vertical cavity heated from the side at $Ra = 5 \times 10^6$, $Pr = 0.71$ DNS data of Versteegh [101].

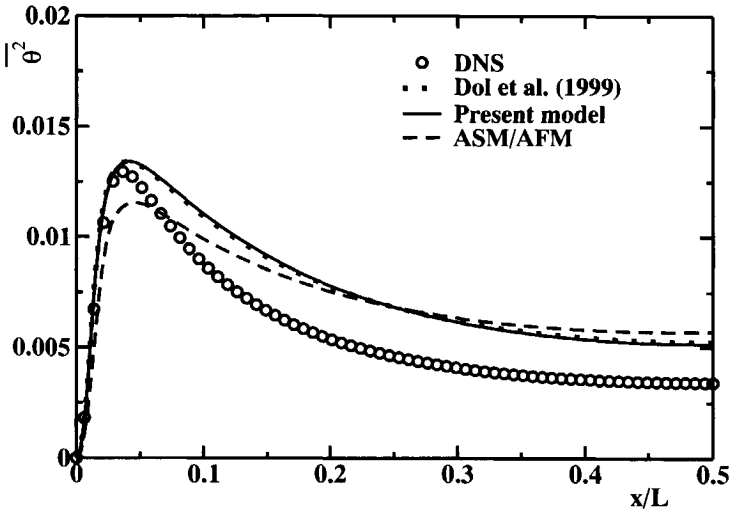

Figure 6.6: The temperature variance $\overline{\theta^2}$ in an infinite vertical cavity heated from the side at $Ra = 5 \times 10^6$, $Pr = 0.71$ DNS data of Versteegh [101].

stress and heat flux equations affects the performance of the algebraic model, the main effect caused by the absence of the transport terms appears only in the vertical heat flux $\overline{\theta v}$. This may be caused by a fact that the buoyancy production and pressure scrambling terms are dominant ones for $\overline{\theta v}$. In addition, the viscous effects are important in the near wall region. Therefore turbulence is strongly generated in this region and this leads to the creation of significant turbulent diffusion. As a consequence, truncation of the transport term causes deterioration of the vertical heat flux.

Dol *et al.*[25] obtained similar profile of $\overline{\theta v}$. This discrepancy was explained in terms of unsatisfactory modelling of turbulent diffusion and slow term of pressure scrambling. Both terms are claimed too dissipative. In the later study, Dol [27] observed that although the turbulent diffusion and the slow term of pressure scrambling were well predicted, significant improvement was not obtained. This disagreement could be overcome by introducing more advanced modelling for the mechanical part. This argument was supported by the fact that when the mechanical part was frozen into DNS, the $\overline{\theta v}$ was very well predicted.

6.3 Simulations with elliptic relaxation model

6.3.1 A side-heated infinite vertical channel

Natural convection in differentially side-heated infinite vertical channel is investigated using the proposed $k-\varepsilon-\overline{v^2}-f-\overline{\theta^2}$ model. In order to calculate the Reynolds stress, the buoyancy extended eddy viscosity is used. The heat flux is calculated using three different approaches, namely SGDH, GGDH, and AFM. The use of these three level modelling approaches is aimed to give insight of how they predict the turbulent flows in the vertical channel. The model has been validated with the DNS data of Versteegh [101] at Rayleigh number under identical conditions as for the second moment closure model in previous section. In order to give a clear view of how the numerical stability is affected by changing y^+, the calculation has been conducted for various values of y^+, namely $y^+ = 0.1,\ 1$ and 2. The non-dimensional wall distance y^+ is defined as:

$$y^+ = \frac{U_\tau\, y}{\nu} \tag{6.1}$$

where $U_\tau = (\tau_w/\rho)^{1/2}$ and $\tau_w = \mu\ \partial U/\partial y$.

Figure (6.7)a shows the mean velocity profile for various y^+ compared with the DNS data. The model agrees well with DNS data in the near wall region. However it deteriorates in $0.05 < x/L < 0.3$ region. It can be seen that variation of y^+ does not affect the performance of the model. The profile of the mean temperature is plotted against DNS in Fig.(6.7)b. It is evident that the model predicts DNS very well.

Figure (6.8)a shows the profiles of the vertical heat flux calculated with different values of y^+. The profiles of vertical heat flux obtained by using SGDH, GGDG, AFM approaches are plotted in Fig.(6.8)b. It is notable that the effect of different approaches on $\overline{\theta v}$ is very significant. As expected, AFM is superior over other approaches. On the other hand, the variation of y^+ on $\overline{\theta u_i}$ is negligibly small, indicating no significant influence of the y^+ in the model's performance.

In general, the proposed $k-\varepsilon-\overline{\theta^2}-f-\overline{\theta^2}$ model predicted reasonably well the natural convection in the side-heated infinite vertical channel. The difference between SGDH, GGDH, and AFM approaches is visible just for the vertical heat flux component $\overline{\theta v}$. Contrary to $\overline{\theta v}$, effect on the normal component of $\overline{\theta u}$ is negligible. In addition, variation of y^+ reveals no significant effect on the model performance. Nevertheless, when y^+ is increased further, the number of calculating points before the maximum value of mean velocity is not sufficient (only 2 points for $y^+ = 5$) and this leads to deterioration of the velocity gradient. When simulation is conducted with $y^+ < 0.01$, numerical problem is observed. The problem is either oscillatory behaviour of residuals or even divergence. This problem is primarily caused by the finite boundary condition of f. It is recommended to use $y^+ \approx 1$ in simulation of natural convection of differentially heated

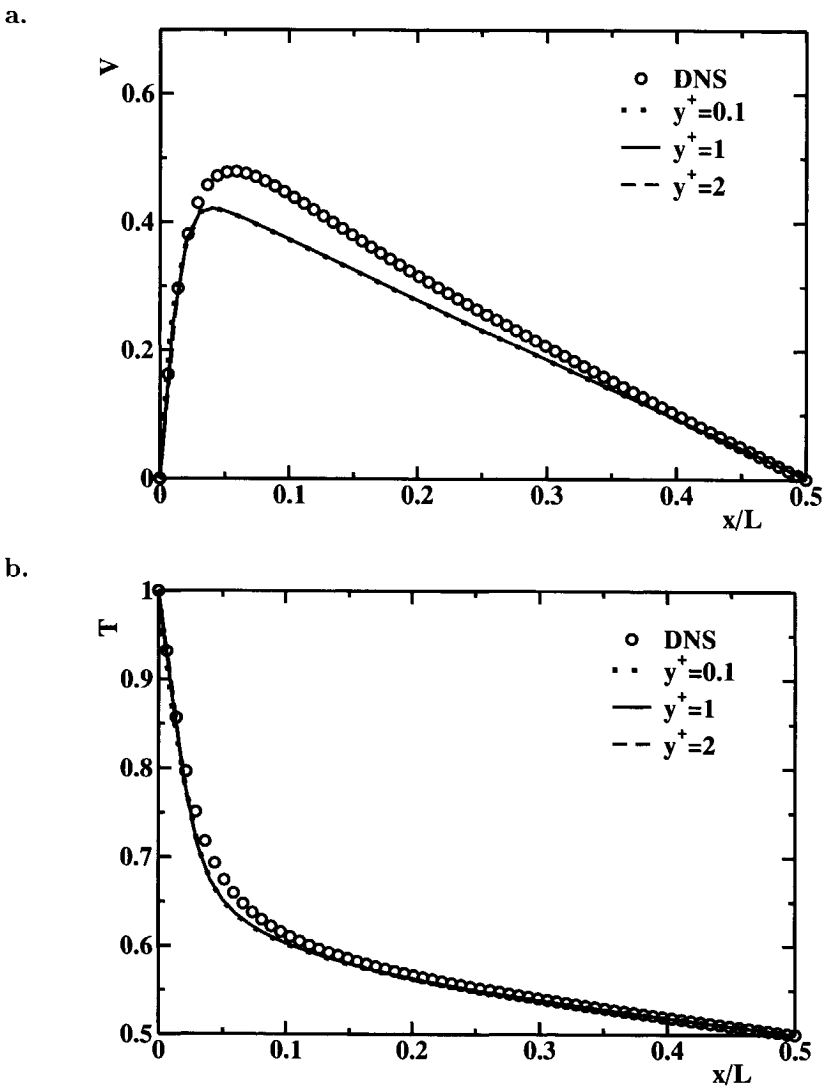

Figure 6.7: The mean vertical velocity distribution (a) and temperature (b) for different values of non-dimensional wall distance, y^+ in an infinite vertical cavity heated from the side at $Ra = 5 \times 10^6$, $Pr = 0.71$ calculated using $k - \varepsilon - \overline{v^2} - f - \overline{\theta^2}$ model.

a.

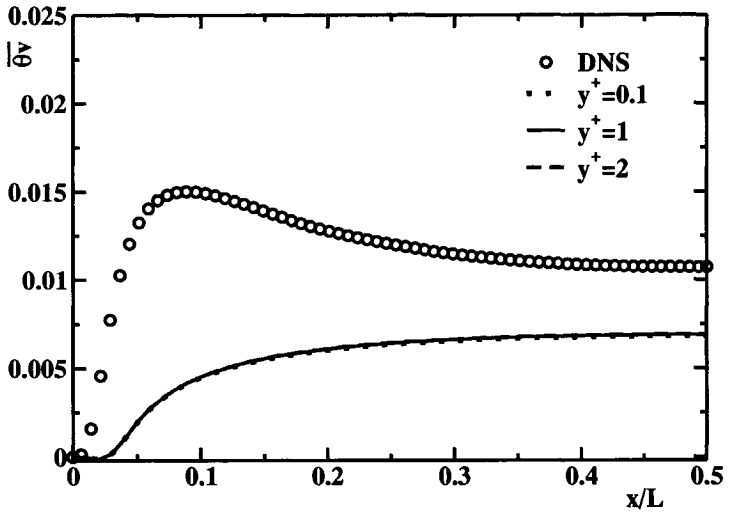

b.

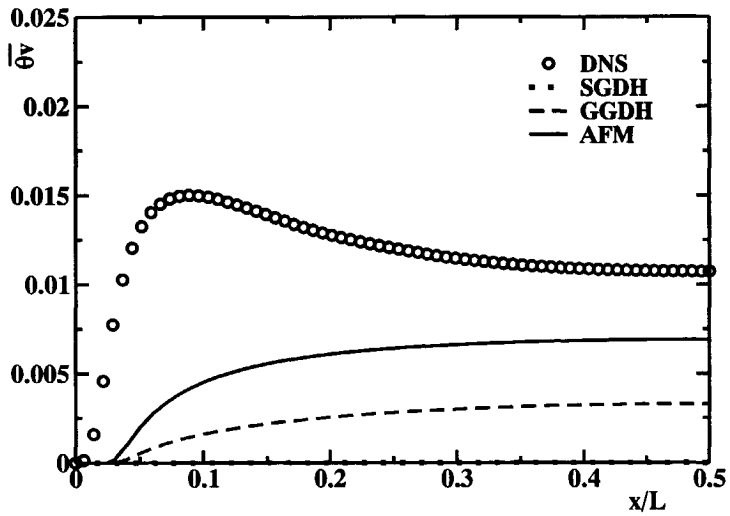

Figure 6.8: The vertical heat flux for different values of non-dimensional wall distance, y^+ (a) and by using different expressions for representation of $\overline{\theta v}$; SGDH,GGDH, and AFM (b) in an infinite vertical cavity heated from the side at $Ra = 5 \times 10^6$, $Pr = 0.71$ calculated using $k - \varepsilon - \overline{v^2} - f - \overline{\theta^2}$ model.

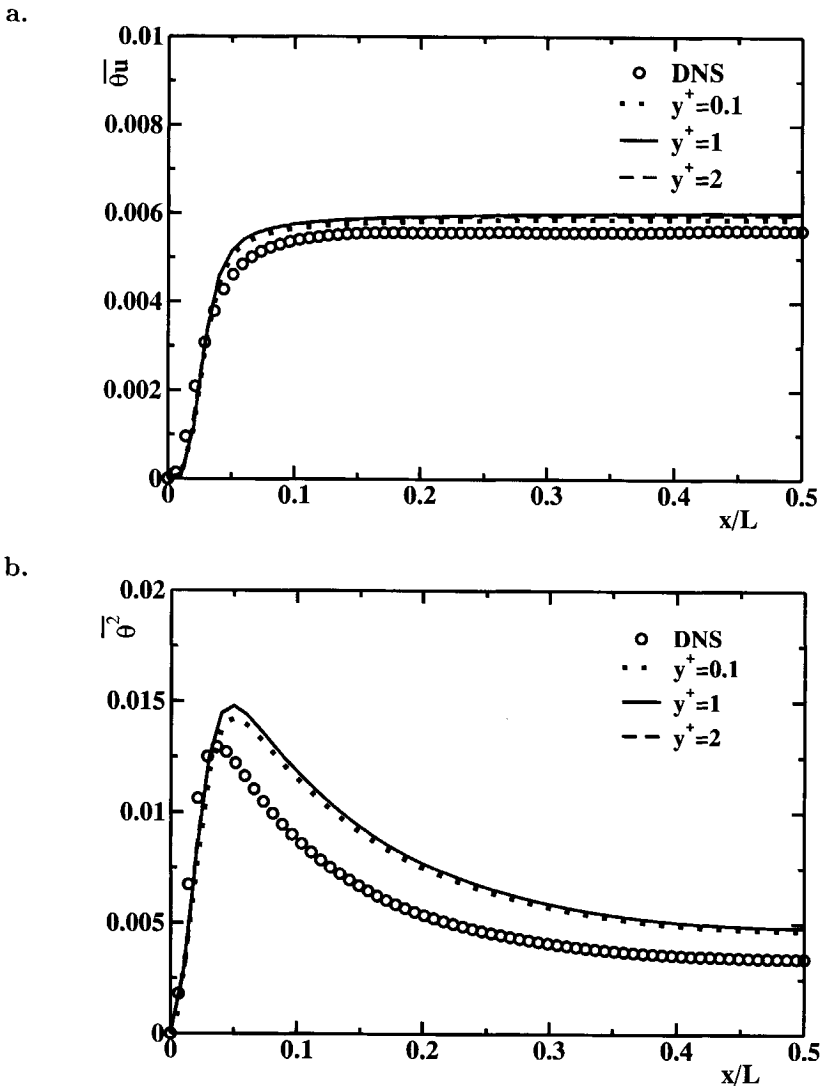

Figure 6.9: The horizontal heat flux (a) and temperature variance (b) for a various y^+ in an infinite vertical cavity heated from the side at $Ra = 5 \times 10^6$, $Pr = 0.71$ calculated using $k - \varepsilon - \overline{v^2} - f - \overline{\theta^2}$ model.

a.

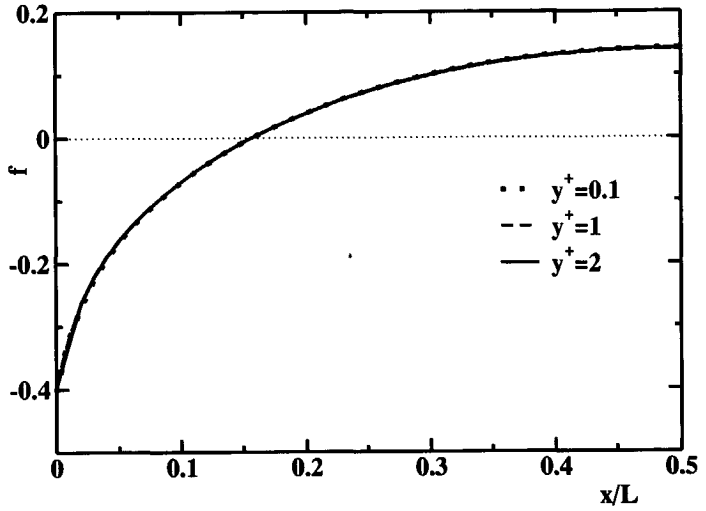

b.

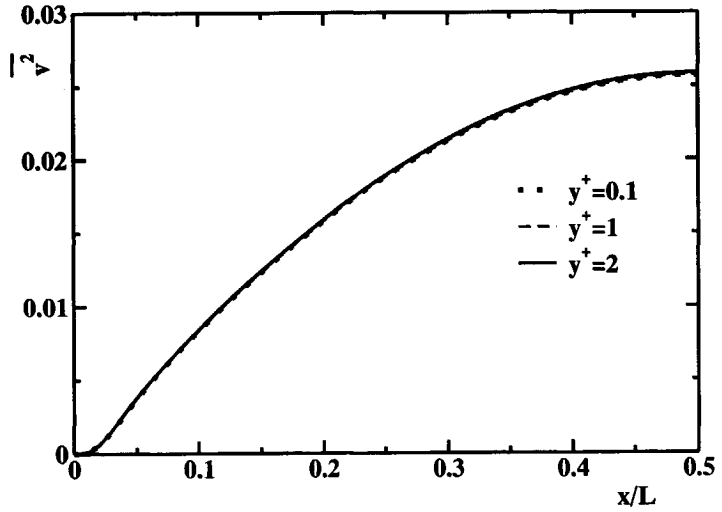

Figure 6.10: The profiles of f (a) and $\overline{v^2}$ (b) for various y^+ in an infinite vertical cavity heated from the side at $Ra = 5 \times 10^6$, $Pr = 0.71$ calculated using $k - \varepsilon - \overline{v^2} - f - \overline{\theta^2}$ model.

vertical channel. The reason lies not only in the stability of numerical simulation, but because it also reproduces good results. As can be seen from Figs.(6.10), the variation of the elliptic relaxation function f and $\overline{v^2}$ is negligible when y^+ is varied.

6.3.2 Natural convection in a side-heated 2D 5:1 aspect ratio enclosure

In this section, natural convection in an enclosure with aspect ratio 5 : 1 is investigated numerically using $k-\varepsilon-\overline{v^2}-f-\overline{\theta^2}$ model. In order to further validate the model, the simulation is carried out at the same condition of the experimental study of Cheesewright *et al.* [9]. The experiment was conducted in an enclosure of 2.5 m height and 0.5 m width of two isothermal vertical walls maintained at temperature 68^o C and 22^o C for the hot and cold walls, respectively, while the remaining horizontal walls are adiabatic. This configuration results in Rayleigh number Ra=5×10^8. The number of grid points for computations is 62×62 control volumes. Variable grid spacing is introduced to resolve steep gradient of velocity and temperature in the near-wall regions. The convergent solution is achieved when the maximum residual is 10^{-6}.

Figure (6.11)a shows the distribution of the y^+ along the isothermal vertical walls. It can be seen that very small y^+ is observed at the upper and lower parts of the walls. This may be the reason for oscillatory behaviour of residuals, especially at the beginning of the calculation. In addition, asymmetric shape of the y^+ along the isothermal hot wall is observed. This is attributed to the development of boundary layer. Similar situation is observed at the opposite cold wall.

The distribution of the local Nusselt numbers along the isothermal walls is shown in Fig.(6.11)b. The main feature of these distribution is characterised by the antisymmetry profile between the hot and cold walls. The maximum Nusselt number of the hot wall occurs at the lower part of the wall, while the maximum Nusselt number at the cold wall takes place at the top part of the enclosure. The transition at the isothermal hot wall occurs at about at $y/H = 0.12$ which is sooner than that calculated using four-equation model of Kenjereš *et al.* [61]. This fact indicates that proposed model predicted more turbulence than the four-equation model.

The results obtained by the proposed model are shown in Figs.(6.12)-(6.13). It can be seen from the velocity vectors in Fig.(6.12)a that boundary layers are characterised by the presence of strong buoyant jet that hits the top wall. From here the jet is turned right creating a strong flow along horizontal adiabatic wall. Some of the fluid is however reflected back towards the core region. This reverse flow vanishes in the middle of the cavity. Similar reverse flow from the bottom part of cold wall is also observed. Figure (6.12)b shows the contour of the turbulent Reynolds number. This contour shows the relatively strong interaction between two separate boundary layers. It is interesting to mention that the contours of turbulent kinetic energy, the horizontal, vertical stresses, and the $\overline{v^2}$ in Figs.(6.12)efgh show a similar pattern. The difference is mainly in their maximum values. The maximum value of the $\overline{v^2}$ is about 2/3 of the

maximum value of the turbulent kinetic energy. Note that the anisotropy can be distinguished by comparing the horizontal to the vertical stresses. This result indicates the significant effect of buoyancy term in the extended eddy viscosity model.

In Fig.(6.14)a the experimental data and computed result of the mean velocity at the mid-height of the cavity are plotted. Predictions show good agreement with experimental velocity data. The velocity maximum is well predicted in the region close to the heated wall. The experimental data is not absolutely symmetrical about the center point of the enclosure because of the imperfect insulation of the horizontal walls. Considering the asymmetry of the experimental data in the cavity due to the heat losses, it is not valuable to compare the computed result in the region near the cold wall.

Figure(6.14)b shows the profile of the turbulent shear stress at $y/H = 0.5$. The model shows reasonably good agreement with the experimental data, especially in proximity of the hot wall. The peak value of computed shear stress is approximately 10% higher compared to the experimental data with a similar slope around the maximum value. Unlike the experimental data, where the shear stress is always positive in the entire enclosure, the model produced steep and narrow negative value in the near wall region.

The comparison between Cheesewright's data and calculated vertical heat flux $\overline{\theta v}$, at $y/H = 0.5$, is shown in Fig.(6.15)a. Similar profile was obtained by Kenjereš [62], where it was shown that calculation using AFM reproduces a substantial improvement over the GGDH approach. The calculated profile for the horizontal heat flux $\overline{\theta u}$ at $y/H = 0.63$ is shown in Fig.(6.15)b. The model overpredicts the experimental data. Nevertheless, the qualitative agreement is observed. The profile of the elliptic relaxation function f is shown in Fig.(6.16). Similar patterns between the hot and cold wall are observed. The maximum values are found in the near wall regions, while far away from the wall they are very small. Note that the profiles at $y/H = 0.9$ and at $y/H = 0.1$ are antisymmetric.

In general, $k-\varepsilon-\overline{v^2}-f-\overline{\theta^2}$ model has demonstrated the ability to predict the flows in natural convection in the side-heated 2D enclosure with moderate aspect ratio. From comparisons shown above, it can be concluded that the proposed model has correctly predicted the experiment of Cheesewright.

a.

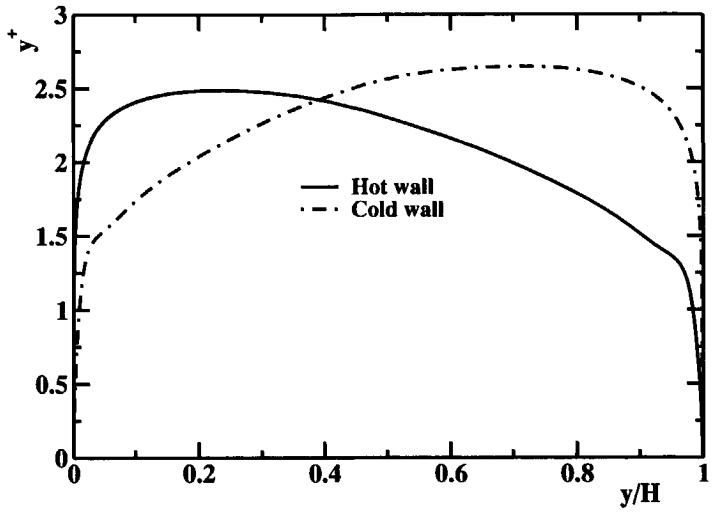

b.

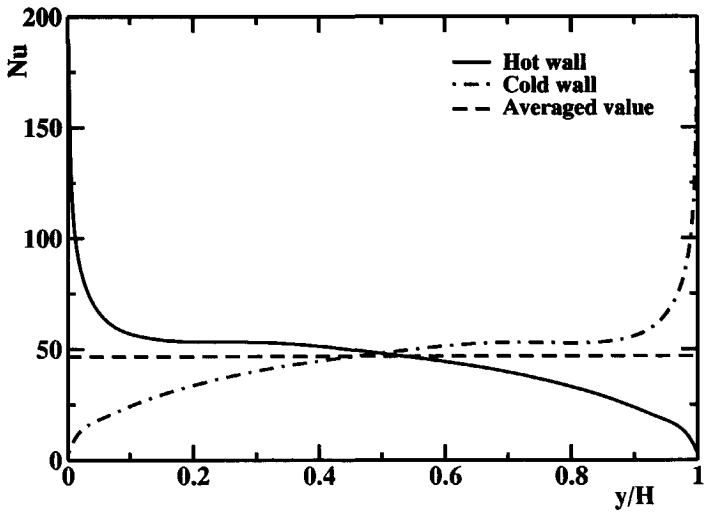

Figure 6.11: The profiles of y^+ (a) and Nu (b) in side-heated 5:1 aspect ratio cavity at $Ra = 5 \times 10^8$.

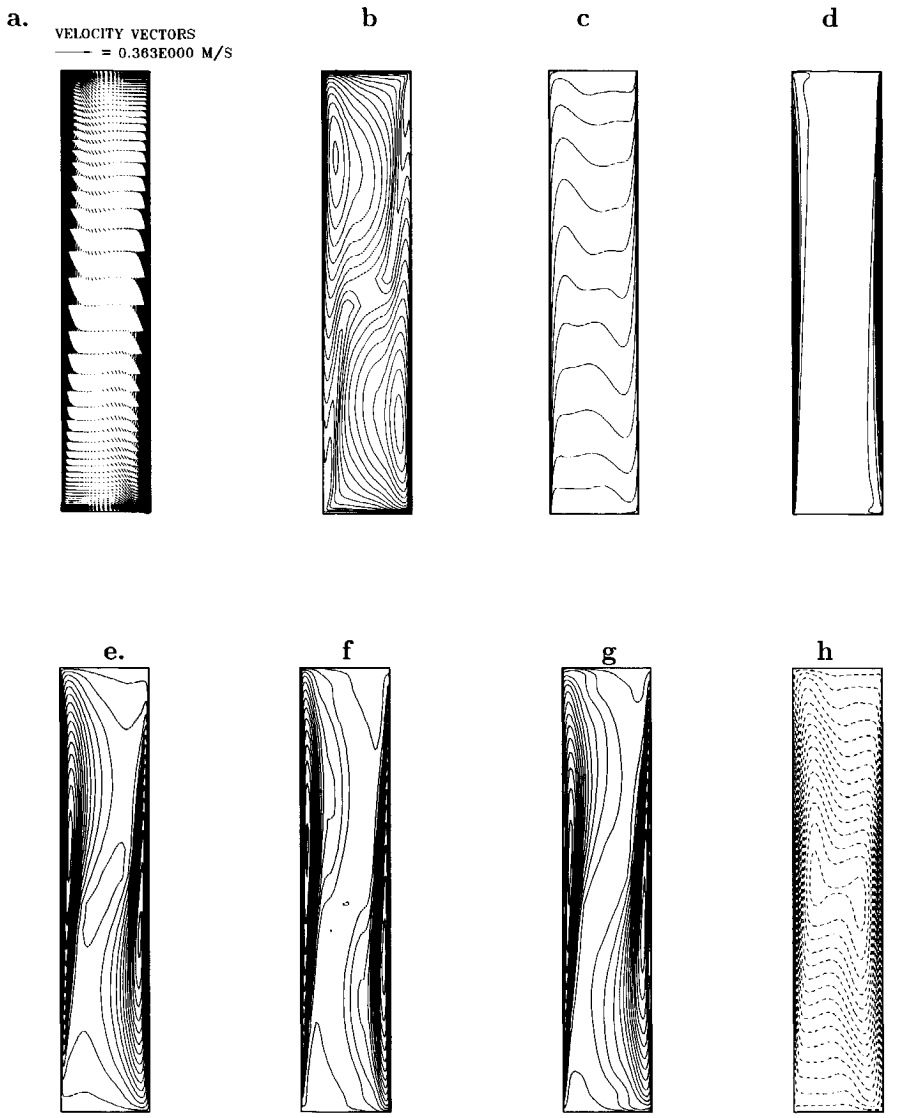

Figure 6.12: Velocity vector and contour distribution of different quantities in side-heated 5:1 aspect ratio cavity at $Ra = 5 \times 10^8$: (a.) velocity vector, (b.) turbulent Reynolds number (max:0.7×10^{-2}; min:0.24×10^{-3}), (c.) temperature (max:68 ^{o} C; min:22 ^{o} C), (d.) temperature variance (max:0.3×10^3 $^oC^2$; min:0.1×10^1 $^oC^2$), (e.) v^2 (max:0.36×10^{-2} m^2/s^2; min:0.1×10^{-3} m^2/s^2), (f.) normal stress (max:0.51×10^{-2} m^2/s^2; min:0.17×10^{-3} m^2/s^2), (g.) vertical stress (max:0.61×10^{-2} m^2/s^2; min:0.21×10^{-3} m^2/s^2), (h.) stream line.

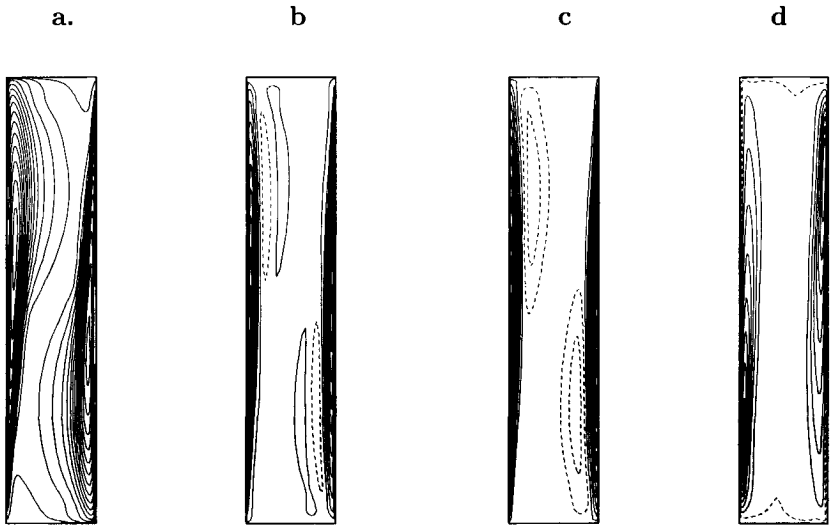

Figure 6.13: Contour distribution of different quantities in side-heated 5:1 aspect ratio cavity at $Ra = 5 \times 10^8$: (a.) turbulent kinetic energy (max:0.7×10^{-2} m^2/s^2; min:0.24×10^{-3} m^2/s^2), (b.) vertical heat flux (max:0.14×10^{-1} m^2/s^2; min:-0.51×10^{-2} m^2/s^2), (c.) horizontal heat flux (max:0.1×10^{-1} m/s^oC; min:-0.1×10^{-2} m/s^oC), (d.) elliptic relaxation function f.(max:2.0; min:-1.0)

a.

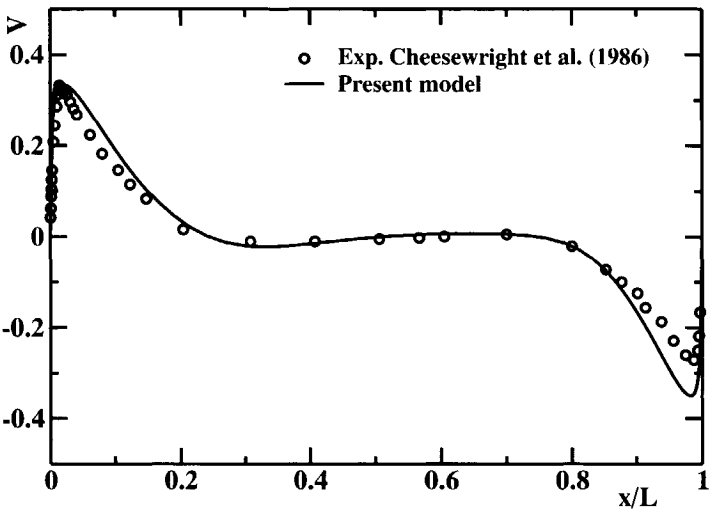

b.

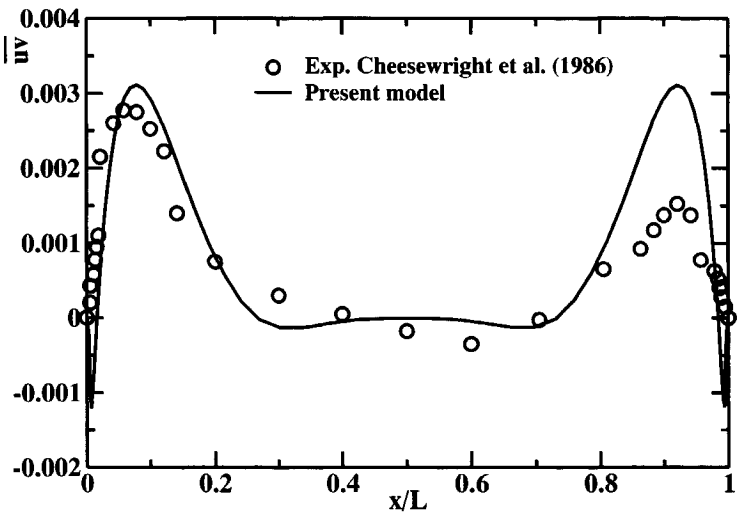

Figure 6.14: The mean velocity (a) and shear stress (b) profiles (at y/H=0.5) in side-heated 5:1 aspect ratio cavity at $Ra = 5 \times 10^8$.

a.

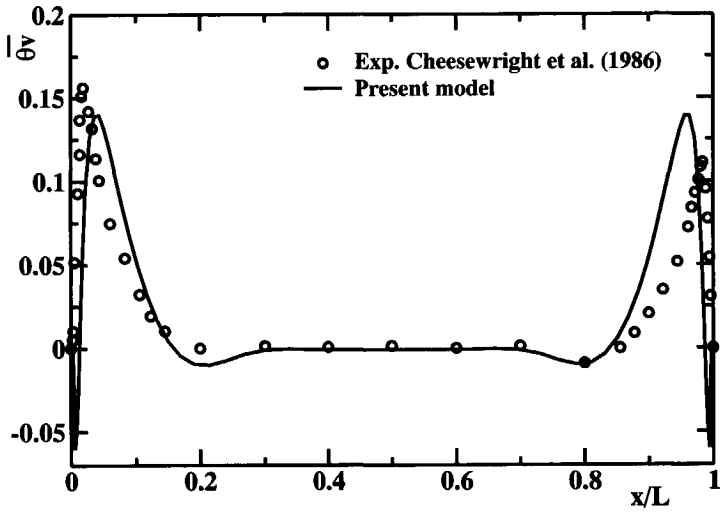

b.

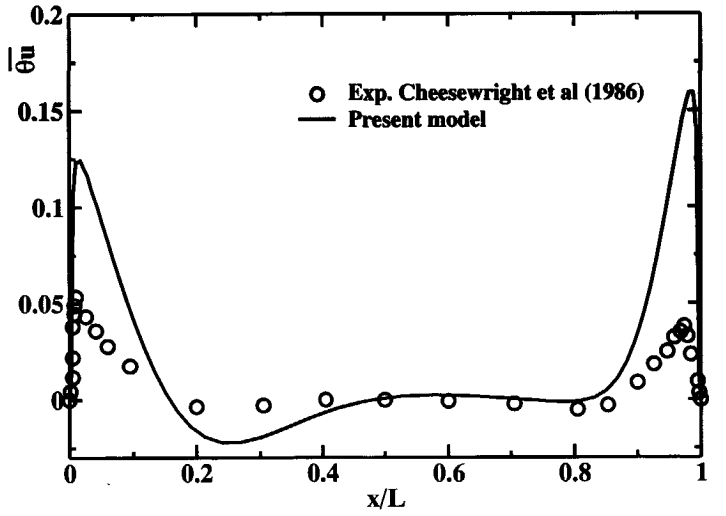

Figure 6.15: The vertical turbulent heat flux (at y/H=0.5) (a) and horizontal heat flux (at $y/H = 0.63$) (b) in side-heated 5:1 aspect ratio cavity at $Ra = 5 \times 10^8$.

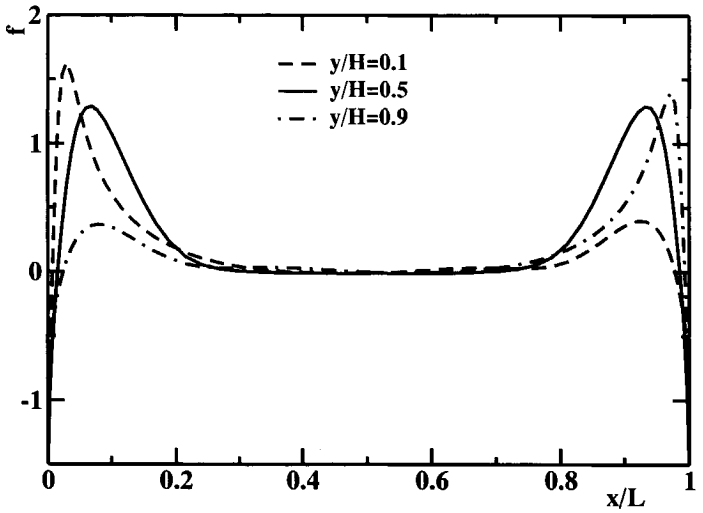

Figure 6.16: The elliptic relaxation function f (at $y/H = 0.1, 0.5$ and 0.9) in side-heated 5:1 aspect ratio cavity at $Ra = 5 \times 10^8$.

6.3.3 A side-heated 3D enclosure with 1:2:3 aspect ratio

This section presents numerical investigation of three dimensional enclosure with height, depth to length aspect ratio of $H : D : L$=1 : 2 : 3. The simulation is performed with grid size of $102 \times 62 \times 42$ of nonuniform mesh clustered towards the wall in order to accurately capture the turbulent fields in the near wall region. This numerical study is compared with the experimental work of Olson *et al.* [84] on the steady state natural convection. The experiment was carried out in three dimensional cavity of 2.5 m high, 7.9 m long and 3.9 m width, with isothermal hot wall at 29.3 °C and opposite cold wall at 10.9 °C. This specification gives a relatively high Rayleigh number, $Ra_H = 3 \times 10^{10}$, or $Ra_L = 9.5 \times 10^{11}$. In addition to the full-scale experiment, Olson *et al.* [84] also performed measurement at small-scale model in order to see possibility for scaling-down but still to keep all interesting physics of flows. Several advantages of using the small scale model could be obtained. For example, much better control of heat-losses and significant reduction of running cost for experimental equipment. It was reported that the main characteristic of the flow were turbulent boundary layers on the isothermal vertical walls, with two horizontal loops, one near the ceiling and one near the floor. In the region far from the boundary layers no motion was detected indicating a stagnant region in the core of the enclosure. In addition, Olson *et al.* [84] observed that the velocities of the full room and the small scale model in the horizontal layers agreed well (within experimental uncertainty).

The velocity contours, turbulent kinetic energy, temperature distribution and temperature variance predicted by the model are shown in Figs.(6.17)a-d, respectively. The velocity field shows a typical boundary layer pattern for the side-heated enclosures. It can be seen that the thin boundary layers are developed along thermally active vertical walls. When the vertical jet hits the top wall, a reverse flow is created. The reverse flow creates a small vertical loop at the upper part of the boundary layer. In a similar manner, the antisymmetrical flow is observed along the cold wall with small vertical loop at the lower part of the wall. At the boundary layer exterior, a stagnant core with very small velocity is observed, indicating weak interaction between two isothermal walls. However, the reverse flows along the horizontal walls are not predicted by the numerical simulation. The contours of the turbulent kinetic energy and temperature variance appear to be concentrated along the isothermal walls.

Figures (6.18)a-d present the contours of $\overline{v^2}$, $\overline{vv}$, $\overline{uu}$, and elliptic relaxation function f. It can be seen that the most significant fields are concentrated in the vertical boundary layers. It is evident that the contours of $\overline{v^2}$, Reynolds stresses, and turbulent kinetic energy have similar pattern[1]. The difference is mainly in their maximum values. Note that due to buoyancy production in the Reynolds

[1]Note that for the adopted coordinate system $\overline{v^2}$ should be compared to $\overline{uu}$ (wall normal stress) to which it reduces in equilibrium flows very close to a wall.

a.

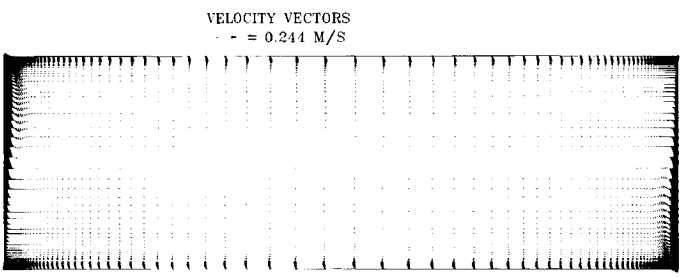

b.

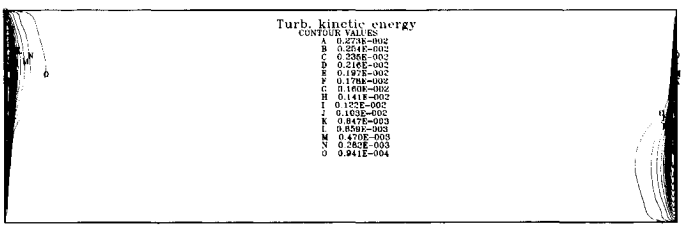

c.

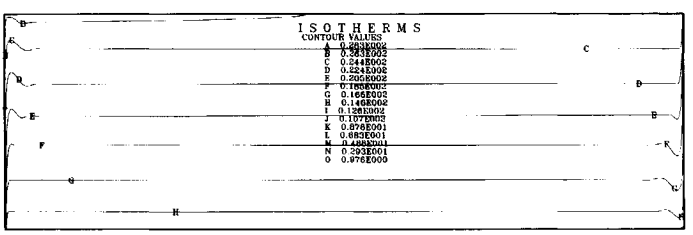

d.

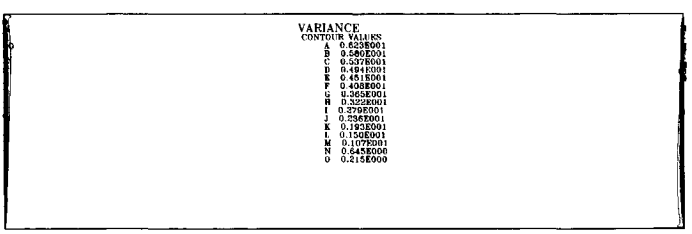

Figure 6.17: The velocity vector, turbulent kinetic energy, temperature, and temperature variance contours of side-heated cavity with aspect ratio $1:2:3$ at $Ra = 3 \times 10^{10}$

a.

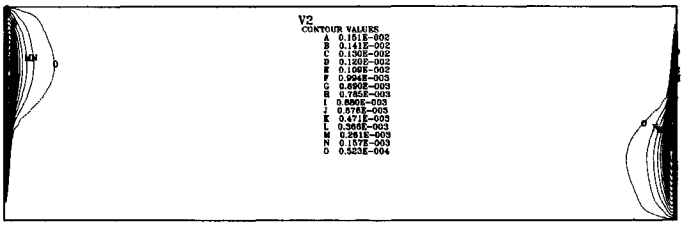

b.

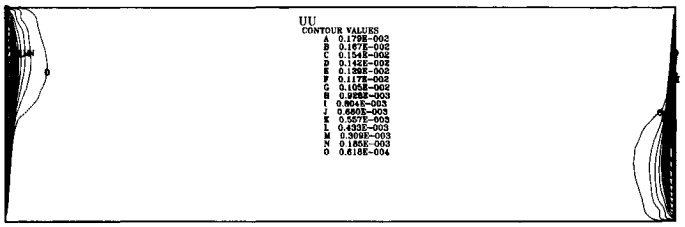

c.

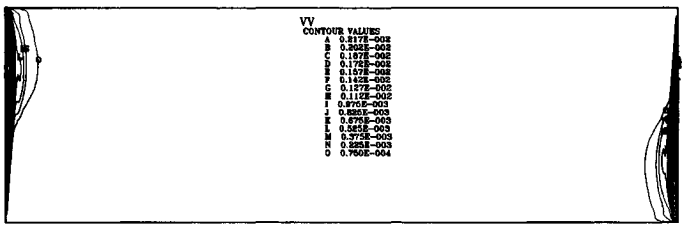

d.

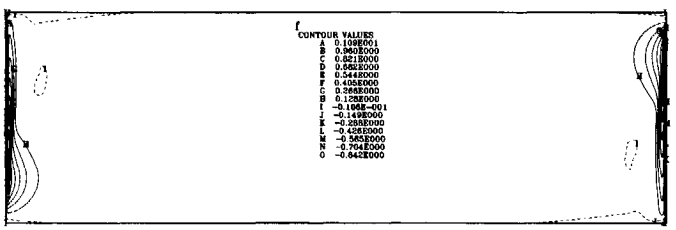

Figure 6.18: The contours of $\overline{v^2}$, $\overline{uu}$, $\overline{vv}$, and f of side-heated cavity with aspect ratio $1:2:3$ at $z/D = 0.5$ at $Ra = 3 \times 10^{10}$.

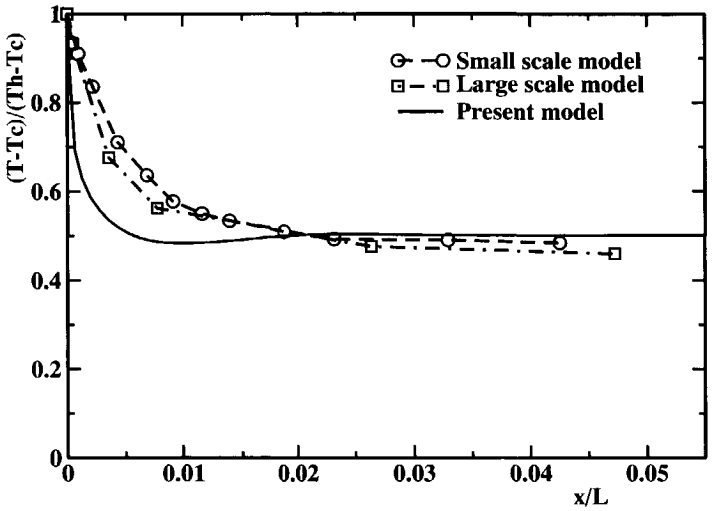

Figure 6.19: The temperature profile at $z/D = 0.5$ of side-heated 3-D cavity with aspect ratio $1:2:3$ at $Ra = 3 \times 10^{10}$

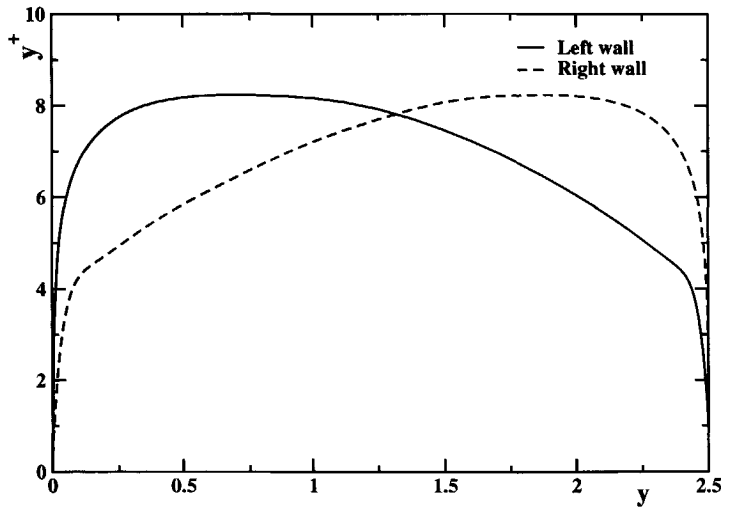

Figure 6.20: The distribution of y^+ at the isothermal walls in side-heated 3-D cavity with aspect ratio $1:2:3$ at $Ra = 3 \times 10^{10}$

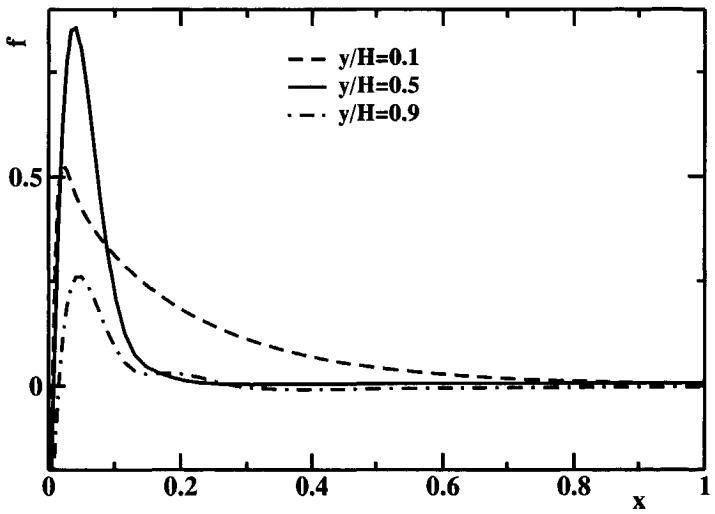

Figure 6.21: The elliptic relaxation function f (at $y/H = 0.1, 0.5$ and 0.9) in the isothermal walls of side-heated 3-D cavity with aspect ratio $1:2:3$ at $Ra = 3 \times 10^{10}$

stress equation, the maximum value of $\overline{vv}$ is considerably higher than that of $\overline{uu}$.

The profile of the mean temperature in proximity of the hot wall are plotted against experiment for the full scale room and the small scale model in Fig.(6.19). Very close to the wall, the calculated temperature decreases very rapidly until $x/L < 0.005$, i.e. about 4 cm from the hot wall, while away from that region, the temperature is almost constant. In general, the computational result captures qualitative profile of the experimental data. However, discrepancy is observed in the near wall region. This discrepancy is mainly attributed to the turbulence level of the flow. The present model obviously overpredicts level of turbulence, causing more pronounced gradients.

Figure (6.20) shows the distribution of y^+ along the vertical walls. The profile is similar to that of the side-heated enclosure with aspect ratio $5:1$, with exception of larger value of almost 200%. Note that the profiles between the left and right walls are antisymmetrical. The profiles of the elliptic relaxation function f at $y/H = 0.1, 0.5$ and 0.9 are shown in Fig.(6.21). It can be seen that f has a significant value only in the near wall region, while in the far away from the wall region f is almost zero.

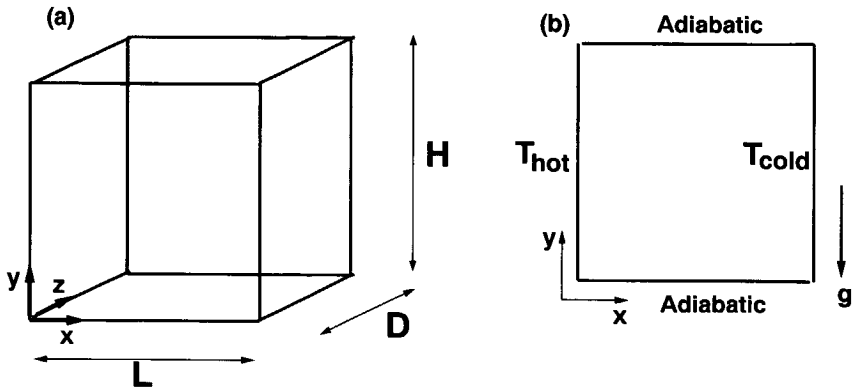

Figure 6.22: The geometrical configuration of cubical cavity (a) and the slice of the plane at $z/D = 0.5$ (b).

6.3.4 A side-heated cubical enclosure

The natural convection inside a cubical cavity has been extensively studied in both the laminar and turbulent regimes. Example is the experimental study of turbulent natural convection in a cubical enclosure heated from the side at a sufficiently high Rayleigh number $Ra = 5 \times 10^{10}$, by Opstelten [85]. The experimental set-up was designed to overcome limitations and to give improvements of previous experiments of Cheeswright *et al.*[9] and King [65]. In order to achieve the high Rayleigh number, the dimension of the cavity is taken as large as possible within the given constraint (size of a laboratory room) and to keep the value of $\beta\Delta T$ relatively small (for which the Boussinesq approximation is valid). Two lateral wall configurations have been tried, with passive or active walls. The lateral wall is called passive one when it is insulated in order to reduce 3D effects caused by heat transfer through the wall. It is called active wall when localised heating is applied to the lateral wall to compensate the flow stratification. In the case with the passive walls, a significant heat loss is found. These heat losses occur due to exchange of heat with environment. The experiment clearly demonstrates the complexity of imposing adiabatic boundary conditions. Despite experimental difficulties, this study provides useful database for validation purposes. Dol and Hanjalić [24] performed numerical simulation of this configuration using second moment closure: for 2D and 3D computations. The model was based on the second moment closure of Peeters and Henkes [89]. Realistic experimental boundary conditions have been applied for these simulations.

The objective of this numerical study is to test the ability of the adopted $k - \varepsilon - \overline{v^2} - f - \overline{\theta^2}$ (5 equation model) in a side-heated cubical enclosure. The numerical simulation is aimed to match with the experimental study of Opstelten

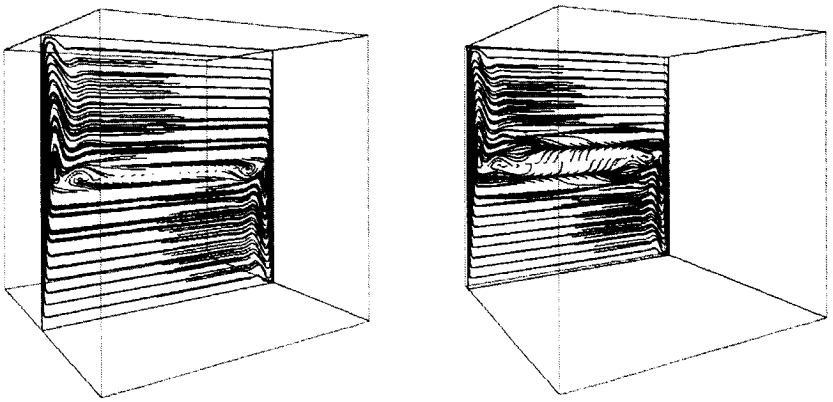

Figure 6.23: The trajectories of massless particles released in characteristic vertical plane in heated from the side cubical enclosure, Ra=5×10^{10}, Pr=0.71: left- z/D=0.5, right- z/D=0.05.

[85] of turbulent natural convection at Rayleigh number $Ra = 5 \times 10^{10}$. A nonuniform grid of $62 \times 62 \times 52$ nodes is used. The mesh is clustered towards walls in order to properly capture turbulent fields. In order to improve convergence, the solution for a lower Rayleigh number ($Ra = 5 \times 10^8$) was used for specification of initial fields. Different underrelaxation factors have been applied to all variables. Convergence of simulations has been accelerated by using small time step at the beginning of the calculation, which was gradually increased as time progressed. The full convergence of computations was declared when all residuals reached 10^{-6}.

The geometrical configuration of the cubical cavity is shown in Fig.(6.22). Analysis is focused in the boundary layer, because the main flow and heat transfer occur in this region. Here, intensive shear and buoyancy productions drive the convection that influence the whole fluid flow in the cavity. It is therefore important to evaluate the model performance in this region. In order to obtain a better insight in the flow pattern, the instantaneous trajectories of massless particles in the central vertical plane and in the proximity of back lateral wall are shown in Fig.(6.23). Figures (6.24)a-b show the velocity vectors and temperature distribution in the mid-plane ($z/D = 0.5$), respectively. The contours of the turbulent kinetic energy (k) and $\overline{v^2}$ are plotted in Figs.(6.25)a-b. Both distributions show a similar pattern, with highest concentration in the near-wall region. Similar contours are observed for Reynolds stress $\overline{uu}$ and $\overline{vv}$.

The non-dimensional vertical velocity (V/V_b, where $V_b = \sqrt{g\beta\Delta TH}$) in the central vertical plane ($z/D = 0.5$) at different heights ($y/H = 0.1, 0.3, 0.5, 0.7$

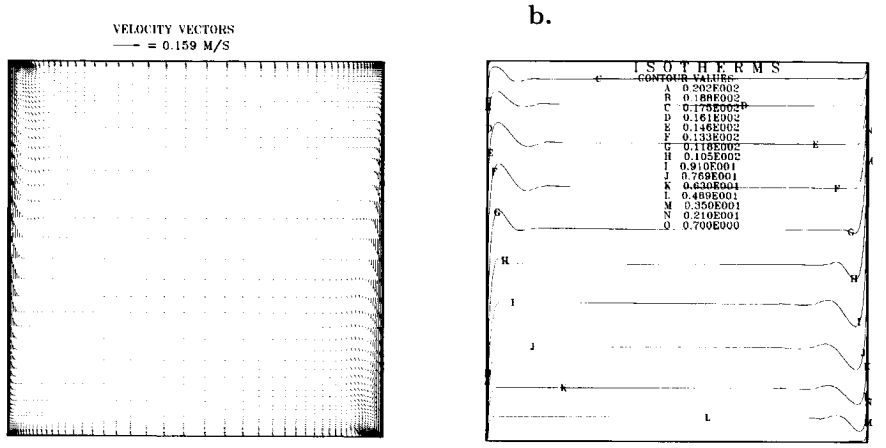

Figure 6.24: The velocity vectors (left) and temperature contours (right); heated from the side cubical enclosure at $z/D = 0.5$, $Ra = 5 \times 10^{10}$.

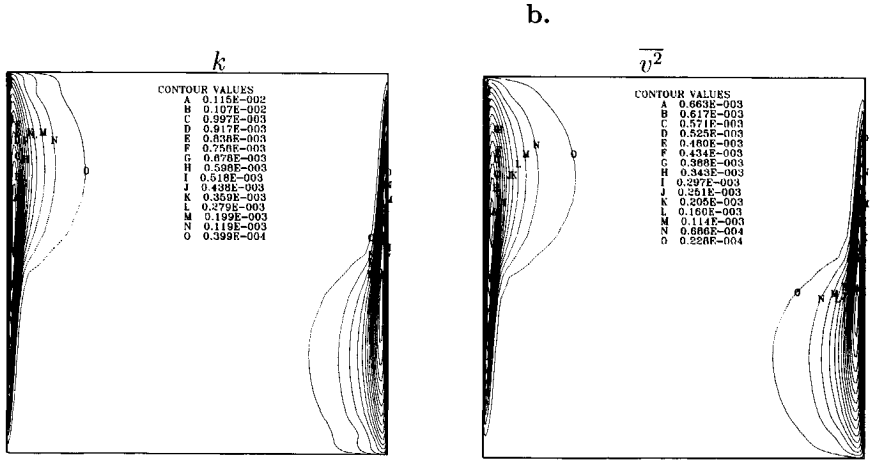

Figure 6.25: The turbulent kinetic energy (a) and $\overline{v^2}$ (b) contours; heated from the side cubical enclosure, $x/L = 0.5$, $Ra = 5 \times 10^{10}$.

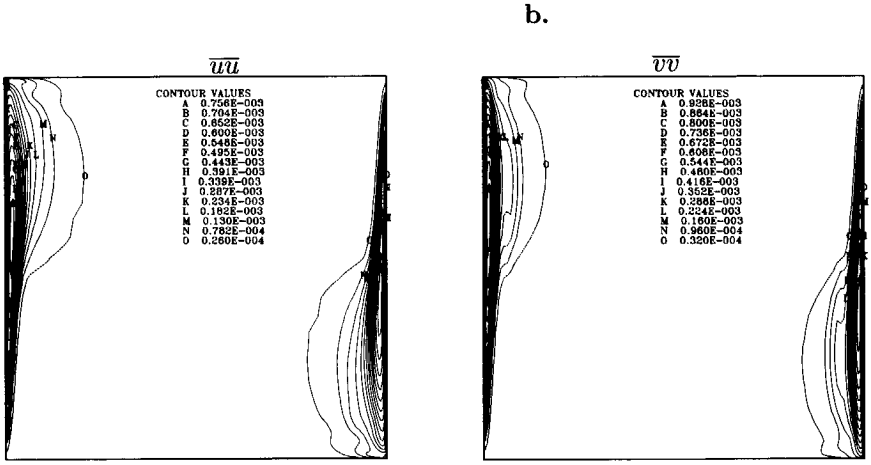

Figure 6.26: The contours of $\overline{uu}$ (a) and $\overline{vv}$ (b) of the heated from the side cubical enclosure; $z/D = 0.5$, $Ra = 5 \times 10^{10}$.

and 0.9) are shown in Figs.(6.27)a-b, (6.28)a-b, and (6.29)a, respectively. In general, the proposed model agrees quite well with the experiment. The proposed model predicts fairly well the vertical velocity in the laminar part of boundary layers ($y/H = 0.1$) shown in Fig.(6.27)a. Similar prediction was observed in the fully turbulent part of boundary layers ($y/H = 0.7$). However, the model slightly underpredicts velocity in the transitional (from laminar to turbulent) part of the boundary layer ($y/H = 0.3$). This discrepancy may be caused by the premature transition predicted by simulations. Figures (6.34)a-b show the horizontal velocities in the near-wall regions. It can be seen that both the second moment closure and the proposed model differ from the experimental data. Note that there is no significant difference between the results obtained by presented model and by second moment closure of Dol and Hanjalić [24].

In order to produce turbulent solution, local triggering was applied by Henkes [50] for low-Reynolds number $k - \varepsilon$ model, followed by Dol and Hanjalić [24] for second moment closure model. Without this treatment, numerical simulation will result in laminar solution. The new $k - \varepsilon - \overline{v^2} - f - \overline{\theta^2}$ proved that the local triggering is not needed in order to get solutions in turbulent regime.

The comparisons between numerically obtained and the measured horizontal and vertical components of the rms velocity fluctuations are shown in Figs.(6.30)a-b and 6.31a-b. Generally, a good agreement between simulations and experiments is obtained. The second moment closure of Dol and Hanjalić [24] exhibits better agreement in the near-wall region for almost all positions (except for $z/D = 0.5$, $y/H = 0.7$), see Fig. (6.31)a. This is not surprising, since the

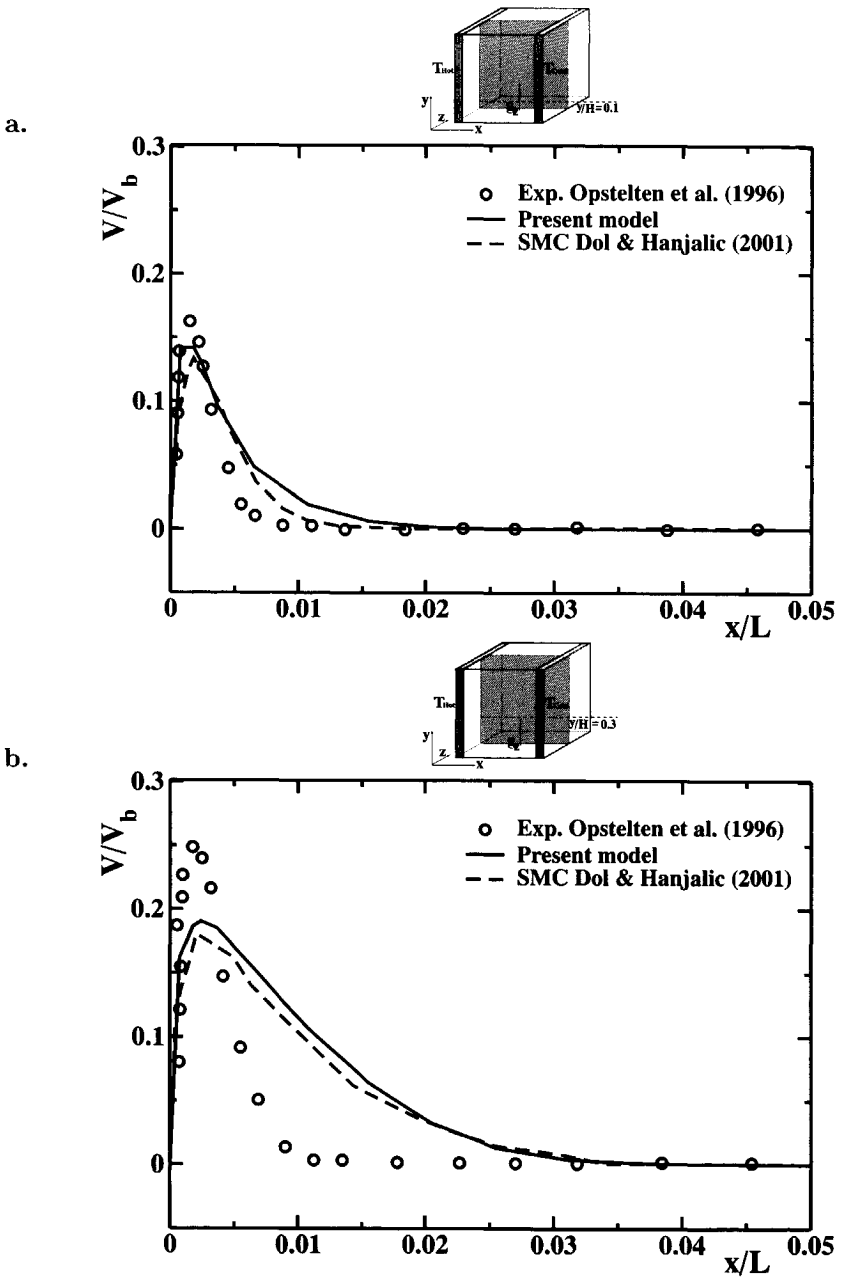

Figure 6.27: The mean velocity V of the heated from the side of the cubical enclosure at $z/D = 0.5$ of (a): $y/H = 0.1$ and (b): $y/H = 0.3$ at $Ra = 5 \times 10^{10}$

a.

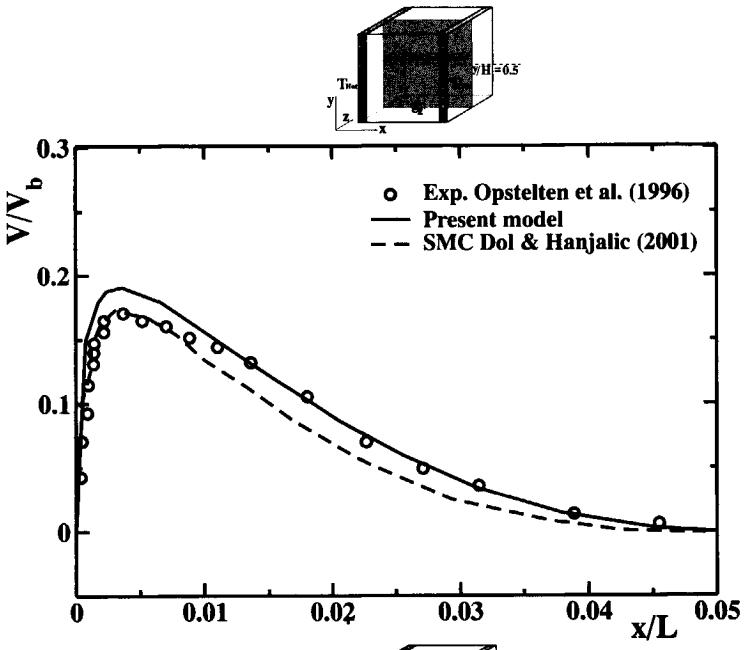

b.

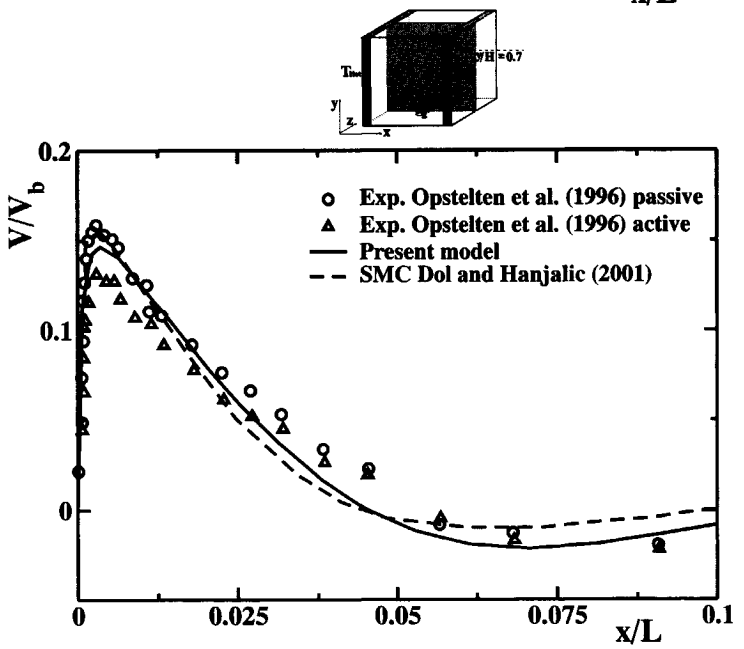

Figure 6.28: The mean velocity V of the heated from the side of the cubical enclosure at $z/D = 0.5$ of (a): $y/H = 0.5$ and (b): $y/H = 0.7$ at $Ra = 5 \times 10^{10}$

a.

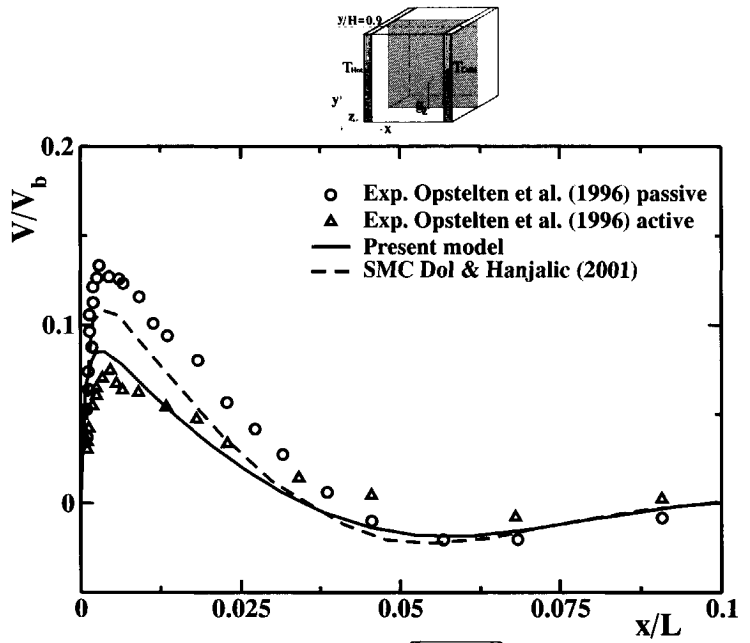

b.

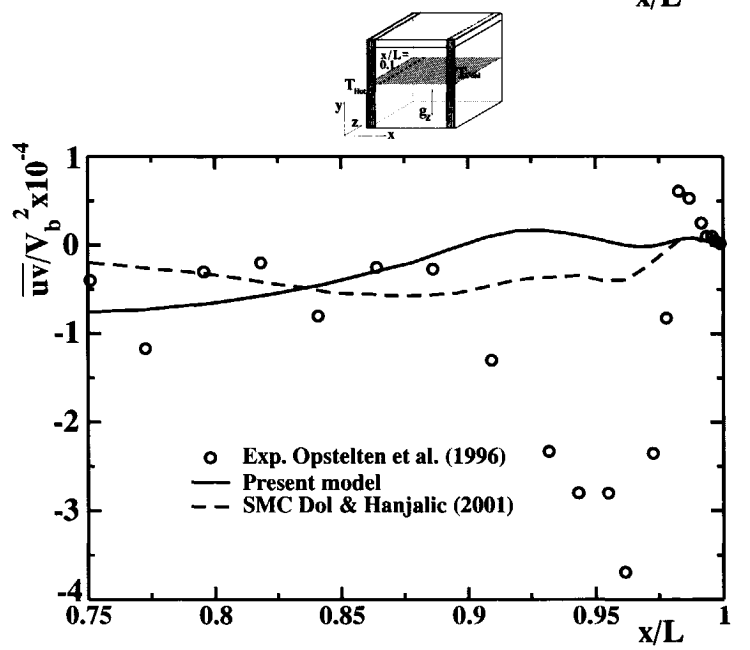

Figure 6.29: The mean velocity (a): V $(y/H = 0.9)$ and shear stress (b): $\overline{uv}$ $(x/L = 0.1)$ of the heated from the side of the cubical enclosure at $z/D = 0.5$ at $Ra = 5 \times 10^{10}$

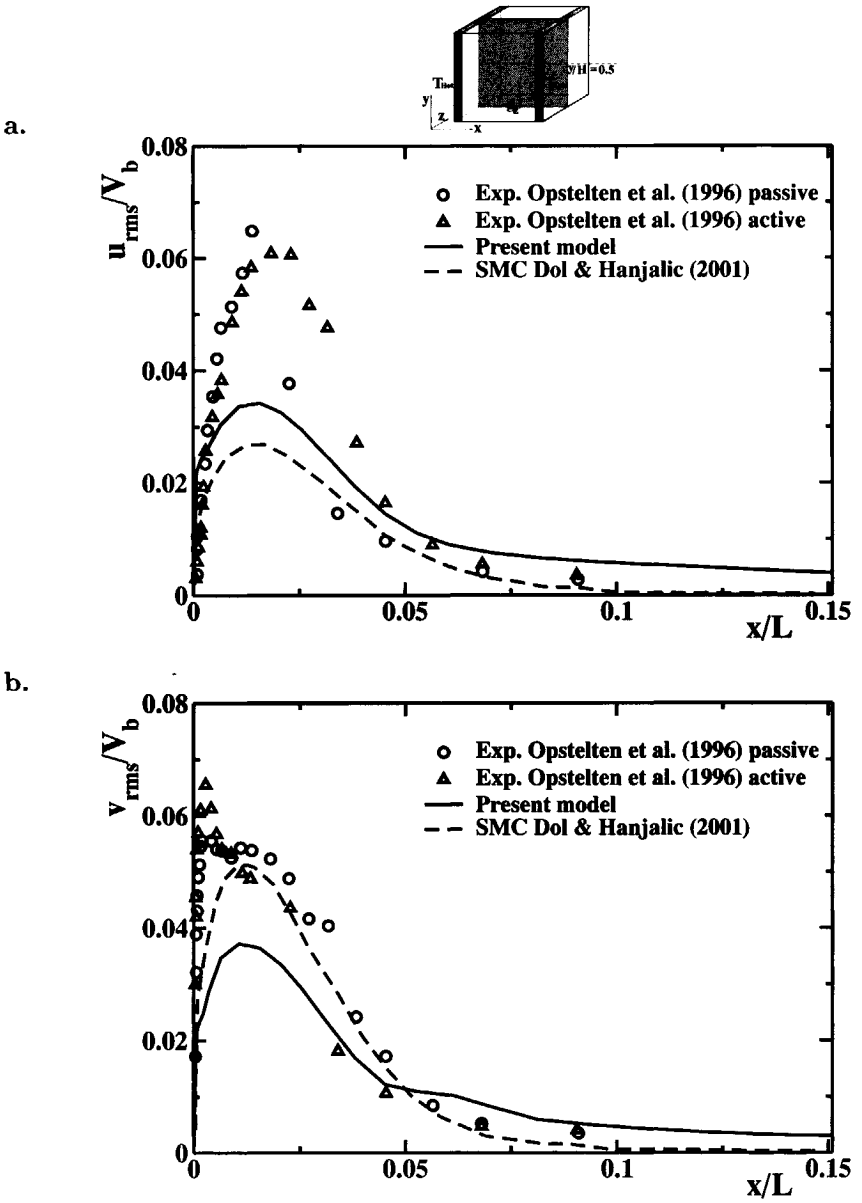

Figure 6.30: The rms velocity fluctuation (a): u_{rms} and (b): v_{rms} of the heated from the side of the cubical enclosure at $z/D = 0.5$ of $y/H = 0.5$ at $Ra = 5 \times 10^{10}$

a.

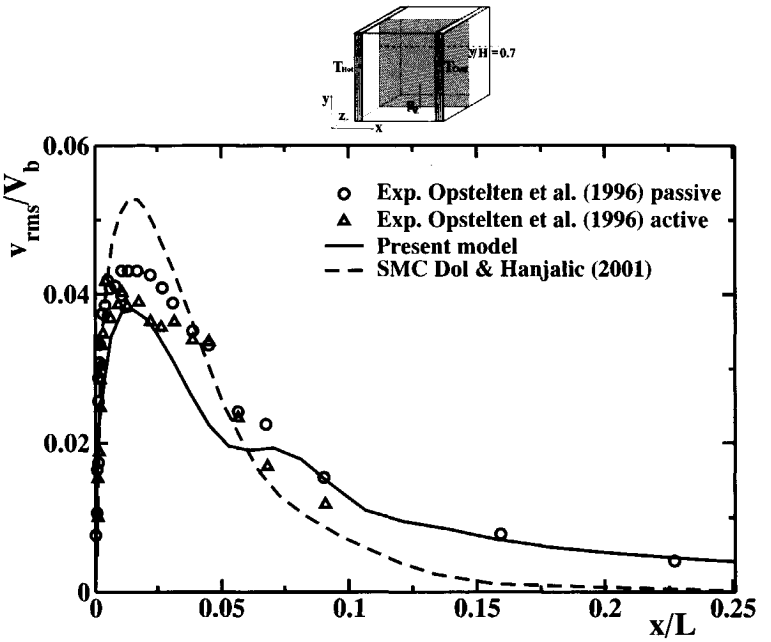

b.

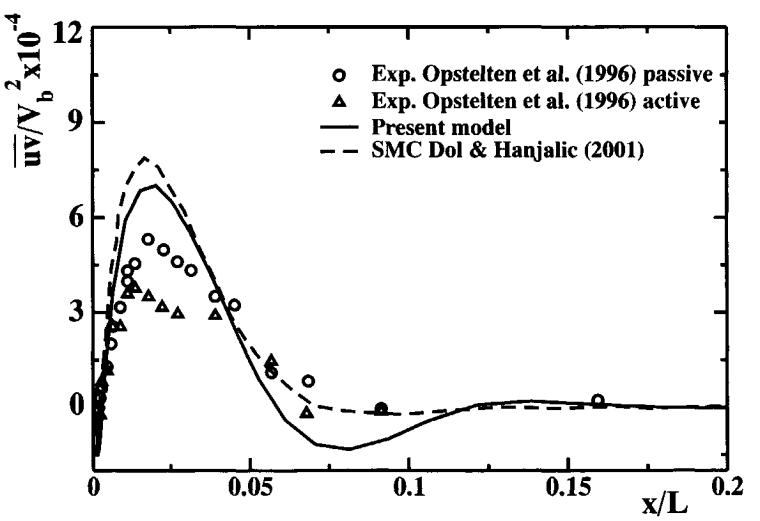

Figure 6.31: The rms velocity fluctuation (a): v_{rms} and shear stress (b): $\overline{uv}$ of the heated from the side of the cubical enclosure at $z/D = 0.5$ of $y/H = 0.7$ at $Ra = 5{\times}10^{10}$

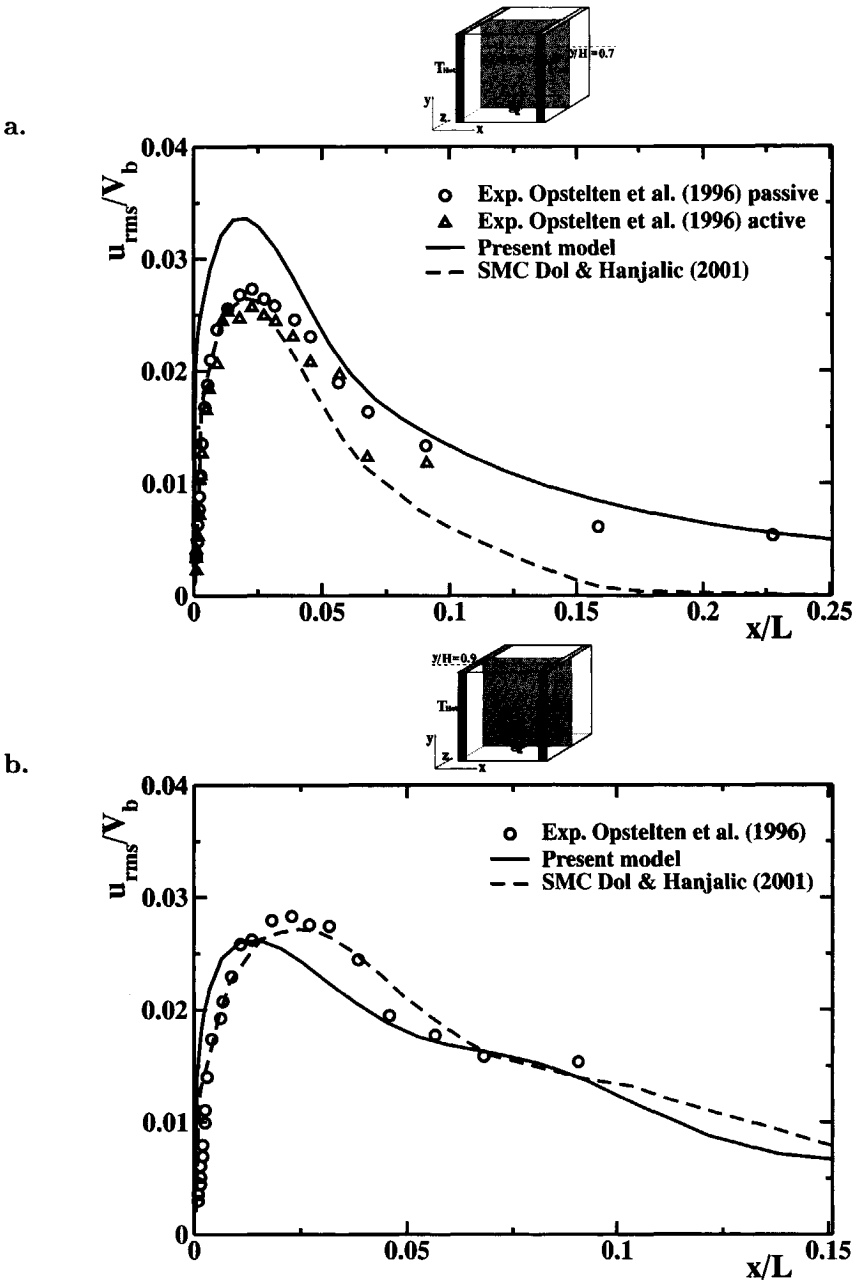

Figure 6.32: The rms velocity fluctuation u_{rms} of the heated from the side of the cubical enclosure at $z/D = 0.5$ of (a): $y/H = 0.7$ and (b): $y/H = 0.9$ at $Ra = 5 \times 10^{10}$

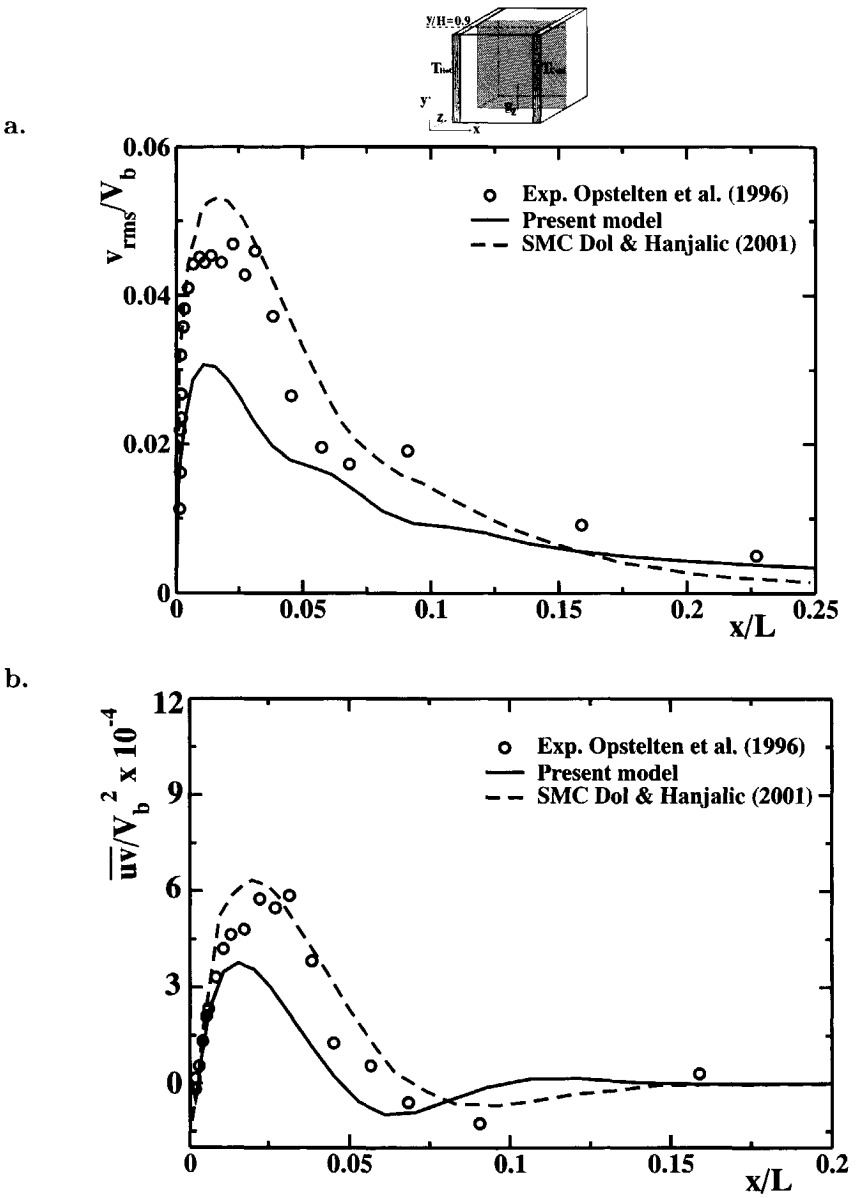

Figure 6.33: The rms velocity fluctuation (a):v_{rms} and shear stress (b): $\overline{uv}$ of the heated from the side of the cubical enclosure at $z/D = 0.5$ of $y/H = 0.9$ at $Ra = 5\times10^{10}$

a.

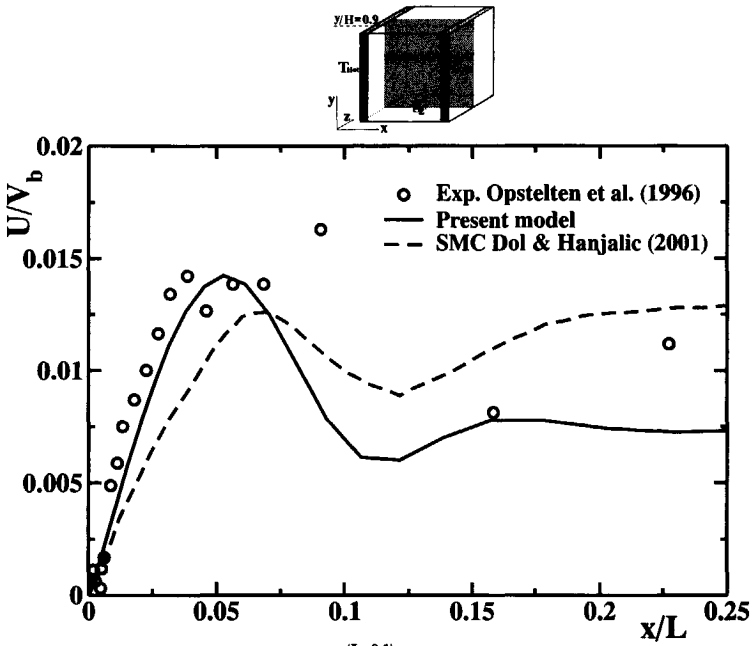

b.

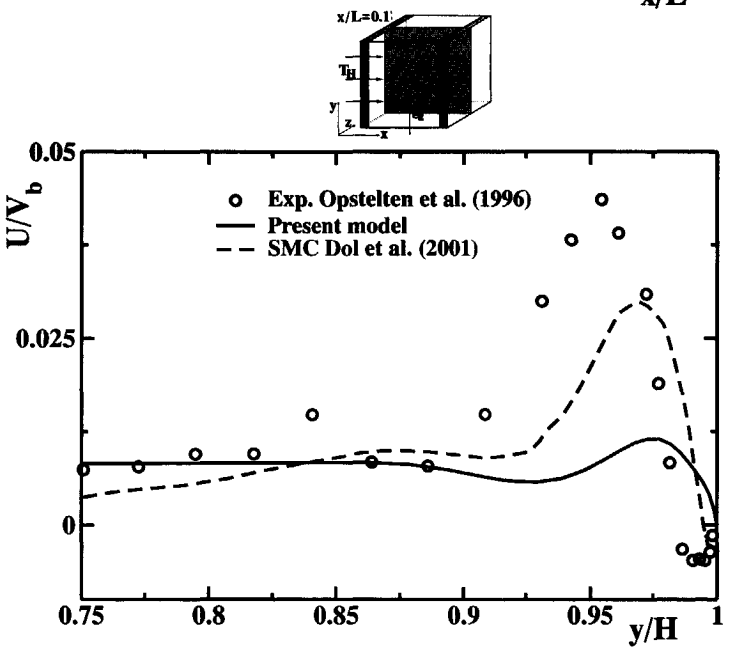

Figure 6.34: The horizontal velocity U at $y/H = 0.9$ (a.) and at $x/L = 0.1$ (b.) of the heated from the side of the cubical enclosure at $Ra = 5 \times 10^{10}$

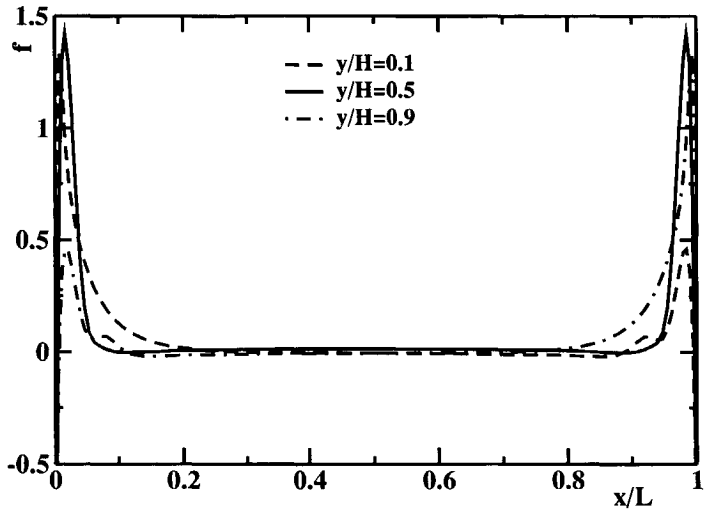

Figure 6.35: The elliptic relaxation function f at $y/H = 0.1, 0.5$ and 0.9 of the heated from the side of the cubical enclosure at $Ra = 5 \times 10^{10}$

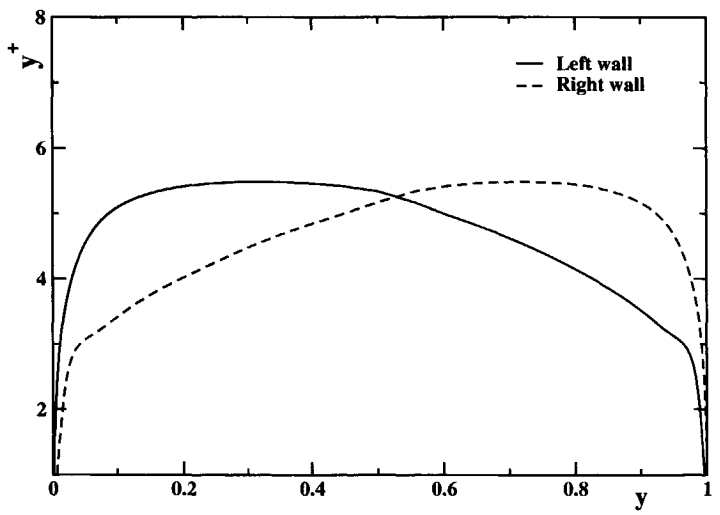

Figure 6.36: The distribution of y^+ at the isothermal walls of the side-heated cubical enclosure at $Ra = 5 \times 10^{10}$

possibility to capture correctly the stress anisotropy in the near-wall region is one of the most prominent features of second moment closure. The present model shows still very acceptable behaviour in the near-wall region and, at our initial surprise, it even outperformed the second moment closure in central region of cubical enclosure. A reason for this probably lies in the elliptical nature of relaxation function (f) compared to empirically assumed dumping functions used by Dol and Hanjalić [24]. In addition, it is important to note that the present $k-\varepsilon-\overline{v^2}-f-\overline{\theta^2}$ model is able to capture anisotropy effects since the buoyancy contribution is taken into account in algebraic representation. The similar conclusions can be drawn from behaviour of the shear stress components, Figs.(6.31)b and (6.33)b. A small negative shear stress is observed only at $y/H = 0.9$. This negative value is also well captured by the proposed model, Fig.(6.33)b.

The profiles of elliptic relaxation function f at different locations, ($y/H = 0.1, 0.5$ and 0.9) are presented in Fig.(6.35). At $y/H = 0.5$ the profile at hot and cold walls are symmetrical, while those at $y/H = 0.1$ and $y/H = 0.9$ are antisymmetrical. Variations of y^+ along the thermally active vertical walls are shown in Fig.(6.36). Note that both distributions exhibit symmetrical shapes. It can be seen that relatively large value of y^+ does not have a significant negative effect on results, indicating a good performance of the $k-\varepsilon-\overline{v^2}-f-\overline{\theta^2}$ model when relatively coarse mesh is applied. This condition is very beneficial for saving computational time as compared to the low-Reynolds model which normally requires very fine mesh for proper calculations.

6.4 Natural convection in heated from below enclosure

Natural convection in enclosures heated from below has been extensively studied both experimentally and numerically, thanks to simplicity of geometry and boundary conditions. Examples of experimental studies can be found in Bénard [3], Fitzjarrald [34], Leong *et al.* [73], and Pallares *et al.* [87]. Similarly, a number of numerical studies have also been conducted by Wörner and Grötzbach [106], Leong *et al.*[72], Kenjereš [62]. Direct numerical simulation of Raleigh-Bénard convection was carried out by Grötzbach [39], Wörner [104] and Kerr [64]. The available DNS data have greatly enhanced the possibilities for model validation.

6.4.1 Natural convection in heated from below 1:1.5 aspect ratio enclosure

The present section considers the application of the 5-equation $k-\varepsilon-\overline{v^2}-f-\overline{\theta^2}$ model in natural convection in heated from below 1 : 1.5 aspect ratio enclosure. The simulation is conducted under the Boussinesq approximation. Two horizontal walls are kept at constant temperature difference, while the remaining walls are adiabatic. The geometry was represented by 82×82 nonuniform collocated grid with a fine spacing near the horizontal walls (necessary for capturing the steep gradients in the thin boundary layers accurately). The simulation is conducted at Rayleigh number $Ra = 2 \times 10^9$, $Pr = 0.71$. In order to obtain convergent solution, underrelaxation is applied to all variables but with different values. The false-time stepping procedure is applied in order to stabilise iterative procedure with $\Delta\tau$=0.1.

It can be seen from the flow pattern in Fig.(6.37)a that a single-circular clockwise rotating flow is produced with rotation center, which is a stagnation point, at the cavity mid-point. In the top left and right bottom corners of the isothermal horizontal walls secondary counter clockwise flows appear. Note that the contours of turbulent Reynolds number, temperature, and stream lines show diagonal symmetry patterns. The contour of the turbulent kinetic energy is shown in Fig.(6.38)a, while the contour of $\overline{v^2}$ is shown in Fig. (6.38)b. It is obvious that the pattern of $\overline{v^2}$ is similar with that of the turbulent kinetic energy. However, its maximum value is about a half of that of the turbulent kinetic energy. The maximum values of the horizontal stress are located in the left-bottom and right-top corners.

The computed temperature profile for Ra=2×10^9 are plotted against the numerical result of Kenjeres [62] in Fig.(6.39)a. In the figure, the measured temperature for Rayleigh number $Ra = 10^6$ of Chu and Goldstein [14] is also presented. Good agreement is observed between 4-equation model of Kenjereš with the experiment. It is obvious that the proposed model agrees well with the 4-equation model of Kenjereš [62]. The local Nusselt number that reflects the heat transfer

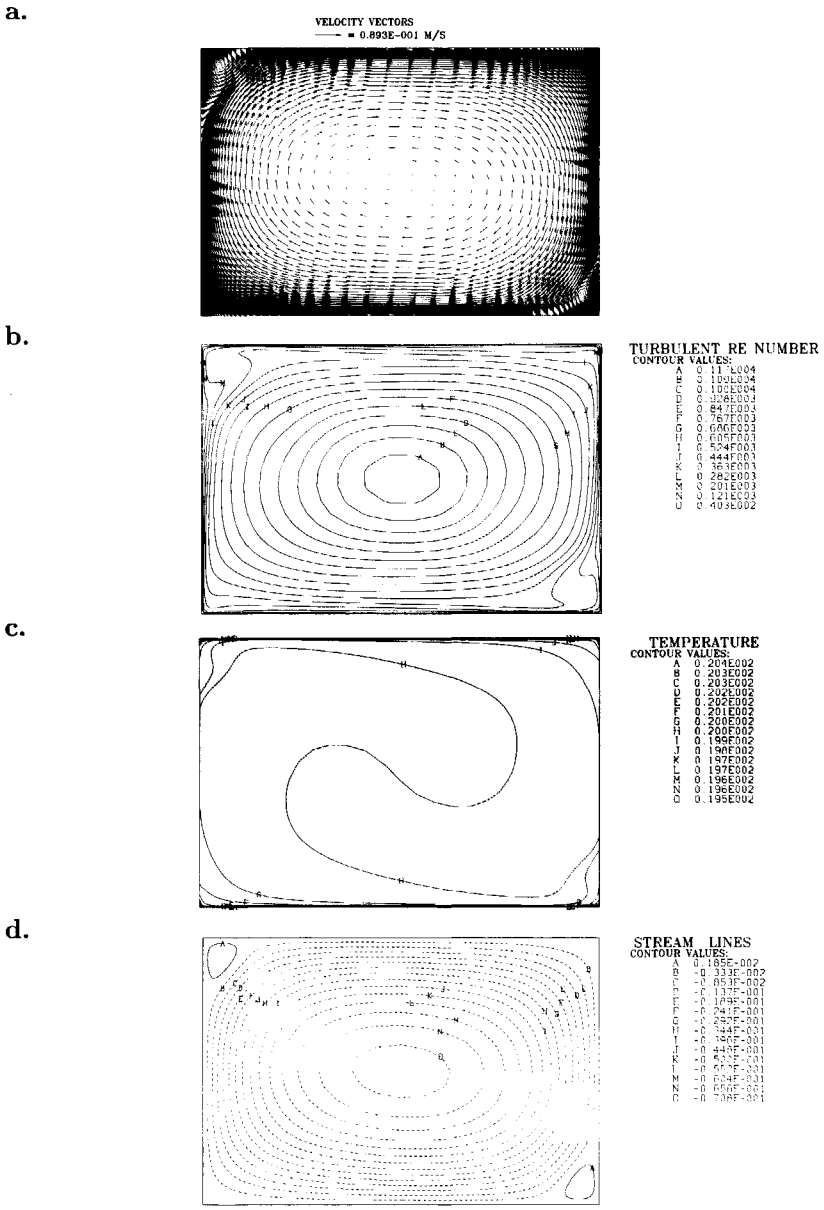

Figure 6.37: Velocity vector, turbulent Reynolds number, temperature, and stream line contours in a rectangular cavity heated from below at $Ra = 2 \times 10^9$.

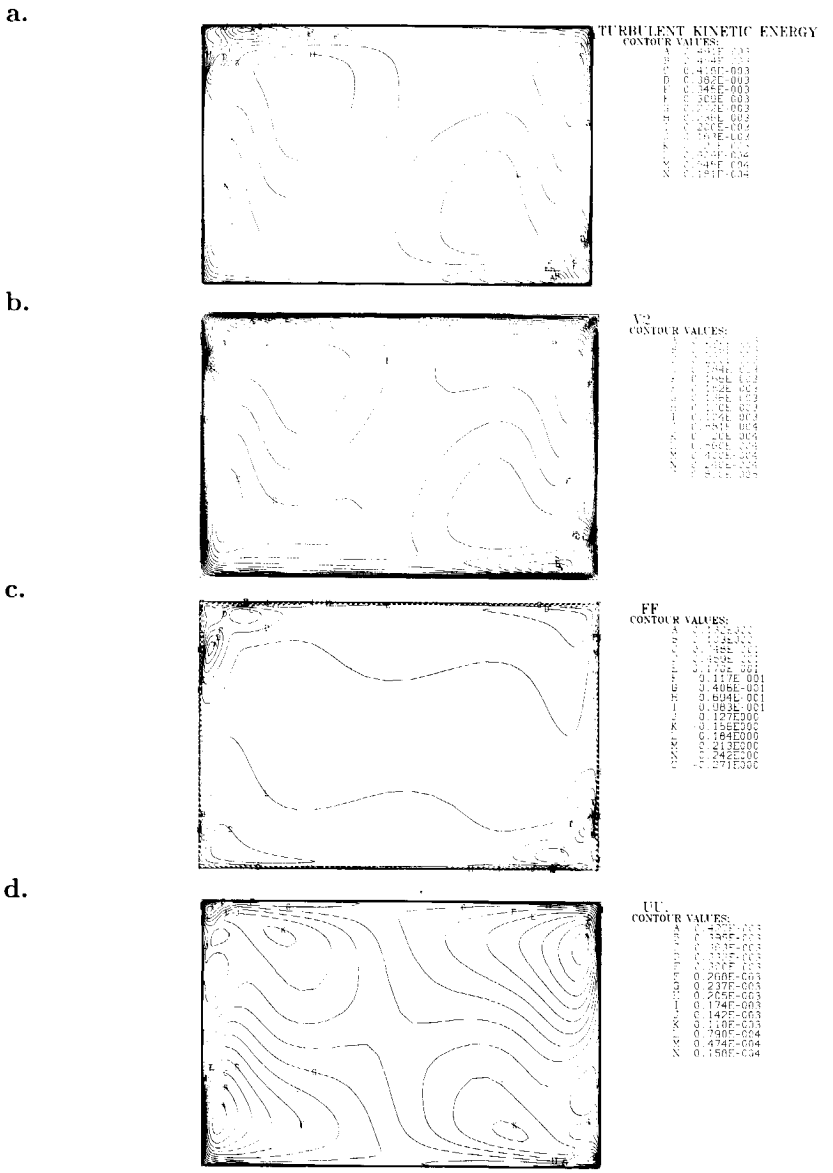

Figure 6.38: Turbulent kinetic energy k, $\overline{v^2}$, $\overline{vv}$, and $\overline{uu}$ contours in a rectangular cavity heated from below at $Ra = 2 \times 10^9$.

a.

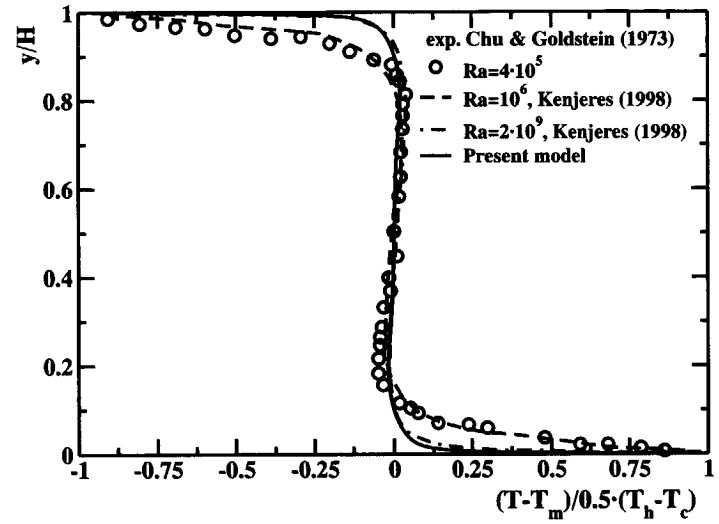

b.

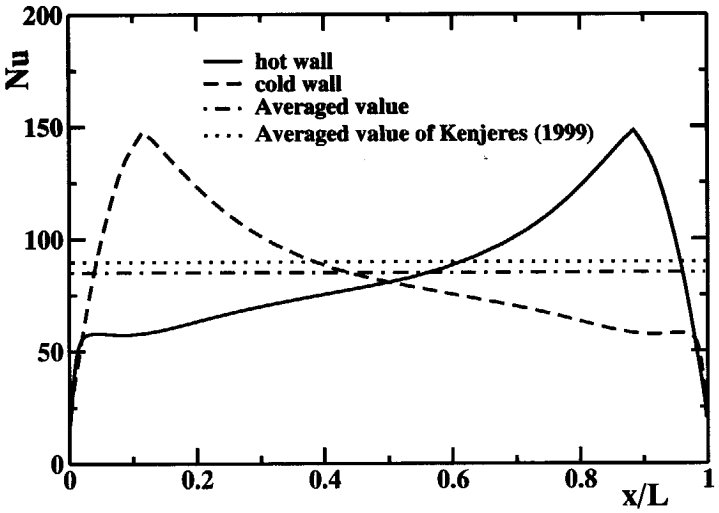

Figure 6.39: The profile of temperature (a) and the local Nusselt numbers (b) at isothermal walls of rectangular cavity heated from below at $Ra = 2 \times 10^9$.

rate at the wall is shown in Fig.(6.39)b. The maximum value of the Nu is located at the border between the secondary eddies and the main circular flow at the wall. A less pronounced peak is found at the other end of the wall. Similar pattern is reported by Kenjereš [62]. Note that the average Nusselt number obtained by

a.

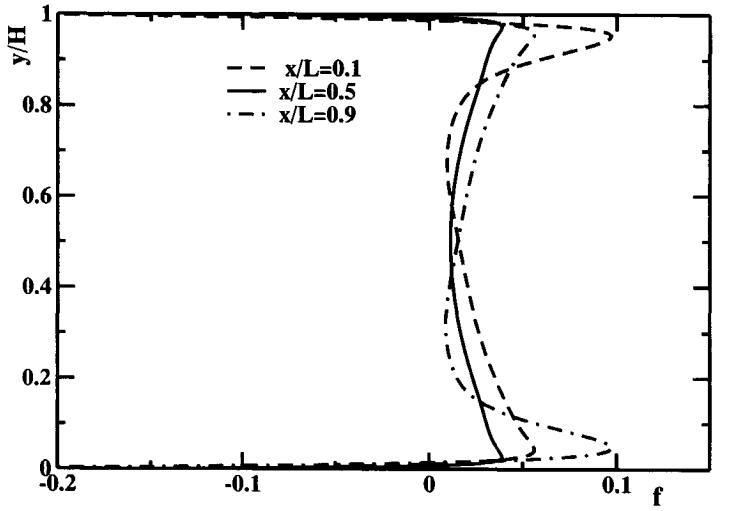

b.

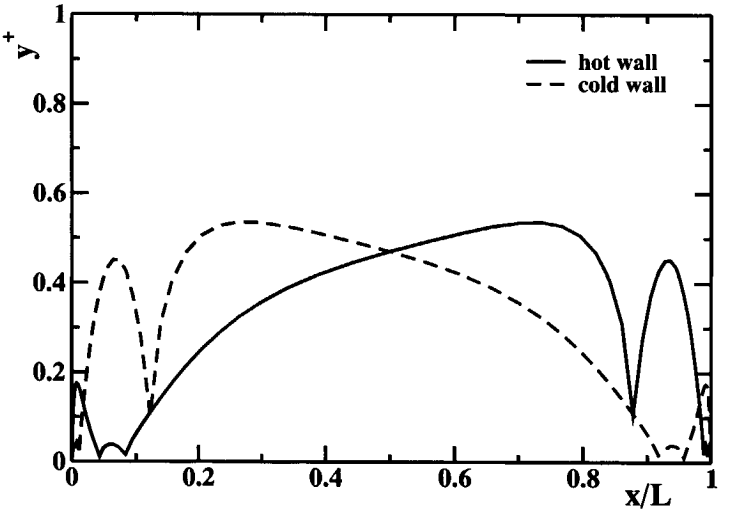

Figure 6.40: The profile of f (a) and the distribution of y^+ (b) at isothermal walls of rectangular cavity heated from below at $Ra = 2 \times 10^9$.

the proposed model is 5% less than the value calculated by using the 4-equation model.

The profile of the elliptic relaxation function f is shown in Fig.(6.40)a. Clearly, a negative value is observed at walls as defined by boundary condition. It then

crosses zero line to reach its peak value at location still close to the side-wall. It is interesting to note that the wall value of f at the isothermal wall is comparable to that of f at the adiabatic wall (see contour of f in Fig.(6.38)). Figure (6.40)b shows the distribution of y^+ along the isothermal horizontal walls. Wavy shape is observed in the near corner regions, while a smooth change is found in the remaining part of enclosure. The secondary eddies are responsible for such distribution of y^+ (velocity gradients exhibit intensive changes).

6.4.2 Conclusions

The differential Reynolds stress and heat flux models are evaluated in the turbulent natural convection in the side-heated infinite vertical channel. In addition, their algebraic forms are evaluated and tested under identical conditions. Validation is made using available DNS data and it is observed that the results agree well with DNS. Although the second moment-closure has produced better results compared to the algebraic model, especially in the prediction of vertical heat flux, there is no significant difference in performances of two modelling levels. Simulations using the $k-\varepsilon-\overline{v^2}-f-\overline{\theta^2}$ have been performed for turbulent natural convection in the side-heated (with several aspect ratios) and heated from below enclosures. For all cases considered, good agreement with available DNS and experimental results is obtained.

CHAPTER 7

Turbulent Mixed Convection Results

7.1 Introduction

Convective heat transfer under combined effects of thermal buoyancy and an externally imposed flow occurs in a number of important technological applications. These combined effects, referred as the mixed convection, may arise, for example, in externally induced flow in heated channels, in the cooling of electronic circuitry by mean of a fan, in indoor-climate situations, etc. With a better understanding of the fundamental mechanism of mixed convection, it is possible to optimise and improve the performance of various industrial applications. For this purpose, a variety of experimental and numerical studies have been performed in the literature under different conditions.

The current chapter presents calculations using the proposed $k-\varepsilon-\overline{v^2}-f-\overline{\theta^2}$ model in turbulent mixed convection of three different situations:

- Enclosure with supply and exhaust under stable thermal stratification: 2D simulations
- Indoor-climate mixed convection under summer cooling condition at low flow rate: 3D simulations
- Indoor-climate mixed convection under summer cooling condition at high flow rate: 3D simulations

The cases considered above are selected because of their relevance in realistic applications. In present investigation, the mixed convection under stable thermal stratification and under summer cooling condition have been validated using experimental data and results of previously performed numerical simulations.

7.2 Enclosure with supply and exhaust under stable thermal stratification: 2D simulations

In this section are performed numerical simulations of mixed convection in a 2D enclosure with supply and exhaust under stable thermal stratification. This configuration corresponds to conditions found in buildings with glassed roofs. The stable thermal stratification suppresses turbulent transport creating local

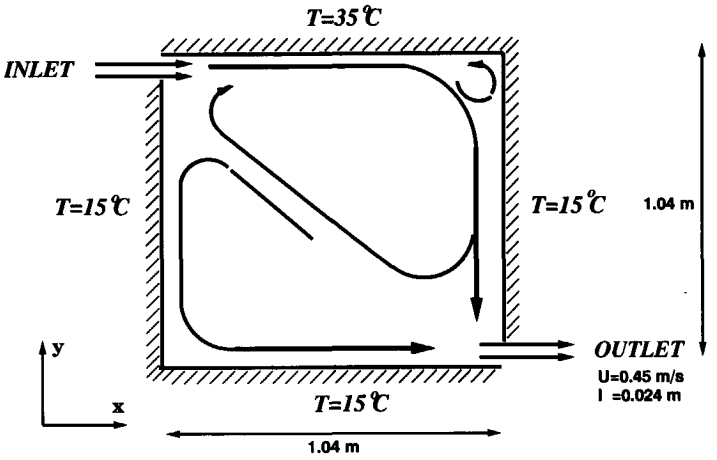

Figure 7.1: The geometrical configuration of the enclosure

coexistence of laminar and turbulent flow regimes. Purpose of this investigation is to extend model validation further to cases with mixed convection conditions.

The similar numerical study was performed by Murakami *et al.* [79]. They developed a new-version of $k-\varepsilon$ model by taking into account algebraic stress/flux representation in which terms were modified in order to provide damping effects of stable thermal stratification. The new damping functions were introduced for shear-stress $\overline{uv}$ and vertical heat flux component $\overline{\theta v}$. However these functions have a relatively complex form and they are introduced just to directly affect $\overline{uv}$ and $\overline{\theta v}$ only. Authors reported significant improvements obtained with the new model compared to standard $k-\varepsilon$ approach with wall functions for three configurations: stable stratified shear flow within a 2D channel, natural convection in 2D side-heated cavity and mixed convection under stable thermal stratification conditions.

The sketch of a two-dimensional enclosure with supply and exhaust under stable thermal stratification is shown in Fig.(7.1). An inlet with 0.018 m width with incoming air of temperature $T = 15^oC$ is placed on the front wall ($H = 1.04\ m$) under the ceiling ($L = 1.04\ m$). Initial specification of uniform inlet profiles resulted in deviation from the experimental data. Then by performing separate simulation, the fully developed profiles of all variables were obtained and used at inlet. On the other side of the wall, an outlet with 0.024 m width is placed on the back wall above the floor. In order to satisfy mass flux balance, a mean velocity is specified at outlet. Temperature in the ceiling is maintained at $T = 35^oC$ and the remaining walls are kept at $T = 15^oC$.

Figure (7.2)a illustrates the flow pattern predicted by the model. It is evident that the velocity field is almost diagonally symmetrical, with intensive flow in the

upper right part of the cavity. The most prominent feature of the flow pattern is the reversed flow from the right bottom corner to the left top corner. Due to this strong jet, the reversed diagonally oriented flow is created. Flow splits into two streams when the corner region is reached. First stream is directed downwards along the left vertical wall and is trapped in the left-bottom corner by incoming diagonal jet. Second stream continues to move in parallel to the incoming horizontal jet. Flow visualisation in experiment of Blay *et al.* [4] shows flow along the diagonal line. The identical flow pattern is reproduced by proposed model. Unlike the result obtained by simulations of Murakami *et al.* [79], where the primary vortex is located in the mid-height of the right side of the cavity, the present model predicted the vortex in the upper part of the cavity. In addition, a secondary vortex is observed at left-bottom cavity corner. This interesting feature might be due to the strong diagonal flow coming from the right-bottom corner. Temperature distribution, turbulent kinetic energy, and $\overline{v^2}$ contours of the flow are shown Fig. (7.2)b, and (7.3)a-b, respectively. As for natural convection cases, similarity between k and $\overline{v^2}$ is observed. In Figs.(7.4)a-b the contours of temperature variance $\overline{\theta^2}$ and heat flux $\overline{\theta u}$ are presented. As expected, the most intensive heat transfer takes place along the horizontal top wall.

The horizontal velocity component (U) in the central vertical line is shown in Fig.(7.5). It can be seen that the present model reproduced well the experimental data, especially in the upper part of the cavity. Similarly, the model of Murakami *et al.* [79] agrees well with the experimental data. However, the present model gives better agreement in the middle of the cavity, while the model of Murakami *et al.* [79] performs slightly better in the lower part of the cavity. Figure (7.6) shows the vertical velocity profile against experiment along the horizontal center line, $y = 0.52\ m$. It is evident that the proposed $k - \varepsilon - \overline{v^2} - f - \overline{\theta^2}$ brings data in close agreement with experiment. Noticeable improvements with the new model compared to model of Murakami *et al.* [79] are achieved in predicting in the maximum velocity profile in the central part of the cavity. The strong non-monotonic behaviour of f distribution across horizontal profiles at different enclosure heights ($y/H = 0.1, 0.5, 0.9$) are observed, Fig.(7.7). The amplitude of changes increases as the right vertical wall is approached. The profiles of y^+ along the vertical walls are shown in Fig.(7.8). The strong variations of y^+ are appearing only in vicinity of horizontal top and bottom walls. Similar distribution of y^+ along the horizontal walls is shown in Fig.(7.9).

It seems that the proposed variant of model works quite well for this case of turbulent mixed convection in a 2D enclosure with supply and exhaust under stable thermal stratification. Although the case considered is relatively complex - characterised by the direct interaction between strong jet with high temperature gradient (at the top wall), velocities are well predicted. In addition, strong fluctuation of y^+, especially in the near inlet region, does not affect the numerical stability.

a. **b.**

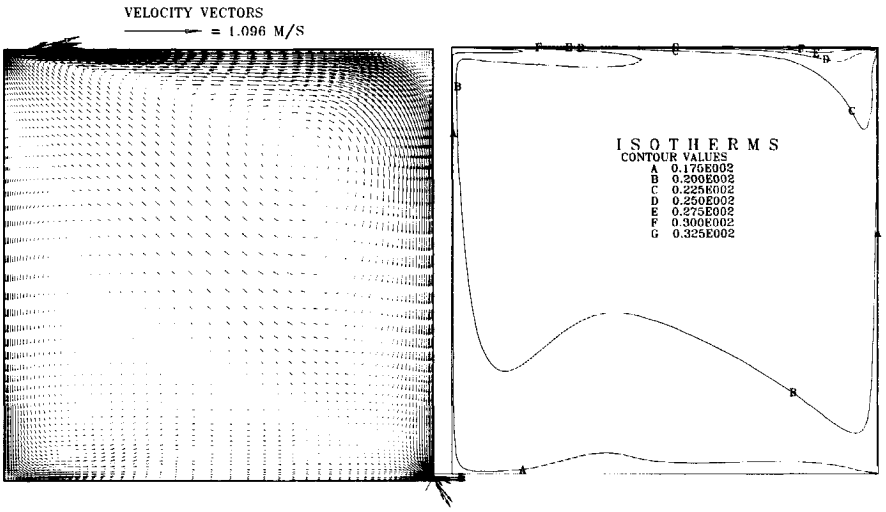

Figure 7.2: The velocity vectors (a.) and temperature distribution (b.) obtained with new $k - \varepsilon - \overline{v^2} - f - \overline{\theta^2}$ model.

a. **b.**

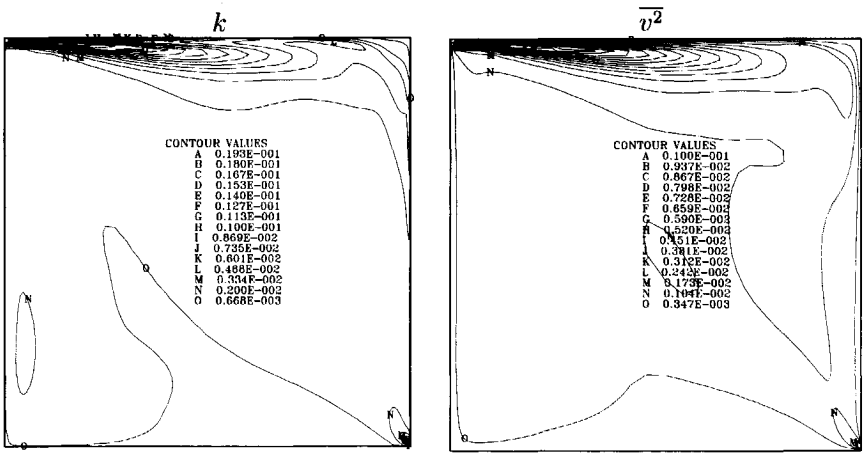

Figure 7.3: The turbulent kinetic energy (a.) and $\overline{v^2}$ (b.) contours obtained with new $k - \varepsilon - \overline{v^2} - f - \overline{\theta^2}$ model.

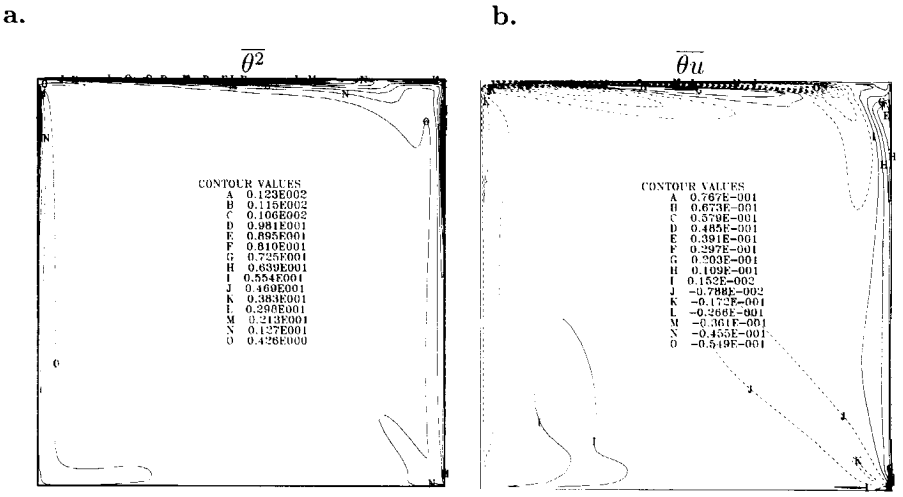

Figure 7.4: The temperature variance $\overline{\theta^2}$ (a.) and heat flux $\overline{\theta u}$ (b.) contours obtained with new $k-\varepsilon-\overline{v^2}-f-\overline{\theta^2}$ model.

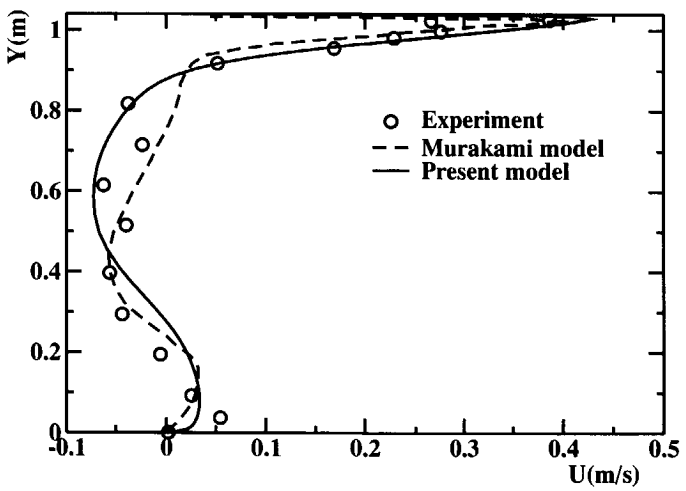

Figure 7.5: Comparison of the horizontal velocity U along the vertical center line $x = 0.52\ m$ with experiment of Blay *et al.* [4]

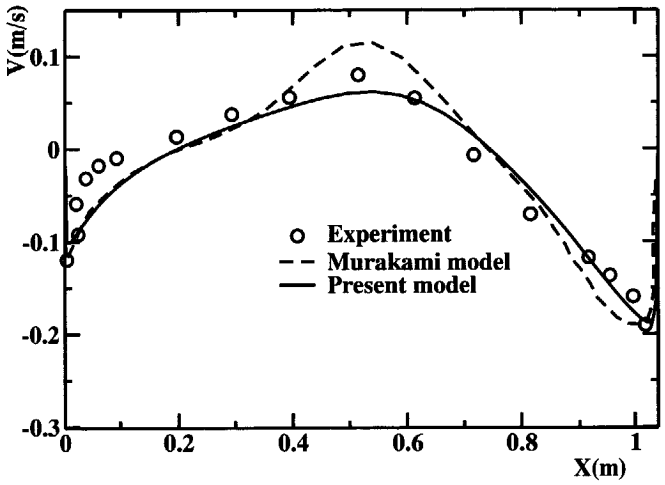

Figure 7.6: Comparison of the vertical velocity V along the horizontal center line $y = 0.52\ m$ with experiment of Blay *et al.* [4].

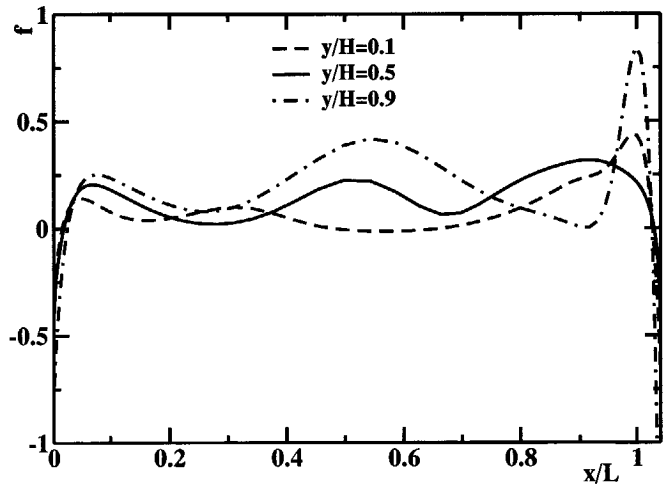

Figure 7.7: The elliptic relaxation function f at $y/H = 0.1, 0.5$ and 0.9 of 2-D mixed convection

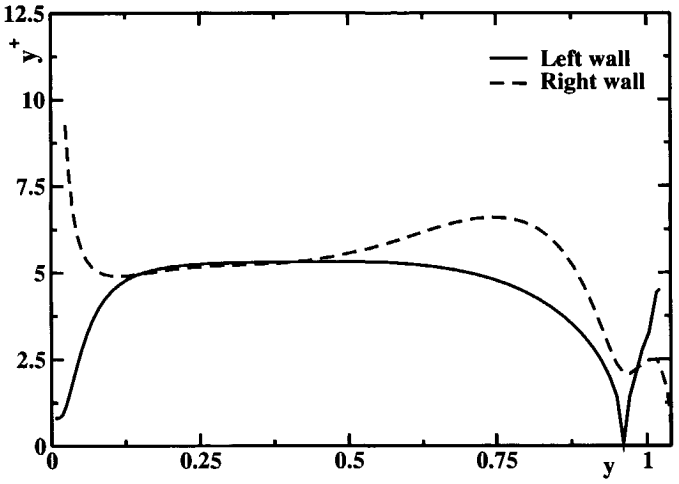

Figure 7.8: The distribution of y^+ along the vertical walls of 2-D mixed convection

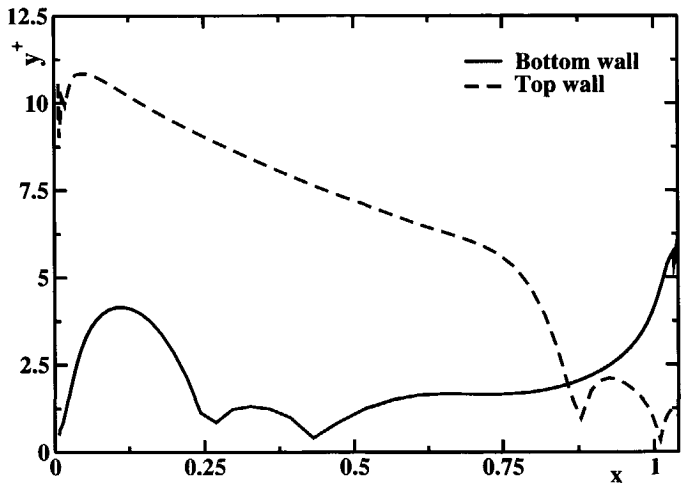

Figure 7.9: The distribution of y^+ along the horizontal walls of 2-D mixed convection

7.3 Indoor-climate mixed convection under summer cooling conditions: 3D simulations

According to an epidemiological survey with more than 10000 participants in the USA and Canada, they spent, on average, about 10% of their time outdoors in summer time and only 2−4% in winter time, Leech *et al.* [70]. Such large fractions of time spent indoors are typical for all industrial countries, especially in seasons when out-doors thermal conditions are too hot or too cold for comfort. Similar statistics is found in industrial cities of tropical countries, where hot weather and humidity may have an adverse impact on occupant comfort. It is therefore important to put a more research attention on indoor-climate investigation.

Thermal comfort is generally defined as that condition of mind which expresses satisfaction with the thermal environment, Höppe [52]. For example, thermal condition in residential or office space has to be considered carefully mainly because of its influence on possible creation of negative conditions which can lead towards dissatisfaction with environment, productivity decrease, and ill health. The dissatisfaction may be caused by the body being too warm or too cold as a whole, or by unwanted heating or cooling of a particular part of the body. Another important parameter involved in the thermal comfort is the moisture content of the inside air. This variable, which is obvious in humid tropical climate, has a significant impact not only on the occupant's comfort, but also on the required energy to heat or to cool specific space. In order to provide indoor thermal comfort, several approaches have been used: natural ventilation, mechanical ventilation (fans) and air-conditioning system. The term 'ventilation' includes all procedures where air in the interior of a closed space is replaced by external air masses, entering through building openings.

Natural ventilation is the cheapest way of providing a comfortable environment in indoor or in workplace, because of its potentials in reduction of energy costs. Many studies dealing with natural ventilation in enclosures can be found in literature. Most of these studies have concentrated on ventilation flows which are solely driven by either the buoyancy force associated with the temperature difference between the fluid inside the enclosure and that of its surroundings, or the wind, Linden *et al.* [75]. The mathematical models have been developed by Cooper and Linden [15] to predict the thermal stratification in enclosures due to buoyancy driven ventilation flows. Wind driven ventilation flows is well understood, particularly with the use of wind tunnel models for the determination of pressure coefficient for model buildings, Hunt and Linden [53]. They investigated the fluid mechanics of combined effects of buoyancy and wind natural ventilation in an enclosure. It was shown that the relationship between the buoyancy and wind effects are non-linear.

Tsutsumi *et al.* [99] conducted the full scale measurement of indoor thermal factors and numerical simulation of indoor air flow. The measurement was carried

out during summer in an apartment building in two operational modes: ventilated and unventilated. The numerical simulation of indoor air flow in a single unit house was carried out to predict the air speed by natural ventilation through opening windows. The standard $k - \varepsilon$ model was applied in the simulation.

Mechanical ventilation by fans is environmentally friendly and is frequently used because of relatively low running costs. For example, Wong and Khoo [105] carried out an investigation on adequacy of mechanical ventilation by fans in providing thermal comfort in Singaporean classrooms. In this study, several aspects are examined: (i) thermal condition in classrooms, (ii) thermal acceptability in classrooms, and (iii) neutral temperature.

Air conditioning system in interior environment of buildings is most frequently used to provide a comfortable indoor environment for occupants. However, the air-conditioning would consume much more energy as compared to natural and mechanical ventilations. Cheong *et al.* [11] examined the thermal comfort conditions of an air-conditioned lecture theater in a Singaporean tertiary institution using both experimental techniques and numerical simulations. It was reported that the measured thermal comfort parameters, such as temperature, airflow rate, and relative humidity are in good agreement with the calculations.

The thermal comfort in a room depends on many parameters such as: humidity, weather season and type of application. Under hot and humid tropical climate, people were found to prefer cooler environment, with slightly higher air velocity, Wong [105]. From Wong [105] study on thermal comfort carried out in tropical countries, such as Singapore and Indonesia, it was shown that temperature of 25.1° C was the optimal value. For European countries where humidity is very low, the preferred temperature may be for some degrees lower than that in tropical countries. It is interesting to note that psychological aspects of thermal comfort play an important role both indoors and outdoors, Höppe [52]. As reported by Rohles [93] in his paper "Temperature or temperament: a psychologist looks at thermal comfort", just adding wood-panels, without any changes of thermal parameters in the chamber, carpets and comfortable furniture, made occupants feel warmer, compared to test without them. Just telling occupants that temperature is higher than it really was, already made them feel warmer.

The mixed convection under summer cooling conditions based on The International Engineering Agency project called ANNEX 20, on the Air flow Pattern in Building project, was carried out by Lemaire [71], Chen [10], Johanson [56], Fossdal [35], Heikkinen [49] and Ewert *et al.*[31]. The experimental work was carried out using thermal anemometry with hot-wire probe and Laser Doppler Anemometry. Heikkinen [49] used constant temperature thermistor anemometers for temperature measurement. The choice of locations for measuring the temperature and velocity was based on the expected flow patterns. In a similar measurement, Fossdal [35] used anemometers and thermocouples. Ewert [32] used Laser Doppler Anemometry to measure local velocity component near supply air diffuser in the test room.

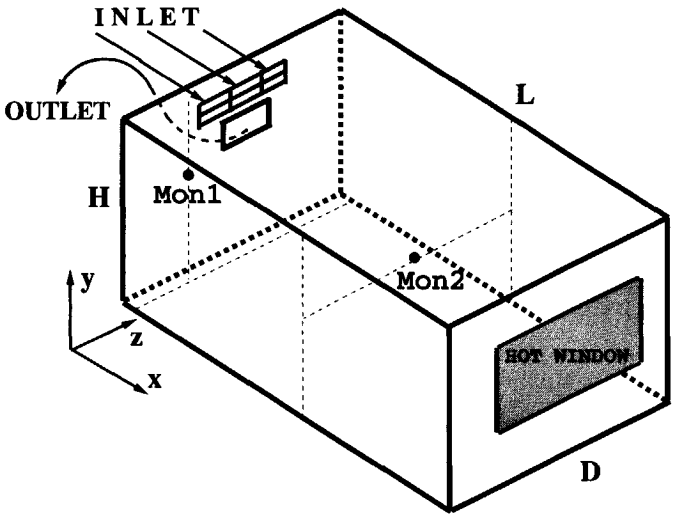

Figure 7.10: Sketch of three-dimensional ventilated room configuration

A numerical study of mixed convection of this situation was conducted by Lemaire [71], Chen [10], Johanson [56]. Several methods of defining inlet boundary condition are introduced: one-slot inlet model, multiple-slot model, and the momentum method. The inlet boundary condition is obtained from manufactures data for various room configurations. Chen [10] used inlet model of multiple slots containing 12 slots and 84 slots, while Emvin [30] used one-slot model of the same nozzles area of diffuser. In order to improve the performance of the model, a local refinement in the near-diffuser region was used by Lemaire [71]. It was shown that the inlet model of multiple slots was superior over the one-slot model. In addition, the numerical prediction showed good agreement with those from measurement.

The motivation of the current work was to predict numerically air flow in rooms using $k - \varepsilon - \overline{v^2} - f - \overline{\theta^2}$ and to compare the numerical result with the available experimental results and in the previous numerical simulations. In the present study we focus on two different flow cases. The first is the case E1 with low air flow rate ($0.0158\ m^3/s$), and the second is the case E2 with high air flow rate ($0.0315\ m^3/s$).

The geometry and basic configuration of the test room is shown in Fig.(7.10). The room configuration used for the research is based on common features of the European working place facilities. The height of the room $H = 2.5\ m$, the length $L = 4.2\ m$, and the width $D = 3.6\ m$. An inlet is centrally located on the front wall at $0.285\ m$ below the ceiling. The width of the inlet is $D_{in} = 0.18\ m$ while the height is $H_{in} = 0.062\ m$. An outlet is situated on the same wall at $1.7\ m$ above the floor and symmetrically situated between the side walls. The height

of the outlet is $H_{out} = 0.2\ m$ and the width is $D_{out} = 0.3\ m$. On the opposite side of the front wall a hot window with surface temperature of 30^oC is situated symmetrically 0.70 m above the floor (H_{win}=1.6 m and D_{win}=2 m). This hot window is expected to produce upwards buoyant flow. The remaining walls are kept at temperature of $21^o\ C$ except the front wall which was kept at $22^o\ C$. In the experimental studies, a HESCO diffuser with 84 tiny nozzles which are distributed over a fairly large area is directed upwards with an angle of 40° with respect to the ceiling. The volume flux of the jet of case E1 is $Q_{in} = 0.0158\ m^3/s$ and for case E2 is $Q_{in} = 0.0315\ m^3/s$.

In this study, the inlet is divided into 6 slots situated symmetrically at the upper part of the front wall. In order to satisfy the experimental specification, the area of the slots are taken as the real diffuser used in the experiment. The inlet velocity is directed upwards with the angle of 40°. Ideally, the inlet should be as similar to the diffuser as possible, consisting of 84 circular nozzles of the same area. However this requirement leads to necessity of using very fine mesh for the simulation. As a consequence, the computational times increases. In addition, very fine mesh in the near wall region produces small y^+ and introduces numerical instabilities in simulation. The simulation uses a non-uniform grid clustered towards the walls for better capturing of turbulence fields in the near wall region. The grid used in this simulation is $52 \times 42 \times 42$. LUDS convection scheme was employed for all variables. The problem was solved in unsteady mode to capture possible inherent unsteadiness. The time integration was performed using the three-level implicit integration scheme.

Because mixed convection is affected by two different processes, it is important to identify in which region forced or natural convection is more dominant. As expected, forced convection is the dominant mechanism of heat transfer in the region close to the inlet. For case E2 where the incoming flow rate is stronger than that of case E1, this region is further extended towards the opposite wall. It is evident that region in which thermal buoyancy prevails is further reduced due to strong cold air supply from inlet. For case E1, the region where buoyancy is the dominant mechanism of heat transfer is significantly larger compared to E2 case.

Figures (7.11)-(7.12) show the flow pattern and temperature contour for cases E1 and E2. A large quantity of fresh cold jet air is supplied by the inlet at the top of the room. It can be seen that the incoming jet of the case E1 is reflected from the upper horizontal wall at about $x/L = 0.25$. On the other hand, the supply air of the case E2 is detaching at almost $x/L = 0.75$ along the ceiling. Here the warm air from the near window region collides with the incoming cold jet. As a results of these interactions unstable flow pattern is observed.

The typical velocity predicted by model is in 0.1 to 0.2 m/s range and it corresponds well to measurement of Fossdal [35] and numerical results of Lemaire [71], but it is slightly underpredicted compared to measurement of Blomqvist [5]. For case E2, the predicted velocity corresponds well to the experimental data of

a.

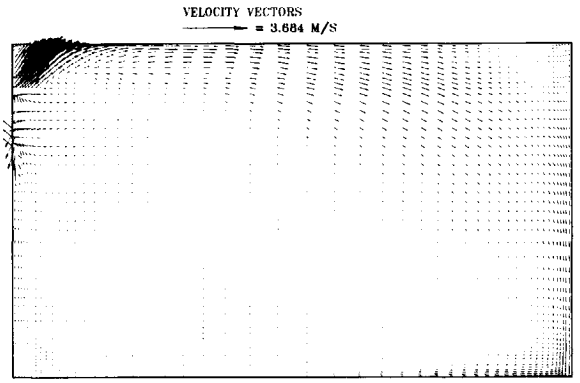

b.

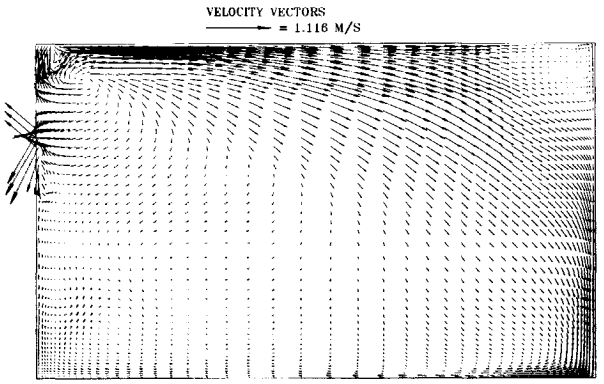

c.

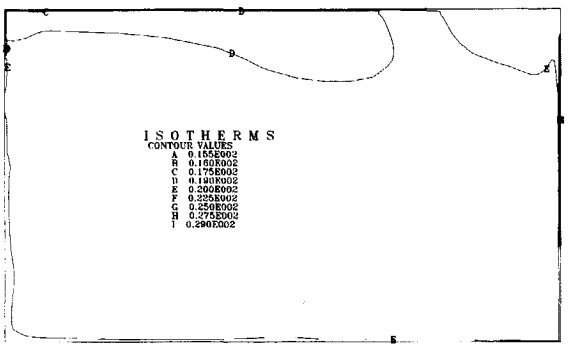

Figure 7.11: The velocity vectors in vertical plane $z/D = 0.5$ (a), at $z/D = 0.51$ (b) and temperature distribution (c) at $z/D = 0.5$ (case E2) for τ=100 *minute*

a.

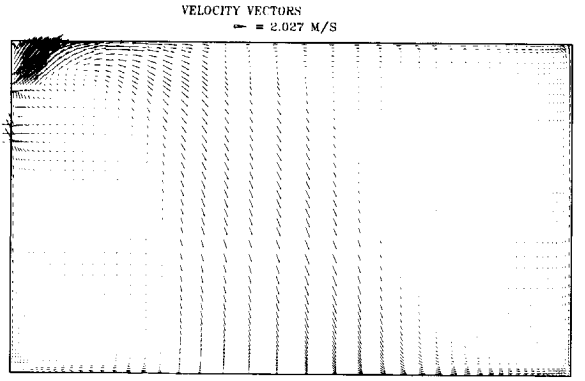

b.

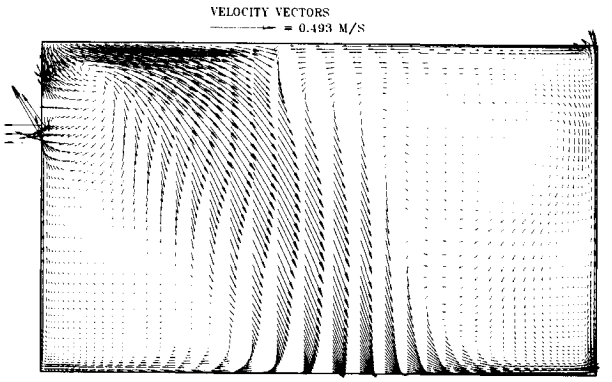

c.

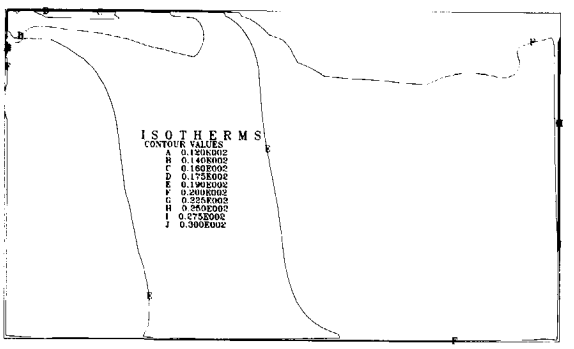

Figure 7.12: The velocity vectors in vertical plane $z/D = 0.5$ (a), at $z/D = 0.51$ (b) and temperature distribution (c) at $z/D = 0.5$ (case E1) for τ=50 *minute*

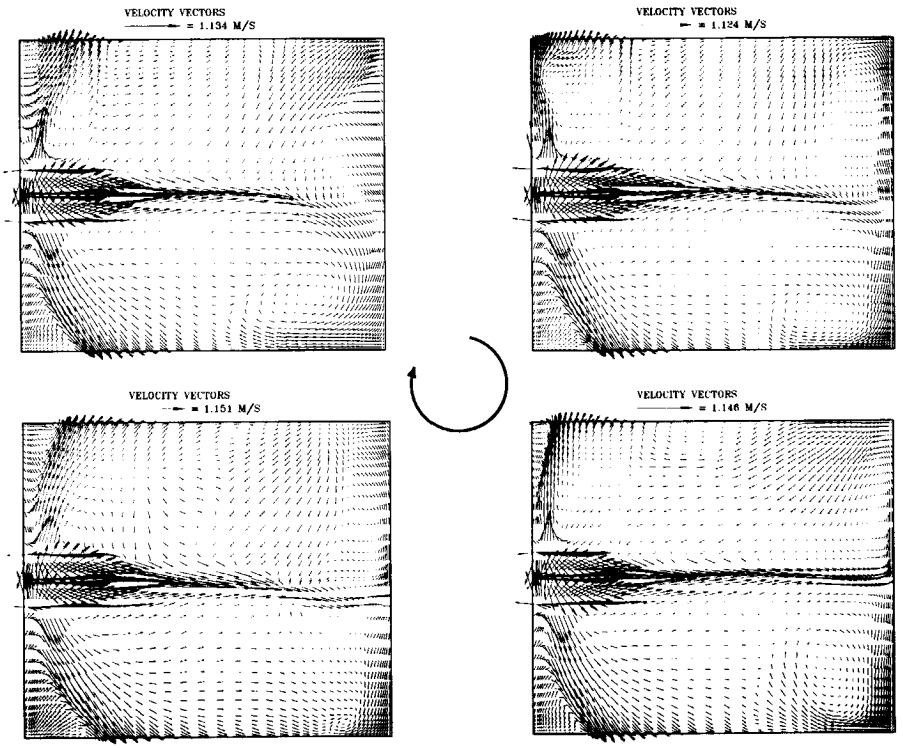

Figure 7.13: The velocity vectors in horizontal plane at $y/H = 0.9$ (case E2) for four different time instants: τ=100, 110, 120 and 130 minute

Heikkinen [49]. In the lower part of the room, the velocity is very small, about 0.05 to 0.1 m/s, with the exception of region below the window where a relatively strong downward flow is observed. In general, the velocity field predicted by present model is consistent with the experimental data.

In order to prevent draft resulting from external flow, it is important to design appropriate ventilation system. One important parameter is the penetration depth of incoming flow. The penetration depth is defined as distance from inlet to a position in which the incoming jet collides with buoyancy jet that is driven by the opposite heated wall. Clearly, a short penetration depth is not desirable, because it causes strong cold jet that enters the occupied zone, which is defined as a region bounded with height of 0.18 m from floor and width with 0.6 m from walls. The penetration depth of case E1 and E2 are 0.25 and 0.76 of the length of the room, respectively. On the other hand, the region close to the back wall,

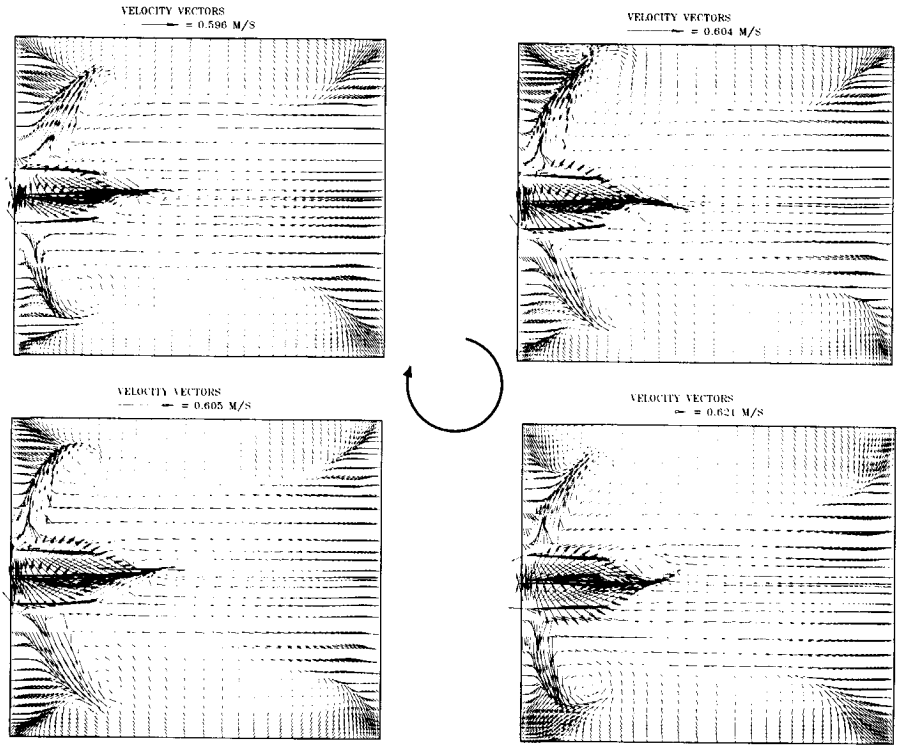

Figure 7.14: The velocity vectors in horizontal plane at $y/H = 0.9$ (case E1) for four different time instants: τ=45, 50, 55 and 60 minute

where the hot window is placed, promotes a different type of convective flow. Since this region is beyond the penetration depth of the incoming jet, the flow is buoyancy driven.

Figure (7.13)-(7.14) show the velocity vectors in the horizontal plane near the ceiling for different time instants. Vortices are found in the near corner region of the back wall. Note that near the front wall, strong span-wise flow is observed. Figure(7.15) shows the time evolution of vertical, horizontal, and span-wise velocity profiles at preselected locations for case E2. At (Mon2) location, the vertical and span-wise velocities are damped at the same level with similar pattern, while the horizontal velocity fluctuates with high amplitude indicating strong jet with unsteadiness, as also shown by Kenjereš *et al.* [63]. Since the Mon2 is within the penetration depth of the incoming jet, most flow is horizontally directed towards the back wall. On the other hand, in the near outlet location (Mon1), the time

a.

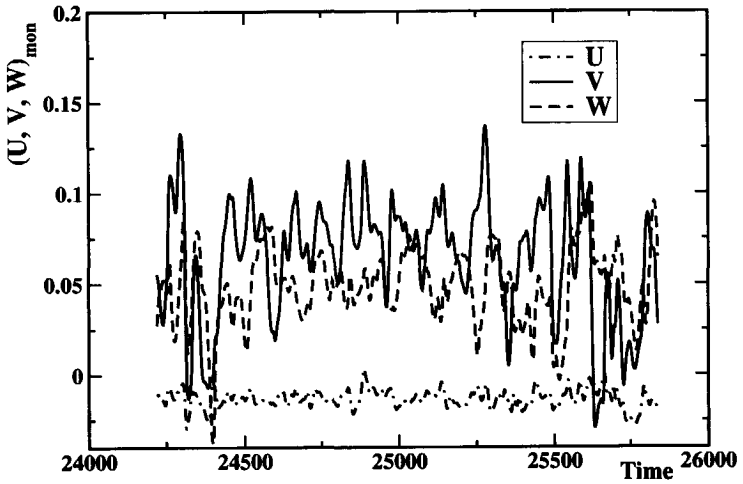

b.

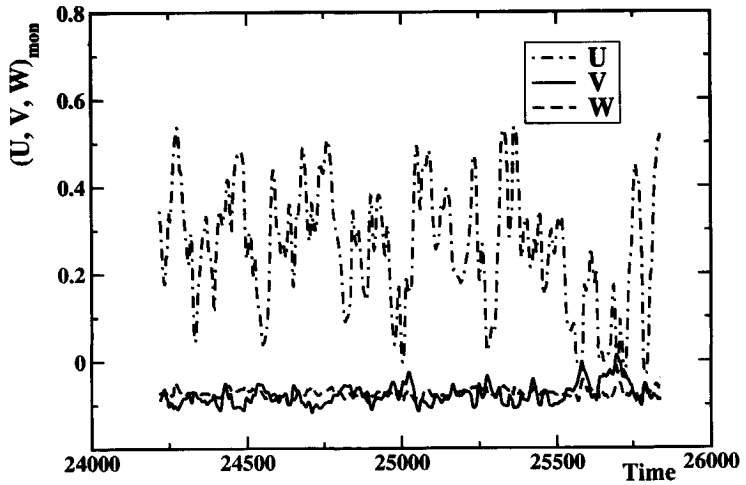

Figure 7.15: Time evolution of velocity components at different monitoring locations: Mon1 (a) and Mon2 (b), Case E2

a.

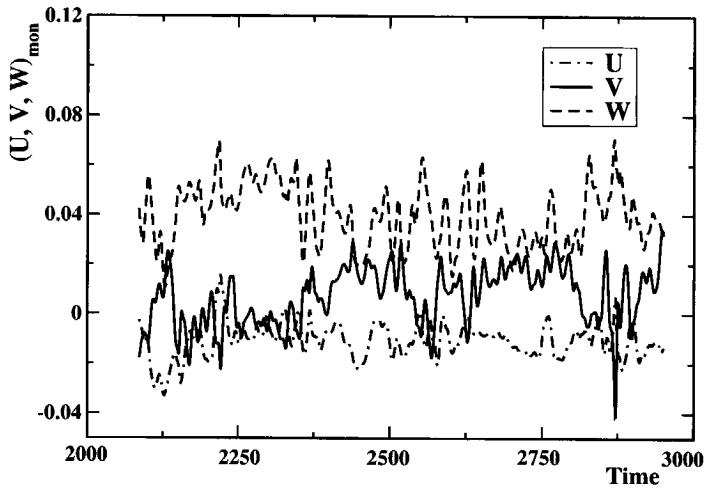

b.

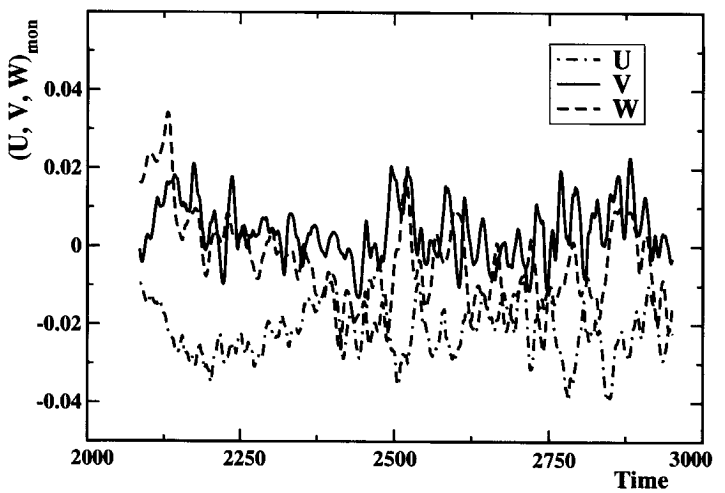

Figure 7.16: Time evolution of velocity components at different monitoring locations: Mon1 (a) and Mon2 (b) Case E1

history of velocities shows that the vertical and span-wise components fluctuate intensively, while the horizontal component is damped. This behaviour can be explained by the presence of the vertical wall which damps horizontal velocity component. Figure(7.16) show the time evolution of the velocity profiles for case E1. Here, at location Mon1, the horizontal component is again damped, while the other components fluctuate with high amplitude. It is worth to mention that synchronised fluctuations between the vertical and span-wise velocity occurs at Mon1, where both components reach maximum and minimum values with almost same period and amplitude.

The calculated velocity profiles and the experimental data of Fossdal [35] and Heikkinen [49] in the vertical plane at x=1.4 m are plotted in Fig.(7.17)a. Surprisingly, both experimental data show an obvious discrepancy, especially close to the floor and ceiling. At $y = 2.25$ m the measured velocity of Heikkinen [49] is about 0.11 m/s, while the velocity measured by Fossdal [35] is about 0.42 m/s. Near the floor, the velocity of experimental data of Heikkinen is about two times larger than measured by Fossdal [35]. Relatively good agreement is observed at the midplane. The proposed model gives values which are in reasonable agreement with experiments and shows significant improvements compared to the numerical results of Chen [10]. Note that close to the floor, both models fail to capture the secondary peak. Figure(7.17)b shows the velocity profiles of vertical plane at x=3.0 m. The proposed model is clearly not able to capture the velocity peak of the experiment in the near floor region. In the middle vertical plane the present simulations show good agreement with experiment of Fossdal [35]. Chen [10] obviously fails to predict this particular flow feature.

Figures(7.18)a-b show the temperature profiles of the proposed model against experimental data in vertical plane x=1.4 m and x=3.0 m, respectively. It can be seen that discrepancy between the two experimental data is about 0.5^o C. Although the present model consistently underpredicts experiment, it is still significantly better than model of Chen [10].

The disagreement between the experimental data and the proposed model may be caused by several factors. First, the inlet jet in experiment is created by a diffuser with 84 circular nozzles, while in present simulation is created by only 6 square nozzles. Although both inlets have the same area, the configuration of the inlet jet and the spacing distance between nozzles might affect flow spreading in the vertical and span-wise directions, and in turn, the penetration depth of the jet. Second, the size of such test room with huge walls may introduce some difficulties to maintain the steady temperature boundary conditions due to heat loses.

Figures (7.19) and (7.21) represent the profiles of the elliptic relaxation function f for case E1 and E2, respectively. All profiles cross the zero line close to the walls. For the profile at $y/H = 0.9$, a large peak is observed, while the others show a minor peak in the same region. The peak for situation at $y/H = 0.9$ is mainly attributed to the location of the inlet. Variations of y^+ on the isothermal

walls are illustrated in Fig. (7.20) and (7.22) for case E1 and E2, respectively. The horizontal variation of y^+ is apparent only in the areas near the end walls. Note that the wiggling shape of y^+ is due to proximity of inlets and outlet. The distribution demonstrates roughly the grid size level of the system. Although the values of y^+ are much larger than what is commonly used in low-Reynolds number model, the present model have reproduced the mean values of temperature and velocity fairly well.

Figures (7.23)-(7.24) show instantaneous trajectories of massless particles in the near wall regions and in the middle of room at characteristic vertical and horizontal planes. In the vertical plane, strong flow is observed in the middle of the room, characterised by dark regions with dense streamlines. It is seen that air jet and the buoyant flows collide in the middle of the room creating strong motion. In the horizontal plane, strong flow is observed only in the upper region.

Trajectories of massless particles for several time instances are shown in Fig. (7.25)-(7.26). The trajectories are taken in the horizontal plane close to the ceiling. In this region, the strong incoming jet exhibits an obvious unsteady behaviour with large periodical pattern. It is important to mention that vortices are observed in the corner regions close to the incoming jet. In this region, the vortices show a periodical pattern: in the first stage, the left vortex (from the inlet) is strong, while the right one (from the inlet) is weak. As the time progresses, the left vortex is becoming weaker while the right one is getting stronger. Finally, the vortices are formed similar as in the first pattern. Periodicity of the flow can also be observed from the changes in direction of the incoming jet. First, the jet is deflected to right. As the time progresses, it is directed straight forward, and then is deflected to the left. In the end, the first pattern is observed again.

The three-dimensional trajectories of massless particles of case E1 and E2 are shown in Figs.(7.27). For E2 case, particles travel along the ceiling and are deflected downwards in proximity of the opposite wall. When the wall is reached, the particles are reflected back and they travel along the floor. An interesting feature can be observed by analysing particles flow patterns for E1 case. After being released from the inlet, the cold jet is deflected downwards in the center of the room. The particles are then bounced upward from the floor. Since the outlet is located near the inlet, some particles are circulated in the region without first traveling in the center of the room.

Figures (7.28)a-b display instantaneous flow fields in terms of isosurfaces of the turbulent kinetic energy for case E1 and E2, respectively. The overall shapes of the isosurfaces for the two cases are qualitatively different. For case E1, intensive turbulent kinetic energy is distributed in front of the inlet, and in the midway of the room down to the floor. For case E2, large turbulent kinetic energy is distributed along the side-top corners and along the ceiling. It should be pointed out that intensive turbulent kinetic energy is observed in front of the hot window, indicating strong generation due to buoyancy. In general, the main pattern of the turbulent kinetic energy for both cases is confined to areas of the main stream.

a.

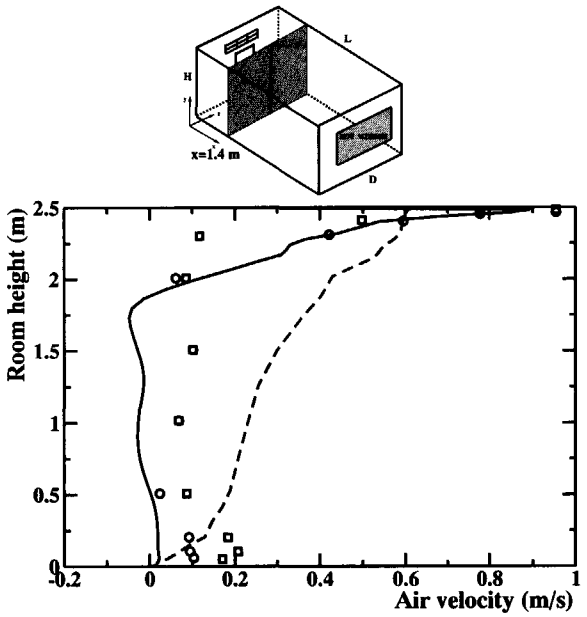

b.

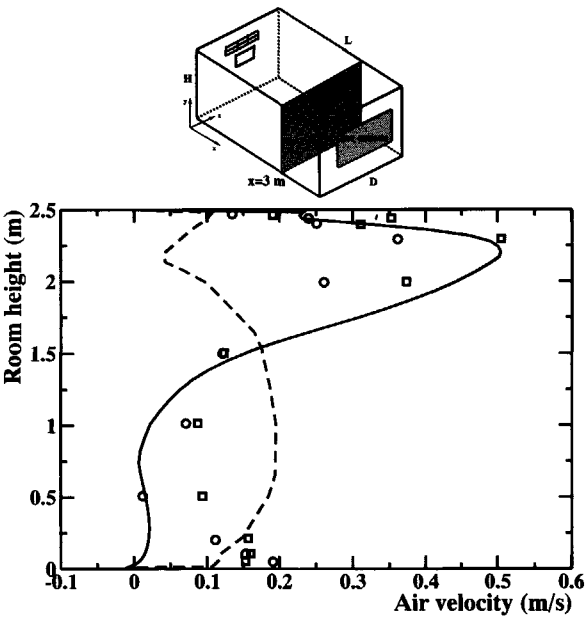

Figure 7.17: The horizontal velocity profiles at: (a) $x = 1.4$m, (b) $x = 3.0$m against experiment of Fossdal [35] ($-\circ-$) and Heikkinen [49] ($-\square-$) standard EVM (Chen [10]) (dashed line) and present model (solid line) for case E2 set up.

a.

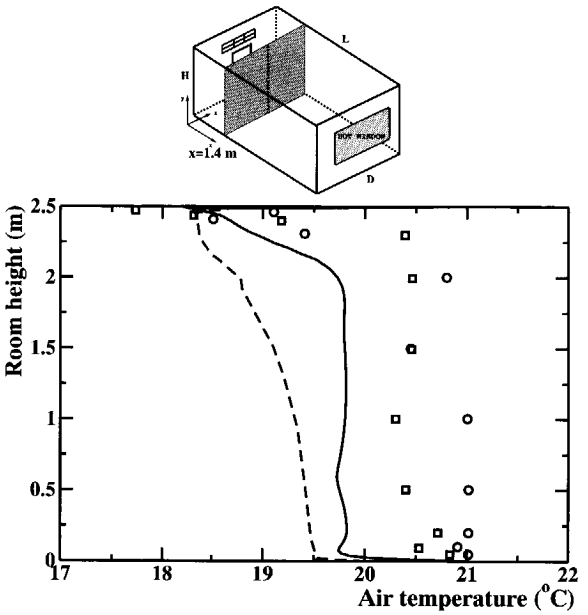

b.

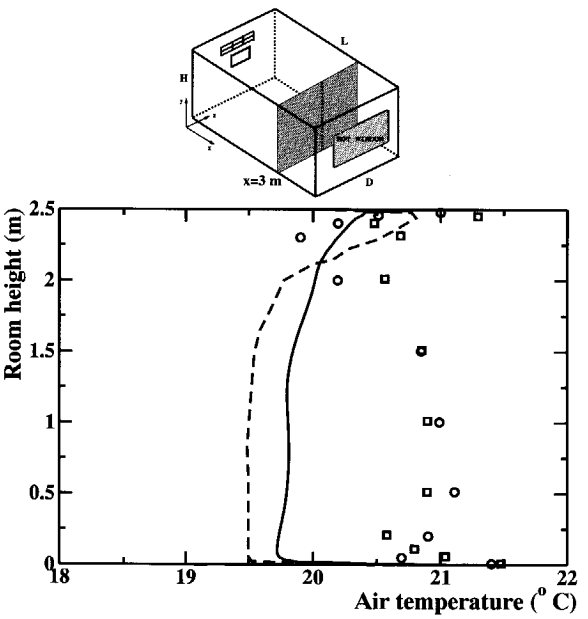

Figure 7.18: The horizontal temperature profiles at: (a) $x = 1.4$m, (b) $x = 3.0$m against experiment of Fossdal [35] ($-\circ-$) and Heikkinen [49] ($-\square-$) standard EVM (Chen [10]) (dashed line) and present model (solid line) for case E2 set up.

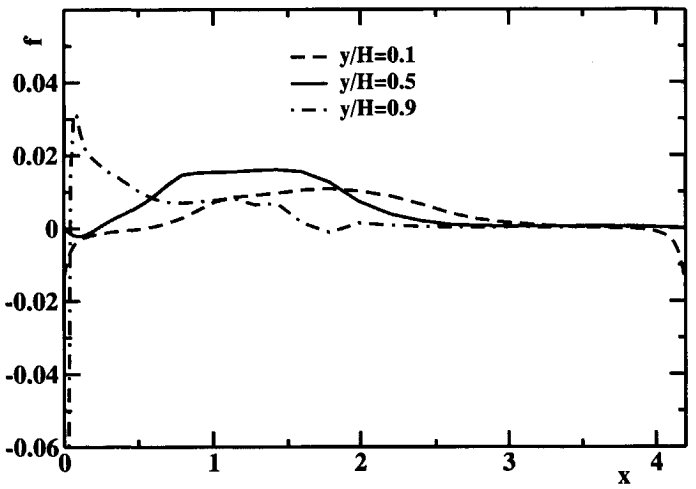

Figure 7.19: The elliptic relaxation function f at $y/H = 0.1, 0.5$ and 0.9 of case E1

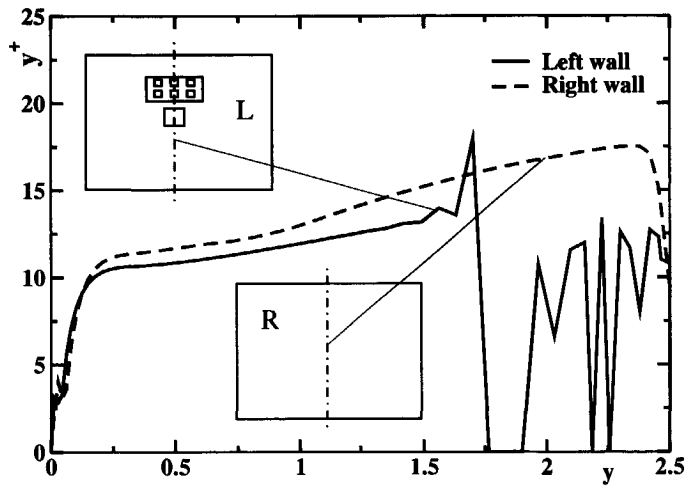

Figure 7.20: The distribution of y^+ along the isothermal walls of case E1

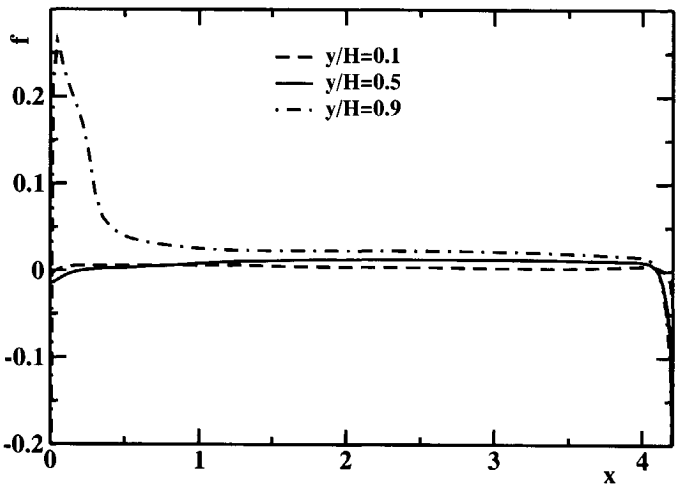

Figure 7.21: The elliptic relaxation function f at $y/H = 0.1, 0.5$ and 0.9 of case E2

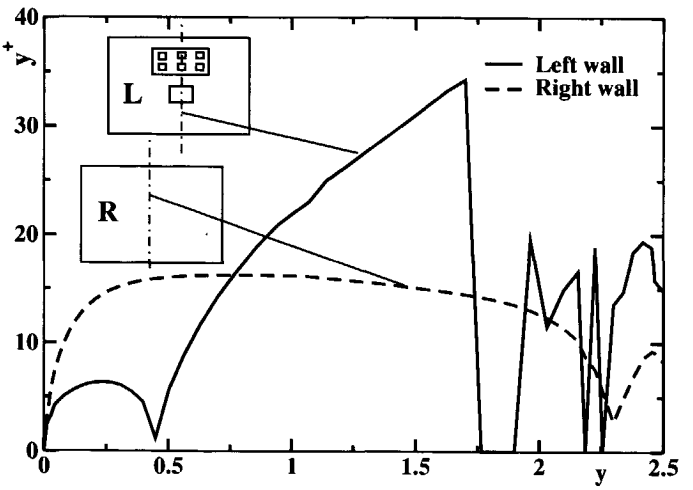

Figure 7.22: The distribution of y^+ along the isothermal walls of case E2

7.3.1 Conclusions

A $k-\varepsilon-\overline{v^2}-f-\overline{\theta^2}$ model has been applied to calculate turbulent mixed convection with supply and exhaust under stable stratification and indoor-climate mixed convection under summer cooling conditions. In the case of 2D mixed convection, the model has reproduced the experiment fairly well. This means that the model is able to predict flows under combined effects of buoyancy and shear force. Simulations of indoor-climate mixed convection show several features:

- unsteady flows with periodical pattern.
- mean temperatures are slightly underpredicted compared to experiment.
- mean velocities are in good agreement with experimental measurements.
- the present model outperformed standard $k-\varepsilon$ model.

Although relatively moderate mesh is employed, the model shows its ability to predict accurately mixed convection. This situation is beneficial for saving computational times, because simulations using a low-Reynolds number model requires significantly finer mesh with a large number of grid points. Despite its simplicity, the proposed model is capable of reasonably predicting flow, heat transfer and turbulence features in flows with strong incoming jets without introducing any ad hoc treatment to the flow condition, indicating a robust and elegant model.

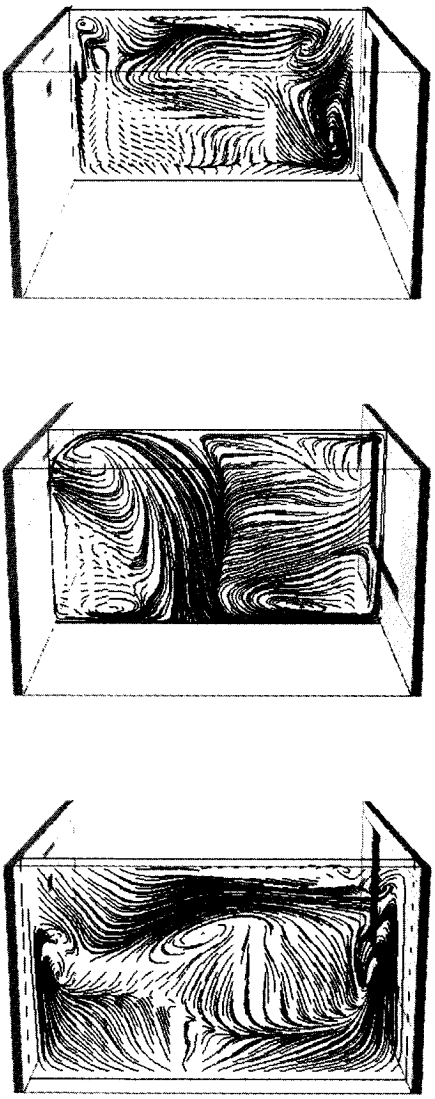

Figure 7.23: Instantaneous trajectories of massless particles in characteristic vertical planes for case E1 at $z/D = 0.9,\ 0.5,\ 0.1$

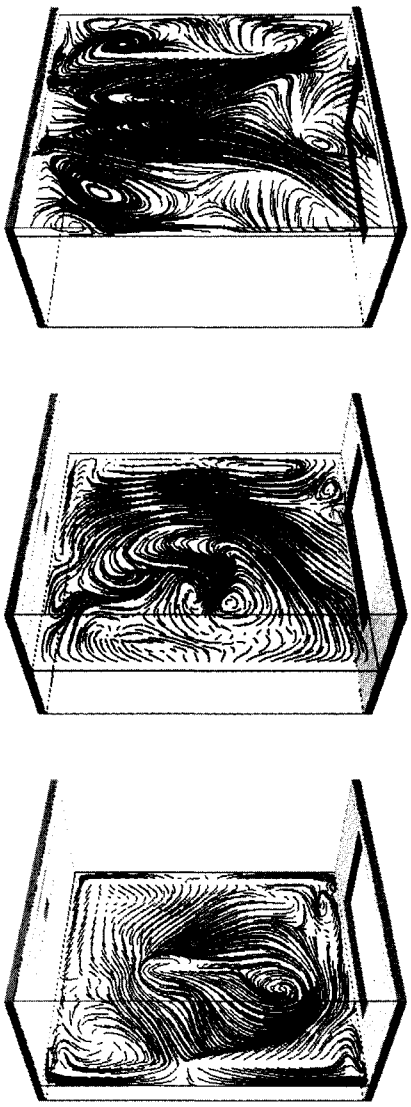

Figure 7.24: Instantaneous trajectories of massless particles in characteristic horizontal planes for case E1 at $y/H = 0.9,\ 0.5,\ 0.1$.

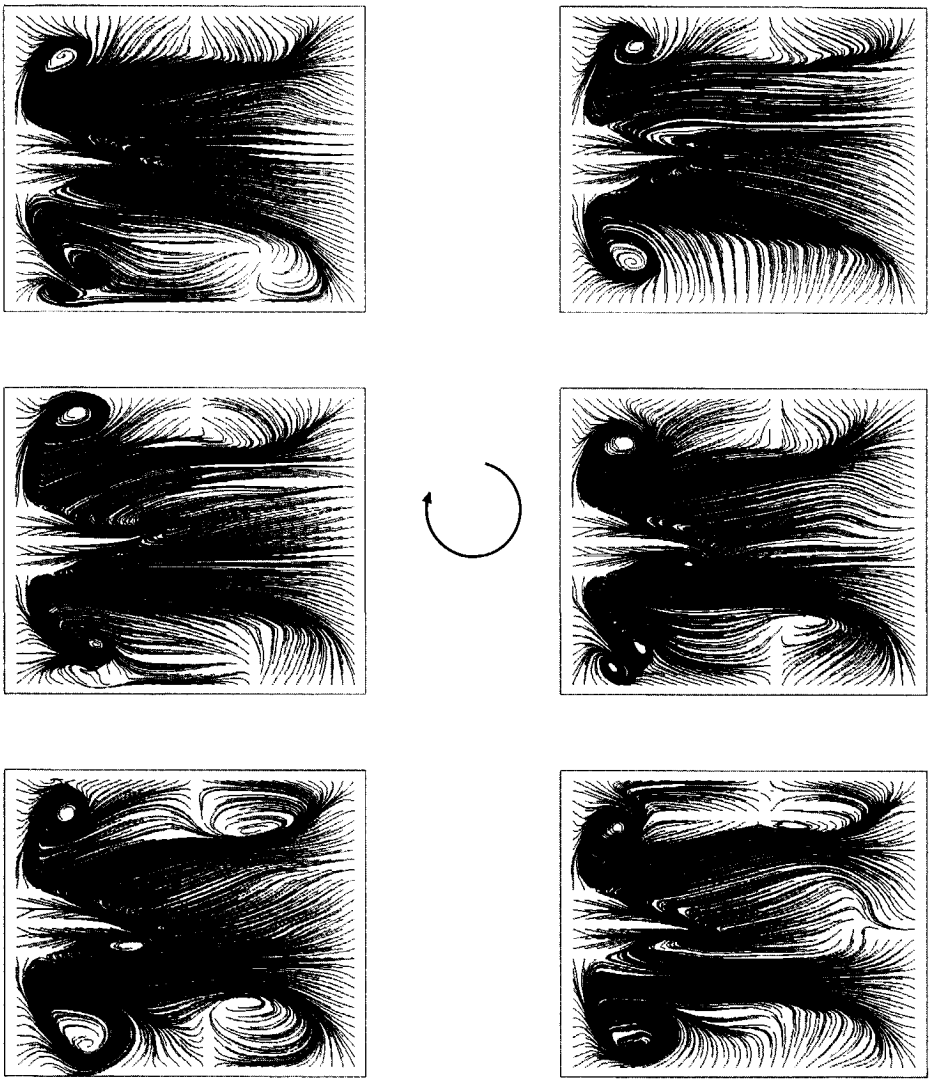

Figure 7.25: Massless particles trajectories of several instantaneous times in horizontal planes ($y/H = 0.92$) for case E1: $\Delta\tau$=5 minute

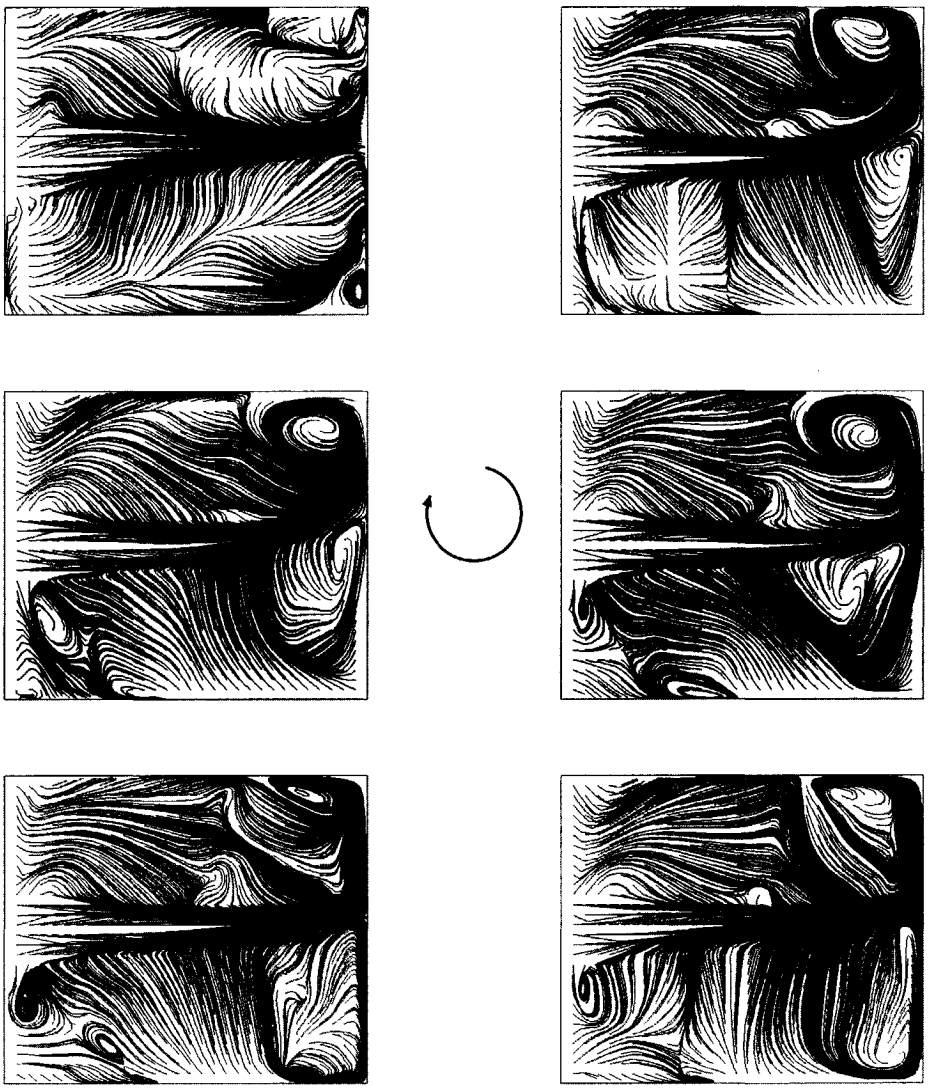

Figure 7.26: Massless particles trajectories of several instantaneous times in horizontal planes ($y/H = 0.92$) for case E2: $\Delta\tau$=10 minute

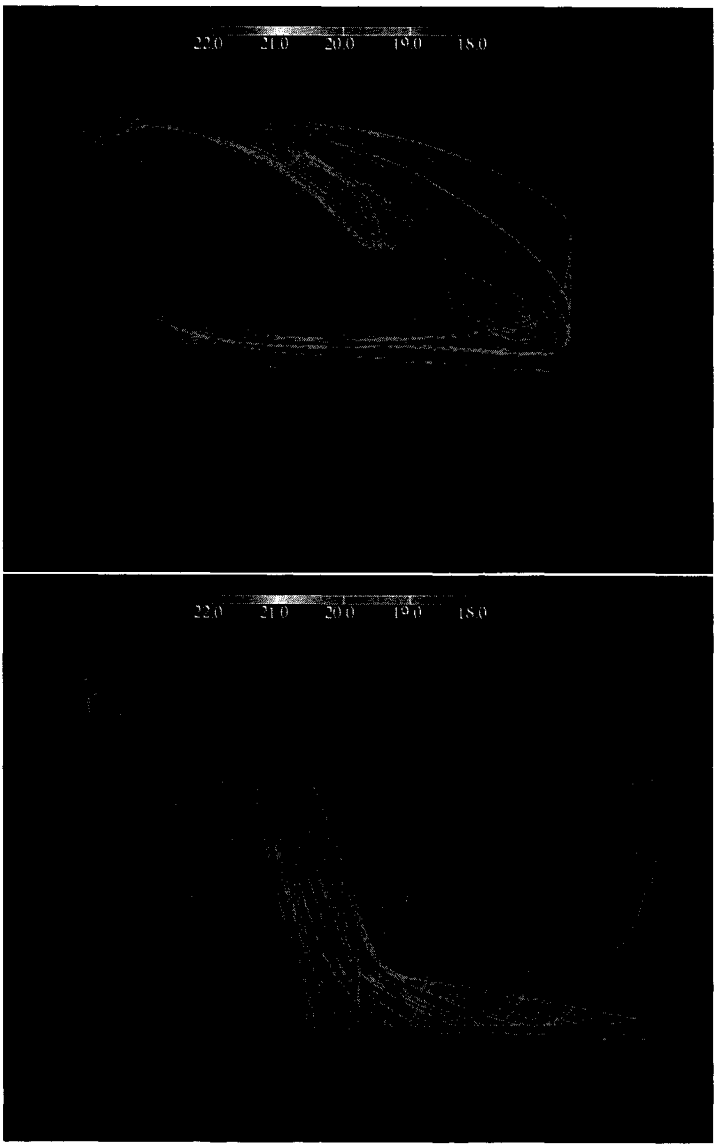

Figure 7.27: The three-dimensional trajectories of particles, coloured by local temperatures, released at diffuser inlet for E1 and E2 situations.

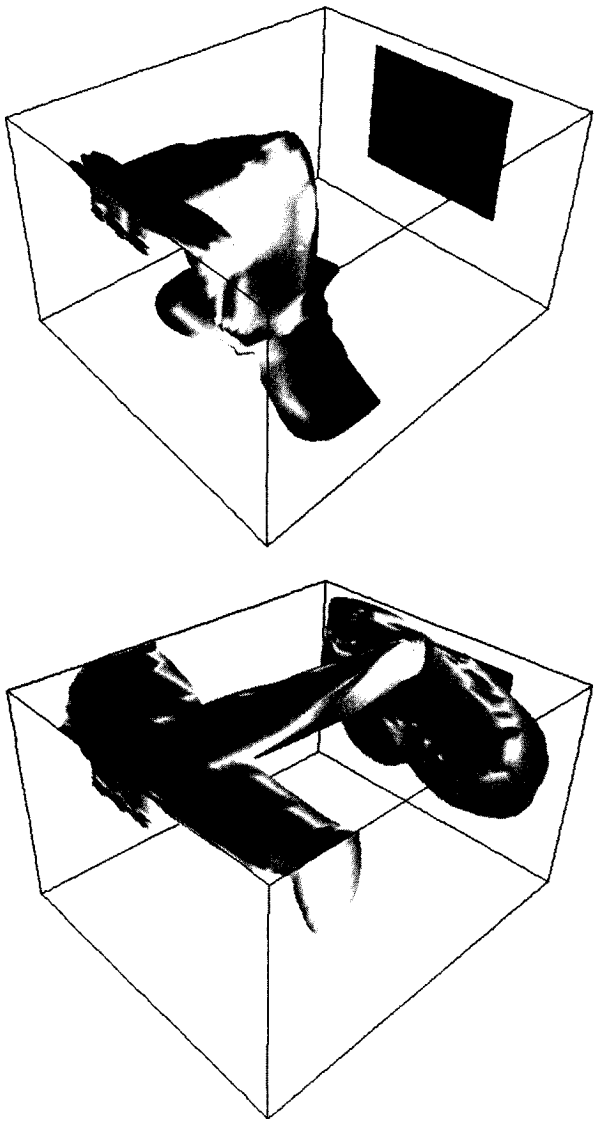

Figure 7.28: The three-dimensional isosurface of turbulent kinetic energy for E1 ($k = 10^{-4}\ m^2/s^2$) and E2 ($k = 2.5 \times 10^{-4}\ m^2/s^2$) situations.

CHAPTER 8

Conclusions

The main goal of this thesis was to improve and to extend the mathematical models of the effects of thermal buoyancy on turbulent flows in enclosures. This work is an extension of the earlier Ph.D. projects of S. Kenjereš [62] and H. Dol [27] in the Section for Thermal and Fluids Sciences, aimed at merging the best outcome of these two theses and expanding and generalizing the model with specific purpose of predicting complex flows driven or affected by thermal buoyancy. The adopted framework are the two advanced turbulence closures with some recent improvements: (i) the second moment closure with the near-wall and low-Re-number modifications, and (ii) the Elliptic Relaxation $k-\varepsilon-\overline{v^2}-f-\overline{\theta^2}$ model. Both of these two model classes have been extensively tested previously in isothermal flows without buoyancy, showing in general very good performances. Because the ultimate target of this work are complex flows, an important concern has been to adopt a moderate level of model complexity which will not deteriorate the computational robustness and which can be managed with the conventional computational methods, such as finite-volume or finite element approach, while still reproducing acceptably accurate main flow, heat transfer and turbulence features. The buoyancy modification of the second moment closure model was focused on the pressure scrambling term, where the new coefficients with scalar flux invariant are introduced. Also the new concept of "homogeneous" dissipation rate has been used to close the Reynolds stress equation. The new version of $k-\varepsilon-\overline{v^2}-f-\overline{\theta^2}$ model has been developed which includes the buoyancy effects. The latter model has been used in connection with an algebraic flux and buoyancy extended eddy viscosity models. Several options for the turbulence time scale in the algebraic flux model have been investigated. All models have been tested in two generic test cases: infinite plane channel with one heated and one cooled wall, positioned vertically or horizontally. In the first case the mean temperature gradient is perpendicular and in the second case it is aligned with the gravitation vector. The following conclusions have been drawn:

- The buoyancy extension of the low-Re-number second moment closure model, based on *a priori* term-by-term validation against the available DNS data for natural convection in a vertical infinite channel at a range of Rayleigh numbers, showed that these extensions improved agreement with the DNS data as compared with models available in the literature. An *a priori* analysis of turbulent natural convection in a horizontal channel heated from below showed improved performance. This improvement is mainly attributed to the use of the scalar (thermal) flux invariant, in terms of which the new coefficients in the pressure scrambling term are formulated.

- The $k-\varepsilon-\overline{v^2}-f-\overline{\theta^2}$ model has been originally developed in order to compromise the complexity, accuracy, and robustness between the advanced second moment closures and the conventional $k-\varepsilon$ eddy-viscosity models. Early validations of this model in various non-buoyant flows showed that the prediction quality, although not perfect, is generally closer to the full second moment closure than to the linear eddy-viscosity models, with only a marginal increase in complexity as compared with the latter model class. Incorporation of buoyancy effects proposed in this thesis confirmed the model features: the test in natural convection in a vertical infinite channel, in two- and three-dimensional side heated cavities, in Rayleigh-Bénard convection, and in mixed convection at a range of Rayleigh numbers, provided significant improvements in reproducing both the mean and turbulence parameters as compared with the conventional $k-\varepsilon$ and similar models.

- This work confirmed earlier findings of Kenjereš [62] that a simple algebraic flux model obtained by truncation of the full differential second-moment flux model is far superior to the eddy diffusivity models, irrespective whether an isotropic ("simple gradient diffusion hypothesis") or tensorial ("generalized gradient diffusion hypothesis") eddy diffusivity is used. The main prerequisite for this success is to keep all flux-production terms in the algebraic expression for heat flux, i.e. the term containing the mean velocity gradient interacting with turbulent heat flux, the term containing mean temperature gradient interacting with turbulent stresses and the buoyancy source of the heat flux.

- An important finding in the present work was the role of the time scale in the algebraic flux model. The use of the conventional mechanical time scale k/ε proved to be not fully adequate, at least in the context of conventional derivation of algebraic models. The new time scale used in the $k-\varepsilon-\overline{v^2}-f-\overline{\theta^2}$ model in the expression for eddy viscosity, which is based on the velocity scale $\overline{v^2}$ and, when used in the algebraic expression for heat flux yielded significant improvements. This time scale seems to represent better the near-wall turbulence dynamics accounting for the wall-blocking effects. It suppresses the heat flux in the near-wall region in accord with the DNS and experimental findings for both the horizontal and vertical configurations.

- Although the Reynolds stress and heat flux are calculated using the eddy viscosity and algebraic flux model, respectively, they can predict major features of flow, heat transfer and turbulence statistics in a range of applications. This may be due to the introduction of buoyancy term in eddy viscosity model and the new time scale in the algebraic flux model. This approach is still less satisfactory as compared to that of advanced second moment closure model, however its appealing simplicity and suitability for

handling complex flows makes it an attractive and preferred option, especially for industrial application.

- It was observed that using very small y_1^+ affects the performance of the $k-\varepsilon-\overline{v^2}-f-\overline{\theta^2}$. The weakness of the model appears to lie in the boundary condition for the elliptic relaxation function (which varies as $1/x_n^4$). This study examined the optimum values for y_1^+, which should be sufficiently small to ensure good near-wall resolution, but still sufficiently large to avoid the numerical problems. In the side heated infinite channel the most appropriate value appeared to be in the range $0.1 < y_1^+ < 2$, while for the two- and three-dimensional enclosures the range can be extended further at $0.1 < y_1^+ < 5$.

- Among the several classes of models considered it has been concluded that the $k-\varepsilon-\overline{v^2}-f-\overline{\theta^2}$ with buoyancy modifications proved to be the best compromise for complex buoyancy driven flows. It is robust and provides results with acceptable accuracy in several generic flows and in a range of application-relevant situations.

BIBLIOGRAPHY

[1] C.A. Armitage. *Computational modelling of double-diffusive flows in stratified media.* PhD thesis, University of Manchester of Science and Technology, Manchester, U.K., 2001.

[2] A. Bejan. *Convective Heat Transfer.* John Wiley and Sons, New York, USA, 1984.

[3] H. Bénard. Les tourbillons cellulaires dans une nappe liquide. *Rev. Gen. Sciences Pure Appl.*, 11:1261–1271, 1900.

[4] D. Blay, S. Mergui, and C Niculae. Confined turbulent mixed convection in the presence of a horizontal buoyant wall jet. In *Fundamental of Mixed Convection, HTD*, volume 213, ASME (1992).

[5] C. Blomqvist. Measurement of test case E (mixed convection, summer cooling). IEA Annex 20 Research Item 1.17, 1991.

[6] M. R. Boudjemadi. *Simulation numérique directe et modélisation de la convection naturelle turbulente dans un canal differentiellement chauffé.* PhD thesis, University of Paris Xi-Orsay, Paris, France, 1997.

[7] R. Boudjemadi, V. Maupu, D. Laurence, and P. Le. Quéré. Budgets of turbulent stresses and fluxes in a vertical slot natural convection flow at Rayleigh Ra=10^5 and 5.4×10^5. *Int. J. Heat and Fluid Flow*, 18:70–79, 1997.

[8] P. Bradshaw, N. N. Mansour, and U. Piomelli. On Local Approximations of the Pressure Strain-Term in Turbulence Modelling. In *Summer Program, 159*, Center for Turbulence Research, Stanford University, U.S.A., 1987.

[9] R. Cheesewright, King K. J., and Ziai S. Experimental data for the validation of computer codes for the prediction of two-dimensional buoyant cavity flows. *Proc. ASME Meeting HTD*, 60:75–86, 1986.

[10] K. S. Chen, A. C. Ku, and C. H. Chou. Investigation of natural convection in partially divided rectangular enclosures both with and without an opening in the partition plate: measurement results. *J. Heat Transfer*, 112:648–652, 1990.

[11] K.W. Cheong and K.Y. Chong. Development and application of an indoor air quality audit to an air-conditioned building in singapore. *Building and Environment*, 36:181–188, 2001.

[12] C. C. Chieng and B.E. Launder. On the calculation of turbulent heat transport downstream from an abrupt pipe expansion. *Num. Heat Transfer, Part B*, 3:189–207, 1980.

[13] P. Y. Chou. On the velocity correlation and the solution of the equation of turbulent fluctuation. *Q. Appl. Math.*, 3:38–54, 1945.

[14] T. Chu and R. J. Goldstein. Turbulent natural convection in a horizontal layer of water. *J. Fluid Mech.*, 60:141–159, 1973.

[15] P. Cooper and P.F. Linden. Natural ventilation of enclosures containing two buoyancy sources. *J. Fluid Mech.*, 311:155–176, 1996.

[16] T. J. Craft. *Second-moment modelling of turbulent scalar transport.* PhD thesis, Faculty of Technology, University of Manchester, Manchester, U.K., 1991.

[17] T. J. Craft, N. Z. Ince, and B. E. Launder. Recent developments in second-moment closure for buoyancy-affected flows. *Dynamics of Atmospheres and Oceans*, 23:99–114, 1996.

[18] T. J. Craft and B. E. Launder. Computation of impinging flows using second-moment closures. In *Proc. 8th Symp. Turbulent Shear Flows*, Technical University of Munich, Germany, 1991.

[19] T. J. Craft, B. E. Launder, and K. Suga. Prediction of turbulent transitional phenomena with a non-linear eddy-viscosity model. *Int. J. Heat and Fluid Flow*, 18(1):15–28, 1997.

[20] A. A. Dafa'Alla and P. L. Betts. Experimental study for natural convection in a tall cavity. Mech. Eng. Rep. TFD/91/6, UMIST, Manchester, U.K., 1991.

[21] B. J. Daly and F. H. Harlow. Transport equations in turbulence. *Phys. Fluids*, 13:2634–2649, 1970.

[22] de Vahl Davis. Natural convection of air in a square cavity: a benchmark numerical solution. *Int. J. Numer. Meth. Fluids*, pages 249–264, 1983.

[23] I. Demirdžić and S. Muzaferija. Numerical method for coupled fluid flow, heat transfer and stress analysis using unstructured moving meshes with cells of arbitrary topology. *Comp. Methods Appl. Mech. Engrg.*, 125:235–255, 1995.

[24] H. S. Dol and K. Hanjalić. Computational study of turbulent natural convection in a side-heated near-cubic enclosure at a high rayleigh number. *Int. J. of Heat and Mass Transfer*, 44:2323–2344, 2001.

[25] H. S. Dol, K. Hanjalić, and S. Kenjereš. A comparative assessment of the second-moment differential and algebraic models in turbulent natural convection. *Int. J. Heat and Fluid Flow*, 18:4–14, 1997.

[26] H. S. Dol, K. Hanjalić, and T.A.M Versteegh. A dns-based thermal second-moment closure for buoyant convection at vertical walls. *J. Fluid Mech.*, 391:211–247, 1999.

[27] H.S. Dol. *Turbulence models for natural convection in side-heated enclosures.* PhD thesis, Delft University of Technology, Delft, The Netherlands, 1998.

[28] P. Durbin. Near-wall turbulence closure modeling without 'damping functions'. *Theor. Comp. Fluid Dynamics*, 3:1–13, 1991.

[29] P. Durbin. A Reynolds stress model for near-wall turbulence. *J. Fluid Mech.*, 249:465–498, 1993.

[30] P. Emvin. *The full multigrid method applied to turbulent flow in ventilated enclosures using structured and unstructured grids.* PhD thesis, Chalmers University of Technology, Goteborg, Sweden, 1997.

[31] M. Ewert, U. Renz, N. Vogel, and M. Zeller. Definition of the flow parameters at the room inlet device-measurements and calculations. IEA Annex 20 Research Item 1.43, 1991.

[32] M. Ewert and M. Zeller. Turbulence parameters at supply opening (measurements). IEA Annex 20 Research Item 1.43, 1991.

[33] J.H. Ferziger and M. Perić. *Computational methods for fluid dynamics.* Springer, Berlin, Germany, 1996.

[34] D. E. Fitzjarrald. An experimental study of turbulent convection in air. *J. Fluid Mech.*, 73:693–719, 1976.

[35] Fossdal. Measurement of test case E (mixed convection, summer cooling). IEA Annex 20 Research Item 1.17, 1991.

[36] S. Fu, B. E. Launder, and D. P. Tselepidakis. Accomodating the Effects of High Strain rates in Modelling the Pressure-Strain Correlation. Technical Report TFD/87/5, Mech. Eng. Dept., UMIST, 1987.

[37] M. M. Gibson and B. E. Launder. On the calculation of horizontal, turbulent, free shear flows under gravitational influence. *J. Heat Transfer*, 2:81–87, 1976.

[38] M. M. Gibson and B. E. Launder. Ground effects on pressure fluctuations in the atmospheric boundary layer. *J. Fluid Mech.*, 86:491, 1978.

[39] G. Grötzbach. Direct numerical simulation of laminar and turbulent Bénard convection. *J. Fluid Mech.*, 119:27–53, 1982.

[40] F.J. Hamady, J.R. Lloyd, H.Q. Yang, and K.T. Yang. Study of local natural convection heat transfer in an inclined enclosure. *Int. J. Heat Mass Transfer*, 32(9):1697–1708, 1989.

[41] K. Hanjalić. Achievements and limitations in modeling and computation of buoyant turbulent flows and heat transfer, special keynote paper. In *Proceedings of the 10th International Heat Transfer Conference*, volume 1, pages 1–18, London,U.K., 1994.

[42] K. Hanjalić. Advanced turbulence closure models: a view of current status and future prospects. *Int. J. Heat and Fluid Flow*, 15:178–203, 1994.

[43] K. Hanjalić and S. Jakirlić. A Model of Stress Dissipation in second moment closures. *Appl. Scientific Research 51*, pages 513–518, 1993.

[44] K. Hanjalić and S. Jakirlić. Contribution towards the second-moment closure modelling of separating turbulent flows. *Computers and Fluids*, 27(2):137–156, 1998.

[45] K. Hanjalić and B. E. Launder. A Reynolds stress model of turbulence and its application to thin shear flows. *J. Fluid Mech.*, 52:609–638, 1972.

[46] K. Hanjalić and B. E. Launder. Contributions towards a Reynolds-stress closure for low-Reynolds-number turbulence. *J. Fluid Mech.*, 74:593–610, 1976.

[47] K. Hanjalić and R. Musemić. Modelling the dynamics of double-diffusive scalar fields at various stability conditions. *Int. J. Heat and Fluid Flow*, 18:360–367, 1997.

[48] K. Hanjalić and S. Vasić. Computation of turbulent natural convection in rectangular enclosures with an algebraic flux model. *Int. J. Heat Mass Transfer*, 36(14):306–324, 1993.

[49] J. Heikkinen. Measurement of test case B2, B3, E2, E3 (isotherm and summer cooling cases). IEA Annex 20 Research Item 1.16 and 1.17, 1991.

[50] R.A.W.M. Henkes. *Natural-convection boundary layers*. PhD thesis, Delft University of Technology, Delft, The Netherlands, 1990.

[51] C.J. Hoogendoorn, I.J Opstelten, and H.S. (1996) Dol. Turbulence natural convection in a cubical enclosures. In *Proc. Turb. Heat Transfer Conf.*, San Diego, USA, 1996.

[52] P. Hoppe. Different aspects of assesing indoor and outdoor thermal comfort. *Energy and Buildings*, 34:661–665, 2002.

[53] G.R. Hunt and P.F. Linden. The fluid mechanics of natural ventilation-displacement ventilation by buoyancy-driven flows assisted by wind. *Building and Environment*, 34:155–176, 1999.

[54] S. Jakirlić. *Reynolds-Spannungs-Modellierung komplexer turbulenter Strömungen.* PhD thesis, Technischen Fakultät der Universität Erlangen-Nürnberg, Erlangen, Germany, 1997.

[55] S. Jakirlić and K. Hanjalić. A new approach to modelling near wall turbulence energy and stress dissipation. *J. Fluid Mech.*, 459:139–166, 2002.

[56] S.H. Johanson, L. Davidson, and E. Olson. Simulation of test case E (mixed convection, summer cooling). IEA Annex 20 Research Item 1.20, 1991.

[57] W.P. Jones and B.E. Launder. Prediction of laminarization with a two-equation model of turbulence. *Int. J. Heat Mass Transfer*, 15:301, 1972.

[58] J. Jovanović, Q.Y. Ye, and F. Durst. Statistical interpretation of the turbulent dissipation rate in wall-bounded flows. *J. Fluid Mech.*, 293:321–347, 1995.

[59] N. Kasagi and M. Nishimura. Direct numerical simulation of combined forced and natural convection in a vertical plane channel. *Int. J. Heat and Fluid Flow*, 18:88–99, 1997.

[60] S. Kenjereš, S.B. Gunarjo, and K. Hanjalić. Natural convection in an air-filled cubical cavity under different angles of inclination: A benchmark study. In *Proc. Int. Symposium on Advances in Computational Heat Transfer*, Palm cave, Australia, 2001.

[61] S. Kenjereš, K. Hanjalić, and S.B. Gunarjo. A t-rans/vles approach to indoor climate simulations. In *2002 ASME Fluids Engineering Division Summer Meeting*, Montreal, Quebec, Canada, 2002.

[62] S. Kenjereš. *Numerical Modelling of Complex Buoyancy Driven Flows.* PhD thesis, Delft University of Technology, Delft, The Netherlands, 1999.

[63] S. Kenjereš, S.B. Gunarjo, and K. Hanjalić. Extension of elliptic relaxation approach to transient natural and mixed convection. *Eurotherm Seminar 74 on Heat Transfer in Unsteady and Transitional Flows*, Eindhoven, The Netherlands, 2003.

[64] R. M. Kerr. Rayleigh number scaling in numerical convection. *J. Fluid Mech.*, 310:139–179, 1996.

[65] K.J. King. *Turbulent natural convection in rectangular air cavities.* PhD thesis, Queen Mary College, London, UK, 1989.

[66] B. E. Launder. Heat and Mass Transport. In P. Bradshow, editor, *Topics in Applied Physics*. Springer, 1976.

[67] B.E Launder. On the effects of a gravitational field on the turbulent transport of heat and momentum. *J. Fluid Mech.*, 67:569, 1975.

[68] B.E. Launder. On the computation of convective heat transfer in complex turbulent flows. *J. Heat Transfer*, 110:1112–1128, 1988.

[69] P. Le Quere. Accurate solutions to the square thermally driven cavity at high rayleigh number. *Computer Fluids*, 20(1):29–41, 1991.

[70] J.A. Leech, R. Burnett, W. Nelson, S.D. Aaron, and M. Raizenne. Outdoor air pollution epidemiologic studies. *Americal Journal of Respiration and Critical Care Medicine*, 161 (3), 2000 A308.

[71] A.D. Lemaire. Simulation of test case E (mixed convection, summer cooling). IEA Annex 20 Research Item 1.20, 1991.

[72] W.H. Leong, K.S. Hollands, and A.P. Brunger. On a physically-realizable benchmark problem in internal natural convection. *Int. J. Heat Mass Transfer*, 41:3817–3828, 1998.

[73] W.H. Leong, K.S. Hollands, and A.P. Brunger. Experimental nusselt numbers for a cubical-cavity benchmark problem in natural convection. *Int. J. Heat Mass Transfer*, 42:1979–1989, 1999.

[74] F.S. Lien and G. Kalitzin. Computational of transonic flow with the $\overline{v^2} - f$ turbulence model. *Int. J of Heat and Fluid Flow*, 22:53–61, 2001.

[75] P.F. Linden, G.F. Lane-Serff, and D.A. Smeed. Emptying filling boxes: the fluid mechanics of natural ventilation. *J. Fluid Mech.*, 212:300–315, 1990.

[76] J. L. Lumley. Computational modelling of turbulent flows. *Adv. Appl. Mech.*, 18:123, 1978.

[77] R. Manceau and K. Hanjalić. A new form of the elliptic relaxation equation to account for wall effects in rans modelling. *Physics of Fluids*, 12:2345–2351, 2000.

[78] A. S. Monin. On the symmetry of turbulence in the surface layer of air. *Izv. Atm. Oceanic Phys.*, 1:45, 1965.

[79] S. Murakami, S. Kato, T. Chikamoto, D. Laurence, and D. Blay. New low-reynolds-number $k\epsilon$ model including damping effect due to buoyancy in a stratified flow field. *Int. J. Heat and Mass Transfer*, 39:3483–3496, 1996.

[80] M. W. Nansteel and R. Greif. Natural convection in undivided and partially divided rectangular enclosures. *J. Heat Transfer*, 103:623–629, 1981.

[81] D. Naot, A. Shavit, and M. Wolfstein. Two-point correlation model and the redistribution of reynolds stresses. *Phys. Fluids*, 16:738, 1973.

[82] L. Neiswanger, G.A. Johnson, and V.P. Carey. An experimental study of high rayleigh number mixed convection in a rectangular enclosure with restricted inlet and outlet openings. *Journal of Heat Transfer*, 109:446 453, 1987.

[83] F. T. M. Nieuwstadt and T. A. M. Versteegh. DNS of natural convection between two vertical, differentially heated walls. *11th Symposium on Turbulent Shear Flows, Grenoble, France, Septembar 1997*, 3:23.7–23.12, 1997.

[84] D. A. Olson, L. R. Glicksman, and H. M. Ferm. Steady state natural convection in empty and partitioned enclosures at high Rayleigh numbers. *J. Heat Transfer*, 112:640 647, 1990.

[85] I.J. Opstelten. *Experimental study on transition characteristics of natural-convection flow.* PhD thesis, Delft University of Technology, Delft, The Netherlands, 1994.

[86] I.J. Opstelten, R.A.W.M. Henkes, and C.J. Hoogendoorn. On instability mechanism of the natural convection flow in a side heated cubical enclosure. In *In Proc. 1st European Conf. Thermal Sciences*, pages 523 529, 1992.

[87] J. Pallares, M.P. Arroyo, F.X. Grau, and F. Giralt. Rayleigh-bénard convection in a cubical cavity: experimental and numerical flow topologies. *Exp. Fluids*, 31 (2):208–218, 2001.

[88] S.V. Patankar. *Numerical heat transfer and fluid flow.* Hemisphere, New York, USA, 1980.

[89] T.W.J. Peeters and R.A.W.M. Henkes. The Reynolds-stress model of turbulence applied to the natural-convection boundary layer along a heated vertical plate. *Int. J. Heat Mass Transfer*, 35(2):403–420, 1992.

[90] M. Perić. *A Finite Volume Method for the Prediction of Three-Dimensional Fluid Flow in Complex Ducts.* PhD thesis, Imperial College, Mech. Eng. Dept., London, U.K., 1985.

[91] W. Rodi. *The Prediction of Free Turbulent Boundary Layers by Use of a 2-Equation Model of Turbulence.* PhD thesis, University of London, London, U.K., 1972.

[92] W. Rodi. A new algebraic realtion for calculating the Reynolds stresses. *ZAMM*, 56:219–221, 1976.

[93] H. Rohles. Temperature or temperament: a psychologist looks at thermal comfort. *ASHRAE Transactions*, 86 (1):5–13, 1980.

[94] J. C. Rotta. Statistiche Theorie nichthomogener Turbulenz. *Z. Phys.*, 20:547–572, 1951.

[95] T. H. Shih and J. L. Lumley. Modelling of pressure correlation terms in reynolds stress and scalar flux equations. Technical Report FD-85-03, Sibley School of Mech. and Aerospace Eng., Cornell University, U.S.A., 1985.

[96] T. H. Shih, J. L. Lumley, and J. Y. Chen. Second order modelling of a passive scalar in a turbulent shear flow. Technical Report FD-85-15, Sibley School of Mech. and Aerospace Eng., Cornell University, U.S.A., 1985.

[97] J.J.M. Sillekens, C.C.M. Rindt, and A.A. van Steenhoven. Development of laminar mixed convection in a horizontal square channel with heated side walls. *Int. J. Heat and Fluid Flow*, 19:270-281, 1998.

[98] T.P. Sommer, R.M.C. C, and Y.G. Lai. A near-wall two-equation model for turbulent heat fluxes. *Int. J. Heat Mass Transfer*, 35:3375–3387, 1992.

[99] J. Tsutsumi, S. Katayama, A. Ishii, H. Ping, and T. Hayashi. Investigation and numerical simulation of the wind effects on thermal comfort in a house. *Journal of Wind Engineering and Industrial Aerodynamics*, 60:267–280, 1996.

[100] J.T. Van der Eyden, Th.H. Van der Meer, and K Hanjalić. Double-diffusive natural convection in trapezoidal enclosures. *Int. J. Heat and Mass Transfer*, 41(13):1885–1898, 1998.

[101] T. A. M. Versteegh. *Numerical simulation of natural convection in a differentially heated vertical channel.* PhD thesis, Delft University of Technology, Delft, The Netherlands, 1998.

[102] T. A. M. Versteegh and F. T. M. Nieuwstadt. Scaling of free convection between two diferentialy-heated infinite vertical plates. *Submitted for publication*, 1996.

[103] P. Wesseling. *An Introduction to Multigrid Methods.* John Willey & Sons Ltd., Chichester, U.K., 1991.

[104] M. Wöerner. Direkte Simulation turbulenter Rayleigh-Bénard Konvektion in flüssigem Natrium. *Dissertation, Uni. of Karlsruhe, KfK 5228, Kernforschungszentrum Karlsruhe*, 1994.

[105] N.H. Wong and S.S. Khoo. Thermal comfort in classrooms in the tropics. *Energy and Buildings*, 35:337–351, 2003.

[106] M. Wörner and G. Grötzbach. Modelling the molecular terms in the turbulent heat flux equation for natural convection. In *10th Symposium on Turbulent Shear Flows*, volume 2, pages P2–73–78, Pennsylvania State University, State College, U.S.A., 1995.

[107] X. Yuan. *Wall functions for numerical simulation of natural convection along vertical surface*. PhD thesis, Swiss Federal Institute of Technology, Zurich, Sweden, 1995.

Summary

Contribution to advanced modelling of turbulent natural and mixed convection

The main objective of this thesis was to develop, improve and extend turbulence models for natural and mixed convection in enclosures. The models targeted were expected to perform well in various configurations, with different boundary conditions and in the range of Rayleigh and Reynolds numbers numbers relevant to practical application. The flows considered are encountered in many engineering applications, such as indoor climate, conventional and renewable space heating and cooling systems, solar engineering, electronics cooling, nuclear engineering and others. The turbulence models developed in this thesis are based on Reynolds Averaged Navier-Stokes Equations (RANS) and to the two classes of advanced closure models: the second moment closures and the elliptic relaxation $k - \varepsilon - \overline{v^2} - f - \overline{\theta^2}$ models.

In the first phase of the research, the study was focused on the buoyancy modification of the second moment closure of Hanjalić and Jakirlić [43] model for the mechanical (isothermal) turbulent flows following the work of Dol *et al.* [26] for the thermal field. The development and validation of various ideas towards the model improvement was first analyzed in *a priori* term-by-term tests based on DNS data. An important enhancement of the mechanical model is the straightforward inclusion of buoyancy in the transport equation for the Reynolds stress, but also in the pressure strain correlation. This introduction of buoyancy is vitally important in order to capture the turbulent fields, especially in the boundary layer region. The modification of the thermal part is mainly focused in the pressure scrambling term, particularly on omitting the less significant terms and optimising the significant ones. In addition, a new model function in terms of scalar flux invariant, is introduced. The use of the scalar flux invariant is supported by the fact that it behaves relatively general in many flows. This replaces the existing model function based on the stress invariant, which showed different behaviour in channel flows when its orientation with respect to the gravity vector is changed. The new second moment closure model is applied in side heated vertical channel for a range of Rayleigh numbers, and they are validated using the DNS data. Algebraic stress and flux models based on the differential second moment closure has also been derived by truncating the convection and diffusion terms in the parent transport equations for Reynolds stress and heat flux. Here, the truncated terms are totally neglected, while the major terms such as shear and buoyancy productions, associated with the gradients of mean velocity and temperature, and with the temperature variance respectively, are kept as in the

transport equations. The second moment closure models are generally superior to algebraic and basic model, but in the flows considered this superiority is not so dramatic and reasonable accuracy has been achieved with algebraic models.

It is well known that the second moment closures demand large computational resources, and also may lead to numerical instabilities when applied in a complex geometry. Concerned with these issues, this study was subsequently focused on the elliptic relaxation approach, specifically on the $k - \varepsilon - \overline{v^2} - f - \overline{\theta^2}$ model, which was extended to account for buoyancy effects. Here the Reynolds stresses are calculated using the buoyancy extended eddy viscosity model, while the heat flux is calculated using an algebraic flux model. The $k - \varepsilon - \overline{v^2} - f - \overline{\theta^2}$ model with an additional transport equation for $\overline{v^2}$, representing an additional velocity scale relevant to near-wall region, and an elliptic equation for the relaxation function f, offers several attractive features: It is simple to solve comparable to the conventional low-Re-number two equation models, it is robust, and it reproduces the near-wall turbulence accurately without a need to employ damping functions.

The model is applied and tested in a range of flows in turbulent natural and mixed convection. For natural convection these include side heated vertical channel, side heated two-dimensional enclosures with various aspect ratio, three-dimensional enclosure, and Rayleigh-Bénard convection. For mixed convection the model was applied in three different situations: in an enclosure with air supply and exhaust under thermal stratification, and in mixed convection under summer cooling condition with high and a low air flow rates.

Most of the numerical results are validated with the available experimental data, DNS, and other results from the literature. The DNS data being only available for very simple flow case of natural convection in infinite channels, have been used for term-by-term model validation. For other cases considered, experimental data available in the literature have been used, such as two-dimensional and three-dimensional side heated enclosures, and in mixed convection under summer cooling condition. In general, the model reproduced reasonable agreement with both DNS and experimental data. This indicates that the model is well formulated. Since the computation using the model covers a range of turbulent flows, it is prospective to employ the model in industrial applications.

Samenvatting

Bijdrage aan de geavanceerde modellering van turbulente natuurlijke en gemengde convectie

Het hoofddoel van dit proefschrift was het ontwikkelen, verbeteren en uitbreiden van turbulentiemodellen voor natuurlijke en gemengde convectie in gesloten ruimten. Van de bedoelde modellen wordt verwacht, dat ze goed presteren onafhankelijk van de vorm van de ruimte, met verschillende randvoorwaarden en voor Rayleigh- en Reynolds-getallen die relevant zijn bij practische toepassingen. De beschouwde stromingen komen bij vele technische toepassingen voor, zoals binnenklimaat, conventionele en duurzame verwarmings- en koelsystemen, toepassingen van zonneënergie, koeling van electronica, nucleaire installaties, enzovoorts. De in dit proefschrift ontwikkelde turbulentiemodellen zijn gebaseerd op de Reynolds-gemiddelde Navier-Stokes vergelijkingen (RANS) en op twee klassen van van geavanceerde sluitingsmodellen: tweede moment sluitingen en de $k-\varepsilon-\overline{v^2}-f-\overline{\theta^2}$ elliptische relaxatie modellen.

In het eerste gedeelte van het onderzoek was de aandacht gericht op de opwaartse kracht modificatie van de tweede moment sluiting volgens van het mechanisch model van Hanjalić and Jakirlić [48] voor isotherme turbulente stromingen. Dit in navolging van het werk van Dol *et al.* [26] voor het temperatuurveld. De ontwikkeling en de geldigheid van de verschillende ideeën voor verbetering van de modellen, werd eerst geanalyseerd in een term-voor-term *a priori* test gebaseerd op DNS gegevens. Een belangrijke verbetering van het mechanisch model is de rechtstreekse opneming van opwaartse kracht niet alleen in de transportvergelijking voor de Reynolds spanning, maar ook in correlaties van drukgradiënt en snelheid. Het opnemen van de effecten van opwaartse kracht is van groot belang om de turbulente effecten juist te beschrijven, met name in grenslagen. De modificatie in de temperatuurvergelijkingen is vooral gericht op de correlatie van drukgradiënten en temperatuur, met name op het weglaten van de minder belangrijke termen en het optimaliseren van de meest bepalende. Daarnaast is er een nieuw model in termen van een scalaire flux-invariantie geïntroduceerd. Het gebruik van invarianties wordt ingegeven door het feit, dat deze zich vrij algemeen gedragen in vele stromingen. Dit vervangt bestaande modelfuncties gebaseerd op de stress-invariantie, welke verschillend gedrag vertoonden in kanaalstromingen afhankelijk van de orientatie van de zwaartekrachtsvector. Het nieuwe tweede moment sluitingsmodel wordt toegepast in een van opzij verwarmd vertikaal kanaal voor een aantal verschillende Rayleigh-getallen en het is gevalideerd met behulp van resultaten verkregen met directe numerieke simulatie. Algebraïsche stress- en fluxmodellen gebaseerd op de differentiële tweede moment sluiting zijn ook afgeleid door afbreking van de convectie- en diffusietermen in de oorspronkelijke transportvergelijkingen voor Reynolds-stress en warmteflux. De afgebroken ter-

men worden hier verwaarloosd, terwijl de belangrijke termen, zoals productie door afschuiving en zwaartekracht, geassocieerd met de gradiënten van gemiddelde snelheid en temperatuur respectievelijk temperatuurvariaties, worden gehouden zoals gegeven in de transportvergelijkingen. Tweede moment sluitingsmodellen zijn over het algemeen superieur aan algebraïsche modellen en aan het basismodel, maar in de hier beschouwde stromingen is deze superioriteit niet zo dramatisch en is een redelijke nauwkeurigheid bereikt met algebraïsche modellen.

Het is wel bekend dat de tweede moment sluiting aanzienlijke rekenkracht vergt en ook kan leiden tot numerieke instabiliteiten wanneer ze wordt toegepast in complexe geometrieën. Rekening houdend met deze eigenschappen, is eze studie vervolgens gericht op een aanpak met elliptische relaxatie, met name op het $k-\varepsilon-\overline{v^2}-f-\overline{\theta^2}$ model, dat was uitgebreid om rekening te houden met zwaartekrachtseffecten. De Reynolds-spanningen worden berekend met een eddy viscositeitsmodel met zwaartekrachtseffecten, terwijl de warmteflux berekend wordt met een algebraïsch flux model. Het $k-\varepsilon-\overline{v^2}-f-\overline{\theta^2}$ model met een toegevoegde transport vergelijking voor $\overline{v^2}$, die een extra snelheidsschaal toevoegt die karakteristiek is voor het gebied nabij de wand, en een elliptische vergelijking voor de relaxatiefunctie f, bieden verschillende aantrekkelijke kenmerken: Het is eenvoudig om de vergelijkingen op te lossen op een vergelijkbare manier als de conventionele twee vergelijkingen modellen voor lage Reynolds-getallen, het is robuust en het reproduceert de turbulentie nabij de wand nauwkeurig, zonder de noodzaak dempingsfuncties te gebruiken.

Het model is toegepast en getest voor een verscheidenheid aan stromingen met turbulente natuurlijke en gemengde convectie. Voor natuurlijke convectie betreffen deze het van opzij verwarmde kanaal, van opzij verwarmde tweedimensionale gesloten ruimten met verschillende breedte-hoogte verhoudingen, driedimensionale gesloten ruimten en Rayleigh-Bénard-convectie. Voor gemengde convectie is het model toegepast in drie verschillende situaties: In een ruimte met toe- en afvoer van lucht bij thermische gelaagdheid en bij gemengde convectie onder zomerse condities, waarbij gekoeld wordt met hoog en laag luchtdebiet.

Het merendeel van de numerieke resultaten is gevalideerd met beschikbare experimentele data, directe numerieke simulatie en andere resultaten uit de literatuur. Resultaten van directe numerieke simulatie, die alleen maar beschikbaar zijn voor de eenvoudige stroming in oneindig lange kanalen, zijn gebruikt voor een term-voor-term model validatie. Voor de andere beschouwde modellen is gebruik gemaakt van experimentele data beschikbaar in de literatuur, zoals de van opzij verwarmde twee- en driedimensionale gesloten ruimten en voor gemengde convectie bij koeling onder zomerse omstandigheden. In het algemeen gaf het model een redelijke overeenstemming met zowel de resultaten uit directe numeriek simulatie als de resultaten uit experimenten. Dit geeft aan dat het model goed is geformuleerd. Aangezien de berekeningen met het model zijn uitgevoerd voor verschillende turbulente stromingen zijn er goede vooruitzichten voor industriële toepassing.

ACKNOWLEDGEMENTS

First of all I would like to thank to my promotor Professor K. Hanjaić for his support, advice, encouragement and help throughout my Ph.D. until the last period of writting this thesis. I would also like to thank to my supervisor Dr. Kenjereš for his help and guidance along the whole years during my Ph.D. He is the one who has guided me to work on Computational Fluid Dynamics from zero until of the end of the thesis. His support and encouragement are acknowledged. In addition, he has been also a nice office mate who made me feeling comfortable while working in the Thermofluids section.

I would like to thank to The Inonesian Government and CICAT for the financial funding. I thank Drs. Paul Althuis for providing support during my stay in The Netherlands. Thanks also to Durk Jellema and Rene Tamboer for their technical support in my Ph.D studies.

Thanks are also due to Ing. Erwin de Beus, for making it possible to perform numerical simulation on the section computers. I would like to thank to Dr. Gerard C.J. Bart and Dr. Harm Jonker for very kindly translating my samenvatting. I would like to thank to Leon who has helped me to solve some technical problems, looking for a doctor when I was not feeling well and for translating the *stellingen*. Thanks also to Werner and Marteen for their help in technical problems. It has been a pleasure to work in the Thermofluids section, where all staff and students have provided good atmosphere and encouragement, thank you all very much.

Support from indonesian students here in The Netherlands is acknowledged, especially Hartono and Suyitno. Special thanks are addressed to Supriyanto and Yogi for their help in my Ph.D studies. Thanks are also addressed to other indonesian students that are too many to be mentioned, for their social support and friendship.

My wife Tripancani, and my sons Esa and Gema have been the source of strength during my Ph.D studies. Thanks for their support, encouragement, patience and love.

Gunarjo Suryanto Budi, Delft, July 2003

About the Author

22 July 1961	Born in Sukoharjo, Indonesia
1976-1980	High School (SMA 2 Wonogiri), Central Jawa
1980-1986	Faculty of Education, Sebelas Maret University, Solo
1994-1995	Master of Science, The University of New England, Australia Graduated on *An optical fibre sensor for use in controlled release technology*, Department of Physics, under supervision of Prof. Dr. G.A. Woolsey.
1999-2003	Ph.D student at the Thermofluids Section, Faculty of Applied Sciences, TU Delft, under supervision of Prof. Dr. K. Hanjalic and Dr. S. Kenjeres
1986-present	Lecturer at Faculty of Education, Palangkaraya University Kalimantan, Indonesia